

THE STRUCTURAL, THERMODYNAMIC AND DIELECTRIC PROPERTIES OF  
ELECTROLYTE SOLUTIONS: A THEORETICAL STUDY

By

PETER GERARD KUSALIK

B.Sc., The University of Lethbridge, 1981

M.Sc., The University of British Columbia, 1984

A THESIS SUBMITTED IN PARTIAL FULFILLMENT OF  
THE REQUIREMENTS FOR THE DEGREE OF  
DOCTOR OF PHILOSOPHY

in

THE FACULTY OF GRADUATE STUDIES  
(Department of Chemistry)

We accept this thesis as conforming  
to the required standard

THE UNIVERSITY OF BRITISH COLUMBIA

February, 1987

© Peter Gerard Kusalik, 1987

In presenting this thesis in partial fulfilment of the requirements for an advanced degree at the University of British Columbia, I agree that the Library shall make it freely available for reference and study. I further agree that permission for extensive copying of this thesis for scholarly purposes may be granted by the head of my department or by his or her representatives. It is understood that copying or publication of this thesis for financial gain shall not be allowed without my written permission.

Department of Chemistry

The University of British Columbia  
1956 Main Mall  
Vancouver, Canada  
V6T 1Y3

Date Feb 26 / 87

## ABSTRACT

In traditional theories for electrolyte solutions the solvent is treated only as a dielectric continuum. A more complete theoretical picture of electrolyte solutions can be obtained by including the solvent as a true molecular species. In this thesis we report results for the structural, thermodynamic, and dielectric properties of model electrolyte solutions which explicitly include a water-like molecular solvent. The ions are modelled simply as charged hard spheres and only univalent ions are considered. The water-like solvent is also treated as a hard sphere into which the low-order multipole moments and polarizability tensor of water are included. The reference hypernetted-chain theory is used to study the model systems. The formalism of Kirkwood and Buff is employed to obtain general expressions relating the microscopic correlation functions and the thermodynamic properties of electrolyte solutions without restricting the nature of the solvent. The low concentration limiting behaviour of these expressions is examined and compared with the macroscopic results determined through Debye-Hückel theory. The influence of solvent polarizability is examined at two theoretical levels. The more detailed approach, the  $R$ -dependent mean field theory, allows us to consider the average local electric field experienced by a solvent particle as a function of its separation from an ion and is shown to have an effect upon the limiting laws of some thermodynamic properties. Model systems for liquid water are investigated over a large range of temperatures and pressures and are found to have dielectric constants which agree reasonably well with experiment. Model aqueous electrolyte solutions are studied both at infinite dilution and at finite concentration, but only at 25°C. The equilibrium dielectric constants of these solutions are qualitatively consistent with those of experiment. A remarkable diversity of behaviour is obtained for our model solutions by simply varying the hard-sphere diameters of the ions. In many cases the behaviour observed for thermodynamic quantities is in accord with experiment. The ion-ion, ion-solvent and solvent-solvent correlation functions of the solutions are examined in detail, revealing a wealth of structural information. Ionic solvation is generally found to be very sensitive to the details of the interactions within the system.

## TABLE OF CONTENTS

ABSTRACT .....	ii
TABLE OF CONTENTS .....	iii
LIST OF TABLES .....	v
LIST OF FIGURES .....	vi
ACKNOWLEDGEMENTS .....	ix
CHAPTER I.	
INTRODUCTION .....	1
CHAPTER II.	
STATISTICAL MECHANICAL THEORY .....	6
1. Introduction .....	6
2. Interaction Potentials .....	9
3. The Ornstein-Zernike Equation .....	23
4. The Hypernetted-Chain Approximation .....	34
5. Method of Numerical Solution .....	38
6. Averages and Potentials of Mean Force .....	41
CHAPTER III.	
THERMODYNAMIC THEORY FOR ELECTROLYTE SOLUTIONS .....	51
1. Introduction .....	51
2. General Expressions .....	52
3. Limiting Behaviour .....	63
CHAPTER IV.	
MEAN FIELD THEORIES FOR POLARIZABLE PARTICLES .....	74
1. Introduction .....	74
2. The Self-Consistent Mean Field Theory .....	76
3. The R-Dependent Mean Field Theory .....	83



CHAPTER V.

RESULTS FOR WATER-LIKE MODELS .....	108
1. Introduction .....	108
2. Choice of Basis Set .....	110
3. Results for Hard-Sphere Models .....	114
4. Results for Soft Models .....	139

CHAPTER VI.

RESULTS FOR MODEL AQUEOUS ELECTROLYTE SOLUTIONS .....	150
1. Introduction .....	150
2. Dielectric Properties .....	156
3. Thermodynamic Properties .....	162
4. Structural Properties .....	202
5. Effects of Including the RDMF .....	238
6. Results Obtained Employing Different Solvents .....	254

CHAPTER VII.

CONCLUSIONS .....	272
-------------------	-----

LIST OF REFERENCES .....	278
--------------------------	-----

APPENDIX A.

TREATMENT OF POTENTIAL TERMS IN $c(12)$ .....	287
---	-----

APPENDIX B.

REPRESENTATIVE EXAMPLES OF EXPONENTIAL INTEGRALS .....	291
--	-----

APPENDIX C.

TRANSFORMATION OF THE ROTATIONAL INVARIANT $\Phi^{123}(12)$ ..	294
--	-----

## LIST OF TABLES

I.	Reduced ion diameters, $d_i^*$ , used in this study	23
II.	Experimental densities of water for the temperatures and pressures examined in this study	109
III.	Numbers of unique projection terms required in HNC basis sets	110
IV.	Projection terms included in $n_{\max}=2$ basis sets	111
V.	Maximum numbers of non-zero terms for any given projection in the HNC binary product	111
VI.	CPU time required per iteration on an FPS 164 array processor	112
VII.	Basis set dependence of $\epsilon$ , the average energies and $g(r=d)$	113
VIII.	Parameters for $u_{SR}(r)$	139
IX.	Model aqueous electrolyte solutions studied	152
X.	Average ion-solvent energies per ion at infinite dilution	268
XI.	Individual ionic partial molar volumes at infinite dilution	270

# LIST OF FIGURES

1.	Molecular axis system for the water molecule .....	18
2.	A charge distribution possessing (a) a square quadrupole and (b) a dipole and a square quadrupole .....	21
3.	The angle $\theta_{is}$ for (a) a positive ion and (b) a negative ion ....	46
4.	An illustration of the method used in determining $\langle \Delta E_{1I}(R) \rangle$ ...	87
5.	An illustration of the method used in determining $\langle \Delta E_{1D}(R) \rangle$ ...	92
6.	An illustration of the method used in determining $\langle \Delta E_{1Q}(R) \rangle$ ...	98
7.	The mean dipole moment of water-like particles as a function of temperature and pressure .....	115
8.	The dielectric constants of water and of water-like models as functions of temperature and pressure .....	118
9.	Radial distribution functions for water-like fluids at 25°C .....	121
10.	The projection $h_{00}^{110}(r)$ .....	124
11.	The projection $h_{00}^{112}(r)$ .....	126
12.	The projection $h_{00}^{123}(r)$ .....	128
13.	The projection $h_{02}^{123}(r)$ .....	130
14.	The projection $h_{00}^{224}(r)$ .....	132
15.	The projection $h_{02}^{224}(r)$ .....	134
16.	The projection $h_{22}^{224}(r)$ .....	136
17.	Soft potentials at 25°C .....	140
18.	Radial distribution functions for soft water-like models at 25°C and $m_e^* = 2.75$ .....	142
19.	Radial distribution functions of water and of water-like fluids at 25°C and $m_e^* = 2.75$ .....	145
20.	Structure factors of water and of water-like fluids at 25°C and $m_e^* = 2.75$ .....	147
21.	The concentration dependence of $\gamma$ .....	154
22.	Comparing theoretical and experimental values for the dielectric constant of aqueous KCl solutions .....	157

23.	The dielectric constants of real and of model aqueous electrolyte solutions as functions of concentration .....	160
24.	Average total ion-ion energies per ion as functions of square root concentration .....	163
25.	Average ion-dipole energies per ion as functions of square root concentration .....	165
26.	Average ion-solvent energies per ion as functions of square root concentration .....	168
27.	Average solvent-solvent energies per solvent as functions of concentration .....	170
28.	Total average energies as functions of concentration .....	173
29.	The square of the Debye screening parameter as a function of concentration .....	176
30.	The product $\rho_2 G_{+-}$ as a function of square root concentration ..	179
31.	$C_{IS}$ as a function of square root concentration .....	182
32.	$G_{+S}$ as a function of square root concentration .....	184
33.	$G_{SS}$ as a function of salt concentration .....	187
34.	Isothermal compressibility as a function of concentration .....	190
35.	Partial molar volume of the solvent as a function of concentration .....	193
36.	Partial molar volume of the solute as a function of square root concentration .....	195
37.	$\ln \gamma_{\pm}$ as a function of square root concentration .....	199
38.	Solvent-solvent radial distribution functions of the pure solvent and of several model electrolyte solutions .....	203
39.	$\langle \cos \theta_{SS}(r) \rangle$ for the pure solvent and for model electrolyte solutions .....	206
40.	Ion-solvent radial distribution functions at infinite dilution .....	208
41.	$\langle \cos \theta_{iS}(r) \rangle$ at infinite dilution .....	211
42.	Ion-solvent radial distribution function for $Cl^-$ .....	214
43.	$\langle \cos \theta_{iS}(r) \rangle$ of $Cl^-$ .....	216
44.	Potentials of mean force at infinite dilution for several pairs of oppositely charged ions .....	219

45.	Concentration dependence of $g_{+-}(r)$ for KCl	223
46.	Concentration dependence of $g_{+-}(r)$ for M <sup>+</sup> I	225
47.	Potentials of mean force at infinite dilution for several pairs of like ions	228
48.	$g_{ii}(r)$ for several ions in model electrolyte solutions at 1.0M	231
49.	$g_{ii}(r)$ for Cl <sup>-</sup> for several model electrolyte solutions	234
50.	Cl <sup>-</sup> /Cl <sup>-</sup> partial structure factors for model NaCl solutions	236
51.	Additional ion-solvent interaction term due to $\Delta p(r)$ for a Na <sup>+</sup> ion at infinite dilution	240
52.	Effect of the RDMF upon $w_{ij}(r)$ for NaCl	242
53.	Effect of the RDMF upon $w_{ij}(r)$ for MBr	244
54.	Effect of the RDMF upon $w_{ii}(r)$ for Na <sup>+</sup>	247
55.	Effect of the RDMF upon $w_{ii}(r)$ for M <sup>+</sup>	249
56.	Effect of the RDMF upon $C_{IS}$	251
57.	Potentials of mean force at infinite dilution for KCl in polarizable and unpolarizable tetrahedral solvents	255
58.	Ion-solvent radial distribution functions at infinite dilution for the tetrahedral and C <sub>2v</sub> octupole solvents	258
59.	$\langle \cos \theta_{is}(r) \rangle$ at infinite dilution for the tetrahedral and C <sub>2v</sub> octupole solvents	261
60.	Potentials of mean force at infinite dilution for LiF in the C <sub>2v</sub> octupole and tetrahedral solvents	263
61.	Like-ion potentials of mean force at infinite dilution for Li <sup>+</sup> and F <sup>-</sup> in the C <sub>2v</sub> octupole and tetrahedral solvents	266

## ACKNOWLEDGEMENTS

I wish to thank my academic advisor, Dr. G.N. Patey, for his guidance and support throughout the past six years, and the Chemistry Department of the University of British Columbia and the Natural Sciences and Engineering Research Council of Canada (NSERC) for their financial support. I am also grateful to my family, particularly my parents, for all their help and encouragement. Most of all I would like to thank my wife, Sheila, for the tremendous sacrifices she has made during the preparation of this thesis.

## CHAPTER I

### INTRODUCTION

The study of electrolyte solutions, particularly aqueous electrolyte solutions, has been one of the most active areas of physical chemistry. The considerable attention received by aqueous electrolyte solutions appears to have two principal motivations. The first arises from an innate interest in water, or in this case, in water as a solvent. Of course, the importance of water as a chemical substance cannot be overstated. Not only is water the only naturally occurring inorganic liquid on earth [1], but its unusual physical properties [2-4] and the fact that all biological processes use it as a solvent [2,5] make water essential to all life on this planet. The second arises from the central role charged species play in many chemical reactions and electrochemical processes [5]. It is little wonder then that aqueous electrolyte solutions have received so much attention.

An electrolyte solution is a homogeneous liquid consisting of an ionic solid, commonly known as a salt, dissolved in a polar solvent, a liquid usually characterized by a *large* dielectric constant. For aqueous solutions the solvent is water. An electrolyte solution is often defined as one having a *high* conductance [3]. In this study we consider only strong electrolytes, *i.e.*, those which can be assumed to fully dissociate (or ionize) in solution. Aqueous electrolyte solutions have been the subjects of numerous experiments and a great deal of experimental data on their macroscopic properties has been accumulated [6-8]. Properties such as density, vapour pressure, and apparent dielectric constant have been measured and their dependence upon salt concentration determined [6-9]. Unfortunately, much of this data has proven difficult to interpret and the details of the underlying microscopic properties remain rather poorly understood [5-12]. We know that the solute exists as a free ionic species in solution, but only recently [13-16] have direct measurements of the microscopic structure in solution (*i.e.*, the ion-ion, ion-solvent, and solvent-solvent distribution functions) been possible. However, these measurements are difficult to perform. Moreover, the results obtained are somewhat ambiguous [13,16] and provide only limited information. Thus,

the details of the microscopic structure of aqueous electrolyte solutions and how they relate to macroscopic properties remain poorly understood. What is needed then is a more complete microscopic understanding of electrolyte solutions in order to more fully understand the macroscopic observations. It is to this point that this thesis is addressed.

The study of electrolyte solutions began during the 19<sup>th</sup> century in that field of chemistry which has now become known as electrochemistry. Investigators [17] were intrigued by the fact that matter was transported in electrolyte conductors but not, of course, in electronic conductors. Clausius [17] noted that ionic solutions obey Ohm's law and concluded that there must be electrically charged particles present. In 1887 van't Hoff [18] published experimental results which clearly indicate that conducting solutions possess colligative properties distinct from those of non-conducting solutions. These results were interpreted by Planck [19] as a possible indication of ionization of the solute. However, the present day theory of electrolyte dissociation in solution is usually credited to Arrhenius [20] who first published his theory in 1887. At the time this seemed like a radical idea, but with the support of a wealth of data it gained general acceptance by the turn of this century.

Many attempts were made during the first decades of this century to develop equilibrium theories, and later dynamical theories, to describe electrolyte solutions and their behaviour. The long-range nature of the ion-ion interactions made it possible to derive [21] limiting laws for many of the properties of dilute electrolyte solutions. These theoretical results were found [21] to be in very good agreement with experiment. The theories of Debye and Hückel [22] and of Onsager [23] stand out today as landmarks. The theory of Debye and Hückel for the equilibrium structure of electrolyte solutions became, and probably remains, the standard approach [3,5,6] used in discussing or describing them.

Much of the work done on the equilibrium theory of electrolyte solutions [6,21,24,25] in the 50 years after the advent of Debye-Hückel theory was concerned with justifying and improving the theory itself. However, the basic approach to electrolyte solutions used by Debye and Hückel [22], in which the solvent is treated simply as a dielectric continuum, remains essentially unchanged. It was actually McMillan and Mayer [26] who formally showed that the solvent need not be explicitly considered as a molecular



species if an effective solvent averaged ion-ion interaction potential is used. Of course, implicit in the above statement is the assumption that all effective many-ion potentials can be ignored [25], although this assumption is really only valid at very low concentration. Within McMillan-Mayer theory [26], the effective ion-ion potential can be written in the form [13]

$$u_{ij}(r) = u_{ij}^S(r) + \frac{q_i q_j}{\epsilon r}, \quad (1.1)$$

where  $r$  is the distance between the ions  $i$  and  $j$ ,  $q_i$  and  $q_j$  are their charges,  $\epsilon$  is the dielectric constant of the solvent and  $u_{ij}^S(r)$  is the short-range ion-ion interaction. Models for electrolyte solutions which are defined in terms of eq. (1.1), *i.e.*, which treat the solvent as a dielectric continuum, are known as *primitive models*. If we take  $u_{ij}^S(r) = 0$ , we obtain the Debye-Hückel primitive model. The restricted and extended primitive models [13,27] result when  $u_{ij}^S(r)$  is a simple hard-sphere potential [27]. The so-called refined primitive models [28,29] attempt to use more realistic short-range ion-ion interactions while also incorporating short-range solvent effects. Primitive model systems have been extensively examined [24,25,27-30] and researchers have been fairly successful at fitting the concentration dependence of many thermodynamic properties of aqueous electrolyte solutions [28] with these simple models. Unfortunately, primitive model studies have given very little insight into the microscopic structure of real aqueous electrolyte solutions because they ignore the molecular nature of the solvent. Therefore, the primitive model is not particularly useful if one wishes to investigate the microscopic properties of electrolyte solutions and determine how they may affect the macroscopic behaviour.

Of course, before one can really even begin to consider investigating model aqueous electrolyte solutions which explicitly include the solvent as a molecular species, one must first be able to study and characterize the pure solvent. The first computer simulation studies [31-33] of water-like models took place almost 20 years ago. Since then numerous other computer simulations [33-49] have been carried out on many different water models. Several of these models have been found to reproduce the microscopic structure and many of the thermodynamic properties of liquid water at normal temperature and pressure quite well [34,36,41,47], although almost all models give rather poor results when studied in the gas or solid phase [36]. Also,

the dielectric properties of two of the more successful models, the MCY [49] and TIP4P [41], have recently been shown to agree quite poorly with those of real water [45,46]. This result has been attributed [46] to the fact that these models neglect molecular polarizability.

Computer simulation techniques have also been used fairly extensively to examine model aqueous electrolyte solutions [34,50-59], with alkali halide solutions receiving the most attention. A variety of ion and solvent models have been employed [34,58,59] to study infinitely dilute solutions (*i.e.*, containing only one ion) and those at moderate to high concentration (*i.e.*,  $>1M$ ). These investigations have concentrated mainly on the determination of the solvent structure around the ions [34,58], for which they obtain reasonable agreement among themselves and with experiment [13,16]. Unfortunately, computer simulation studies of aqueous electrolyte solutions are somewhat limited as to the systems and the properties which can be examined. This is due mainly to the fact that they consider systems of only a small number of particles. Hence, the ion-ion and long-range ion-solvent structure and the many thermodynamic properties which depend upon them (*e.g.*,  $\gamma_{\pm}$ ,  $\bar{V}_2$ , etc.) are not currently accessible through computer simulation. Moreover, one can not study solutions at low concentration.

Integral equation methods, commonly used in liquid state theory [27,33,60], have been used very successfully to investigate primitive model electrolyte solutions [24,25,27,28,30]. They have also been shown to be very useful in the study of multipolar fluids [27,61-72]. Solutions of hard-sphere ions in a dipolar solvent [73-78] were examined extensively with integral equation techniques. More recent work [79-82] has focussed upon the calculation of ion-ion potentials of mean force at infinite dilution in water-like solvents. Unlike computer simulation, integral equation theories consider an infinite system and will, in principle, yield all equilibrium properties of the solution. Furthermore, the entire concentration range can, for the most part, be investigated with integral equation theories.

In the present study we will use integral equation methods first to examine a water-like solvent and then to study model aqueous electrolyte solutions, both at infinite dilution and at finite concentration. We stress that we can consider only equilibrium properties of these systems because of our choice of an integral equation approach. The solvent model we shall

investigate is a simple one which incorporates a set of known (measured) molecular properties of the water molecule with no freely adjustable parameters. When determining the properties of this water-like solvent, particular attention will be paid to its dielectric constant, since  $\epsilon$  represents the ability of the solvent to screen the coulombic forces between ions that are far apart (*cf.* eq. (1.1)). Model aqueous electrolyte solutions will then be studied. The structural, thermodynamic and dielectric properties of these systems and their dependence upon salt concentration will be determined. The results obtained will be compared with those of real solutions. These comparisons will be mostly qualitative in nature. Their basic purpose will be to help identify which microscopic properties are important in ionic hydration and in determining the macroscopic properties of aqueous electrolyte solutions. We also hope to demonstrate the usefulness of the current approach. It should also be noted that in the present study a great deal of theoretical formalism is introduced and derived, most of which can be applied to more general models than those examined here. Most of the work presented in this thesis is being prepared for publication [83,84], or has been submitted or accepted for publication [85,86].

In Chapter II we define the models considered in this study and describe the specific integral equation theory (the reference hypernetted-chain [68]) employed. A general formalism which relates certain thermodynamic properties of electrolyte solutions to integrals of radial distribution functions is outlined in Chapter III. The low concentration behaviour of our expressions is examined and the limiting laws obtained. These limiting laws are in terms of microscopic properties and can be compared with the macroscopic (*i.e.*, Debye-Hückel) results. In Chapter IV we discuss two levels of theory in which the polarizability of the solvent can be taken into account. We find that polarization can have long-range effects which may influence the limiting laws of some thermodynamic quantities. The results obtained for the pure solvent are given in Chapter V, while in Chapter VI we present our findings for model aqueous electrolyte solutions, both at infinite dilution and finite concentration. Finally, Chapter VII will summarize all the results presented in this thesis, pointing out areas which need further investigation and indicating possible extensions of the present study.

## CHAPTER II

### STATISTICAL MECHANICAL THEORY

#### 1. Introduction

Statistical mechanics plays an essential role in the present day study of real systems [27,33,87]. Its principal function is often viewed as being a bridge between the disciplines of thermodynamics and quantum (or classical) mechanics. Thermodynamics is primarily concerned with the measurement and interpretation of the macroscopic, or bulk, properties of materials while quantum mechanics is, at present, restricted to the study of individual (or very small numbers of) atoms or molecules within materials. Like thermodynamics and quantum mechanics, statistical mechanics embodies a very large theoretical framework built upon only a small number of axioms. This development is not given here but may be found in introductory books [87-89] on statistical mechanics.

Statistical mechanics provides several different approaches through which to study matter [87,88]. Distribution function language [27,33,87] is frequently used in such studies since it allows a complete but compact description of the microscopic structure. Knowledge of the probability distribution functions is sufficient, in general, to determine all thermodynamic properties of a liquid system. In all statistical mechanical studies of matter, we start by first defining a microscopic model for the system of interest. It is usually sufficient to define such a model by specifying the interaction potential between particles of the system. Then given this interaction potential, statistical mechanical theory provides us with a means of determining the average microscopic structure which in turn specifies the macroscopic properties of the system. This chapter will outline the theoretical approach we have used.

In this thesis we are concerned with the study of systems in the liquid state. Most liquids and solutions can be reasonably described using classical statistical mechanics [27,33]. Liquid hydrogen, liquid helium, and solvated electrons are some of the few exceptions. Two basic approaches are currently employed to study classical fluid systems; they are computer simulation and

approximate methods.

Computer simulation [27,33,87] can be regarded as essentially an exact method although it usually requires considerable computational resources. All but the simplest model systems require several hours on a powerful computer to obtain statistically meaningful results, even with present day super-computers. In order to keep such times on a reasonable scale only small systems, usually consisting of 100-1000 particles, are studied. As a result quantities which are very sensitive to boundary conditions, such as dielectric constants, or systems which have long-range forces, such as electrolyte solutions, pose major problems for computer simulation.

A great deal of effort has been spent in developing approximate theories [27,33,60,87]. Up until the advent of the modern computer some 25 years ago, they represented the only means through which model systems could be studied. Approximate theories do not suffer from the statistical or boundary condition problems present in computer simulation. Also, they usually require much less computation than do computer simulations. However, being approximate, they can only give estimates for the unique set of properties that exist for a given model system.

Integral equation theories are one set of approximate methods which have been used extensively in the study of fluids [27,33,60,61,87]. Most integral equation theories can be written as two coupled equations. One of these, the Ornstein-Zernike (OZ) equation [90], is a basic relationship in the equilibrium theory of fluids. The OZ equation is an exact relationship. A second equation is required to close the system of equations, hence the term *closure* is given to this expression. An integral equation theory is usually known by the name given the closure equation. At present only approximate closures exist. Therefore, it is the closure approximation which determines the accuracy of the integral equation theory. Also for all but the simplest cases, these theories must be solved numerically.

There are several different integral equation theories which have been extensively studied [27,33,60,87]. These include the Mean Spherical Approximation (MSA) [91], the Percus-Yevick (PY) [92] theory, and the Hypernetted-Chain (HNC) [93-97] theory. Further discussions of these theories can be found elsewhere [27,33,60,87]. Of importance here is the fact that the HNC theory is known [27,60,87] to be superior for fluid systems possessing

long-range interactions (*e.g.*, charged systems).

Until recently, it was not possible to solve the HNC theory for systems characterized by non-spherical potentials. As a result further approximations were made to the HNC closure in order to obtain several related theories, including the linearized HNC (LHNC) [62] and quadratic HNC (QHNC) [63] approximations. The LHNC and QHNC theories have been used extensively to study systems with non-spherical interaction potentials and have been shown to give good results for some multipolar fluids [61-65,67,69]. However, recent advances [68] have made the use of the full HNC and the closely related reference HNC (RHNC) [68] possible in the investigation of systems possessing anisotropic potentials. The models studied include dipolar hard spheres [68] and Stockmayer particles [70], as well as dipole linear quadrupole systems [71]. Very recently, the HNC was used to examine liquid crystal models [98] as well as hard ellipsoids and spherocylinders [99,100]. In all cases the HNC has been found to agree reasonably well with computer simulation results.

In this chapter we are concerned with the development of the classical statistical mechanical theory necessary to study model water and electrolyte solution systems using integral equation methods, primarily the RHNC theory. Since the water molecule has  $C_{2v}$  symmetry [4], we have restricted ourselves to model systems in which all species have at least  $C_{2v}$  symmetry. We shall consider the simplifications that result from this restriction. Section 2 of this chapter will deal with the interaction potentials used in this study. In section 3 we describe that generalized reduction of the OZ equation for a multi-component system employing the rotational invariant language [68,101-103] outlined in section 2. A discussion of the HNC and RHNC closures and their application is given in section 4. Section 5 of this chapter will outline some of the techniques used to obtain a numerical solution to the equations of sections 3 and 4. Finally, in section 6 we will summarize the relationships used to calculate some of the average properties of polar solvents and electrolyte solutions. In Chapter III we will examine how other thermodynamic properties of electrolyte solutions may be obtained from Kirkwood-Buff [104] theory.

## 2. Interaction Potentials

In the study of real systems and their physical properties the development of *useful* models and the potentials that characterize them is an essential step. For a model to be useful it must be simple enough to enable us to produce meaningful results with resources currently available, yet it must have a sufficient degree of sophistication so as to adequately represent the system of interest.

The interactions which determine most bulk properties of liquids, and of matter in general, are essentially electrostatic in nature [33]. They arise from the coulombic interactions between nuclei and electrons. At this level we could treat any system exactly by solving the many-body Schrödinger equation describing the motion of all nuclei and electrons. Unfortunately, such a task is several orders of magnitude beyond our present day capabilities.

In order to simplify the model, we first use the Born-Oppenheimer approximation [105] in which the heavier nuclei are held fixed while we determine the electronic distributions. The ground electronic states are then used to determine average charge distributions and polarizabilities. A second approximation is made in assuming that all molecules are rigid. We ignore all intramolecular vibrational and rotational modes. (This may not be a good approximation for large polymeric molecules.) A third simplification arises from the fact that the behaviour of the particles within most fluids at ordinary temperatures can be described classically, as was mentioned above. Hence we find it convenient to restrict ourselves to classical mechanics and classical statistical mechanics.

Subject to the above assumptions, the total interaction potential,  $u_N$ , will depend only upon the positions and orientations of all particles within the system. We write [33]

$$u_N = u(\underline{x}_1, \underline{x}_2, \dots, \underline{x}_N) , \quad (2.1)$$

where  $\underline{x}_i$  represents the positional and angular coordinates of particle  $i$ , and  $N$  is the total number of particles in the system. In general, this  $N$ -body interaction potential is very complicated, particularly for liquid systems, and the  $N$ -body problem is very difficult to solve. To allow further simplification,

we express [33] the total interaction potential as an expansion

$$u(\underline{x}_1, \dots, \underline{x}_N) = \sum_{i < j} u^{(2)}(\underline{x}_i, \underline{x}_j) + \sum_{i < j < k} u^{(3)}(\underline{x}_i, \underline{x}_j, \underline{x}_k) + \dots, \quad (2.2)$$

in which the first term is the sum of all unique pair interactions, the second term is the sum of all unique 3-body interactions, and so on. It is generally agreed that for most liquids the pair interaction potential is the dominant term [27,33]. In most statistical mechanical studies higher order terms are usually neglected or the pair potential is modified in an attempt to take into account higher order terms [27,33]. In Chapter IV we will describe how the many-body problem of polarizability can be reduced to an *effective* pair potential.

It is convenient to write the pair interaction potential term of eq. (2.2) as [106]

$$u^{(2)}(\underline{x}_1, \underline{x}_2) \equiv u(12) = u^*(12) + u^e(12), \quad (2.3)$$

where  $u^*(12)$  is the interaction due to the overlap and instantaneous anisotropies of the charge distributions of the particles, and  $u^e(12)$  is the interaction due to permanent anisotropies or net charges associated with the charge distributions of the particles. Thus  $u^*(12)$  contains the short-range repulsive terms and the long-range dispersion terms of the interaction. It can be approximated by potentials such as the hard-sphere or Lennard-Jones [106] interactions.  $u^e(12)$  is the electrostatic interaction between two non-overlapping charge distributions. It is usually described in one of two ways: either using point charge models or using multipole expansions.

A point charge model uses a small set of discrete charges in place of the continuous charge distribution of the molecule of interest. Hence  $u^e(12)$  is given by

$$u^e(12) = \sum_{i < j} \left[ \frac{q_i^{(1)} q_j^{(2)}}{r_{ij}} \right], \quad (2.4)$$

where  $q_i$  is the  $i^{\text{th}}$  charge on particle 1,  $q_j$  is the  $j^{\text{th}}$  charge on particle 2, and  $r_{ij}$  is the separation between points  $i$  and  $j$ . In general, the larger the



number of discrete charges, the more closely the real charge distribution can be mimicked. It has been found [39] that for simple molecules relatively few point charges are necessary to give a reasonable description of their electrostatic interaction.

$u^e(12)$  may also be described in terms of multipole expansions. The electric potential produced at a point  $t$  by an arbitrary charge distribution can always be expressed as a Taylor series in spherical harmonics known as a multipole expansion [106,107]. In a similar fashion, the electrostatic interaction between two non-overlapping charge distributions is given by [72,102,106]

$$u^e(12) = \sum_{\substack{mn1 \\ \mu\nu}} \left[ (-1)^m \delta_{m+n,1} \left[ \frac{(2l+1)!}{2m! 2n!} \right]^{\frac{1}{2}} \right. \\ \left. \times \frac{\bar{Q}_m^\mu \bar{Q}_n^\nu}{f^{mn1} r^{l+1}} \Phi_{\mu\nu}^{mn1}(\Omega_1, \Omega_2, \hat{r}) \right] , \quad (2.5)$$

where  $\delta$  is a Kronecker delta function,  $r$  is the separation between the centres (*i.e.*, the points of expansion) of particles 1 and 2, and the rotational invariants,  $\Phi_{\mu\nu}^{mn1}(\Omega_1, \Omega_2, \hat{r})$ , are defined below. The multipole moments,  $\bar{Q}_m^\mu$ , are defined for a discrete charge distribution by [72,102,106]

$$\bar{Q}_m^\mu = \sum_a \left[ e_a (r_a)^m R_{\mu 0}^{m*}(\theta_a, \phi_a) \right] , \quad (2.6a)$$

where the coordinates  $(r_a, \theta_a, \phi_a)$  of the charge  $e_a$  are given in the molecular (rotating) frame of reference. The generalized spherical harmonic [72,108]

$$R_{\mu 0}^{m*}(\theta, \phi) = \left[ \frac{4\pi}{2m+1} \right]^{\frac{1}{2}} Y_m^\mu(\theta, \phi) \\ = i^{|\mu|-\mu} \left[ \frac{(m-|\mu|)!}{(m+|\mu|)!} \right]^{\frac{1}{2}} P_m^\mu(\cos\theta) e^{i\mu\phi} , \quad (2.6b)$$

where  $Y_m^\mu(\theta, \phi)$  is a spherical harmonic [106] and  $P_m^\mu(\cos\theta)$  is an associated Legendre polynomial [106]. We note that for a continuous charge distribution the multipole moments will be given by an expression analogous to eq. (2.6a), except now the sum over discrete charges will be replaced by integrals over

the charge distribution [106].

For an isotropic system we would expect  $u(12)$  to be translationally and rotationally invariant. That is to say, the interaction observed between particles 1 and 2 will be invariant to the position and orientation of the frame of reference attached to the vector joining the two particles, with respect to the lab fixed frame. Translational invariance is retained by eq. (2.5) by noting that  $r$  is just the interparticle separation. The functions  $\Phi_{\mu\nu}^{mnl}(\Omega_1, \Omega_2, \hat{r})$ , which fulfill the requirement of rotational invariance in eq. (2.5), are known as rotational invariants. They are defined by [68,101]

$$\Phi_{\mu\nu}^{mnl}(\Omega_1, \Omega_2, \hat{r}) = f^{mnl} \sum_{\alpha\beta\gamma} \begin{pmatrix} m & n & l \\ \alpha & \beta & \gamma \end{pmatrix} R_{\alpha\mu}^m(\Omega_1) R_{\beta\nu}^n(\Omega_2) R_{\gamma 0}^l(\hat{r}) , \quad (2.7)$$

where  $m, n, l$  are positive integers,  $R_{\alpha\mu}^m(\Omega)$  is again a generalized Wigner spherical harmonic [108],  $\Omega = (\theta, \phi, \psi)$  is the set of Euler angles [87,108] for each particle,  $\hat{r}$  is the orientation of the vector from particle 1 to particle 2 and  $\begin{pmatrix} \cdot & \cdot & \cdot \\ \cdot & \cdot & \cdot \end{pmatrix}$  is the usual 3-j symbol [109]. The orientations  $\Omega_1, \Omega_2, \hat{r}$  are the sets of angles of rotation from the lab fixed frame to the molecular fixed frame [87]. The sum in eq. (2.7) is only over those values of  $\alpha, \beta, \gamma$  for which the 3-j symbol evaluates to a non-zero value. The triangle condition [109] in the 3-j symbol requires that

$$|m-n| \leq l \leq m+n . \quad (2.8a)$$

From the definition of the generalized Wigner spherical harmonics we have

$$|\mu| \leq m \quad \text{and} \quad |\nu| \leq n . \quad (2.8b)$$

In eq. (2.7)  $f^{mnl}$  can be any non-zero constant. In this thesis we will make use of two different definitions:

$$f^{mnl} = \frac{l!}{\begin{pmatrix} m & n & l \\ 0 & 0 & 0 \end{pmatrix}} , \quad (2.9a)$$

$$f^{mnl} = \left[ (2m+1)(2n+1) \right]^{\frac{1}{2}} . \quad (2.9b)$$

We will alternate between eqs. (2.9a) and (2.9b) when it is convenient to do so.

The rotational invariant functions generated by eq. (2.7) form a basis set of orthogonal polynomials [101] which will span the complete space of orientations of particles 1 and 2. Equation (2.5) is an expansion in this rotational invariant basis set. The expansion is such that the coefficients will only depend upon the interparticle separation  $r$  and all angular dependence is in the functions  $\Phi_{\mu\nu}^{mnl}(\Omega_1, \Omega_2, \hat{r})$ . Using  $f^{mnl}$  as given by eq. (2.9b), we rewrite eq. (2.5) as

$$u^e(12) = \sum_{mnl} u_{\mu\nu}^{mnl}(r) \Phi_{\mu\nu}^{mnl}(\Omega_1, \Omega_2, \hat{r}) , \quad (2.10a)$$

where

$$u_{\mu\nu}^{mnl}(r) = (-1)^m \delta_{m+n, l} \left[ \frac{(2l+1)!}{(2m+1)!(2n+1)!} \right]^{\frac{1}{2}} \frac{\bar{Q}_m^\mu \bar{Q}_n^\nu}{r^{l+1}} . \quad (2.10b)$$

We can expand eq. (2.3) in a similar manner. Later we will find it very convenient to expand other functions in this same basis set.

A rotational invariant expansion must also satisfy two other symmetry conditions of isotropic fluids. Since the labels 1 and 2 are totally arbitrary for an isotropic fluid, exchange of these labels should leave  $u^e(12)$  unchanged. It has been shown [101,110,111] that this condition requires that the invariant expansion coefficients satisfy

$$u_{\mu\nu}^{mnl}(r) = (-1)^{m+n} u_{\nu\mu}^{nml}(r) . \quad (2.11)$$

We also have the requirement that  $u^e(12)$  must remain unchanged under symmetry operations on the individual particles. Conditions for several symmetry groups are given in Blum and Torruella [101]. In this study we will make use of the following requirements:

i) for spherical symmetry in both particles

$$m, n, l, \mu, \nu = 0 , \quad (2.12a)$$

ii) for linear symmetry in both particles

$$\mu, \nu = 0 , \quad (2.12b)$$

iii) for  $C_{2v}$  symmetry in both particles

$$\mu, \nu = \text{even} \quad (2.12c)$$

and

$$u_{\mu\nu}^{mnl}(r) = u_{\pm\mu\pm\nu}^{mnl}(r) . \quad (2.12d)$$

Blum and Torruella [101] also showed that since  $u^e(12)$  must be real then

$$\left[ u_{\mu\nu}^{mnl}(r) \right]^* = (-1)^{m+n+l+\mu+\nu} u_{-\mu-\nu}^{mnl}(r) . \quad (2.13)$$

Together eqs. (2.12c), (2.12d) and (2.13) imply that at least for particles of  $C_{2v}$  symmetry

$$m+n+l = \text{even} \quad (2.14)$$

and  $u_{\mu\nu}^{mnl}(r)$  must be real. The conditions given by eqs. (2.12) and (2.14) serve simply to remove some of the basis functions from the rotational invariant expansion.

Let us now return to eq. (2.5). The sum in eq. (2.5) is infinite where  $m, n, l, \mu, \nu$  are subject to the restrictions given by eqs. (2.8), (2.12) and (2.14). We know that the multipole expansion for non-overlapping charge distributions must be convergent [106], in which case  $u^e(12)$  must be given equivalently by eqs. (2.4) and (2.5). Also, as we go to higher moments in the expansion and  $l$  becomes larger, the terms in eq. (2.5) become shorter ranged as their  $(1/r)$  dependence increases. Therefore, we would expect the multipole expansion to converge quickly at large separations while converging more slowly at short-range. This property of multipole expansions will be used in discussing the models used in this study.

The multipole expansion is frequently given in Cartesian tensor form [107,112], whereas eq. (2.5) is really a spherical tensor form [113] of the same expansion. In Cartesian notation the first four moments ( $n = 0,1,2,3$ ) of a discrete charge distribution are [107,112,114]

$$q = \sum_a e_a , \quad (2.15a)$$

$$\mu_i = \sum_a e_a r_{ia} , \quad (2.15b)$$

$$\Theta_{ij} = \frac{1}{2} \sum_a e_a (3r_{ia}r_{ja} - r_a^2 \delta_{ij}) \quad (2.15c)$$

and

$$\Omega_{ijk} = \frac{1}{2} \sum_a e_a \left[ 5r_{ia}r_{ja}r_{ka} - r_a^2 (r_{ia}\delta_{jk} + r_{ja}\delta_{ik} + r_{ka}\delta_{ij}) \right] , \quad (2.15d)$$

where  $q$  is the net charge,  $\mu_i$  are the components of the dipole vector, and  $\Theta_{ij}$  and  $\Omega_{ijk}$  are the components of the quadrupole and octupole tensors, respectively. In eqs. (2.15) the sum is over the discrete charges  $e_a$  and  $r_i, r_j, r_k$  are the  $i, j, k$  components, respectively, of the vector  $\underline{r}$  given in the molecular axis frame. We again point out that for a continuous charge distribution the sums over charges in eqs. (2.15) become integrals over the charge distribution. A common convention, and one we will use, is to choose this reference frame such that the origin (*i.e.*, the point about which the expansion is made) is at the molecular centre of mass and the axis of highest symmetry is labelled the  $z$ -axis.

An electric multipole moment has, in general,  $(2n+1)$  independent components. However, this number can be greatly reduced by molecular symmetry [107,114]; of most importance here is the reduction under  $C_{2v}$  symmetry. From Kielich [107] we have that for  $C_{2v}$  symmetry, the dipole, quadrupole and octupole moments have 1, 2 and 2 mutually independent components, respectively. Thus, the dipole moment is given by the scalar  $\mu_z$  and the quadrupole tensor has the form

$$\underline{\Theta} = \begin{bmatrix} \Theta_{xx} & 0 & 0 \\ 0 & \Theta_{yy} & 0 \\ 0 & 0 & \Theta_{zz} \end{bmatrix} , \quad (2.16a)$$

where we require [107] that

$$\Theta_{xx} + \Theta_{yy} + \Theta_{zz} = 0 . \quad (2.16b)$$

To specify the octupole tensor it is sufficient to give  $\Omega_{xxz}, \Omega_{yyz}$  and  $\Omega_{zzz}$

where  $\Omega_{xxz} + \Omega_{yyz} + \Omega_{zzz} = 0$ .

The Cartesian representation is the form most often used in the literature to specify the multipole moments of specific molecules. In this study it is convenient to work with multipole moments as defined by eq. (2.6a). To find expressions relating the two representations we use eqs. (2.6) and (2.15) along with explicit forms for the associated Legendre polynomials [106] and the relationships  $z_a = r_a \cos \theta$  and  $x_a + iy_a = r_a \sin \theta e^{i\phi}$ . It is then easy to show that in general

$$\bar{Q}_0^0 = q , \quad (2.17a)$$

$$\bar{Q}_1^0 = \mu_z , \quad (2.17b)$$

$$\bar{Q}_2^0 = \Theta_{zz} , \quad (2.17c)$$

$$\bar{Q}_1^{\pm 1} = \frac{\pm 1}{\sqrt{2}} (\mu_x \pm i\mu_y) , \quad (2.18a)$$

$$\bar{Q}_2^{\pm 1} = \frac{\pm 2}{\sqrt{6}} (\Theta_{xz} \pm i\Theta_{yz}) \quad (2.18b)$$

and

$$\bar{Q}_2^{\pm 2} = \frac{1}{\sqrt{6}} (\Theta_{xx} - \Theta_{yy} \pm 2i\Theta_{xy}) . \quad (2.18c)$$

If we restrict ourselves to  $C_{2v}$  symmetry where  $\mu_x = \mu_y = \Theta_{xy} = \Theta_{xz} = \Theta_{yz} = 0$  [107], we have immediately from eqs. (2.18) that

$$\bar{Q}_1^1 = \bar{Q}_1^{-1} = 0 , \quad (2.19a)$$

$$\bar{Q}_2^1 = \bar{Q}_2^{-1} = 0 \quad (2.19b)$$

and

$$\bar{Q}_2^2 = \bar{Q}_2^{-2} = \frac{1}{\sqrt{6}} (\Theta_{xx} - \Theta_{yy}) . \quad (2.19c)$$

In a similar fashion we can show that for  $C_{2v}$  symmetry the components of the octupole moment are given by

$$\bar{Q}_3^0 = \Omega_{zzz} , \quad (2.20a)$$

$$\bar{Q}_3^1 = \bar{Q}_3^{-1} = 0 , \quad (2.20b)$$

$$\bar{Q}_3^2 = \bar{Q}_3^{-2} = \frac{3}{\sqrt{30}} (\Omega_{xxz} - \Omega_{yyz}) \quad (2.20c)$$

and

$$\bar{Q}_3^3 = \bar{Q}_3^{-3} = 0 . \quad (2.20d)$$

We note that eqs. (2.17) and (2.19) are consistent with the results of Carnie *et al.* [72]. Price *et al.* [113] give similar relationships between the Cartesian and spherical multipole moments. It is also obvious from eqs. (2.17), (2.19) and (2.20) that for  $C_{2v}$  symmetry we have the required 1, 2 and 2 independent non-zero components of the dipole, quadrupole and octupole moments, respectively.

It is clearly the case that particles of spherical symmetry will possess only an  $n=0$  moment (net charge) as given by eq. (2.15a). Thus the charge distributions of spherical ions, such as the alkali halides, are completely represented by a single point charge at their centre. It follows from eq. (2.5) that the electrostatic interaction between two such ions,  $i$  and  $j$ , is itself spherically symmetric, so we write

$$u_{ij}^e(12) = u_{ij}^e(r) = \frac{q_i q_j}{r} , \quad (2.21)$$

where  $\Phi_{00}^{000}(\Omega_1, \Omega_2, \hat{r}) = 1$  is understood and  $q_i, q_j$  are the charges of the ions. For non-spherical particles eq. (2.5) remains, in principle, an infinite sum subject to symmetry conditions, such as those represented by eqs. (2.12).

The gas phase dipole and quadrupole moments of water have been measured [115]. In this study we will take the permanent dipole moment,  $\mu$ , as being 1.855D [118] ( $D=10^{-18}$  esu.cm.). The non-zero components of the quadrupole moment [119] are  $\Theta_{xx} = 2.63B$ ,  $\Theta_{yy} = -2.50B$  and  $\Theta_{zz} = -0.13B$ , where  $B=10^{-26}$  esu.cm.<sup>2</sup> and the molecular axis system is defined as it appears in Figure 1. This definition for the molecular axis frame for water will be used universally throughout this thesis. For the higher moments of water we must rely on quantum chemistry to give us reasonable estimates. There have been many large scale CI and SCF calculations done for the water molecule, but only a few of these [115-117] report multipole moments higher than quadrupole order. In this study we will use the octupole moment of Neumann and Moskowitz [116] who reported the values  $\Omega_{xxz} = 2.30F$ ,  $\Omega_{yyz} = -0.96F$  and  $\Omega_{zzz} = -1.34F$ , where  $F=10^{-34}$  esu.cm.<sup>3</sup>. Their calculated values of the dipole and quadrupole moments are in reasonable agreement (within 8%) of the

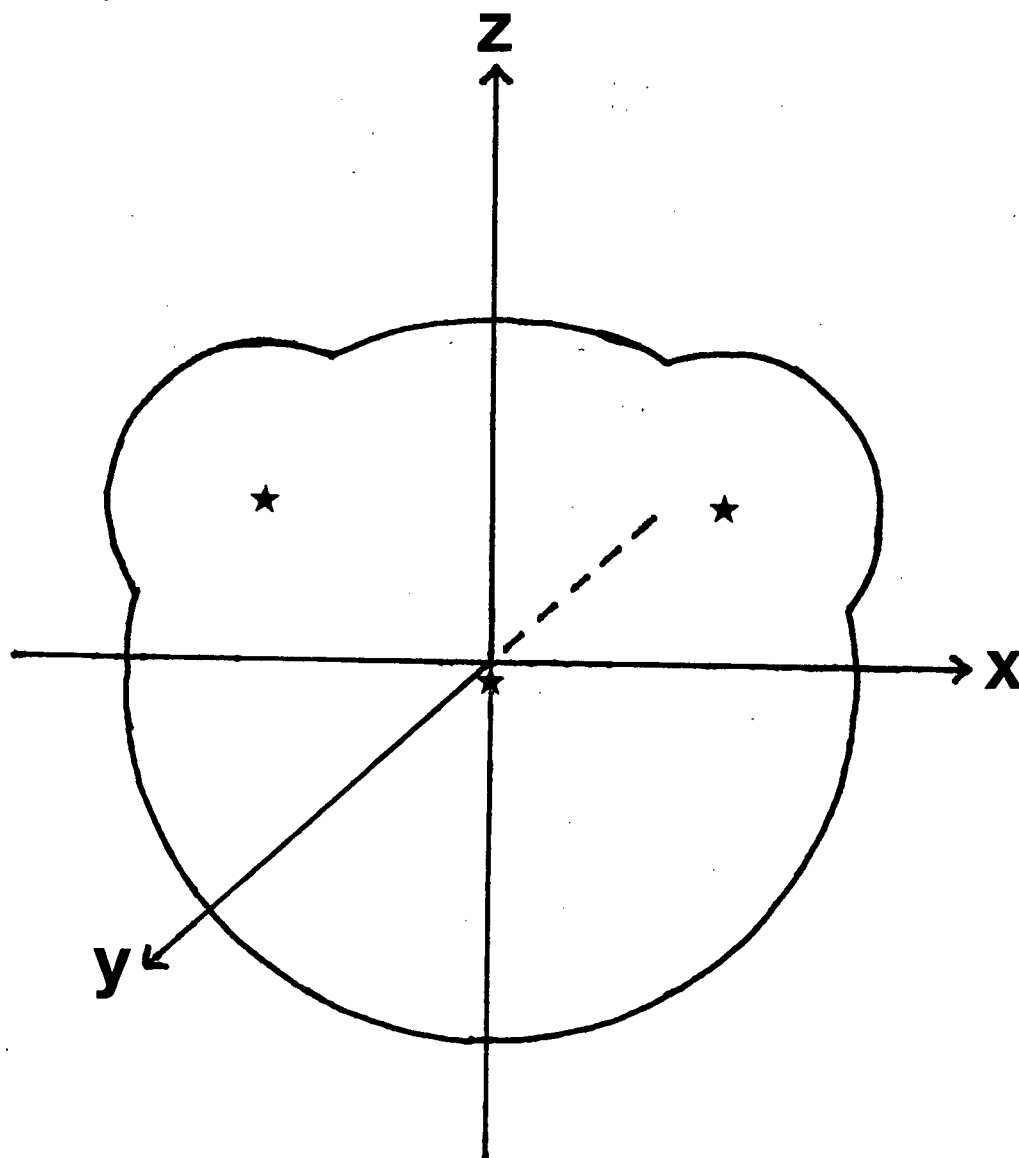


Figure 1. Molecular axis system for the water molecule. The stars indicate the atomic centres.



measured values. More recent calculations [115,117] for water using larger basis sets show little improvement in their results for the dipole and quadrupole moments. Moreover, their reported octupole moments are in good agreement with Neumann and Moskowitz [116]. The hexadecapole moment of water has also been calculated [115,117] and a very recent publication [117] reports multipole moments up to and including the  $n=6$  moment.

In this study we have chosen to ignore the hexadecapole and all higher moments. Hence we have truncated the sum in eq. (2.5) to octupole order (*i.e.*, required  $m,n \leq 3$ ). We might expect properties such as the dielectric constant and processes such as ion solvation to be dominated by long-range electrostatic interactions and thus not be particularly sensitive to this truncation of the multipole expansion. Several early studies [62,66,73-78] of polar solvents and electrolyte solutions considered electrostatic interactions only up to dipole order. This model was found to be quite unsatisfactory for water, giving very poor results for its dielectric properties and generally a poor description of ion hydration. More recent studies [67,79-81] have indicated that the addition of the quadrupole moment to the solvent model greatly improves the results. The dielectric properties seem to be approaching those of real water [67]. For model aqueous electrolyte solutions at infinite dilution the ion hydration appears more reasonable, much more like what is believed to be the case in real solutions [79-81,120]. Therefore, for most of the electrolyte solutions studied here, all those examined at finite concentration, the electrostatic interaction will contain terms only up to quadrupole order. The influence of the octupole terms will be examined for the pure water-like solvent as well as for electrolyte solutions at infinite dilution.

Carnie and co-worker [67,72] have pointed out that to a good approximation the quadrupole tensor of water can be expressed as

$$\underline{\Theta}_S = \begin{bmatrix} \Theta_S & 0 & 0 \\ 0 & -\Theta_S & 0 \\ 0 & 0 & 0 \end{bmatrix} \quad (2.22)$$

by setting  $\Theta_{zz}$  to zero in eq. (2.16). Such a quadrupole tensor is totally specified by the single parameter  $\Theta_S$ , which we shall refer to as a square quadrupole moment (it is also known as a tetrahedral quadrupole moment

[67,72]). In Figure 2(a) we have illustrated the simplest charge distribution that has a *square* quadrupole as its lowest order moment. It is a charge distribution where two positive and two negative charges of equal magnitude have been placed at opposite corners of a square. In Figure 2(b) we have illustrated what we will refer to as a *tetrahedral* charge distribution, in which the four charges are now located at the vertices of a regular tetrahedron. This point charge model, which possesses a dipole and square quadrupole as its two lowest order moments, has been used to represent the real charge distribution of water (*i.e.*, the BNS model [44]). Carnie *et al.* [67] have shown that  $u^e(12)$  is subject to an additional symmetry condition if both particles 1 and 2 have only dipole and square quadrupole moments. In this case, in addition to eqs. (2.12c) and (2.12d), we require that [72]

$$(\mu + \nu + 21) \text{ MOD } 4 = 0 . \quad (2.23)$$

Thus, if we consider moments only up to quadrupole order, restricting ourselves to a square quadrupole moment will result in a smaller number of basis functions. We point out that the tetrahedral charge distribution does not represent a special symmetry group, since if we include the octupole moment we return to general  $C_{2v}$  symmetry. The tetrahedral point charge model does have an interesting property in that it will interact with positive or negative charges equivalently. Therefore a solvent with a tetrahedral charge distribution will solvate simple spherical ions of equal size symmetrically. This property will prove useful in the present study.

Now let us return to eq. (2.3) to consider the remaining term,  $u^*(12)$ , in the expression for the total pair interaction potential. In this study we take  $u^*(12)$  to be spherically symmetric, *i.e.*,  $u^*(12) = u^*(r)$ . This is frequently done for water-like models [35-39,44,67] since the water molecule is roughly spherical (see Figure 1) and results in a much simpler pair potential. We choose to represent  $u^*(r)$  with the simplest possible pair interaction, the hard-sphere potential. The hard-sphere potential,  $u_{a\beta}^{HS}(r)$ , between two particles  $a$  and  $\beta$  is given by [27,33]

$$u_{a\beta}^{HS}(r) = \begin{cases} \infty; & r < d_{a\beta} \\ 0; & r > d_{a\beta} \end{cases} , \quad (2.24a)$$

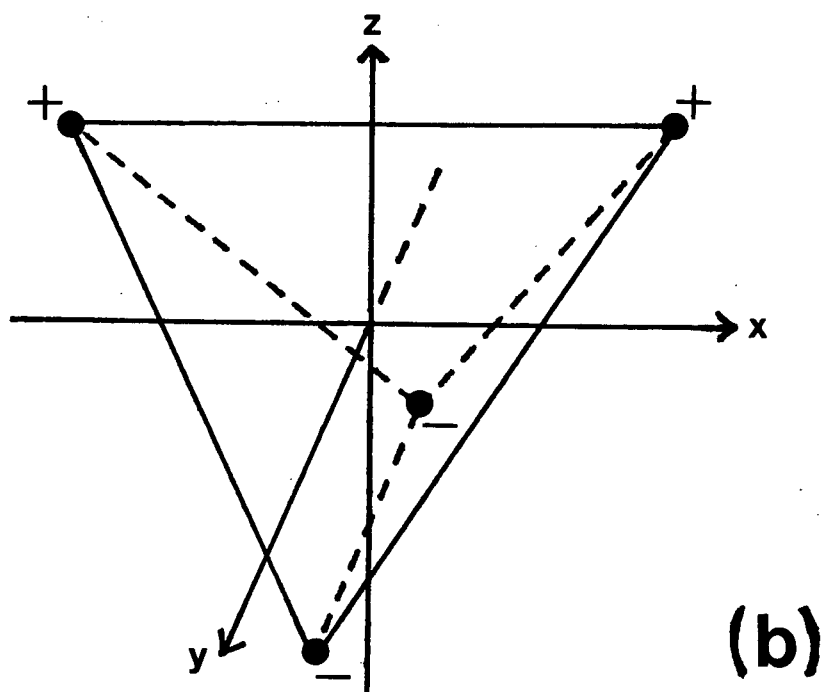
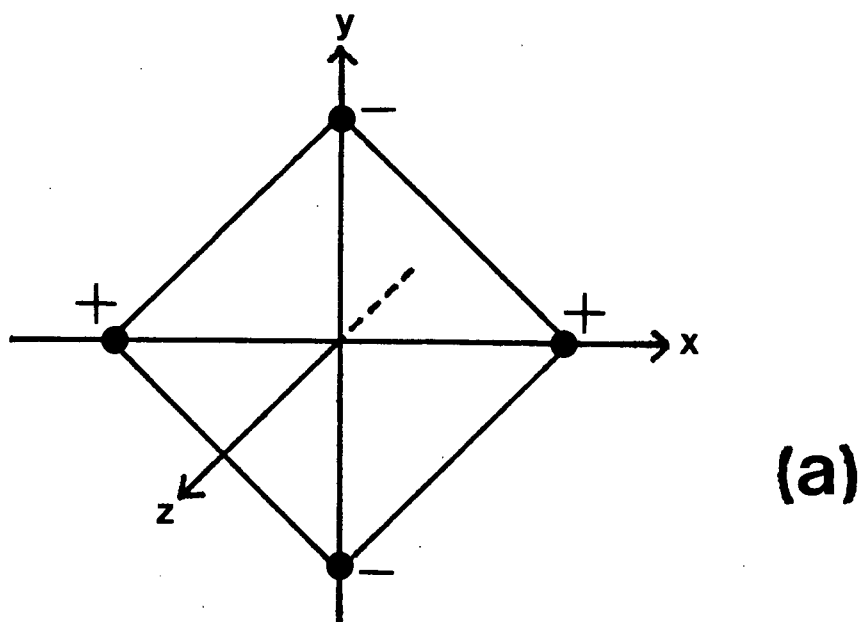


Figure 2. A charge distribution possessing (a) a square quadrupole and (b) a dipole and a square quadrupole.

where

$$d_{a\beta} = \frac{d_a + d_\beta}{2}, \quad (2.24b)$$

with  $d_a$  being the diameter of particle  $a$ . It is clear from eq. (2.24a) that the hard-sphere interaction is a purely repulsive potential. In approximating  $u^*(r)$  with  $u_{a\beta}^{HS}(r)$  we are making two further assumptions: first that the short-range repulsions between the particles can be reasonably represented by the hard-sphere potential, and second that the long-range dispersion forces are small compared to the electrostatic forces in the systems of interest. The validity of these assumptions and their influence upon properties of interest shall be discussed later.

The hard-sphere potential requires that we specify hard-sphere diameters for our particles. Although the exact values are somewhat arbitrary, for water a value of  $d_s \approx 2.8\text{\AA}$  is a reasonable choice. It is consistent with O-O structure as measured by diffraction experiments [121,122] and has been used in previous studies [67,79-81].

For ions in solution, the choice is not quite so obvious. We would expect the radius of an ion in solution to be close to its crystal radius. For the alkali halides however, there are several estimates of the crystal radii [123,124]. Recent X-ray electron density measurements of ionic crystals seem to be the most physically realistic method of defining ionic radii. To be consistent with previous work [80,81], we have chosen to use the radii of Morris [124] as determined in this manner. Table I summarizes the values of the ion diameters used in this study. They are expressed as reduced ion diameters (*i.e.*, in terms of solvent diameters),  $d_i^* = d_i/d_s$ , where  $d_s = 2.8\text{\AA}$ . The values have also been rounded to the nearest 0.04 to accommodate the grid width used in the numerical calculations (*i.e.*,  $0.02d_s$ ), as discussed below. Included in Table I are reduced diameters for the alkali halides, as well as those of four other ions which appear at the bottom of the table. Two of the ions,  $\text{Eq}^+$  and  $\text{Eq}^-$  which have no real counterparts, are the same size as the solvent and will be used simply to test solvation effects. The two other ions,  $\text{M}'^+$  and  $\text{M}^+$ , are almost twice the size of the solvent. They are similar in size to tetraalkylammonium ions and will be useful in investigating large ion effects.

TABLE I. Reduced ion diameters,  $d_i^*$ , used in this study.

ION	$d_i^*$
Li <sup>+</sup>	0.68
Na <sup>+</sup> ,F <sup>-</sup>	0.84
K <sup>+</sup>	1.08
Rb <sup>+</sup> ,Cl <sup>-</sup>	1.16
Cs <sup>+</sup> ,Br <sup>-</sup>	1.28
I <sup>-</sup>	1.44
M <sup>+</sup>	1.80
M <sup>+</sup>	1.96
Eq <sup>+</sup> ,Eq <sup>-</sup>	1.00

Finally we should point out that we have not ignored terms in the interaction potential due to the polarizability of the particles in our systems. These terms will be treated on a mean field level (*i.e.*, by ignoring fluctuations) and will be included as effective interactions in our pair potentials. Details of how this can be done at two different levels are given in Chapter IV.

### 3. The Ornstein-Zernike Equation

In liquid state theory the pair distribution function,  $g(\Omega_1, \Omega_2, \underline{r}) = g(12)$ , is of fundamental importance [27,33]. It is a measure of the probability density of finding particle 1 with orientation  $\Omega_1$  and particle 2 with orientation  $\Omega_2$  at the separation  $\underline{r}$ . For a system defined using only pair potentials, knowledge of  $g(12)$  is sufficient to completely describe the equilibrium thermodynamics of such a system. The radial distribution function,  $g(r)$ , is the angle-averaged pair distribution function and is obtained by integrating  $g(12)$  over all orientations of particles 1 and 2. More detailed discussions of distribution functions can be found elsewhere [27,81,87]. One important property of  $g(12)$ , and of distribution functions in general, is that they are normalized such that

$$g(12) \rightarrow 1 \quad \text{as} \quad r \rightarrow \infty. \quad (2.25)$$

In the development of integral equation theories [27,33,60] it is convenient to

introduce the pair correlation function

$$h(12) = g(12) - 1 , \quad (2.26)$$

which measures the departure of the pair distribution function from its limiting value.

In 1914, Ornstein and Zernike [90] defined a relationship in which  $h(12)$  is expressed as a sum of a direct part involving only particles 1 and 2, and an indirect part which takes into account all correlations involving other particles. This expression is known as the OZ equation. When generalized to a mixture [125], it can be written in the form

$$h_{\alpha\beta}(12) = c_{\alpha\beta}(12) + \frac{1}{8\pi^2} \sum_{\gamma} \left[ \rho_{\gamma} \int h_{\alpha\gamma}(13) c_{\gamma\beta}(32) d\mathbf{x}_3 \right] , \quad (2.27)$$

where  $\rho_{\gamma} = N_{\gamma}/V$  is the number density of species  $\gamma$  and the integration is over all positions and orientations of particle 3 of species  $\gamma$ . The sum in eq. (2.27) is over all species in the system. The original authors [90] called  $c(12)$  the direct correlation function. The second term of eq. (2.27) is a convolution and is often called the indirect part of  $h(12)$ .

As stated earlier, the OZ equation is a basic relationship in liquid state theory and is common to many integral equation theories [27,33,60]. The OZ equation is now regarded as a definition of the direct correlation function, since  $c(12)$  has no simple physical interpretation. More detailed discussions of the OZ equation and how it can be derived through diagrammatic expansions or functional differentiation appear in several text books dealing with liquid state theory [27,87].

In order to make the convolution in the OZ equation tractable, one has only to Fourier transform eq. (2.27) with respect to the interparticle position vector  $\underline{r}$ . We then have [101,110]

$$\tilde{h}_{\alpha\beta}(12) - \tilde{c}_{\alpha\beta}(12) = \frac{1}{8\pi^2} \sum_{\gamma} \left[ \rho_{\gamma} \int \tilde{h}_{\alpha\gamma}(13) \tilde{c}_{\gamma\beta}(32) d\Omega_3 \right] , \quad (2.28)$$

where the integration is now over all orientations of particle 3 and the  $\sim$  denotes the usual Fourier transform [126,127]. If all particles in the system

have spherical symmetry, then the integration over  $\Omega_3$  is trivial and eq. (2.28) reduces to a simple algebraic form which is easy to solve numerically [81]. However, this is not the case for systems which may include anisotropic terms in their pair potentials. Blum and Torruella [101] recognized that eq. (2.28) could be reduced for systems with non-spherical pair potentials by expanding  $h(12)$  and  $c(12)$  in terms of the rotational invariants defined in the previous section. The reduction given below closely follows that of Blum [101-103] but the expressions have been generalized to multi-component systems. The notation and definitions used are those of the more recent literature [68]. Also, the description given here will only summarize the important results. Discussions of the underlying mathematical details can be found elsewhere [110,111].

Analogous to eq. (2.10a), we write the expansions

$$b_{a\beta}^{(12)} = \sum_{\substack{mnl \\ \mu\nu}} b_{\mu\nu;a\beta}^{mnl}(r) \Phi_{\mu\nu}^{mnl}(\Omega_1, \Omega_2, \hat{r}) \quad (2.29a)$$

and

$$\tilde{b}_{a\beta}^{(12)} = \sum_{\substack{mnl \\ \mu\nu}} \tilde{b}_{\mu\nu;a\beta}^{mnl}(k) \Phi_{\mu\nu}^{mnl}(\Omega_1, \Omega_2, \hat{k}) , \quad (2.29b)$$

where  $b_{a\beta}^{(12)}$  can be  $c_{a\beta}^{(12)}$  or  $h_{a\beta}^{(12)}$ ,  $\tilde{b}_{a\beta}^{(12)}$  can be  $\tilde{c}_{a\beta}^{(12)}$  or  $\tilde{h}_{a\beta}^{(12)}$ , and  $\Phi_{\mu\nu}^{mnl}(\Omega_1, \Omega_2, \hat{r})$  and  $\Phi_{\mu\nu}^{mnl}(\Omega_1, \Omega_2, \hat{k})$  are defined by eq. (2.7). The coefficients  $b_{\mu\nu;a\beta}^{mnl}(r)$  are given by

$$b_{\mu\nu;a\beta}^{mnl}(r) = \frac{\int b_{a\beta}^{(12)} \left[ \Phi_{\mu\nu}^{mnl}(\Omega_1, \Omega_2, \hat{r}) \right]^* d\Omega_1 d\Omega_2}{\int \Phi_{\mu\nu}^{mnl}(\Omega_1, \Omega_2, \hat{r}) \left[ \Phi_{\mu\nu}^{mnl}(\Omega_1, \Omega_2, \hat{r}) \right]^* d\Omega_1 d\Omega_2} , \quad (2.30)$$

and the k-space projections,  $\tilde{b}_{\mu\nu;a\beta}^{mnl}(k)$ , are the Hankel transforms

$$\tilde{b}_{\mu\nu;a\beta}^{mnl}(k) = 4\pi i^{-1} \int_0^\infty r^2 j_1(kr) b_{\mu\nu;a\beta}^{mnl}(r) dr , \quad (2.31)$$

where  $j_1(kr)$  is a spherical Bessel function of order 1 [128]. In general, high order (i.e.,  $l \geq 2$ ) Hankel transforms are very difficult to treat numerically since

they can not make use of fast Fourier transform techniques [126]. Thus a two-step method of performing these transforms has been introduced [102]. First we define the integral (*hat*) transforms

$$\hat{c}_{\mu\nu;a\beta}^{mn1}(r) = c_{\mu\nu;a\beta}^{mn1}(r) - \int_r^\infty \left[ \frac{c_{\mu\nu;a\beta}^{mn1}(s)}{s} P_1^e(r/s) \right] ds \quad \text{for } l \text{ even,} \quad (2.32a)$$

and

$$\hat{c}_{\mu\nu;a\beta}^{mn1}(r) = c_{\mu\nu;a\beta}^{mn1}(r) - r \int_r^\infty \left[ \frac{c_{\mu\nu;a\beta}^{mn1}(s)}{s^2} P_1^o(r/s) \right] ds \quad \text{for } l \text{ odd,} \quad (2.32b)$$

in which the polynomials  $P_1^e(x)$  and  $P_1^o(x)$  are given by

$$P_{2t+1}^e(x) = 2 \sum_{i=0}^t \left[ \frac{(-1)^{t-i} x^{2i}}{i! (t-i)!} \frac{(t+i+3/2)!}{(i+1/2)!} \right], \quad (2.33a)$$

$$P_{2t+3}^o(x) = 2 \sum_{i=0}^t \left[ \frac{(-1)^{t-i} x^{2i}}{i! (t-i)!} \frac{(t+i+5/2)!}{(i+3/2)!} \right], \quad (2.33b)$$

for  $t \geq 0$  and

$$P_1^o(x) = P_0^e(x) = 0, \quad (2.33c)$$

where we use the general definition of  $z!$  [128]. The  $k$ -space projections,  $\hat{c}_{\mu\nu;a\beta}^{mn1}(k)$ , can then be written [102] as zeroth order (Fourier) and first order Hankel transforms of  $\hat{c}_{\mu\nu;a\beta}^{mn1}(r)$ . Explicitly we have

$$\hat{c}_{\mu\nu;a\beta}^{mn1}(k) = 4\pi \int_0^\infty r^2 j_0(kr) \hat{c}_{\mu\nu;a\beta}^{mn1}(r) dr \quad \text{for } l \text{ even} \quad (2.34a)$$

and

$$\hat{c}_{\mu\nu;a\beta}^{mn1}(k) = 4\pi i \int_0^\infty r^2 j_1(kr) \hat{c}_{\mu\nu;a\beta}^{mn1}(r) dr \quad \text{for } l \text{ odd,} \quad (2.34b)$$

where

$$j_0(x) = \frac{\sin x}{x} \quad (2.35a)$$

and



$$j_1(x) = \frac{\sin x}{x^2} - \frac{\cos x}{x} . \quad (2.35b)$$

We note that the transforms (2.34) can be computed using fast Fourier transform techniques.

The expansions for  $\tilde{c}_{a\beta}(12)$  and  $\tilde{h}_{a\beta}(12)$  can then be inserted into eq. (2.28). After performing the necessary angular integrations and simplifying, one obtains [102]

$$\tilde{h}_{\mu\nu;a\beta}^{mnl}(k) - \tilde{c}_{\mu\nu;a\beta}^{mnl}(k) = \sum_{\gamma} \rho_{\gamma} \left[ \sum_{l_2 l_1 i} \left[ z_{mni}^{l_2 l_1 l} \right. \right. \\ \left. \left. \times \sum_{\omega=-i}^i (-1)^{\omega} \tilde{h}_{\mu\omega;a\gamma}^{mil_1}(k) \tilde{c}_{-\omega\nu;\gamma\beta}^{inl_2}(k) \right] \right] , \quad (2.36a)$$

where

$$z_{mni}^{l_2 l_1 l} = (-1)^{m+n+i} \frac{[2l+1]}{[2i+1]} \frac{f_{mnl}^{mil_1} f_{mnl}^{inl_2}}{f_{mnl}^{mnl}} \left\{ \begin{matrix} l_2 l_1 l \\ m n i \end{matrix} \right\} \left( \begin{matrix} l_2 l_1 l \\ 0 0 0 \end{matrix} \right) \quad (2.36b)$$

and  $\left\{ \begin{matrix} \cdot & \cdot & \cdot \\ \cdot & \cdot & \cdot \end{matrix} \right\}$  is the usual 6-j symbol [109]. Following Blum [102] we now introduce the  $\chi$ -transform

$$\tilde{c}_{\mu\nu;a\beta}^{mn;\chi}(k) = \sum_l \begin{pmatrix} m & n & l \\ \chi & -\chi & 0 \end{pmatrix} \tilde{c}_{\mu\nu;a\beta}^{mnl}(k) , \quad (2.37)$$

in which the sum over  $l$  is from  $|m-n|$  to  $m+n$ . It is convenient at this time to define the function

$$\eta_{a\beta}(12) = h_{a\beta}(12) - c_{a\beta}(12) , \quad (2.38)$$

which, unlike  $h_{a\beta}(12)$  or  $c_{a\beta}(12)$ , will be a smooth continuous function of  $r$  for hard core models. For the choice of  $f_{mnl}^{mnl}$  given by eq. (2.9b), it has been shown [102] that we can rewrite eq. (2.36) as

$$\tilde{N}_{\mu\nu;a\beta}^{mn;\chi}(k) = \sum_{\gamma} \rho_{\gamma} \sum_i \left[ \sum_{\omega=-i}^i (-1)^{\chi+\omega} \left[ \tilde{N}_{\mu\omega;a\gamma}^{mi;\chi}(k) + \tilde{C}_{\mu\omega;a\gamma}^{mi;\chi}(k) \right] \right. \\ \left. \times \tilde{C}_{-\omega\nu;\gamma\beta}^{in;\chi}(k) \right] , \quad (2.39)$$

where  $\tilde{N}_{\mu\nu;a\beta}^{mn;\chi}(k)$  is the  $\chi$ -transform of  $\tilde{\eta}_{\mu\nu;a\beta}^{mn1}(k)$  as defined by eq. (2.37). By comparing eqs. (2.36) and (2.39), we see that the  $\chi$ -transform has split the general OZ equation into smaller independent sets of equations which should be easier to invert numerically. Also, the numerical constant  $Z_{mni}^{121,1}$  has been greatly simplified.

Again following Blum [103], we define the matrices  $\tilde{N}_{a\beta}^{\chi}$  and  $\tilde{C}_{a\beta}^{\chi}$  whose  $(i,j)^{th}$  elements are  $\tilde{N}_{\mu\nu;a\beta}^{mn;\chi}(k)$  and  $\tilde{C}_{\mu\nu;a\beta}^{mn;\chi}(k)$ , respectively, where

$$i = m(m+1) + \mu + 1 \quad (2.40a)$$

and

$$j = n(n+1) + \nu + 1 . \quad (2.40b)$$

Equations (2.40) follow from the fact that there are, in general,  $(2m+1)$  values of  $\mu$  allowed for each  $m$ . The general OZ equation (2.39) can then be written as

$$\tilde{N}_{a\beta}^{\chi} = \sum_{\gamma} (-1)^{\chi} \left[ \tilde{N}_{a\gamma}^{\chi} + \tilde{C}_{a\gamma}^{\chi} \right] \rho_{\gamma} P \tilde{C}_{\gamma\beta}^{\chi} , \quad (2.41)$$

where  $\rho_{\gamma} = \rho_{\gamma} I$  is a diagonal matrix. The elements of matrix  $P$  are given by

$$P_{ij} = \begin{cases} (-1)^{\mu} & \text{for } \begin{cases} i=m(m+1)-\mu+1 \\ j=m(m+1)+\mu+1 \end{cases} \\ 0 & \text{otherwise} \end{cases} . \quad (2.42)$$

Now, for an  $n$ -component system, we introduce the matrices  $\tilde{N}^{\chi}$  and  $\tilde{C}^{\chi}$  whose  $(a,\beta)$  elements are  $\tilde{N}_{a\beta}^{\chi}$  and  $\tilde{C}_{a\beta}^{\chi}$ , respectively. We also define

$$\underline{\rho} = \text{diag}(\rho_1, \rho_2, \dots, \rho_n) \quad (2.43a)$$

and

$$\underline{P} = \text{diag}(P, P, \dots, P) . \quad (2.43b)$$

We then rewrite eq. (2.41) as

$$\underline{\tilde{N}}^{\chi} = (-1)^{\chi} \left[ \underline{\tilde{N}}^{\chi} + \underline{\tilde{C}}^{\chi} \right] \underline{P} \underline{P} \underline{\tilde{C}}^{\chi} , \quad (2.44a)$$

which we can rearrange to obtain

$$\underline{\tilde{N}}^{\chi} = \underline{\tilde{C}}^{\chi} \underline{P} \underline{P} \underline{\tilde{C}}^{\chi} \left[ (-1)^{\chi} \underline{I} - \underline{P} \underline{P} \underline{\tilde{C}}^{\chi} \right]^{-1} . \quad (2.44b)$$

Thus, for each value of  $\chi$  we must construct the  $\underline{\tilde{C}}^{\chi}$  matrix and then solve eq. (2.44b) to determine a  $\underline{\tilde{N}}^{\chi}$  matrix.

Once the values of  $\tilde{N}_{\mu\nu; a\beta}^{mn; \chi}(k)$  are known the projections  $\tilde{\eta}_{\mu\nu; a\beta}^{mnl}(k)$  are easily obtained using the inverse  $\chi$ -transform

$$\tilde{\eta}_{\mu\nu; a\beta}^{mnl}(k) = (2l+1) \sum_{\chi} \begin{pmatrix} m & n & 1 \\ \chi & \chi - \chi & 0 \end{pmatrix} \tilde{N}_{\mu\nu; a\beta}^{mn; \chi}(k) , \quad (2.45)$$

in which the sum over  $\chi$  is from  $-\min(m,n)$  to  $\min(m,n)$ . Finally, the projections  $\eta_{\mu\nu; a\beta}^{mnl}(r)$  are found by inverting the transforms defined by eqs. (2.34) and (2.32). The inverse Hankel transforms are given by

$$\hat{\eta}_{\mu\nu; a\beta}^{mnl}(r) = \frac{1}{2\pi^2} \int_0^{\infty} k^2 j_0(kr) \tilde{\eta}_{\mu\nu; a\beta}^{mnl}(k) dk \quad \text{for } l \text{ even}, \quad (2.46a)$$

$$\hat{\eta}_{\mu\nu; a\beta}^{mnl}(r) = \frac{-i}{2\pi^2} \int_0^{\infty} k^2 j_1(kr) \tilde{\eta}_{\mu\nu; a\beta}^{mnl}(k) dk \quad \text{for } l \text{ odd}, \quad (2.46b)$$

and the inverse hat transforms by

$$\eta_{\mu\nu; a\beta}^{mnl}(r) = \hat{\eta}_{\mu\nu; a\beta}^{mnl}(r) - \frac{1}{r^3} \int_0^r s^2 \hat{\eta}_{\mu\nu; a\beta}^{mnl}(s) P_1^e(s/r) ds \quad \text{for } l \text{ even}, \quad (2.47a)$$

$$\eta_{\mu\nu; a\beta}^{mnl}(r) = \hat{\eta}_{\mu\nu; a\beta}^{mnl}(r) - \frac{1}{r^4} \int_0^r s^3 \hat{\eta}_{\mu\nu; a\beta}^{mnl}(s) P_1^o(s/r) ds \quad \text{for } l \text{ odd}, \quad (2.47b)$$

where  $P_1^e(x)$  and  $P_1^o(x)$  are defined by eqs. (2.33).

Hence, given a set of coefficients  $c_{\mu\nu;a\beta}^{mnl}(r)$  we now have the necessary relationships, as given in eqs. (2.32)–(2.35) and (2.44b)–(2.47), to calculate the set of projections  $\eta_{\mu\nu;a\beta}^{mnl}(r)$  which satisfy the general OZ equation (2.27) for a mixture of non-spherical particles. We should point out that in general  $\tilde{\mathbf{C}}^X$  and  $\tilde{\mathbf{N}}^X$  will be complex matrices and complex arithmetic must be used to solve eq. (2.44b).

In principle, the expansions in rotational invariants (*cf.* eq. (2.29)) are infinite sums. For obvious numerical reasons we must truncate the basis set at some point to make it finite. We do this by requiring that [68,70,71]

$$m, n \leq n_{\max} . \quad (2.48a)$$

This is not a unique choice for restricting the basis set. However, the finite set of rotational invariants that satisfy eq. (2.48a) does have the special property of being a closed set under the generalized convolution of the OZ equation. That is to say, this particular set will generate only itself when the angular integration in eq. (2.28) is performed. We will also examine the effects of imposing an additional condition

$$l \leq l_{\max} . \quad (2.48b)$$

Having truncated the basis set by imposing eqs. (2.48), it follows from eqs. (2.37) and (2.45) that eq. (2.44b) need only be solved for  $|x| \leq n_{\max}$ . At this point we recall that we have also truncated the electrostatic pair potential (*cf.* eq. (2.10)) in an equivalent manner to eq. (2.48a). The two truncations need not occur at the same value of  $n_{\max}$ , however, it is obvious that the basis sets generated by eqs. (2.48) must always contain all terms we wish to include in the pair potential. Patey and co-workers [68,70,71] have found rapid basis set convergence for several dipolar and dipolar-quadrupolar models. They observed that a value of  $n_{\max}$  of four or five was sufficient to converge properties such as the average energy and dielectric constant. Furthermore, they found that higher order projections (*i.e.*,  $n=4,5$ ) only weakly couple to the low order ones (*i.e.*,  $n=0,1$ ).

It is easily shown [103] that the matrices  $\tilde{\mathbf{N}}_{a\beta}^X$  and  $\tilde{\mathbf{C}}_{a\beta}^X$  have dimensions  $D \times D$  where

$$D = (n_{\max} + 1)^2 . \quad (2.49a)$$

For  $|x| > 0$ , it follows from the definition of the  $x$ -transform and the properties of the 3-j symbol [109] that these matrices will contain rows and columns of zeros, corresponding to  $m, n < |x|$ . The number of such zero rows (or columns) will be

$$\{(\chi-1) + 1\}^2 = \chi^2. \quad (2.49b)$$

We eliminate these zero rows and columns from the matrices by defining new indices

$$i_\chi = m(m+1) + \mu - \chi^2 + 1 \quad (2.50a)$$

and

$$j_\chi = n(n+1) + \nu - \chi^2 + 1 \quad (2.50b)$$

to replace those defined in eqs. (2.40). The new dimensionality is

$$D_\chi = (n_{\max} + 1)^2 - \chi^2. \quad (2.51)$$

For an  $n$ -component system, the matrices  $\tilde{\mathbf{N}}^\chi$  and  $\tilde{\mathbf{C}}^\chi$  will then have dimensions  $(nD_\chi) \times (nD_\chi)$ . We define the indices

$$g_\chi = D_\chi(\alpha-1) + i_\chi \quad (2.52a)$$

and

$$h_\chi = D_\chi(\beta-1) + j_\chi \quad (2.52b)$$

such that the  $(g_\chi, h_\chi)^{\text{th}}$  element of  $\tilde{\mathbf{N}}^\chi$  will be  $\tilde{N}_{\mu\nu; \alpha\beta}^{mn; \chi}(k)$ , and similarly for  $\tilde{\mathbf{C}}^\chi$ . Also, eq. (2.42) is now replaced by

$$P_{i_\chi j_\chi} = \begin{cases} (-1)^\mu & \text{for } \begin{cases} i_\chi = m(m+1) - \mu - \chi^2 + 1 \\ j_\chi = m(m+1) + \mu - \chi^2 + 1 \end{cases} \\ 0 & \text{otherwise} \end{cases} \quad (2.52c)$$

Let us now consider the simplifications that arise if we restrict ourselves to systems in which all the particles have at least  $C_{2v}$  symmetry. First we will examine the results of imposing eq. (2.14). Immediately, the properties of the 3-j symbol allow us to rewrite the  $x$ -transform, eq. (2.37), as

$$\tilde{C}_{\mu\nu;a\beta}^{mn;\chi}(k) = \sum_{\chi} \begin{pmatrix} n & m & 1 \\ \chi & -\chi & 0 \end{pmatrix} \tilde{C}_{\mu\nu;a\beta}^{mn1}(k) , \quad (2.53)$$

and then using the relationship given by eq. (2.11) for the exchange of labels, we have

$$\tilde{C}_{\nu\mu;\beta a}^{nm;\chi}(k) = (-1)^{m+n} \tilde{C}_{\mu\nu;a\beta}^{mn;\chi}(k) . \quad (2.54a)$$

It also follows immediately from the properties of 3-j symbols that

$$\tilde{C}_{\mu\nu;a\beta}^{mn;-\chi}(k) = \tilde{C}_{\mu\nu;a\beta}^{mn;\chi}(k) , \quad (2.54b)$$

and similarly for  $\tilde{N}_{\mu\nu;a\beta}^{mn;\chi}(k)$ . Clearly then, the OZ equation as expressed by eq. (2.39) will be invariant to the sign of  $\chi$  for systems with  $C_{2v}$  symmetry. Thus we need only solve the OZ equation for  $\chi$  in the range  $[0, n_{\max}]$ . In this case the inverse  $\chi$ -transform, eq. (2.45), becomes

$$\tilde{\eta}_{\mu\nu;a\beta}^{mn1}(k) = (2l+1) \sum_{\chi} a_{\chi} \begin{pmatrix} m & n & 1 \\ \chi & -\chi & 0 \end{pmatrix} \tilde{N}_{\mu\nu;a\beta}^{mn;\chi}(k) , \quad (2.55a)$$

where the sum over  $\chi$  is from 0 to  $\min(m,n)$  and

$$a_{\chi} = \begin{cases} 1 & \text{for } \chi=0 , \\ 2 & \text{for } \chi>0 . \end{cases} \quad (2.55b)$$

We have already pointed out that in general  $\tilde{C}_{\mu\nu;a\beta}^{mn;\chi}(k)$  and  $\tilde{N}_{\mu\nu;a\beta}^{mn;\chi}(k)$  are complex. However, for  $m+n+1=\text{even}$  we find that there can be no mixing of real and imaginary projections by eq. (2.37). Thus,  $\tilde{C}_{\mu\nu;a\beta}^{mn;\chi}(k)$  can only be real for  $m+n=\text{even}$ , or pure imaginary for  $m+n=\text{odd}$ , and similarly for  $\tilde{N}_{\mu\nu;a\beta}^{mn;\chi}(k)$ .

Now let us examine simplifications that result from imposing eqs. (2.12c) and (2.12d). We immediately obtain

$$\tilde{C}_{\mu\nu;a\beta}^{mn;\chi}(k) = \tilde{C}_{\pm\mu\pm\nu;a\beta}^{mn;\chi}(k) . \quad (2.56)$$

Then using eq. (2.56) and eq. (2.12c), we can rewrite the general OZ equation,

as expressed by eq. (2.39), as

$$\tilde{N}_{\mu\nu; a\beta}^{mn; \chi}(k) = \sum_{\gamma} \rho_{\gamma} \sum_i \left[ \sum_{\omega=0}^i (-1)^{\chi} a_{\omega} \left[ \tilde{N}_{\mu\omega; a\gamma}^{mi; \chi}(k) + \tilde{C}_{\mu\omega; a\gamma}^{mi; \chi}(k) \right] \right. \\ \left. \times \tilde{C}_{\omega\nu; \gamma\beta}^{in; \chi}(k) \right] , \quad (2.57a)$$

where

$$a_{\omega} = \begin{cases} 1 & \text{for } \omega=0 \\ 2 & \text{for } \omega>0 \end{cases} . \quad (2.57b)$$

In matrix notation, the general OZ equation (2.44b) will be unchanged but the forms of the matrices will change. If we examine the changes in dimensionality upon applying only eq. (2.12c), it is easily shown that

$$D'_{\chi} = [ (n_{\max}+1)^2 + 1 ] / 2 - [ \chi^2 + 1 ] / 2 . \quad (2.58a)$$

To determine the dimensionality,  $D_{\chi}^C$ , under both  $C_{2v}$  symmetry conditions, we observe that in eq. (2.57a) we have essentially decreased the number of terms in the sum over  $\omega$  by a factor of 2, except for the  $(n_{\max}+1)$  terms for which  $\omega=0$ . For  $\chi=0$  we have

$$D_0^C = [ D'_0 + n_{\max} + 1 ] / 2 \\ = [ (n_{\max} + 2)^2 ] / 4 . \quad (2.58b)$$

We then generalize to obtain

$$D_{\chi}^C = [ (n_{\max} + 2)^2 ] / 4 - [ (\chi+1)^2 ] / 4 . \quad (2.59a)$$

In a similar fashion we determine that

$$i_{\chi}^C = [ (m+1)^2 ] / 4 + [ \mu/2 ] - [ (\chi+1)^2 ] / 4 + 1 \quad (2.59b)$$

and

$$j_{\chi}^C = [ (n+1)^2 ] / 4 + [ \nu/2 ] - [ (\chi+1)^2 ] / 4 + 1 . \quad (2.59c)$$

We remark that the divisions in eqs. (2.58) and (2.59) are to be taken as integer divisions. For systems of  $C_{2v}$  symmetry, eqs. (2.59) can be used to replace eqs. (2.50) and (2.51). However, the indices  $g_{\chi}$  and  $h_{\chi}$  will still be

given by eqs. (2.52a) and (2.52b) with  $D_X$ ,  $i_X$  and  $j_X$  replaced by  $D_X^C$ ,  $i_X^C$  and  $j_X^C$ , respectively. If we examine eq. (2.57), comparing it with eq. (2.39), we find that the matrix  $P$  will no longer be given by eq. (2.42). Matrix  $P$  will now be diagonal, given by

$$P_{i_X^C i_X^C} = \begin{cases} 1 & \text{for } \mu=0 , \\ 2 & \text{for } \mu>0 , \end{cases} \quad (2.60)$$

where the index  $i_X^C$  is defined by eq. (2.59b).

#### 4. The Hypernetted-Chain Approximation

The hypernetted-chain (HNC) approximation was developed simultaneously by several authors [93-97] some 25 years ago. It can be derived from functional Taylor series or cluster series expansions for  $c(12)$  which is given exactly by [27,87]

$$c(12) = h(12) - \ln g(12) - \beta u(12) + B(12) , \quad (2.61)$$

where  $\beta=1/kT$ . The function  $B(12)$  represents a class of diagrams known as elementary clusters [33] or bridge diagrams [27,87] which are not easily expressed as simple functions of  $h(12)$ . The HNC equation is obtained [27,33,87] by setting  $B(12)=0$ . The name *hypernetted-chain* equation reflects the fact that the HNC approximation,

$$c(12) = h(12) - \ln g(12) - \beta u(12) , \quad (2.62a)$$

includes contributions to  $c(12)$  from classes of diagrams known [33] as simple chains, netted chains and bundles. It is believed [27,87] that  $B(12)$  is short-ranged, having a  $h(12)^2$  dependence at large  $r$ . Therefore, the HNC is thought to have the correct long-range behaviour, *i.e.*,  $c(12) \rightarrow -\beta u(12)$  as  $r \rightarrow \infty$ . The HNC closure is often rewritten in the form

$$c(12) = \exp[\eta(12) - \beta u(12)] - \eta(12) - 1 , \quad (2.62b)$$

where  $\eta(12)$  is defined in eq. (2.38).



The HNC approximation has been used widely [27,33,60,87] to study model systems defined by spherical potentials. For example, the HNC has been found [60,87] to be particularly successful for primitive model electrolyte solutions. Until recently, in order to study systems with angle-dependent interactions, further approximations were made to the HNC closure. The LHNC [62] and QHNC [63] closures were obtained by making a particular expansion of the logarithm in eq. (2.62a) and retaining terms to only linear and quadratic order, respectively. (A further discussion of the LHNC approximation will be included at the end of this section.) Recently however, Fries and Patey [68] have shown how it is possible to analytically expand the full HNC in terms of rotational invariants. The following is essentially a summary of their work.

In order to eliminate the logarithmic term from eq. (2.62a), we take the partial derivative with respect to  $r$  holding all angular variables fixed. Using the definition

$$W(12) = -\eta(12) + \beta u(12) , \quad (2.63)$$

we obtain

$$\frac{\partial c(12)}{\partial r} = -h(12) \frac{\partial W(12)}{\partial r} - \frac{\partial \beta u(12)}{\partial r} . \quad (2.64)$$

Later we shall see that  $W(12)$  is really a dimensionless angle-dependent potential of mean force (*cf.* eq. (2.100)). We now re-integrate eq. (2.64), taking advantage of the fact that as  $r \rightarrow \infty$ ,  $c(12) \rightarrow -\beta u(12) \rightarrow 0$ . One immediately has the result

$$c(12) = \int_r^\infty h(12) \frac{\partial W(12)}{\partial r} dr - \beta u(12) . \quad (2.65)$$

In this form the HNC can then be expanded in rotational invariants, where the binary product,  $h(12)[(\partial W(12)/\partial r)]$ , can be expressed as a sum over a single invariant. In particular, Fries and Patey [68] have shown that

$$\phi_{\mu_1 \nu_1}^{m_1 n_1 l_1} \phi_{\mu_2 \nu_2}^{m_2 n_2 l_2} = \sum_{mnl} P_{\mu\nu}^{mnl} \phi_{\mu\nu}^{mnl} , \quad (2.66a)$$

in which the numerical coefficient

$$P_{\mu\nu}^{mnl} = \frac{f^{m_1 n_1 l_1} f^{m_2 n_2 l_2}}{f^{mnl}} (2m+1)(2n+1)(2l+1)(-1)^{m+n+l+\mu_1+\nu_1+\mu_2+\nu_2} \\ \times \left\{ \begin{matrix} m_1 & n_1 & l_1 \\ m_2 & n_2 & l_2 \\ m & n & l \end{matrix} \right\} \left( \begin{matrix} m_1 & m_2 & m \\ \mu_1 & \mu_2 & \mu \end{matrix} \right) \left( \begin{matrix} n_1 & n_2 & n \\ \nu_1 & \nu_2 & \nu \end{matrix} \right) \left( \begin{matrix} l_1 & l_2 & l \\ 0 & 0 & 0 \end{matrix} \right) \quad (2.66b)$$

and  $\left\{ \begin{matrix} \cdot & \cdot & \cdot \\ \cdot & \cdot & \cdot \\ \cdot & \cdot & \cdot \end{matrix} \right\}$  is the usual 9-j symbol [108]. Thus we have

$$c_{\mu\nu}^{mnl}(r) = \sum_{m_1 n_1 l_1} \sum_{m_2 n_2 l_2} \left[ P_{\mu\nu}^{mnl} \int_r^\infty h_{\mu_1 \nu_1}^{m_1 n_1 l_1}(r) \frac{\partial W_{\mu_2 \nu_2}^{m_2 n_2 l_2}(r)}{\partial r} dr \right] \\ - \beta u_{\mu\nu}^{mnl}(r) , \quad (2.67)$$

where the sums are over all allowed projections.

For models with hard-sphere potentials (*cf.* eq. (2.24)), it follows immediately from eq. (2.62b) that

$$c(12) = -1 - \eta(12) \quad \text{for } r < d, \quad (2.68)$$

which is an exact closure. Thus for the models considered in this study, eq. (2.68) will replace eq. (2.67) when  $r < d$ .

To improve the accuracy of the HNC closure, Fries and Patey [68] employed a well known perturbation technique first suggested by Lado [129]. This technique separates the pair potential and correlation functions into reference and perturbation parts. Explicitly, we write

$$X(12) = \Delta X(12) + X_R(r) , \quad (2.69)$$

where  $X(12)$  can be  $c(12)$ ,  $h(12)$ ,  $\eta(12)$ , or  $u(12)$  and  $X_R(r)$  is the same function for some spherically symmetric reference system. Then applying eq. (2.69) to eq. (2.62a), we obtain the reference HNC (RHNC) closure given by

$$c(12) = \Delta h(12) + \ln g_R(r) - \ln g(12) - \beta \Delta u(12) + c_R(r) . \quad (2.70)$$

This method assumes that exact results for  $g_R(r)$  and  $c_R(r)$  can be readily obtained. One can then proceed as before and derive the result

$$\Delta c_{\mu\nu}^{mnl}(r) = \int_r^\infty \left[ \sum_{\substack{m_1 n_1 l_1 \\ \mu_1 \nu_1}} \sum_{\substack{m_2 n_2 l_2 \\ \mu_2 \nu_2}} \left[ p_{\mu\nu}^{mnl} \Delta h_{\mu_1 \nu_1}^{m_1 n_1 l_1}(r) \frac{\partial \Delta w_{\mu_2 \nu_2}^{m_2 n_2 l_2}(r)}{\partial r} \right] \right. \\ \left. + h_R(r) \frac{\partial \Delta w_{\mu\nu}^{mnl}(r)}{\partial r} - \Delta h_{\mu\nu}^{mnl}(r) \frac{\partial \ln g_R(r)}{\partial r} \right] dr - \beta u_{\mu\nu}^{mnl}(r) . \quad (2.71)$$

The RHNC closure is easily generalized to mixtures. Clearly, in eq. (2.70) we see that there can be no coupling between different pairs of components in the HNC equation. Hence, for multicomponent systems, we have only to apply eq. (2.71) to each unique component pair,  $\alpha\beta$ .

In the present study the appropriate hard-sphere fluid is the clear choice of reference system. The *exact* hard-sphere radial distribution functions,  $g_{\alpha\beta}^{HS}(r)$ , are determined using the Lee-Levesque [130] generalization of the Verlet-Weis [131] fit to Monte Carlo data. Again, because of the hard-sphere potential, we only apply eq. (2.71) for  $r > d_{\alpha\beta}$  and use eq. (2.68) when  $r < d_{\alpha\beta}$ . Expanding eq. (2.68) in rotational invariants, we have that for  $r < d_{\alpha\beta}$

$$c_{00;\alpha\beta}^{000}(r) = -1 - \eta_{00;\alpha\beta}^{000}(r) \quad (2.72a)$$

and

$$c_{\mu\nu;\alpha\beta}^{mnl}(r) = -\eta_{\mu\nu;\alpha\beta}^{mnl}(r) \quad (2.72b)$$

for  $mnl \neq 000$ . Equation (2.71) need not be used for spherically symmetric components. In such cases it is numerically expedient to directly apply eq. (2.70), which we can rewrite as

$$c_{\alpha\beta}(r) = g_{\alpha\beta}^{HS}(r) \exp \left[ \Delta \eta_{\alpha\beta}(r) - \beta \Delta u_{\alpha\beta}(r) \right] - \eta_{\alpha\beta}(r) - 1 . \quad (2.73)$$

In this thesis we will also report a few results obtained using the reference LHNC (RLHNC) theory [62,74,81]. For hard core models, the RLHNC closure is equivalent to the RHNC closure for  $r < d_{\alpha\beta}$  (cf. eqs. (2.72)). When  $r > d_{\alpha\beta}$ , we can show [81] that the RLHNC is given by

$$c_{00;a\beta}^{000}(r) = g_{a\beta}^{HS}(r) \exp \left[ \Delta \eta_{00;a\beta}^{000}(r) - \beta \Delta u_{00;a\beta}^{000}(r) \right] - \eta_{00;a\beta}^{000}(r) - 1 \quad (2.74a)$$

and

$$\Delta c_{\mu\nu;a\beta}^{mnl}(r) = h_{00;a\beta}^{000}(r) \left[ \Delta \eta_{\mu\nu;a\beta}^{mnl}(r) - \beta \Delta u_{\mu\nu;a\beta}^{mnl}(r) \right] - \beta \Delta u_{\mu\nu;a\beta}^{mnl}(r) \quad (2.74b)$$

for  $mnl \neq 000$ . We point out that in the RLHNC theory,  $h_{00;a\beta}^{000}(r) = h_{a\beta}^{HS}(r)$  for a single component system, but this is not true for a multi-component system. Examination of eq. (2.74a) reveals that there is no coupling of the anisotropic projections into  $c_{00;a\beta}^{000}(r)$  in the RLHNC closure approximation. Therefore, the angle-dependent terms of the pair interaction potential between components  $a\beta$  can have no effect on  $g_{00;a\beta}^{000}(r)$ . This deficiency and its consequences will be discussed later. However, comparing eqs. (2.74a) and (2.73) we see that the RLHNC approximation is equivalent to the RHNC approximation for spherically symmetric components.

## 5. Method of Numerical Solution

In the previous two sections we have described how the two equations which compose the RHNC theory can be solved by expanding them in terms of rotational invariants. Hence we have two set of equations, the OZ and the RHNC equations, and two sets of unknowns, the  $\eta_{\mu\nu;a\beta}^{mnl}(r)$  and  $c_{\mu\nu;a\beta}^{mnl}(r)$  coefficients. The equations must be solved numerically and so the projections,  $\eta_{\mu\nu;a\beta}^{mnl}(r)$  and  $c_{\mu\nu;a\beta}^{mnl}(r)$ , must be represented with a set of discrete points on a numerical grid of width  $\Delta r$ . In this study we will use a value of  $\Delta r = 0.02d_s$ , which is consistent with previous work [68,70,71,79-81]. It represents a reasonable compromise between data storage, computational requirements and numerical accuracy. The necessary Hankel transforms are performed using fast Fourier transform techniques [126,127] and thus we require  $2^n$  grid points. For the calculations done on pure solvent systems, we find that 512 points are sufficient. For ionic solutions we find that more

points are usually necessary to accommodate the longer ranged correlations. The number of points varies with concentration as the screening length changes. At 1.0 molar, 1024 points are required, while concentrations between 0.1 and 0.02 molar need 4096 points.

The RHNC theory is solved by iterating the RHNC and OZ equations in a manner similar to that used in earlier work [68,81]. The iterative cycle begins with an initial guess for one of the functions. In this study we have chosen  $c_{\mu\nu;a\beta}^{\text{mnl}}(r)$ . This guess is usually a converged result from a previous calculation at slightly different conditions (e.g., concentration, total density, temperature, etc.). We then solve the OZ equation to determine a set of coefficients  $\eta_{\mu\nu;a\beta}^{\text{mnl}}(r)$ . This set along with our initial guess for  $c_{\mu\nu;a\beta}^{\text{mnl}}(r)$  is used as input into the RHNC closure which returns a new estimate for  $c_{\mu\nu;a\beta}^{\text{mnl}}(r)$ . Direct substitution of the new estimate for the initial guess will not provide a stable solution unless the initial guess is already very close to the *correct* result. However, convergence can usually be obtained by mixing successive approximations. The (i+1) approximation is given by

$$c_{\mu\nu;a\beta}^{\text{mnl}}(r)^{(i+1)} = (1 - \sigma_{\mu\nu;a\beta}^{\text{mnl}}) c_{\mu\nu;a\beta}^{\text{mnl}}(r)^{(i)} + \sigma_{\mu\nu;a\beta}^{\text{mnl}} c_{\mu\nu;a\beta}^{\text{mnl}}(r)^{(\text{new})}, \quad (2.75)$$

where the mixing parameter,  $\sigma_{\mu\nu;a\beta}^{\text{mnl}}$ , determines how much of the previous and new estimates are taken and it satisfies  $0 < \sigma_{\mu\nu;a\beta}^{\text{mnl}} < 1$ . Separate mixing parameters are used for each projection to speed convergence and their values are allowed to increase as convergence is approached. The iteration continues in this manner until a desired state of convergence is attained.

However, unlike the mixing procedures used in previous studies in which  $\eta_{\mu\nu;a\beta}^{\text{mnl}}(r)$  [81], or both  $\eta_{\mu\nu;a\beta}^{\text{mnl}}(r)$  and  $c_{\mu\nu;a\beta}^{\text{mnl}}(r)$  [68,70,71], were mixed, in this study we have chosen to mix only the functions  $c_{\mu\nu;a\beta}^{\text{mnl}}(r)$ . For the model systems being considered here, this is a better procedure. The functions which are actually mixed are short-range c's; they are the projections  $c_{\mu\nu;a\beta}^{\text{mnl}}(r)$  with the potential terms subtracted, as described in Appendix A. This method has several obvious advantages. These short-range c's contain no long-range tails due to the pair potential. As a result, they can be readily truncated to reduce storage requirements. The long-range tail

of  $c_{\alpha\beta}^{(12)}$  will always be given exactly, and hence it is relatively easy to obtain solutions after making adjustments to the potential. For electrolyte solutions, particularly at low concentration,  $c_{\alpha\beta}^{(12)}$  will change very little with a small shift in the concentration, whereas  $\eta_{\alpha\beta}^{(12)}$  will show much larger changes because of its dependence upon the screening length.

Experience with the present systems would also indicate that, in general, the convergence is faster and larger changes in parameters are tolerated when  $c_{\mu\nu;\alpha\beta}^{mnl}(r)$  is being mixed. The one obvious disadvantage is that  $c_{\alpha\beta}^{(12)}$  is discontinuous for hard-sphere models. Thus we would expect it to be more difficult to change diameters in a multi-component system.

The iterative procedure described above is a task well suited for an automated program. Such a program has been written and was used to generate all the results, both for one and three component systems, presented in this thesis. The program uses the general forms of the multipole potential (cf. eq. (2.10a)) and the OZ and RHNC equations as described in the previous sections of this chapter. This same program is also being used to study several different systems, including liquid crystal models [98], as well as models for pure ammonia [132] and ions dissolved in ammonia. It has been extended in order to study four component systems, in particular systems consisting of a colloidal particle in an electrolyte solution [133]. With only slight modifications, the program is being used to investigate systems of hard ellipsoids [99] and spherocylinders [100].

All one dimensional integrals required by the Hankel transforms are calculated using the trapezoidal rule. However, for the integration in the HNC equation (cf. eq. (2.71)), the trapezoidal rule was found to be inadequate near contact (i.e.,  $r \approx d_{\alpha\beta}$ ) for some of the systems studied here. Hence, a higher order rule [134] ( $n=6$ ) was used in this region for these systems. The numerical derivatives needed in the HNC closure were computed using a standard 4<sup>th</sup> order central difference formula [134]. Comparison with results obtained using only a 2<sup>nd</sup> order formula showed almost no change.

Care must also be taken in computing the binary product in the HNC closure equation. The number of terms in the double sum for a given projection will grow as the square of the total number of projections. Fortunately, for as many as 90% of these terms, the  $P_{\mu\nu}^{mnl}$  is zero. Even so, for large basis sets several hours on a large computer are required in order

to calculate a complete set of  $P_{\mu\nu}^{mnl}$  coefficients. Therefore it becomes important to compute the coefficients only once for a given model, storing them in a file in such a fashion so as to avoid storing zero values. A further reduction in storage can be achieved by storing only unique values. It was also found that for very large basis sets, many of the non-zero terms of the double sum could be ignored because they were very small. Another means of saving substantial amounts of time when computing the binary product in the HNC equation is to limit the range in  $r$  over which the calculations are done. For most projections, particularly those with larger  $m$  or  $n$ , the contribution from the binary product is relatively short-range. For the model systems considered here the contribution to most projections is essentially zero after the first 200-300 points. By automating a truncation procedure, the binary product is computed only over that range in  $r$  where its contribution to  $c_{\mu\nu;a\beta}^{mnl}(r)$  is significantly different from zero. Of course, this range will vary with the projection being considered. A further discussion of computational details and their relationships to basis set will be included in Chapter V.

When studying multipolar models using integral equation methods, care must be taken in treating the long-range tails in  $c_{\mu\nu;a\beta}^{mnl}(r)$  due to the electrostatic potential. This is particularly true here, where the ion-ion and some ion-solvent  $\tilde{c}_{\mu\nu;a\beta}^{mnl}(k)$ 's will have divergent behaviour at small  $k$  [74,135] due to the long-range nature of the charge-charge and charge-dipole interactions. A further discussion of how we treat these and other long-range tails can be found in Appendix A.

## 6. Averages and Potentials of Mean Force

In section 2 of this chapter we have defined the models we will investigate. The RHNC theory has been described in sections 3 and 4, and the scheme for numerical solution is outlined in section 5. In this section we will examine in detail how average properties of our systems can be calculated once we have solved the RHNC theory. We should again point out that the RHNC is an approximate theory and will give only approximate results for the correlation functions of our system. Hence, any properties determined using these correlation functions will only be estimates of the true values for the

model system.

The RHNC approximation, or any related integral equation theory, will provide us with numerical solutions for  $h_{a\beta}(12)$  and  $c_{a\beta}(12)$  which satisfy the OZ and RHNC equations (to within numerical accuracy). General statistical mechanical theory [30,33] tells us that for a model system defined by only a pair potential, knowledge of the pair distribution function,  $g_{a\beta}(12)$ , is sufficient to completely describe the thermodynamic properties of that system. It can be shown [27,33] from the definition of  $g_{a\beta}(12)$  that the average value,  $M_{a\beta}$ , of any mechanical quantity,  $m_{a\beta}(12)$ , associated with the pair  $a\beta$  is given by the general expression

$$M_{a\beta} = \frac{1}{(8\pi^2)^2 V} \int g_{a\beta}(12) m_{a\beta}(12) d\Omega_1 d\Omega_2 d\underline{r} , \quad (2.76)$$

where  $V$  is the volume of the system. Now the total interaction potential for a multi-component system (*cf.* eq. (2.2)) is given by

$$u_{tot} = \frac{1}{2} \sum_{a\beta} \sum_i^{N_a} \sum_j^{N_\beta} u_{ij}(12) , \quad (2.77)$$

where  $N_a$  and  $N_\beta$  are the numbers of particles of species  $a$  and  $\beta$  in the system. We have, of course, assumed that the system is completely characterized by a pair potential. Using eqs. (2.76) and (2.77) one obtains [27,33,74] an expression for the total average configurational energy

$$\frac{U_{TOT}}{N} = \frac{1}{2} \rho_T \sum_{a\beta} \chi_a \chi_\beta \frac{1}{(8\pi^2)^2} \int g_{a\beta}(12) u_{a\beta}(12) d\Omega_1 d\Omega_2 d\underline{r} , \quad (2.78)$$

where  $N$  is the total number of particles in the system,  $\rho_T = N/V$  is the total number density and  $\chi_a = N_a/N$  is the mole fraction of species  $a$ . Expanding  $g_{a\beta}(12)$  and  $u_{a\beta}(12)$  in terms of rotational invariants, and using the orthogonality condition [110,111]

$$\begin{aligned} & \int \Phi_{\mu\nu}^{mnl}(\Omega_1, \Omega_2, \hat{r}) \left[ \Phi_{\mu_1\nu_1}^{m_1n_1l_1}(\Omega_1, \Omega_2, \hat{r}) \right]^* d\Omega_1 d\Omega_2 \\ &= (-1)^{m+n+l} \delta_{mm_1} \delta_{nn_1} \delta_{ll_1} \delta_{\mu\mu_1} \delta_{\nu\nu_1} \left[ \frac{(f^{mnl})^2 (8\pi^2)^2}{(2m+1)(2n+1)(2l+1)} \right] \end{aligned} \quad (2.79a)$$



and

$$\int_0^\pi \int_0^{2\pi} d\underline{r} = 4\pi r^2 dr , \quad (2.79b)$$

we have

$$\frac{U_{TOT}}{N} = \frac{2\pi}{\rho_T} \sum_{a\beta} \rho_a \rho_\beta \sum_{mn1} \left[ \frac{(f^{mn1})^2}{(2m+1)(2n+1)(2l+1)} \times \int_0^\infty r^2 g_{\mu\nu;a\beta}^{mn1}(r) u_{\mu\nu;a\beta}^{mn1}(r) dr \right] . \quad (2.80)$$

Here we note that  $g_{\mu\nu;a\beta}^{mn1}(r) = h_{\mu\nu;a\beta}^{mn1}(r)$  for  $mn1 \neq 000$ . We will use eq. (2.80) to calculate all average energies reported in this thesis. Care must be taken in computing some terms such as the ion-dipole energy at infinite dilution and the ion-ion energies. The contribution to the energy from each individual ion-ion pair is divergent. However, for a charge neutral system these divergences cancel and the total ion-ion energy,  $U_{II}$ , is a meaningful quantity.

Also of interest in this study will be the total average energy,  $U_{a\beta}$ , of single component pairs within the system. It is usually convenient to express these energies per  $N_a$  rather than  $N$ . After eq. (2.80) we write

$$\frac{U_{a\beta}}{N_a} = 2\pi a_{a\beta} \rho_\beta \sum_{mn1} \left[ \frac{(f^{mn1})^2}{(2m+1)(2n+1)(2l+1)} \times \int_0^\infty r^2 g_{\mu\nu;a\beta}^{mn1}(r) u_{\mu\nu;a\beta}^{mn1}(r) dr \right] , \quad (2.81a)$$

where

$$a_{a\beta} = \begin{cases} 1 & \text{if } a=\beta , \\ 2 & \text{if } a \neq \beta . \end{cases} \quad (2.81b)$$

Another average quantity we can calculate for our systems is the average pressure as given by the compressibility factor,  $Z = PV/NkT$ . From the virial expression for the equation of state (cf. eq. (2.28) of Ref. 27), together with eq. (2.76) we have that

$$Z = 1 - \frac{\rho_T}{6kT} \sum_{a\beta} \chi_a \chi_\beta \frac{1}{(8\pi^2)^2} \int r g_{a\beta}^{(12)} \frac{\partial u_{a\beta}^{(12)}}{\partial r} d\Omega_1 d\Omega_2 d\underline{r} . \quad (2.82)$$

Equation (2.82) is often referred to as the pressure or virial equation. We determine  $Z$  by again expanding  $g_{a\beta}(12)$  and  $u_{a\beta}(12)$  in rotational invariants. In evaluating eq. (2.82), the required derivative of the multipolar potential is easy to perform analytically, while for the hard-sphere potential we must use the identity [27]

$$\frac{\partial u_{a\beta}(12)}{\partial r} = -kT \delta(r=d_{a\beta}) , \quad (2.83)$$

where  $\delta$  is the Dirac delta function. We must again treat the ion-ion terms and the ion-solvent terms carefully.

In general, we can also determine average quantities as functions of particle separation. Let us define

$$M_{a\beta}(r) = \left\langle \sum^{N_{a\beta}(r)} m_{a\beta}^{\square}(12) \right\rangle \quad (2.84)$$

as the average total value of  $m_{a\beta}^{\square}(12)$  at  $r$ , where  $\langle \dots \rangle$  denotes the ensemble average.  $m_{a\beta}^{\square}(12)$  is some property of the particles of species  $\beta$  to be evaluated at a distance  $r$  from a particle of species  $a$ , and  $N_{a\beta}(r)$  is the number of particles of species  $\beta$  at the separation  $r$ . Using eqs. (2.76) and (2.79b), and recalling that [13,27]

$$4\pi r^2 \rho_{\beta} g_{00;a\beta}^{000}(r) dr = \langle N_{a\beta}(r) \rangle , \quad (2.85a)$$

we have the expression

$$M_{a\beta}(r) = \frac{\langle N_{a\beta}(r) \rangle}{(8\pi^2)^2 g_{00;a\beta}^{000}(r)} \int g_{a\beta}(12) m_{a\beta}^{\square}(12) d\Omega_1 d\Omega_2 . \quad (2.85b)$$

If we assume there is very little correlation between  $M_{a\beta}(r)$  and  $\langle N_{a\beta}(r) \rangle$ , then the average  $M_{a\beta}(r)$  per particle is given by

$$\begin{aligned} \langle m_{a\beta}^{\square}(r) \rangle &\approx \frac{M_{a\beta}(r)}{\langle N_{a\beta}(r) \rangle} \\ &\approx \frac{1}{(8\pi^2)^2 g_{00;a\beta}^{000}(r)} \int g_{a\beta}(12) m_{a\beta}^{\square}(12) d\Omega_1 d\Omega_2 . \end{aligned} \quad (2.86)$$

In the study of liquids, the average orientations of the molecules as functions of separation are usually of interest. We define  $\langle \Phi_{\mu\nu;a\beta}^{mnl}(r) \rangle$  as being the average orientation of a particle of species  $\beta$  at a distance  $r$  from a particle of species  $a$ . Expanding  $g_{a\beta}(12)$  in eq. (2.86) and taking advantage of the orthogonality of rotational invariants as given in eq. (2.79a), we obtain

$$\langle \Phi_{\mu\nu;a\beta}^{mnl}(r) \rangle = \frac{(f^{mnl})^2}{(2m+1)(2n+1)(2l+1)} \left[ \frac{h_{\mu\nu;a\beta}^{mnl}(r)}{g_{00;a\beta}^{000}(r)} \right], \quad (2.87)$$

where we have assumed that  $m+n+l=\text{even}$ . The average orientation of solvent molecules around an ion is an important property of electrolyte solutions and will be examined in this study. The averages of most interest are

$$\langle P_1(\cos\theta_{is}) \rangle = \langle \cos\theta_{is} \rangle \quad (2.88a)$$

and

$$\langle P_2(\cos\theta_{is}) \rangle = \frac{3}{2} \langle \cos^2\theta_{is} \rangle - \frac{1}{2}, \quad (2.88b)$$

where  $\theta_{is}$  is the angle between the dipole vector and the vector joining the ion,  $i$ , and the solvent,  $s$ . In Figure 3 we have illustrated our convention in choosing  $\theta_{is}$  for positive and negative ions. This convention guarantees that  $\cos\theta_{is}$  will be positive for favourable dipole orientations for both positive and negative ions. For the choice of  $f^{mnl}$  given by eq. (2.9a), and using explicit forms for the rotational invariants [61,81], it is easy to show that eqs. (2.88) can be written as

$$\langle P_1(\cos\theta_{+s}) \rangle(r) = \frac{h_{00;+s}^{011}(r)}{3g_{00;+s}^{000}(r)}, \quad (2.89a)$$

$$\langle P_1(\cos\theta_{-s}) \rangle(r) = \frac{-h_{00;-s}^{011}(r)}{3g_{00;-s}^{000}(r)}, \quad (2.89b)$$

and

$$\langle P_2(\cos\theta_{is}) \rangle(r) = \frac{2h_{00;is}^{022}(r)}{5g_{00;is}^{000}(r)}, \quad (2.89c)$$

where  $+$  and  $-$  denote the positively and negatively charged ionic species. It

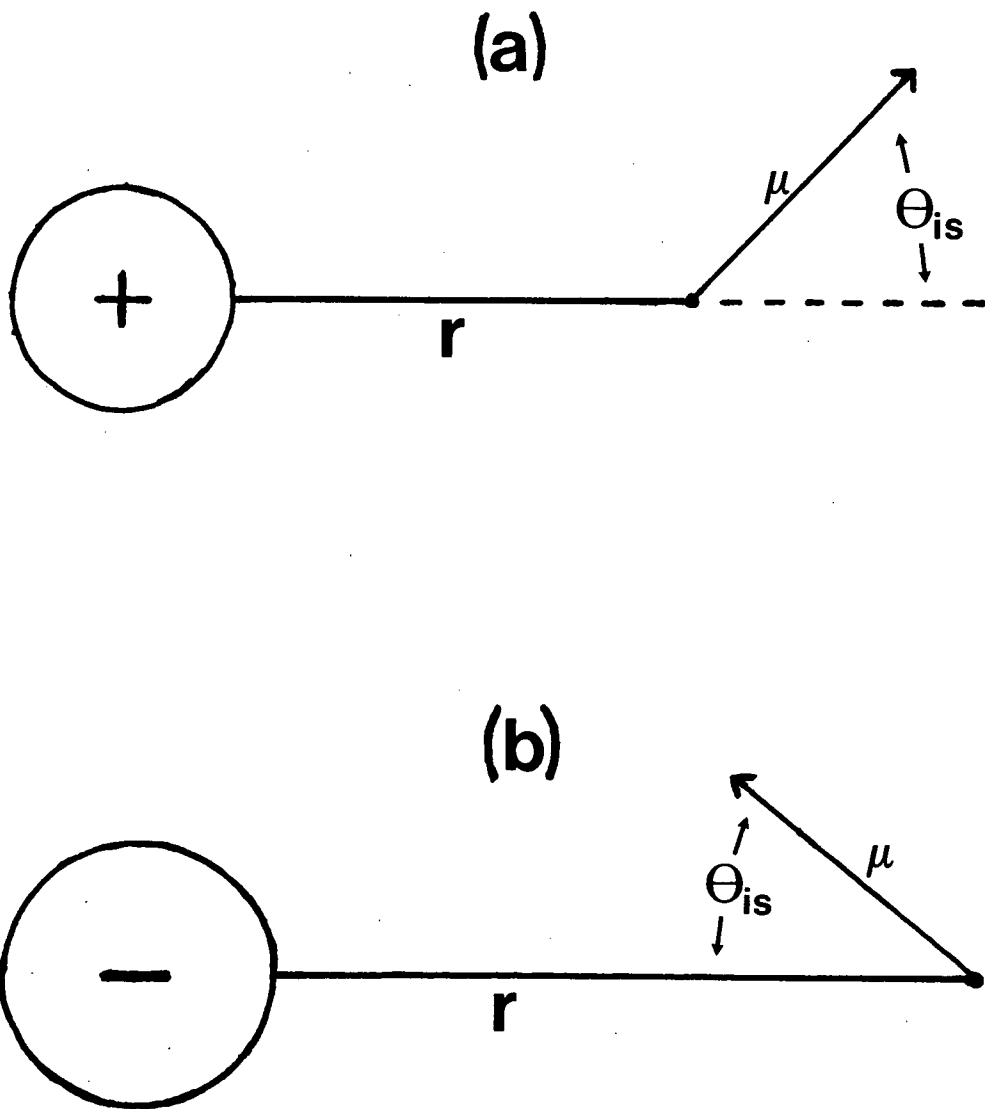


Figure 3. The angle  $\theta_{is}$  for (a) a positive ion and (b) a negative ion.

is also easy to demonstrate that for a random distribution of dipole orientations

$$\langle P_1(\cos\theta_{is}) \rangle(r) = \langle P_2(\cos\theta_{is}) \rangle(r) = 0 . \quad (2.90)$$

Clearly then, eq. (2.90) must represent the large  $r$  limits of these averages. From any introductory textbook in statistics [136], we have that the standard deviation,  $\sigma$ , of a distribution,  $y$ , is given by

$$\sigma = (\langle y^2 \rangle - \langle y \rangle^2)^{\frac{1}{2}} , \quad (2.91)$$

where  $\sigma$  is a measure of the width of the distribution. Therefore we can easily compute the standard deviation of  $(\cos\theta_{is})$  using eqs. (2.88) and (2.89).

The equilibrium, or static, dielectric constant is another quantity we will calculate since it is an important property of polar solvents and of electrolyte solutions [8,10,81,137]. For a pure solvent, the static dielectric constant,  $\epsilon$ , is well defined [81,137-140] and is readily measured. For electrolyte solutions the equilibrium dielectric constant,  $\epsilon_s$ , is theoretically well defined [61,81], but the measured dielectric constant,  $\epsilon^*(\omega)$ , diverges at low frequencies,  $\omega$ , of the applied field [10,81]. This is due to the conducting properties of ionic solutions. Hence, one defines [10,81] an apparent dielectric constant,  $\epsilon_a$ , for electrolyte solutions given by

$$\epsilon_a = \lim_{\omega \rightarrow 0} \left[ \epsilon^*(\omega) - \frac{4\pi\lambda}{i\omega} \right] , \quad (2.92)$$

where  $\lambda$  is the zero-frequency conductivity. However,  $\epsilon_a$  is not a true equilibrium quantity since several authors [10,21,141] have shown that it contains dynamical contributions. These dynamical contributions are not well understood and  $\epsilon_s$  can not, at present, be unambiguously determined experimentally for electrolyte solutions. Thus, for electrolyte solutions we would not expect exact agreement between the dielectric constants calculated for model systems and those determined experimentally using eq. (2.92). However, the agreement that is obtained should give a further indication of how large the dynamical contributions to  $\epsilon_a$  may be.

In this study we will make use of three different expressions for determining the dielectric constant of a pure solvent. The first is the Kirkwood [138,142] relationship

$$\frac{(\epsilon-1)(2\epsilon+1)}{9\epsilon} = yg , \quad (2.93a)$$

where

$$y = \frac{4\pi\rho_s\mu^2}{9kT} , \quad (2.93b)$$

in which  $\mu$  is the dipole moment of the solvent. The Kirkwood g-factor can be expressed [61,62] as

$$g = 1 + \frac{4\pi\rho_s}{3} \int_0^\infty r^2 h_{00;ss}^{110}(r) dr . \quad (2.93c)$$

It has been shown [143] that the dielectric constant can be obtained through the limit

$$h_{00;ss}^{112}(r) \rightarrow \frac{(\epsilon-1)^2}{4\pi\rho_sy\epsilon r^3} \quad \text{as } r \rightarrow \infty . \quad (2.94)$$

We will also determine  $\epsilon$  using the relationship [74]

$$\epsilon = \frac{1 - \frac{\rho_s}{3} [\tilde{c}_{00;ss}^{110}(k=0) + 2\tilde{c}_{00;ss}^{112}(k=0)]}{1 - \frac{\rho_s}{3} [\tilde{c}_{00;ss}^{110}(k=0) - \tilde{c}_{00;ss}^{112}(k=0)]} , \quad (2.95a)$$

where

$$\tilde{c}_{00;ss}^{112}(k=0) = \frac{-4\pi\mu^2}{3kT} \quad (2.95b)$$

and it follows from eq. (2.31) that

$$\tilde{c}_{00;ss}^{110}(k=0) = 4\pi \int_0^\infty r^2 c_{00;ss}^{110}(r) dr . \quad (2.95c)$$

For electrolyte solutions, eq. (2.95a) is still a valid route [74] to the dielectric constant. However, eqs. (2.93a) and (2.94) are no longer valid because of the Debye screening of  $h_{00;ss}^{112}(r)$  and  $h_{00;ss}^{110}(r)$ . Levesque *et al.* [74] have shown that for a screened ionic system

$$\frac{\epsilon_s - 1}{3} = yg , \quad (2.96)$$

where  $y$  and  $g$  are still given by eqs. (2.93b) and (2.93c). Chan *et al.* [135]

have also found that

$$\epsilon_s = \frac{4\pi}{kT} \sum_{ij} \rho_i \rho_j q_i q_j \tilde{h}_{ij}^{(2)} , \quad (2.97a)$$

where the sums are over ionic species and

$$\tilde{h}_{ij}^{(2)} = \frac{-4\pi}{6} \int_0^\infty h_{ij}(r) r^4 dr , \quad (2.97b)$$

in which  $h_{ij}(r)$  is understood to be the spherically symmetric ion-ion pair correlation function. Equations (2.97) are known as the Stillinger-Lovett [144] second moment condition. It is important to point out that for the HNC (and LHNC) theory, the three formulas valid for a pure solvent (eqs. (2.93), (2.94) and (2.95)) and the three formulas valid for electrolyte solutions (eqs. (2.95), (2.96) and (2.97)) must, in principle, all yield  $\epsilon$  consistently for their respective systems.

In this study we examine many electrolyte solutions at infinite dilution. In discussing such systems it is convenient to introduce the ion-ion potential of mean force,  $w_{ij}(r)$ , defined by [27]

$$\beta w_{ij}(r) = -\ln g_{ij}(r) , \quad (2.98)$$

where  $g_{ij}(r)$  is the ion-ion radial distribution function and  $\beta=1/kT$ . At infinite dilution,  $w_{ij}(r)$  is the potential associated with the solvent averaged force acting between the two ions,  $i$  and  $j$ . It includes all solvent effects that influence the ion-ion correlations. The ion-ion potential of mean force at infinite dilution is a measure of the free energy change of the system in taking the two ions from infinite separation to some separation  $r$ . Pettitt and Rossky [82] have exploited this relationship to determine the entropic and energetic contributions to  $w_{ij}(r)$ . We point out that  $w_{ij}(r)$  at infinite dilution is the solvent averaged ion-ion potential required by McMillan-Mayer theory [26] and it clearly follows from eq. (1.1) that

$$w_{ij}(r) \rightarrow \frac{q_i q_j}{\epsilon r} \quad \text{as } r \rightarrow \infty . \quad (2.99)$$

Thus this effective ion-ion potential could be used to perform McMillan-Mayer level theory for model electrolyte solutions at finite concentration, as was

done by Pettitt and Rossky [82].

In the HNC theory, we rewrite eq. (2.98) using the HNC equation (2.62a) to obtain

$$\beta w_{ij}(r) = \beta u_{ij}(r) - \eta_{ij}(r) . \quad (2.100)$$

However, since all our calculations are done using the RHNC approximation, we will report the ion-ion potentials of mean force as given by

$$\beta w_{ij}(r) = \beta \Delta u_{ij}(r) - \Delta \eta_{ij}(r) + \ln g_{ij}^{HS}(r) , \quad (2.101)$$

which is the correct expression for hard-sphere ions in the RHNC theory.

Finally, we note that whenever a dielectric constant, energy, or other average quantity is computed, the required integrations are usually performed using both trapezoidal and Simpson's rule [134]. This is done, in part, to check our numerical accuracy. In most cases it is the result obtained using Simpson's rule which is reported.



## CHAPTER III

### THERMODYNAMIC THEORY FOR ELECTROLYTE SOLUTIONS

#### 1. Introduction

In the statistical mechanical theory of multi-component systems the formalism of Kirkwood and Buff [104] often provides a convenient route to the thermodynamic properties. The Kirkwood-Buff approach is well known [87-89]. It uses grand canonical concentration fluctuation relationships in order to relate certain thermodynamic functions to integrals of the type

$$G_{a\beta} = 4\pi \int_0^{\infty} r^2 h_{a\beta}(r) dr , \quad (3.1a)$$

where for notational convenience we use

$$h_{a\beta}(r) \equiv h_{00;a\beta}^{000}(r) = g_{00;a\beta}^{000}(r) - 1 \quad (3.1b)$$

and  $g_{00;a\beta}^{000}(r)$  is the radial distribution function defined in Chapter II. This makes the Kirkwood-Buff theory particularly useful in extracting thermodynamic properties from the integral equation theories discussed in the previous chapter. In this study we would like to be able to apply the Kirkwood-Buff method to model electrolyte solutions in which the solvent has been included as a discrete molecular species.

For mixtures of uncharged particles, each species is an independently variable component and the expressions given by Kirkwood and Buff [104] can be directly applied. However, for electrolyte solutions where one has correlation functions between dependent constituents rather than independent components (*i.e.*, the concentrations of individual ions cannot be varied independently), the computational application of the Kirkwood-Buff theory is not immediately obvious. The ambiguity stems from the fact that when charge neutrality conditions are applied, all Kirkwood-Buff expressions [104] for the thermodynamic properties (*e.g.*, the partial molecular volume of the salt, the compressibility of solution, etc.) are indeterminate. This problem has been previously recognized and dealt with by Friedman and Ramanathan [145] for model electrolyte solutions which treat the solvent at the continuum level.

Several other authors [13,146,147] have employed the Kirkwood-Buff formalism in order to relate the structure and thermodynamics of real electrolyte solutions. However, the results reported are either limited to particular systems and thermodynamic properties or are not applicable to the present study.

In this chapter we will use the Kirkwood-Buff expressions to derive more general results for electrolyte solutions. The model we will consider incorporates the solvent as a true molecular species, and hence the relationships obtained are directly applicable to real systems. Although we will only give expressions explicitly for a two component salt/solvent system, the method we will outline in this chapter is totally general and can be readily applied to solutions of more than one salt. We will also examine the low concentration limiting behaviours of our expressions and compare these with macroscopic results obtained through Debye-Hückel theory [6].

## 2. General Expressions

The exact formulation of Kirkwood and Buff [104] expresses the thermodynamic properties of a multi-component system in terms of a matrix  $\underline{B}$ . The elements of  $\underline{B}$  are defined by

$$B_{a\beta} = \rho_a \delta_{a\beta} + \rho_a \rho_\beta G_{a\beta} , \quad (3.2)$$

where  $G_{a\beta}$  is given by eq. (3.1a) and  $\rho_a = N_a/V$  is again the number density of species  $a$ . If we consider a mixture of  $m$  species and denote the chemical potential of species  $a$  by  $\mu_a$ , the partial molecular volume by  $\bar{V}_a$ , and the isothermal compressibility of the system by  $\chi_T$ , then the relevant relationships given by Kirkwood and Buff [104] can be expressed as follows:

$$\frac{V}{kT} \left[ \frac{\partial \mu_a}{\partial N_\beta} \right]_{T, V, N_\gamma} = \frac{1}{kT} \left[ \frac{\partial \mu_a}{\partial \rho_\beta} \right]_{T, \rho_\gamma} = \frac{|\underline{B}|_{a\beta}}{|\underline{B}|} , \quad (3.3a)$$

$$\frac{V}{kT} \left[ \frac{\partial \mu_a}{\partial N_\beta} \right]_{T, P, N_\gamma} = \frac{1}{kT} \left[ \frac{\partial \mu_a}{\partial \rho_\beta} \right]_{T, \rho_\gamma} - \frac{\bar{V}_a \bar{V}_\beta}{kT \chi_T} , \quad (3.3b)$$

$$\bar{V}_\gamma = \left[ \frac{\partial V}{\partial N_\gamma} \right]_{T, P, N_a} = \frac{1}{S} \sum_{\beta=1}^m \rho_\beta |\underline{B}|_{\gamma\beta} , \quad (3.3c)$$

$$kT\chi_T = \frac{1}{S} |\underline{B}| , \quad (3.3d)$$

where

$$S = \sum_{a, \beta=1}^m \rho_a \rho_\beta |\underline{B}|_{a\beta} , \quad (3.3e)$$

$|\underline{B}|$  is the determinant of  $\underline{B}$ , and  $|\underline{B}|_{a\beta}$  indicates the cofactor of the element  $B_{a\beta}$ . Also if we label the solvent as component 1 and the remaining species by integers ranging from 2...m, the derivative of the osmotic pressure,  $\Pi$ , with respect to  $\rho_a$  is given by

$$\frac{1}{kT} \left[ \frac{\partial \Pi}{\partial \rho_a} \right]_{T, \mu_1, \rho_{\gamma \neq 1}} = \sum_{\beta=2}^m \rho_\beta \frac{|\underline{B}'|_{a\beta}}{|\underline{B}'|} , \quad (3.4a)$$

where the elements of  $\underline{B}'$  are defined by

$$B'_{a\beta} = \rho_a \delta_{a\beta} + \rho_a \rho_\beta G_{a\beta} ; \quad a, \beta \neq 1 . \quad (3.4b)$$

It should be emphasized that eqs. (3.3) and (3.4) apply to ionic solutions in only a formal sense. This is because single ion properties can not be evaluated by thermodynamic methods [6,7]. However, the physically meaningful quantities that apply to the electrically neutral salt can be obtained from the single ion expressions:

Although the method described below can be applied to any electrolyte solution, we shall write explicit results only for a two component system consisting of a solvent and a salt of the general type  $M_{\nu_+} X_{\nu_-}$ . Throughout this chapter, the solute (salt) will be referred to as component 2 and the subscripts s, + and - will denote the solvent and the positively and negatively charged ionic species. Also, it is convenient to introduce the parameter  $\nu = \nu_+ + \nu_-$ , as well as the relationships  $\rho_+ = \nu_+ \rho_2$ ,  $\rho_- = \nu_- \rho_2$  and  $\rho_+ = (\nu_+/\nu_-) \rho_-$ . Also, since the salt molecule is electrically neutral, we have that  $q_+ = -(\nu_-/\nu_+) q_-$ . For electrolyte solutions, we have charge neutrality conditions which can be expressed as [74,135,148,149]

$$\sum_i \rho_i q_i G_{ij} = -q_j \quad (3.5a)$$

and

$$\sum_i \rho_i q_i G_{is} = 0 . \quad (3.5b)$$

For the systems we will consider, eqs. (3.5a) and (3.5b) can be rewritten in the form

$$G_{+-} = G_{++} + \frac{1}{\rho_+} = G_{--} + \frac{1}{\rho_-} \quad (3.5c)$$

and

$$G_{+s} = G_{-s} . \quad (3.5d)$$

As mentioned earlier, the charge neutrality conditions render indeterminate all thermodynamic quantities obtained by direct substitution into the Kirkwood-Buff equations. Therefore, in order to proceed it is necessary to employ a formalism which allows the charge neutral limit to be taken analytically in such a way that useful determinate expressions are obtained for the thermodynamic properties. One way of doing this in a general systematic manner is described below.

We begin by realizing that

$$G_{a\beta} = \tilde{h}_{a\beta}(k=0) \equiv \tilde{h}_{a\beta}^{(0)} , \quad (3.6a)$$

where

$$\tilde{h}_{a\beta}(k) = \frac{4\pi}{k} \int_0^\infty r h_{a\beta}(r) \sin(kr) dr \quad (3.6b)$$

follows immediately from eqs. (2.34a) and (2.35a). At finite ion concentration  $h_{a\beta}(r)$  is screened and decays exponentially at large  $r$  (as will be discussed below). Hence at small  $k$ ,  $\tilde{h}_{a\beta}(k)$  can be expanded in the form [73,74,135]

$$\tilde{h}_{a\beta}(k) = \tilde{h}_{a\beta}^{(0)} + k^2 \tilde{h}_{a\beta}^{(2)} + \dots , \quad (3.6c)$$

where the second moment,  $\tilde{h}_{a\beta}^{(2)}$ , is given by eq. (2.97b). Thus we can introduce the matrix  $\tilde{\mathbf{B}}(k)$  whose elements are

$$\tilde{B}_{a\beta}(k) = \rho_a \delta_{a\beta} + \rho_a \rho_\beta \tilde{h}_{a\beta}(k) . \quad (3.7)$$

This then allows determinate expressions for the thermodynamic properties to be obtained by taking the  $k \rightarrow 0$  limit of the appropriate  $k$ -dependent quantities.

For the  $M_{\nu_+} X_{\nu_-}$  /solvent system we consider,  $\tilde{\underline{B}}(k)$  has the explicit form

$$\tilde{\underline{B}}(k) = \begin{bmatrix} \rho_+^2 \tilde{h}_{++}^\dagger(k) & \rho_+ \rho_- \tilde{h}_{+-}(k) & \rho_+ \rho_s \tilde{h}_{+s}(k) \\ \rho_+ \rho_- \tilde{h}_{+-}(k) & \rho_-^2 \tilde{h}_{--}^\dagger(k) & \rho_- \rho_s \tilde{h}_{-s}(k) \\ \rho_+ \rho_s \tilde{h}_{+s}(k) & \rho_- \rho_s \tilde{h}_{-s}(k) & \rho_s^2 \tilde{h}_{ss}^\dagger(k) \end{bmatrix}, \quad (3.8a)$$

where

$$\tilde{h}_{aa}^\dagger(k) = \tilde{h}_{aa}(k) + \frac{1}{\rho_a} \quad (3.8b)$$

and we have made use of the requirement that  $h_{a\beta}(r) = h_{\beta a}(r)$ , in which  $a, \beta = +, -, s$ . In order to take the required  $k \rightarrow 0$  limits, it is necessary to know the small  $k$  behaviour of the determinant  $|\tilde{\underline{B}}(k)|$  and of the sum

$$\tilde{S}(k) = \sum_{a\beta} \rho_a \rho_\beta |\tilde{\underline{B}}(k)|_{a\beta}, \quad (3.9)$$

where again  $|\tilde{\underline{B}}(k)|_{a\beta}$  denotes the cofactor of the element  $\tilde{\underline{B}}_{a\beta}(k)$ . Using eq. (3.7) together with the charge neutrality conditions given by eqs. (3.5c) and (3.5d), one finds that at small  $k$

$$|\tilde{\underline{B}}(k)|_{++} = \rho_-^2 \rho_s^2 \left[ \tilde{h}_{+-}^{(0)} \tilde{h}_{ss}^{\dagger(0)} - [\tilde{h}_{+s}^{(0)}]^2 + k^2 [\tilde{h}_{ss}^{\dagger(0)} \tilde{h}_{--}^{(2)} + \tilde{h}_{+-}^{(0)} \tilde{h}_{ss}^{(2)} - 2\tilde{h}_{+s}^{(0)} \tilde{h}_{-s}^{(2)}] + \dots \right], \quad (3.10a)$$

$$|\tilde{\underline{B}}(k)|_{+-} = |\tilde{\underline{B}}(k)|_{-+} = \rho_+ \rho_- \rho_s^2 \left[ [\tilde{h}_{+s}^{(0)}]^2 - \tilde{h}_{+-}^{(0)} \tilde{h}_{ss}^{\dagger(0)} + k^2 [\tilde{h}_{+s}^{(0)} [\tilde{h}_{+s}^{(2)} + \tilde{h}_{-s}^{(2)}] - \tilde{h}_{+-}^{(0)} \tilde{h}_{ss}^{(2)} - \tilde{h}_{ss}^{\dagger(0)} \tilde{h}_{+-}^{(2)}] + \dots \right], \quad (3.10b)$$

$$|\underline{\tilde{B}}(k)|_{--} = \rho_+^2 \rho_s^2 \left[ \tilde{h}_{+-}^{(0)} \tilde{h}_{ss}^{\dagger(0)} - [\tilde{h}_{+s}^{(0)}]^2 + k^2 [\tilde{h}_{ss}^{\dagger(0)} \tilde{h}_{++}^{(2)} + \tilde{h}_{+-}^{(0)} \tilde{h}_{ss}^{(2)} - 2\tilde{h}_{+s}^{(0)} \tilde{h}_{+s}^{(2)}] + \dots \right], \quad (3.10c)$$

$$|\underline{\tilde{B}}(k)|_{+s} = |\underline{\tilde{B}}(k)|_{s+} = \rho_+ \rho_-^2 \rho_s \left[ k^2 [\tilde{h}_{+s}^{(0)} [\tilde{h}_{+-}^{(2)} - \tilde{h}_{--}^{(2)}] + \tilde{h}_{+-}^{(0)} [\tilde{h}_{-s}^{(2)} - \tilde{h}_{+s}^{(2)}]] + \dots \right], \quad (3.10d)$$

$$|\underline{\tilde{B}}(k)|_{-s} = |\underline{\tilde{B}}(k)|_{s-} = \rho_+^2 \rho_- \rho_s \left[ k^2 [\tilde{h}_{+s}^{(0)} [\tilde{h}_{+-}^{(2)} - \tilde{h}_{++}^{(2)}] + \tilde{h}_{+-}^{(0)} [\tilde{h}_{+s}^{(2)} - \tilde{h}_{-s}^{(2)}]] + \dots \right] \quad (3.10e)$$

and

$$|\underline{\tilde{B}}(k)|_{ss} = \rho_+^2 \rho_-^2 \left[ k^2 [\tilde{h}_{+-}^{(0)} [\tilde{h}_{++}^{(2)} + \tilde{h}_{--}^{(2)} - 2\tilde{h}_{+-}^{(2)}]] + \dots \right]. \quad (3.10f)$$

We remark that in the  $k \rightarrow 0$  limit  $|\underline{\tilde{B}}(k)|_{+s} = |\underline{\tilde{B}}(k)|_{-s} = |\underline{\tilde{B}}(k)|_{ss} = 0$ . The explicit forms for the cofactors can then be used to show that as  $k \rightarrow 0$ ,

$$|\underline{\tilde{B}}(k)| \rightarrow \rho_+^2 \rho_-^2 \rho_s^2 [\tilde{h}_{ss}^{\dagger(0)} \tilde{h}_{+-}^{(0)} - [\tilde{h}_{+s}^{(0)}]^2] D k^2 + \dots, \quad (3.11a)$$

$$\tilde{S}(k) \rightarrow \rho_+^2 \rho_-^2 \rho_s^2 [\tilde{h}_{ss}^{\dagger(0)} + \tilde{h}_{+-}^{(0)} - 2\tilde{h}_{+s}^{(0)}] D k^2 + \dots, \quad (3.11b)$$

where

$$D = \tilde{h}_{++}^{(2)} + \tilde{h}_{--}^{(2)} - 2\tilde{h}_{+-}^{(2)}. \quad (3.11c)$$

It is also obvious from eqs. (3.11a) and (3.11b) that as  $k \rightarrow 0$ , both  $\tilde{S}(k)$  and  $|\underline{\tilde{B}}(k)| \rightarrow 0$ .

First we shall derive explicit expressions for the volumetric properties. For the present system the partial molecular volume of the salt,  $\bar{V}_2$ , is defined by [6]

$$\bar{V}_2 = \left[ \frac{\partial V}{\partial N_2} \right]_{T,P,N_S} = \nu_+ \bar{V}_+ + \nu_- \bar{V}_- , \quad (3.12)$$

where  $\bar{V}_+$  and  $\bar{V}_-$  are given by eq. (3.3c). It then follows that the appropriate k-dependent quantity is

$$\tilde{\bar{V}}_2(k) = \nu_+ \tilde{\bar{V}}_+(k) + \nu_- \tilde{\bar{V}}_-(k) , \quad (3.13a)$$

where

$$\tilde{\bar{V}}_i(k) = \frac{1}{\tilde{S}(k)} \sum_{a=+,-,s} \left[ \rho_a | \tilde{B}(k) |_{ia} \right] . \quad (3.13b)$$

Now using eqs. (3.10) and (3.11b) and collecting terms, we find that the resulting expression contains the factor  $Dk^2$  in both its numerator and its denominator. We then simply cancel this common factor to obtain

$$\lim_{k \rightarrow 0} \tilde{\bar{V}}_2(k) = \frac{\tilde{h}_{ss}^{\dagger}(0) - \tilde{h}_{+s}^{(0)}}{\rho_2 [\tilde{h}_{ss}^{\dagger}(0) - \tilde{h}_{+-}^{(0)} - 2\tilde{h}_{+s}^{(0)}]} , \quad (3.14)$$

which in the convenient  $G_{\alpha\beta}$  notation gives

$$\bar{V}_2 = \frac{1 + \rho_s (G_{ss} - G_{+s})}{\rho_2 [1 + \rho_s (G_{ss} + G_{+-} - 2G_{+s})]} . \quad (3.15)$$

Clearly eq. (3.15) is the desired determinate expression for  $\bar{V}_2$ .

In a similar fashion we define the k-dependent quantity  $\tilde{\bar{V}}_s(k)$ . Then inserting eqs. (3.10) and (3.11b) and taking the  $k \rightarrow 0$  limit, we obtain the partial molecular volume of the solvent,

$$\bar{V}_s = \frac{G_{+-} - G_{+s}}{1 + \rho_s (G_{ss} + G_{+-} - 2G_{+s})} . \quad (3.16)$$

It is easy to see that eqs. (3.15) and (3.16) satisfy the required relationship

$$\rho_s \bar{V}_s + \rho_2 \bar{V}_2 = 1 . \quad (3.17a)$$

From eq. (3.15) we immediately have that

$$\lim_{\rho_s \rightarrow 0} \bar{V}_2 = \frac{1}{\rho_2} . \quad (3.17b)$$

Also, since in eq. (3.16) only  $G_{+-}$  is divergent in the limit  $\rho_2 \rightarrow 0$  (as shown below), it follows that

$$\lim_{\rho_2 \rightarrow 0} \bar{V}_s = \frac{1}{\rho_s} . \quad (3.17c)$$

Obviously eqs. (3.17b) and (3.17c) represent the correct single component results for the partial molecular volumes. Finally, we note that for the particular case when  $\nu_+ = 1$ , eq. (3.16) can easily be shown to be equivalent to the expression given by Enderby and Neilson [13].

In general, the isothermal compressibility [27] of a system is given by

$$kT\chi_T = -\frac{1}{\bar{V}} \left[ \frac{\partial \bar{V}}{\partial P} \right]_{T,N} = \frac{1}{\rho_T} \left[ \frac{\partial \rho_T}{\partial P} \right]_{T,N} . \quad (3.18)$$

It should be pointed out that when  $k$  appears in the combination  $kT$ , as in eq. (3.18), it refers to the Boltzmann constant and is not to be confused with  $k$  in the Fourier transform. By analogy with eq. (3.3d), we define the  $k$ -dependent isothermal compressibility

$$kT\tilde{\chi}_T(k) = \frac{1}{\tilde{S}(k)} |\tilde{B}(k)| . \quad (3.19)$$

The  $k \rightarrow 0$  limit follows immediately from eqs. (3.11a) and (3.11b), and yields the relationship

$$kT\chi_T = \frac{G_{+-} + \rho_s(G_{+-}G_{ss} - G_{+s}^2)}{1 + \rho_s(G_{ss} + G_{+-} - 2G_{+s})} , \quad (3.20)$$

which agrees with the result previously given by Levesque *et al.* [74].

Equations (3.15), (3.16) and (3.20) will be used to determine the volumetric properties of the model electrolyte solutions being considered in this study.

We also point out that these expressions are totally general and can be applied directly to those solutions which contain only a single salt.



The chemical potential is a fundamental quantity in thermodynamics [6,150] and is particularly useful in describing non-ideal behaviour in solutions [1,5,7]. Using notation consistent with Harned and Owen [6], we express the chemical potential of species  $a$  as

$$\begin{aligned}\mu_a &= \mu_a^0 + kT \ln a_a = \mu_{a;m}^0 + kT \ln(\gamma_a m_a) \\ &= \mu_{a;c}^0 + kT \ln(y_a c_a) ,\end{aligned}\quad (3.21)$$

where  $a_a$  is the activity of species  $a$ ,  $m_a$  and  $c_a$  are concentrations expressed as molality and molarity,  $\gamma_a$  and  $y_a$  are activity coefficients, and  $\mu_a^0$ ,  $\mu_{a;m}^0$  and  $\mu_{a;c}^0$  are the chemical potentials of the standard states. Since  $\mu_a$  must be independent of the concentration scale in which  $a_a$  is expressed, the chemical potential of the standard state will contain a term dependent on the choice of scale. Thus we find  $\mu_{a;m}^0 \neq \mu_{a;c}^0$  and it follows that  $\gamma_a \neq y_a$ . Expressions relating the logarithms of the various activity coefficients can be easily obtained (*cf.* eqs. (1-8-13)-(15) of Ref. 6) and it can be shown that the differences between the logarithms of the activity coefficients always have a linear dependence on concentration at low solute concentration. We point out that the molarity activity coefficient,  $y_a$ , remains unchanged if the concentration scale is expressed as a number density.

For the electrolyte solutions being considered here, the chemical potential of the solute (salt),  $\mu_2$ , is given by

$$\mu_2 = \nu_+ \mu_+ + \nu_- \mu_- , \quad (3.22a)$$

where the single ion quantities are defined by eq. (3.21). If we introduce the mean activity coefficient of the salt defined [6] such that

$$y_{\pm} = y_+^{\nu_+} y_-^{\nu_-} , \quad (3.22b)$$

then it follows from eqs. (3.21) and (3.22a) that

$$\mu_2 = \mu_{2;\rho}^0 + kT \ln(\nu_+^{\nu_+} \nu_-^{\nu_-}) + \nu kT \ln(y_{\pm} \rho_2) . \quad (3.22c)$$

We take the partial derivative of eq. (3.22c) with respect to  $\rho_2$  holding  $T$  and  $\rho_s$ , or  $T$  and  $P$ , fixed to obtain

$$\left[ \frac{\partial \ln y_{\pm}}{\partial \rho_2} \right]_{T, \rho_S \text{ or } P} = \frac{1}{\nu kT} \left[ \frac{\partial \mu_2}{\partial \rho_2} \right]_{T, \rho_S \text{ or } P} - \frac{1}{\rho_2} . \quad (3.23)$$

Expressions for the right hand side of eq. (3.23) can now be found by applying the Kirkwood-Buff equations.

Using eq. (3.22a) together with the mathematical relationship

$$\left[ \frac{\partial \mu_i}{\partial \rho_2} \right] = \sum_{j=+, -} \nu_j \left[ \frac{\partial \mu_i}{\partial \rho_j} \right]_{\rho_{k \neq j}} ; \quad i = + \text{ or } - , \quad (3.24a)$$

one immediately finds that

$$\left[ \frac{\partial \mu_2}{\partial \rho_2} \right] = \nu_+^2 \left[ \frac{\partial \mu_+}{\partial \rho_+} \right]_{\rho_-} + \nu_+ \nu_- \left[ \left[ \frac{\partial \mu_+}{\partial \rho_-} \right]_{\rho_+} + \left[ \frac{\partial \mu_-}{\partial \rho_+} \right]_{\rho_-} \right] + \nu_-^2 \left[ \frac{\partial \mu_-}{\partial \rho_-} \right]_{\rho_+} , \quad (3.24b)$$

where in addition to the variables specifically indicated  $T$  and  $\rho_S$  or  $P$  are also held constant. The partial derivatives,  $(\partial \mu_a / \partial \rho_\beta)$ , required in the constant volume case are given by eq. (3.3a). Again, in order to obtain determinate results it is necessary to define

$$\frac{1}{kT} \left[ \frac{\partial \tilde{\mu}_a}{\partial \rho_\beta} \right]_{T, \rho_\gamma}^{(k)} = \frac{|\tilde{B}(k)|_{a\beta}}{|\tilde{B}(k)|} . \quad (3.25)$$

Substituting eq. (3.25) into the right hand side of eq. (3.24b) and using eqs. (3.10) and (3.11a), then simplifying and taking the  $k \rightarrow 0$  limit yields the determinate result

$$\frac{1}{kT} \left[ \frac{\partial \mu_2}{\partial \rho_2} \right]_{T, \rho_S} = \frac{1 + \rho_S G_{SS}}{\rho_2^2 [G_{+-} + \rho_S (G_{SS} G_{+-} - G_{+S}^2)]} . \quad (3.26)$$

From eqs. (3.3b), (3.12) and (3.24b) we can show that the constant pressure derivative can be expressed as

$$\frac{V}{kT} \left[ \frac{\partial \mu_2}{\partial N_2} \right]_{T, P, N_S} = \frac{1}{kT} \left[ \frac{\partial \mu_2}{\partial \rho_2} \right]_{T, \rho_S} - \frac{\bar{V}_2^2}{kT \chi_T} . \quad (3.27a)$$

Inserting results from eqs. (3.15), (3.20) and (3.26) we obtain

$$\frac{V}{kT} \left[ \frac{\partial \mu_2}{\partial N_2} \right]_{T, P, N_S} = \frac{\rho_S}{\rho_2^2 [1 + \rho_S (G_{SS} + G_{+-} - 2G_{+S})]} . \quad (3.27b)$$

Clearly, eq. (3.27b) does not represent the constant pressure derivative required in eq. (3.23). In order to proceed, we introduce the relationship

$$\frac{1}{kT} \left[ \frac{\partial \mu_2}{\partial \rho_2} \right]_{T, P} = \frac{V}{kT} \left[ \frac{\partial \mu_2}{\partial N_2} \right]_{T, P, N_S} / V \left[ \frac{\partial \rho_2}{\partial N_2} \right]_{T, P, N_S} , \quad (3.28a)$$

where  $N_S$  is being implicitly held fixed on the left-hand side of the equation. However,  $\rho_S$  can not be held fixed because the volume is allowed to vary. It can easily be shown that

$$\left[ \frac{\partial \rho_2}{\partial N_2} \right]_{T, P, N_S} = \frac{1}{\bar{V}} (1 - \rho_2 \bar{V}_2) = \frac{1}{\bar{V}} \rho_S \bar{V}_S . \quad (3.28b)$$

Then combining eqs. (3.27b) and (3.28), and using eq. (3.16) we obtain

$$\frac{1}{kT} \left[ \frac{\partial \mu_2}{\partial \rho_2} \right]_{T, P} = \frac{1}{\rho_2^2 (G_{+-} - G_{+S})} . \quad (3.29)$$

Expressions for the mean activity coefficients now follow immediately from eqs. (3.23), (3.26) and (3.29). Explicitly, we have

$$\left[ \frac{\partial \ln y_{\pm}}{\partial \rho_2} \right]_{T, \rho_S} = \frac{1}{\rho_2} \left[ \frac{1 + \rho_S G_{SS}}{\nu \rho_2 [G_{+-} + \rho_S (G_{SS} G_{+-} - G_{+S}^2)]} - 1 \right] \quad (3.30a)$$

and

$$\left[ \frac{\partial \ln y_{\pm}}{\partial \rho_2} \right]_{T, P} = \frac{1}{\rho_2} \left[ \frac{1}{\nu \rho_2 (G_{+-} - G_{+S})} - 1 \right] . \quad (3.30b)$$

Equations (3.30) will be used in this study to calculate derivatives of the mean activity coefficient. Again, these are general expressions for two component salt/solvent systems but results for more complex mixtures could be found with relative ease.

In a similar manner, we can also derive relationships involving the solvent chemical potential. In particular, we can show that

$$\frac{1}{kT} \left[ \frac{\partial \mu_s}{\partial \rho_s} \right]_{T, \rho_2} = \frac{G_{+-}}{\rho_s [G_{+-} + \rho_s (G_{ss} G_{+-} - G_{+s}^2)]} \quad (3.31a)$$

and

$$\begin{aligned} \frac{1}{kT} \left[ \frac{\partial \mu_2}{\partial \rho_s} \right]_{T, \rho_2} &= \frac{1}{kT} \left[ \frac{\partial \mu_s}{\partial \rho_2} \right]_{T, \rho_s} \\ &= \frac{-G_{+s}}{\rho_2 [G_{+-} + \rho_s (G_{ss} G_{+-} - G_{+s}^2)]} . \end{aligned} \quad (3.31b)$$

Finally, we will consider the osmotic pressure. The derivative of the osmotic pressure with respect to  $\rho_2$  is given by

$$\left[ \frac{\partial \Pi}{\partial \rho_2} \right]_{T, \mu_s} = \sum_{i=+,-} \nu_i \left[ \frac{\partial \Pi}{\partial \rho_i} \right]_{T, \mu_s, \rho_{j \neq i}} , \quad (3.32)$$

where  $(\partial \Pi / \partial \rho_i)$  is defined by eq. (3.4a). Again direct substitution into eq. (3.32) leads to an indeterminate result when the charge neutrality condition (3.5c) is applied. Therefore, proceeding as before we define the matrix  $\tilde{\mathbf{B}}'(k)$  (cf. eq. (3.4b)) and the  $k$ -dependent derivatives analogous to eq. (3.4a). Substituting the  $k$ -dependent quantities for  $(\partial \Pi / \partial \rho_i)$  into eq. (3.32) and taking the  $k \rightarrow 0$  limit yields the expression

$$\frac{1}{kT} \left[ \frac{\partial \Pi}{\partial \rho_2} \right]_{T, \mu_s} = \frac{1}{\rho_2 G_{+-}} . \quad (3.33)$$

For 1:1 electrolytes this result is equivalent to that given in Ref. 74, although eq. (3.33) is a more general relationship.

### 3. Limiting Behaviour

In order to determine the limiting behaviour as  $\rho_2 \rightarrow 0$  of the expressions given in the previous section, it is first necessary to deduce the low concentration limiting laws for  $G_{+-}$ ,  $G_{+S}$  and  $G_{SS}$ . For continuum level theories of electrolyte solutions only  $G_{+-}$  is relevant and this function has been previously considered by Rasaiah and Friedman [151]. The ion-ion distribution function,  $g_{+-}(r)$ , can be written in the form

$$g_{+-}(r) = \exp[-\beta w_{+-}(r)] , \quad (3.34)$$

where  $w_{+-}(r)$  is the ion-ion potential of mean force (cf. eq. (2.98)). For both continuum and molecular solvents it is possible to show [61] that as  $r \rightarrow \infty$  and  $\kappa \rightarrow 0$ ,

$$w_{+-}(r) \rightarrow \frac{-q_+ q_-}{\epsilon r} e^{-\kappa r} , \quad (3.35a)$$

where

$$\kappa = \left[ \frac{4\pi}{\epsilon kT} \sum_i \rho_i q_i^2 \right]^{\frac{1}{2}} \quad (3.35b)$$

is the usual Debye screening parameter and  $\epsilon$  is the dielectric constant of the pure solvent. For a solution containing only a single salt we have

$$\kappa = \left[ \frac{4\pi}{\epsilon kT} |q_+ q_-| \nu \rho_2 \right]^{\frac{1}{2}} . \quad (3.35c)$$

If we now expand the exponential in eq. (3.34) and keep terms to order  $[\beta w_{+-}(r)]^2$ , eqs. (3.1), (3.35a) and (3.35c) yield (see Appendix B) the limiting law

$$G_{+-} = \frac{1}{\nu \rho_2} + \frac{A}{\sqrt{\nu \rho_2}} + \dots , \quad (3.36a)$$

where

$$A = \frac{\pi^{\frac{1}{2}}}{2} \left[ \frac{|q_+ q_-|}{\epsilon kT} \right]^{\frac{3}{2}} . \quad (3.36b)$$

We emphasize that eq. (3.36a) holds for both continuum and molecular level theories of electrolyte solutions.

In order to obtain limiting expressions for  $G_{+S}$  and  $G_{SS}$ , it is necessary to reintroduce the direct correlation function,  $c_{\alpha\beta}^{(12)}$ , and to apply the OZ

equation, both of which are described in the previous chapter. Our analysis will require that we know the long-range behaviour of  $c_{a\beta}(12)$ . Therefore, we must restrict ourselves to systems which can be described by pairwise or effective pairwise additive potentials.

For the present purposes, the only relevant projections are  $h_{00;a\beta}^{000}(r)$ . From the OZ equation, as given by (2.36a), we have that

$$\begin{aligned} \tilde{h}_{00;a\beta}^{000}(k) - \tilde{c}_{00;a\beta}^{000}(k) &= \sum_{\gamma} \rho_{\gamma} \left[ \sum_m z_{00m}^{mm0} \right. \\ &\quad \times \left. \left[ \sum_{\omega=-m}^m (-1)^{\omega} \tilde{h}_{0\omega;a\gamma}^{0mm}(k) \tilde{c}_{-\omega 0;\gamma\beta}^{m0m}(k) \right] \right], \quad (3.37) \end{aligned}$$

where  $z_{00m}^{mm0}$  is a nonzero coefficient given by eq. (2.36b). Obviously, it is the small  $k$  dependence of this expression which is required here. In order to reduce eq. (3.37) further, we take advantage of a property of the Hankel transforms,  $\tilde{b}_{\mu\nu;a\beta}^{mnl}(k)$  (cf. eq. (2.31)). It can be shown (by using explicit forms for the spherical Bessel functions and expanding the sin and cos terms) that if  $b_{\mu\nu;a\beta}^{mnl}(r)$  decays faster than  $1/r^3$ , then

$$\tilde{b}_{\mu\nu;a\beta}^{mnl}(k=0) = 0 \quad \text{for } l > 0. \quad (3.38a)$$

Of course, for all electrolyte solutions at finite concentrations, screening ensures that  $h_{0\nu;a\beta}^{0mm}(r)$  decays exponentially, and hence

$$\tilde{h}_{0\nu;a\beta}^{0mm}(k=0) = 0 \quad \text{for } m > 0. \quad (3.38b)$$

Thus, if we consider the  $k \rightarrow 0$  limit of eq. (3.37), we can then apply eq. (3.38b) to obtain the expression

$$G_{as} - C_{as} = \sum_{\gamma} \rho_{\gamma} G_{a\gamma} C_{\gamma s}, \quad (3.39a)$$

where for notational convenience we have introduced

$$C_{a\beta} = \tilde{c}_{00;a\beta}^{000}(k=0) = 4\pi \int_0^{\infty} r^2 c_{00;a\beta}^{000}(r) dr. \quad (3.39b)$$

Equation (3.39a) is an exact relationship subject only to the restriction that the potentials describing our system be pairwise additive.

For the systems being considered here we can explicitly write out the terms in the sum of eq. (3.39a) and then rearrange to obtain

$$G_{+s}(1 - \rho_s C_{ss}) = (1 + \rho_+ G_{++})C_{+s} + \rho_- G_{+-}C_{-s} \quad (3.40a)$$

and

$$G_{-s}(1 - \rho_s C_{ss}) = (1 + \rho_- G_{--})C_{-s} + \rho_+ G_{+-}C_{+s} , \quad (3.40b)$$

which, when combined with the charge neutrality condition (3.5c), yield the result

$$G_{+s} = G_{-s} = \left[ \frac{\nu_+ C_{+s} + \nu_- C_{-s}}{1 - \rho_s C_{ss}} \right] \rho_2 G_{+-} . \quad (3.41)$$

Equation (3.41) is in fact the origin of the charge neutrality condition (3.5d). Also, since eq. (3.41) is obtained with the aid of the charge neutrality condition (3.5c), it holds only for  $\rho_2 > 0$ .

At this point it is interesting to note that if we examine eq. (3.37) at small  $k$ , we have a relationship analogous to eq. (3.39a), namely

$$\begin{aligned} \tilde{h}_{00;as}^{000}(k) = & \left[ \tilde{c}_{00;as}^{000}(k) + \rho_+ \tilde{h}_{00;a+}^{000}(k) \tilde{c}_{00;+s}^{000}(k) \right. \\ & \left. + \rho_- \tilde{h}_{00;a-}^{000}(k) \tilde{c}_{00;-s}^{000}(k) \right] \left[ \frac{1}{1 - \rho_s \tilde{c}_{00;ss}^{000}(k)} \right] . \end{aligned} \quad (3.42a)$$

The small  $k$  behaviour of  $\tilde{h}_{00;ij}^{000}(k)$  (an apparent  $1/k^2$  divergence) will dominate this expression, and so it follows that  $\tilde{h}_{00;as}^{000}(k)$  must also have the same small  $k$  dependence. Therefore, at large  $r$  we can write that

$$h_{00;is}^{000}(r) \rightarrow a_{is} \rho_2 h_{+-}(r) \quad (3.42b)$$

and

$$h_{00;ss}^{000}(r) \rightarrow a_{ss} \rho_2^2 h_{+-}(r) , \quad (3.42c)$$

where  $a_{as}$  is a constant dependent on the values of  $\tilde{c}_{00;as}^{000}(k)$  at small  $k$ . We remark that if  $c_{00;+s}^{000}(r) = c_{00;-s}^{000}(r)$  (i.e., the ions are solvated equivalently), then  $a_{as} = 0$ . The long-range tails in  $h_{00;as}^{000}(r)$  that are a result of eqs. (3.42b) and (3.42c) will be discussed in more detail in later chapters.

Inspection of eqs. (3.41) and (3.36a) shows that at low concentration  $G_{+S} = G_{-S}$  will have a term due to  $\rho_2 G_{+-}$  which varies like  $\sqrt{\rho_2}$ . We might also expect  $C_{iS}$  ( $i = +$  or  $-$ ) to have a  $\sqrt{\rho_2}$  dependence at low concentration, so we write

$$C_{IS} \equiv \nu_+ C_{+S} + \nu_- C_{-S} = (\nu_+ C_{+S}^0 + \nu_- C_{-S}^0) + S_c \sqrt{\rho_2} + \dots, \quad (3.43)$$

where the superscript  $o$  indicates the infinite dilution result. It is not possible, at present, to obtain an exact expression for the slope  $S_c$ . However, the HNC equation (2.62a) can be used to find an approximate form for  $S_c$ .

We start by expanding the logarithm in eq. (2.62a) for large  $r$  and using eq. (2.25), which immediately yields the result

$$c_{a\beta}(12) \rightarrow \frac{1}{2}[h_{a\beta}(12)]^2 - \beta u_{a\beta}(12) \quad \text{as } r \rightarrow \infty. \quad (3.44)$$

We then expand  $c(12)$ ,  $h(12)$ , and  $u(12)$  in rotational invariant as in Chapter II. It is possible to deduce, with that aid of eq. (3.42b), that as  $\rho_2 \rightarrow 0$  and  $r \rightarrow \infty$ ,

$$c_{00;is}^{000}(r) \rightarrow \frac{1}{6}[h_{00;is}^{011}(r)]^2 - \beta u_{00;is}^{000}(r). \quad (3.45)$$

Thus for nonpolarizable particles the first term in eq. (3.45) is the leading concentration dependent term and it is sufficient to determine the limiting HNC slope for  $C_{iS}$ . It is known from the work of Høye and Stell [61,152] that in the limits  $\rho_2 \rightarrow 0$  and  $r \rightarrow \infty$ ,

$$h_{00;is}^{011}(r) \rightarrow \beta \left[ \frac{\epsilon-1}{\epsilon} \right] \left[ \frac{q_i \mu}{3y} \right] \frac{1+\kappa r}{r^2} e^{-\kappa r}, \quad (3.46)$$

where  $y$  has been defined in eq. (2.93b). Now substituting eqs. (3.45) and (3.46) into eq. (3.39b), it is possible to show, after considerable manipulation (see Appendix B), that as  $\rho_2 \rightarrow 0$ ,

$$C_{iS} \rightarrow C_{iS}^0 - \left[ \pi \beta^2 \left[ \frac{\epsilon-1}{\epsilon} \right]^2 \frac{q_i^2 \mu^2}{9y^2} \right] \kappa + \dots. \quad (3.47)$$



Combining eqs. (3.43) and (3.47) along with eq. (3.35c), and then rearranging gives

$$S_c = \frac{-A\nu^{\frac{3}{2}}(\epsilon-1)^2}{\rho_s \gamma \epsilon} . \quad (3.48)$$

Again we note that eq. (3.48) is approximate, and furthermore holds only for fluids of nonpolarizable particles. The accuracy of the HNC estimate for  $S_c$  will be discussed below.

From eqs. (3.36a), (3.41) and (3.43) we have the limiting law

$$G_{+s} = G_{-s} = G_{+s}^{0+} + \left[ \frac{S_c}{\nu} + \frac{A}{\sqrt{\nu}}(\nu_+ C_{+s}^0 + \nu_- C_{-s}^0) \right] \sqrt{\rho_2} , \quad (3.49a)$$

where

$$G_{+s}^{0+} = G_{-s}^{0+} = \lim_{\rho_2 \rightarrow 0^+} G_{+s} = \frac{\nu_+ C_{+s}^0 + \nu_- C_{-s}^0}{\nu(1 - \rho_s C_{ss}^0)} . \quad (3.49b)$$

We point out that  $\rho_2 \rightarrow 0^+$  is the appropriate limit here since eq. (3.41) holds only for  $\rho_2 > 0$ .

It is interesting to apply the infinite dilution limit (*i.e.*,  $\rho_+ = \rho_- = 0$ ) to eqs. (3.40) to obtain

$$G_{+s}^0 = \frac{C_{+s}^0}{1 - \rho_s C_{ss}^0} \quad (3.50a)$$

and

$$G_{-s}^0 = \frac{C_{-s}^0}{1 - \rho_s C_{ss}^0} . \quad (3.50b)$$

It is obvious that these expressions do not agree with eq. (3.49b), and hence  $G_{+s}$  and  $G_{-s}$  must be discontinuous at  $\rho_2 = 0$ . Moreover, it follows from eqs. (3.49b) and (3.50) that

$$G_{+s}^{0+} = G_{-s}^{0+} = (\nu_+ G_{+s}^0 + \nu_- G_{-s}^0) / \nu . \quad (3.51)$$

Clearly,  $G_{+s}^{0+}$  and  $G_{-s}^{0+}$  are just the weighted averages of  $G_{+s}^0$  and  $G_{-s}^0$ . In terms of the Fourier transforms,  $\tilde{h}_{00;is}^{000}(k)$  ( $i = +$  or  $-$ ), this discontinuous behaviour can be expressed in the form

$$\lim_{\rho_2 \rightarrow 0} \lim_{k \rightarrow 0} \tilde{h}_{00;is}^{000}(k) \neq \lim_{k \rightarrow 0} \lim_{\rho_2 \rightarrow 0} \tilde{h}_{00;is}^{000}(k) . \quad (3.52)$$

The left and right hand sides of eq. (3.52) give eqs. (3.49a) and (3.50), respectively. We note that this discontinuous behaviour in  $G_{a\beta}$  (for a charged-uncharged pair) was also indicated in earlier considerations [149] of this function at the second virial coefficient level.

The limiting form for  $G_{ss}$  can also be obtained by considering the OZ equation as expressed by eq. (3.39a). It can be shown that

$$G_{ss} = \frac{(\rho_+ C_{+s} + \rho_- C_{-s})G_{+s} + C_{ss}}{1 - \rho_s C_{ss}} , \quad (3.53)$$

from which it follows that at low concentration

$$G_{ss} = \frac{C_{ss}^0}{1 - \rho_s C_{ss}^0} + O(\rho_2) . \quad (3.54)$$

We also point out that

$$\frac{1}{1 - \rho_s C_{ss}^0} = 1 + \rho_s G_{ss}^0 = \rho_s kT \chi_T^0 , \quad (3.55)$$

where  $\chi_T^0$  is the isothermal compressibility of the pure solvent. Equation (3.55) is a well known result [27], which can be obtained from the one component limit of eq. (3.3d) or from the  $\rho_2 \rightarrow 0$  limit of eq. (3.20).

We can now examine the limiting behaviours of the thermodynamic functions discussed in the previous section. First let us consider the mean activity coefficient. Substituting eqs. (3.36a), (3.49a) and (3.54) into eqs. (3.30), it can be shown that in the limit  $\rho_2 \rightarrow 0$ ,

$$\left[ \frac{\partial \ln \gamma_{\pm}}{\partial \rho_2} \right]_{T, \rho_s} \rightarrow \left[ \frac{\partial \ln \gamma_{\pm}}{\partial \rho_2} \right]_{T, P} \rightarrow \frac{-A\sqrt{\nu}}{\sqrt{\rho_2}} . \quad (3.56)$$

Equation (3.56) agrees with the derivative of the usual Debye-Hückel limiting law [6] for  $\ln \gamma_{\pm}$ , where it follows from the discussion in the previous section that the limiting law for the mean activity coefficients must be independent of the concentration scale.

Now let us consider the limiting behaviour of the derivative of the osmotic pressure. Combining eqs. (3.33) and (3.36a) we immediately obtain

$$\frac{1}{kT} \left[ \frac{\partial \Pi}{\partial \rho_2} \right]_{T, \mu_s} \rightarrow \frac{\nu}{1 + A\sqrt{\nu \rho_2}} \rightarrow \nu(1 - A\sqrt{\nu \rho_2}) . \quad (3.57)$$

We recall [150] that the osmotic pressure is a measure of the change in chemical potential of the solvent due to the presence of the salt. A more frequently used measure of the solvent chemical potential is the osmotic coefficient [6,7],  $\phi$ , defined by

$$\phi = \frac{-1000}{\nu M_s m} \ln a_s , \quad (3.58)$$

where  $M_s$  is the molecular weight of the solvent,  $m$  is the concentration in molality and  $a_s$  is the solvent activity. If we assume the solvent is incompressible over the pressure change of  $\Pi$ , then the osmotic pressure is related [6,7] to the osmotic coefficient by

$$\Pi = \frac{\nu k T M_s}{1000 \bar{V}_s} \phi m . \quad (3.59)$$

The limiting law for  $\phi$  (cf. eq. (3-5-12) of Ref. [6]) can be written as

$$\phi \rightarrow 1 - \frac{2}{3} A \sqrt{\nu \rho_2} \quad \text{as } \rho_2 \rightarrow 0 . \quad (3.60)$$

At very low concentration eq. (3.59) can be rearranged to give

$$\Pi = \nu k T \phi \rho_2 . \quad (3.61)$$

Now substituting eq. (3.60) into (3.61) and taking the derivative with respect to  $\rho_2$ , we again obtain eq. (3.57). Clearly, the limiting behaviours of the osmotic pressure and of the osmotic coefficient are simply related.

The limiting behaviour of the partial molecular volume,  $\bar{V}_2$ , is of particular importance and requires careful attention. From eq. (3.15) and the limiting expressions (3.36a), (3.49a) and (3.54), it is possible to show that as  $\rho_2 \rightarrow 0$ ,

$$\bar{V}_2 \rightarrow \left[ \frac{1 + \rho_s G_{ss}^0}{\rho_s \rho_2 G_{+-}} \right] - \frac{G_{+s}}{\rho_2 G_{+-}} , \quad (3.62a)$$

or using eq. (3.41)

$$\bar{V}_2 \rightarrow \left[ \frac{1 + \rho_s G_{ss}^0}{\rho_s \rho_2 G_{+-}} \right] - \left[ \frac{\nu_+ C_{+s} + \nu_- C_{-s}}{1 - \rho_s C_{ss}^0} \right] . \quad (3.62b)$$

Now applying eqs. (3.36a), (3.43) and (3.55) we obtain the limiting law expression

$$\bar{V}_2 = \bar{V}_2^0 + S_V \sqrt{\rho_2} , \quad (3.63)$$

where

$$\bar{V}_2^0 = \nu_+ kT \chi_T^0 (1 - \rho_s C_{+s}^0) + \nu_- kT \chi_T^0 (1 - \rho_s C_{-s}^0) \quad (3.64a)$$

$$= \nu kT \chi_T^0 - \rho_s kT \chi_T^0 (\nu_+ C_{+s}^0 + \nu_- C_{-s}^0) \quad (3.64b)$$

and

$$S_V = AkT\nu^{\frac{3}{2}} \left[ -\chi_T^0 - \frac{\chi_T^0 \rho_s S_C}{A\nu^{\frac{3}{2}}} \right] . \quad (3.65)$$

We remark that as one would expect,  $\bar{V}_2^0$  splits into two independent terms which depend upon the interaction of the positive and negative ions with the solvent (*cf.* eq. (3.64a)). It is also interesting to note that  $\bar{V}_2^0$  can be written as the sum of two terms, only one of which depends upon the ion-solvent interactions, as in eq. (3.64b).

It is very instructive to compare eq. (3.65) with the exact macroscopic (*i.e.*, Debye-Hückel) result for  $S_V$ , which can be expressed in the form [6]

$$S_V = AkT\nu^{\frac{3}{2}} \left[ -\chi_T^0 + 3 \left[ \frac{\partial \ln \epsilon}{\partial P} \right]_T \right] , \quad (3.66)$$

where again  $\epsilon$  is the pure solvent dielectric constant. Clearly, our microscopic result for  $S_V$ , as given by eq. (3.65), is functionally equivalent to eq. (3.66). Comparing eqs. (3.65) and (3.66) we obtain the differential equation

$$\left[ \frac{\partial \ln \epsilon}{\partial P} \right]_T = \frac{-x_T^0 \rho_S S_C}{3A\nu^{\frac{3}{2}}} . \quad (3.67)$$

If we introduce the identity

$$\left[ \frac{\partial \ln \epsilon}{\partial P} \right]_T = \frac{1}{\epsilon} \left[ \frac{\partial \epsilon}{\partial \rho_S} \right]_T \rho_S x_T^0 , \quad (3.68)$$

which follows from eq. (3.18), we can then rewrite eq. (3.67) as

$$\frac{1}{\epsilon} \left[ \frac{\partial \epsilon}{\partial \rho_S} \right]_T = \frac{-S_C}{3A\nu^{\frac{3}{2}}} . \quad (3.69)$$

We note that at least for systems characterized by pairwise additive potentials, eqs. (3.67) and (3.69) are exact expressions.

If the HNC result for  $S_C$  (*i.e.*, eq. (3.48)) is substituted into eq. (3.69), then we obtain the differential equation

$$\left[ \frac{\partial \epsilon}{\partial \rho_S} \right]_T = \frac{(\epsilon - 1)^2}{3\rho_S y} . \quad (3.70)$$

This is exactly the equation obtained by Rasaiah *et al.* [153] in their consideration of electrostriction in polar fluids at the HNC level. Equation (3.70) integrates to give [153]

$$\frac{\epsilon - 1}{\epsilon + 2} = y , \quad (3.71)$$

which is the Debye approximation for the dielectric constant [61] of the pure solvent. Of course, eq. (3.71) is not a very accurate theory and overestimates  $\epsilon$ . This means that one cannot expect the HNC theory to give very accurate values for  $S_V$  since the HNC approximation appears to overestimate the effect of electrostriction. Rasaiah [154] has shown that when bridge diagrams missing in the HNC approximation are included in the closure, improved results are obtained.

In the LHNC theory, it clearly follows from eq. (2.74a) and eqs. (3.39b) and (3.43) that  $S_C = 0$ . As discussed earlier, this is a result of the lack of coupling between the anisotropic potential terms and the radial distribution function in the LHNC closure equation. This is consistent with the observation of Rasaiah *et al.* [153] that the LHNC approximation does not predict

electrostriction in polar fluids.

We now examine the low concentration behaviour of the partial molecular volume of the solvent,  $\bar{V}_s$ . First we rewrite eq. (3.17a) as

$$\bar{V}_s = \frac{1}{\rho_s} (1 - \rho_2 \bar{V}_2) . \quad (3.72)$$

Then inserting eq. (3.63) into eq. (3.72) one immediately has the limiting law

$$\bar{V}_s = \frac{1}{\rho_s} (1 - \rho_2 \bar{V}_2^0) . \quad (3.73)$$

Clearly,  $\bar{V}_s$  has a linear dependence on  $\rho_2$  at low concentration and its limiting slope will be almost totally determined by  $\bar{V}_2^0$  unless  $\rho_s$  has a strong  $\rho_2$  dependence.

Finally, from eqs. (3.20), (3.36a), (3.49a) and (3.54) we can show that at low concentration

$$\chi_T \rightarrow \chi_T^0 + O(\rho_2) . \quad (3.74)$$

Thus we find that the compressibility also has a  $\rho_2$  dependence in the limit  $\rho_2 \rightarrow 0$ .

It also possible to deduce limiting laws for some of the average energy terms. In order to simplify the expressions slightly, we will consider only symmetric electrolytes (*i.e.*,  $\nu_+ = \nu_- = 1$ ). Using eq. (2.81a), eq. (2.10b), and eqs. (3.34), (3.35) and (3.46) we can show that at low concentration

$$\frac{U_{II}}{N_i} = -2 \left[ \frac{2\pi\beta}{\epsilon} \right]^{\frac{1}{2}} |q_+ q_-|^{\frac{3}{2}} \sqrt{\rho_2} \quad (3.75)$$

and

$$\frac{U_{iD}}{N_i} = \frac{U_{iD}^0}{N_i} + 2 \left[ \frac{\epsilon-1}{\epsilon} \right] \left[ \frac{2\pi\beta}{\epsilon} \right]^{\frac{1}{2}} |q_+ q_-|^{\frac{3}{2}} \sqrt{\rho_2} , \quad (3.76)$$

where  $U_{II}/N_i$  is the total average ion-ion energy per ion and  $U_{iD}/N_i$  is the average ion-dipole energy per ion. In a similar manner, we can obtain an expression for the dipole-dipole energy by inserting the long-range low concentration form for  $h_{00;ss}^{112}(r)$  (*cf.* eq. (2.35a) and Ref. 61) into eq. (2.81a). Integrating and then simplifying yields the result

$$\frac{U_{DD}}{N_i} = \frac{U_{DD}^0}{N_i} + \frac{3}{d_s} \left[ \frac{\epsilon-1}{\epsilon} \right]^2 |q_+ q_-|^{\frac{3}{2}} - 4 \left[ \frac{\epsilon-1}{\epsilon} \right]^2 \left[ \frac{2\pi\beta}{\epsilon} \right]^{\frac{1}{2}} |q_+ q_-|^{\frac{3}{2}} \sqrt{\rho_2} . \quad (3.77)$$

It is interesting to note that for systems in which the pure solvent has a large dielectric constant, the limiting slopes of the first two energy terms, *i.e.*, eqs. (3.75) and (3.76), are almost equal in magnitude but opposite in sign. The limiting slope of the dipole-dipole energy (the last term in eq. (3.77)) is also very similar in form, and since there are two ionic species present, it will be almost cancelled by the two ion-dipole terms.

In subsequent chapters, in particular Chapter VI, we will use the expressions derived in section 2 of this chapter to compute the various thermodynamic properties of the electrolyte solutions being studied. We will also test the validity of the limiting laws given in this section and examine the ranges over which they hold.

## CHAPTER IV

### MEAN FIELD THEORIES FOR POLARIZABLE PARTICLES

#### 1. Introduction

In Chapter II we have developed a theoretical approach and the necessary methodology with which to study liquid systems of several components. One requirement of this theory was that the total interaction potential of the system contain only pairwise additive terms (*cf.* eq. (2.2)). As mentioned earlier, most statistical mechanical studies of fluid systems [33] use only pair potentials to describe the interactions within the systems being investigated. However, recent studies of polar-polarizable fluids using both approximate theories [61,67,155-158] and computer simulations [158-162] have shown that the many-body interactions due to molecular polarizability are important in determining the equilibrium properties of the systems. The importance of polarization effects in water [35-38,67] and in electrolyte solutions [38,54] is now well known. Thus, in this study we have chosen to include polarizability in the models we will consider.

In general, the many-body problem of polarizability is difficult to treat. In the current theoretical framework (*i.e.*, the RHNC theory as described in Chapter II) it is not possible to treat it exactly. Fortunately, recent work [61,67,156] has demonstrated that it is possible to take into account the influence of many-body interactions due to polarizability through effective pair potentials. The self-consistent mean field (SCMF) approximation [67] has been shown [158,163] to be an accurate means of reducing the many-body potential when applied to a fluid of polarizable particles with dipole and square quadrupole moments. For purely dipolar fluids, the SCMF approximation is equivalent to the 1-R theory of Wertheim [156]. Unlike other methods, however, the SCMF theory uses approximations that are distinctly physical in nature. It is also easily generalized to include contributions to the average local electric field from higher order multipole moments. In section 2 of this chapter, we will extend the SCMF theory of Carnie and Patey [67] to include ion and octupole terms in order to facilitate its application to the systems being studied here.



In the SCMF theory the pairwise additive potentials, which result from the reduction of the many-body interactions of a polarizable system, are written in terms of an effective permanent dipole moment,  $m_e$ , as described below. This effective dipole moment is an average molecular property of the system, that is, it is the same for all molecules. It will depend upon the polarizability and permanent multipole moments of the model, as well as upon other properties of the model and the state parameters of the system. Within the SCMF approximation, the systems characterized by this effective dipole moment will have the same structural and dielectric properties as the true polarizable fluid.

The SCMF theory has been previously used [79-81] in the study of model electrolyte solutions at infinite dilution. There the effective moment,  $m_e$ , must simply be that of the pure solvent. At finite concentrations we might expect the effective dipole moment to vary due to the presence of the ions and the resulting changes in the solvent structure. We know that at small separations ( $\sim 3\text{\AA}$ ) an ion is surrounded by an intense electric field ( $\sim 10^8 \text{V/cm.}$ ) which will greatly alter the local solvent structure. Hence, the average local solvent electric field might be expected to change appreciably. Moreover, we would also expect an ion itself to significantly alter the local field in its immediate vicinity. Thus it would be very interesting to be able to examine the average local electric field experienced by a solvent molecule in solution as a function of its separation,  $R$ , from an ion, and thereby determine the  $R$ -dependence of the average dipole moment of a solvent molecule.

If we consider an ion and only one polarizable solvent molecule, it can be shown [139,140] that the dipole moment,  $p$ , induced in the molecule will be given by

$$p = aq/r^2, \quad (4.1a)$$

where

$$a = \frac{1}{3} \text{Tr } \underline{a} \quad (4.1b)$$

is the isotropic polarizability of the molecule,  $\underline{a}$  being its polarizability tensor, and  $q$  is the charge on the ion. It immediately follows that the interaction between the charge and the induced moment is

$$u_{qp}(r) = \frac{-aq^2}{2r^4} . \quad (4.1c)$$

However, in solution an ion is surrounded by more than one solvent molecule. These molecules will order in some fashion around the ion, and this must give rise to local changes in the electric field around the ion. At finite concentration the ion will also be surrounded by other ions which will tend to screen its charge and again alter the local electric field. Thus, we would expect eqs. (4.1a) and (4.1c) to be poor approximations in a dense system such as an electrolyte solution.

In this chapter we will describe two different levels of theory in which a polarizable solvent may be studied. The first is the SCMF approximation [67] which we will outline in section 2. In section 3 of this chapter we will develop a second and more detailed formalism through which we can estimate the average local field experienced by a solvent at a distance  $R$  from an ion. As in the SCMF theory, we will follow a mean field approach (*i.e.*, we will ignore fluctuations). This  $R$ -dependent mean field (RDMF) theory gives rise to an effective spherical potential between the ion and the solvent at  $R$ . Moreover, this spherical potential is found to have an effect on the limiting laws for thermodynamic quantities, such as  $\bar{V}_2$ , which depend upon the ion-solvent correlations.

## **2. The Self-Consistent Mean Field Theory**

The SCMF theory of Carnie and Patey [67] reduces the many-body problem of polarization into a problem involving an effective pairwise additive potential. It does so by ignoring fluctuations in the local electric field. The following is simply an extension of the SCMF approximation [67] to include octupole and ion field contributions thus making it applicable to the systems of interest in this study.

In general, we will consider a system which contains three molecular species, one of these being a polar-polarizable solvent. The two ionic species, designated  $+$  and  $-$ , are assumed to be simple spherical ions possessing only charges and no higher order multipole moments. The polarizability of these

ions must also be spherically symmetric. When solvated, these ions will experience no net average polarization since the average electric field generated at the centre of such an ion by the surrounding solvent must be zero. Therefore, we can ignore the polarizability of simple spherical ions at a mean field level. (Of course, we have already chosen to ignore all dispersion terms for the models we will consider.)

For the solvent, we start by writing the total instantaneous dipole moment of the  $j^{\text{th}}$  solvent molecule as

$$\underline{m}_j = \underline{\mu}_j + \underline{p}_j , \quad (4.2a)$$

where  $\underline{\mu}_j$  is the permanent dipole moment of the solvent,

$$\underline{p}_j = \underline{a} \cdot (\underline{E}_1)_j \quad (4.2b)$$

is the instantaneous induced dipole moment and  $(\underline{E}_1)_j$  is the total instantaneous electric field felt by the solvent  $j$ . If we let  $\langle \underline{E}_1 \rangle$  be the average electric field experienced by a solvent molecule, then the average total dipole moment,  $\langle \underline{m} \rangle = \underline{m}'$ , (measured in the molecular frame) of each molecule is given by

$$\underline{m}' = \underline{\mu} + \underline{a} \cdot \langle \underline{E}_1 \rangle . \quad (4.3)$$

For molecules of  $C_{2v}$  (or higher) symmetry in an isotropic fluid, we know that  $\langle \underline{E}_1 \rangle$  will be non-zero only in the direction of  $\underline{\mu}$ . This immediately implies that  $\underline{\mu}$ ,  $\langle \underline{E}_1 \rangle$  and  $\underline{m}'$  are all in the same direction. As a result, we can write

$$\langle \underline{E}_1 \rangle = C(m') \underline{m}' , \quad (4.4)$$

where the scalar  $C(m')$  will depend upon the properties of the system. If one inserts eq. (4.4) into eq. (4.3) and then iterates the result with itself, one obtains

$$\underline{m}' = \underline{\mu} + C(m') \underline{a}' \cdot \underline{\mu} , \quad (4.5a)$$

where we define

$$\underline{a}' = \underline{a} + C(m') \underline{a} \cdot \underline{a}' \quad (4.5b)$$

as being a renormalized polarizability. This renormalized polarizability of a

molecule in a fluid of polarizable particles plays the same role as  $\underline{a}$  does for an isolated molecule. It will describe the fluctuations of the total dipole moment of a polarizable molecule in solution about its mean value and thus one can write

$$\begin{aligned}\langle m^2 \rangle &= m'^2 + (\langle p^2 \rangle - \langle p \rangle^2) \\ &= m'^2 + 3a'kT, \end{aligned} \quad (4.6a)$$

where

$$a' = \frac{1}{3} \text{Tr } \underline{a}' \quad (4.6b)$$

and  $\langle m^2 \rangle$  is just the mean square dipole moment of the solvent.

In order to determine an expression for the scalar  $C(m')$ , we now examine the configurational energy of the polarizable system. For the system we are considering, the instantaneous configurational energy is given by

$$\begin{aligned}u_N &= u_{HS} + u_{II} + u_{IQ} + u_{IO} + u_{QQ} + u_{QO} + u_{OO} - \frac{1}{2} \sum_j \underline{m}_j \cdot (\underline{E}_{1D})_j \\ &\quad - \sum_j \underline{m}_j \cdot (\underline{E}_{1Q})_j - \sum_j \underline{m}_j \cdot (\underline{E}_{1O})_j - \sum_j \underline{m}_j \cdot (\underline{E}_{1I})_j + \frac{1}{2} \sum_j \underline{p}_j \cdot (\underline{E}_1)_j, \quad (4.7)\end{aligned}$$

in which the sums over  $j$  are over the number of solvent molecules,  $N_s$ , and where

$$(\underline{E}_1)_j = (\underline{E}_{1D})_j + (\underline{E}_{1Q})_j + (\underline{E}_{1O})_j + (\underline{E}_{1I})_j. \quad (4.8)$$

$\underline{E}_{1D}$ ,  $\underline{E}_{1Q}$ ,  $\underline{E}_{1O}$  and  $\underline{E}_{1I}$  are the dipolar, quadrupolar, octupolar and total ionic field contributions, respectively. In eq. (4.7)  $u_{HS}$  is the instantaneous hard-sphere energy and  $u_{II}$ ,  $u_{IQ}$ ,  $u_{IO}$ ,  $u_{QQ}$ ,  $u_{QO}$  and  $u_{OO}$  are the total instantaneous ion-ion, ion-quadrupole, ion-octupole, quadrupole-quadrupole, quadrupole-octupole and octupole-octupole energies, respectively. The first term of the second line of eq. (4.7) is the total dipole-dipole contribution to the energy, followed by the dipole-quadrupole, dipole-octupole and total ion-dipole terms. The last term in eq. (4.7) is the energy of polarization. Since all the solvent molecules present are equivalent, the total average energy can be expressed as

$$U_{TOT} = U^\dagger - \frac{1}{2}N_S \langle \underline{\mu} \cdot \underline{E}_{1D} \rangle - N_S \langle \underline{\mu} \cdot \underline{E}_{1Q} \rangle - N_S \langle \underline{\mu} \cdot \underline{E}_{1O} \rangle - N_S \langle \underline{\mu} \cdot \underline{E}_{1I} \rangle \\ - \frac{1}{2}N_S \langle \underline{p} \cdot \underline{E}_{1Q} \rangle - \frac{1}{2}N_S \langle \underline{p} \cdot \underline{E}_{1O} \rangle - \frac{1}{2}N_S \langle \underline{p} \cdot \underline{E}_{1I} \rangle , \quad (4.9a)$$

where

$$U^\dagger = U_{HS} + U_{II} + U_{IQ} + U_{IO} + U_{QQ} + U_{QO} + U_{OO} . \quad (4.9b)$$

In the SCMF theory one ignores fluctuations in the electric field and assumes that  $\langle \underline{p} \cdot \underline{E}_1 \rangle = \langle \underline{p} \rangle \cdot \langle \underline{E}_1 \rangle$ . Using this assumption and the fact that for molecules of  $C_{2v}$  symmetry the average electric field must always be directed along the permanent dipole moment, we can rewrite eq. (4.9a) in the form

$$U_{TOT} = U^\dagger - \frac{1}{2}N_S \mu \langle E_{1D} \rangle - \frac{1}{2}N_S (m' + \mu) \left[ \langle E_{1Q} \rangle + \langle E_{1O} \rangle + \langle E_{1I} \rangle \right] . \quad (4.10)$$

If we now let

$$C(m') = C_D(m') + C_Q(m') + C_O(m') + C_I(m') , \quad (4.11)$$

then it clearly follows from eqs. (4.4) and (4.8) that

$$\langle \underline{E}_{1D} \rangle = C_D(m') \underline{m}' , \quad (4.12a)$$

$$\langle \underline{E}_{1Q} \rangle = C_Q(m') \underline{m}' , \quad (4.12b)$$

$$\langle \underline{E}_{1O} \rangle = C_O(m') \underline{m}' \quad (4.12c)$$

and

$$\langle \underline{E}_{1I} \rangle = C_I(m') \underline{m}' . \quad (4.12d)$$

Inserting eqs. (4.12) into eq. (4.10) yields

$$U_{TOT} = U^\dagger - \frac{1}{2}N_S \mu m' C_D(m') \\ - \frac{1}{2}N_S m' (m' + \mu) \left[ C_Q(m') + C_O(m') + C_I(m') \right] . \quad (4.13)$$

To obtain estimates for the average local fields, or for  $C(m')$ , we now define an effective system characterized by an effective pair potential. This system should have very similar structure to the polarizable system (the structures must become identical if fluctuations are unimportant), and hence one assumes that they will have the same local fields. For this effective system the instantaneous configurational energy will be given by

$$u_N = \sum_{j < k} u_{jk}(12) + \sum_j \frac{p_j^2}{2a}, \quad (4.14)$$

where the sum over  $j$  and  $k$  is over all particles of all species present. The second term in eq. (4.14) represents the polarization energy which will be non-zero only for solvent molecules. The pair potential,  $u_{jk}(12)$ , is described in detail in Chapter II. Of importance here are the terms (as given by eq. (2.10b) and eqs. (2.17), (2.19) and (2.20)) which involve the dipole moment, including

$$u_{00;ss}^{112}(r) = -\sqrt{10/3} \left[ \frac{m_j m_k}{r^3} \right], \quad (4.15a)$$

$$u_{00;ss}^{123}(r) = -\sqrt{7} \left[ \frac{m_j \Theta_{zz}}{r^4} \right], \quad (4.15b)$$

$$u_{00;ss}^{134}(r) = -\sqrt{12} \left[ \frac{m_j \Omega_{zzz}}{r^5} \right] \quad (4.15c)$$

and

$$u_{00;is}^{011}(r) = \frac{q_j m_k}{r^2}, \quad (4.15d)$$

where  $m_j$  and  $m_k$  are the total instantaneous dipole moments of solvents  $j$  and  $k$ . To facilitate the simplification of the pair potential, one again ignores fluctuations in the local field. In eq. (4.14) we replace  $p_j^2$  by  $\langle p^2 \rangle$ . Consequently, the polarization energy becomes a constant term which can be dropped without altering the physics of the effective system. In eq. (4.15a) we use

$$m_j m_k = \langle m^2 \rangle = m_e^2, \quad (4.16)$$

where  $m_e$  is an effective permanent dipole moment. In all other potential

terms involving the dipole moment (*e.g.*, eqs. (4.15b)-(d)), one could replace  $m_j$  by  $m'$ . However, the effective potential would then involve two parameters,  $m'$  and  $m_e$ , and considerable effort would be required to determine the self-consistent average local field for the polarizable system. Therefore it is convenient, from a computational viewpoint, to ignore the difference between  $m'$  and  $m_e$  (for the systems we will consider this difference is only 2-4%) and to use  $m_e$  in place of  $m'$  in the effective pair potential. Thus the pair potential of the effective system becomes equivalent to that of a nonpolarizable system in which we have replaced the permanent dipole moment by  $m_e$ .

We have yet to determine an explicit form for  $C(m')$ . For the effective system we know that

$$U_{DD}^e = -\frac{1}{2}N_s m_e \langle E_{1D} \rangle^e, \quad (4.17a)$$

$$U_{DQ}^e = -N_s m_e \langle E_{1Q} \rangle^e, \quad (4.17b)$$

$$U_{DO}^e = -N_s m_e \langle E_{1O} \rangle^e \quad (4.17c)$$

and

$$U_{ID}^e = -N_s m_e \langle E_{1I} \rangle^e, \quad (4.17d)$$

where the superscript  $e$  indicates the effective system. Since the effective and polarizable systems are assumed to have the same structure, it immediately follows that

$$\langle E_{1Q} \rangle^e = \langle E_{1Q} \rangle \quad (4.18a)$$

and similarly for  $\langle E_{1O} \rangle$  and  $\langle E_{1I} \rangle$ , but

$$\langle E_{1D} \rangle^e = \frac{m_e}{m'} \langle E_{1D} \rangle. \quad (4.18b)$$

Combining eqs. (4.18) and eqs. (4.17) and then using eqs. (4.12), one simply rearranges to obtain the desired expressions

$$C_D(m') = \frac{-2U_{DD}^e}{N_s m_e^2}, \quad (4.19a)$$

$$C_Q(m') = \frac{-U_{DQ}^e}{N_s m_e m'} , \quad (4.19b)$$

$$C_O(m') = \frac{-U_{DO}^e}{N_s m_e m'} \quad (4.19c)$$

and

$$C_I(m') = \frac{-U_{ID}^e}{N_s m_e m'} . \quad (4.19d)$$

We note that although the effective and polarizable systems have the same structure, their total average energies must be different since in the effective system we have ignored the polarization energy. Substituting eqs. (4.19) into eq. (4.13) we find that the energy of the polarizable fluid is given by

$$U_{TOT} = U^\dagger + \frac{\mu m'}{m_e} U_{DD}^e + \frac{m' + \mu}{2m_e} [U_{DQ}^e + U_{DO}^e + U_{ID}^e] . \quad (4.20)$$

Patey *et al.* [163] have also shown that the dielectric constant,  $\epsilon$ , of the polarizable system is simply that of the effective system and does not depend upon the method used to obtain the properties of the effective system.

In order to solve the SCMF theory, we must first determine the average energies of the effective system at several values of  $m_e$  while all other parameters are held fixed. Of course, in this study we employ the RHNC theory, as described in Chapter II, to perform this task. The energies must then be accurately fit to interpolating curves (here we have used cubic splines [134]) so that  $C(m')$  is known as a function of  $m_e$ . For given values of  $\mu$ ,  $\underline{a}$  and  $\chi_s = N_s/N$ , eqs. (4.5), (4.6) and (4.19) are solved iteratively, to give values of  $m'$ ,  $\underline{a}'$  and  $m_e$  that are consistent with the given molecular and state parameters.



### 3. The R-Dependent Mean Field Theory

The RDMF theory, as outlined below, is directly applicable only to solutions of spherically symmetric ions, although extensions to more general systems may be possible. In the following derivation we restrict ourselves to a tetrahedral solvent model, that is a solvent model with only a dipole and a square quadrupole, as described in Chapter II. For simplicity, we will again consider solutions of only a single salt in which the ions are spherically symmetric. Also, all particles will be treated as hard spheres where the hard-sphere contact distances,  $\bar{d}_{\alpha\beta}$ , are given by eq. (2.24b).

The problem we will be addressing will be that of an ion being immersed into a multipolar-polarizable solvent which may or may not contain other ions. The RDMF theory will examine the changes in the average local field which are a result of the presence of an ion. Considering only the case of a spherically symmetric ion allows us to take advantage of the fact that the fluid surrounding the ion must be isotropic from the viewpoint of the ion. Thus, we need only examine the dependence of the average local field upon  $R$ , the distance from the ion. Furthermore, all additional average fields generated in the surrounding fluid, due to the presence of the ion, must be directed radially at or away from the ion, and hence appear as though they are being produced by additional (screening) charges placed at the centre of the ion. We will determine the average local fields at  $R$  by considering the average interaction between the dipole of a solvent particle fixed at a distance  $R$  from the ion and all other particles in the system. The average interaction can then be easily related to the average local electric fields.

The electric field experienced by a solvent molecule at a distance  $R$  from an ion will, in general, have both ion and solvent components. For the electrolyte solutions being considered here, the average local electric field at  $R$  will be given by

$$\langle \underline{E}_1(R) \rangle = \langle \underline{E}_{1D}(R) \rangle + \langle \underline{E}_{1Q}(R) \rangle + \langle \underline{E}_{1I}(R) \rangle . \quad (4.21)$$

We point out that this expression is just an  $R$ -dependent analogue of eq. (4.8). We now rewrite eq. (4.21) in the form

$$\langle \underline{E}_1(R) \rangle = \langle \underline{E}_1 \rangle + \langle \Delta \underline{E}_1(R) \rangle , \quad (4.22a)$$

where  $\langle \underline{E}_1 \rangle$  is just the average local field of the bulk solution as given by the SCMF theory.  $\langle \Delta \underline{E}_1(R) \rangle$  is the correction to the bulk field when a solvent particle is at a distance  $R$  from an ion, that is to say, it gives the change in the average local field at  $R$  due to the presence of the ion. For the present system we can express this correction term as

$$\langle \Delta \underline{E}_1(R) \rangle = \langle \Delta \underline{E}_{1D}(R) \rangle + \langle \Delta \underline{E}_{1Q}(R) \rangle + \langle \Delta \underline{E}_{1I}(R) \rangle . \quad (4.22b)$$

As in the SCMF theory, we wish to determine the average total molecular dipole moment. In the present context, we have

$$\underline{m}'(R) = \underline{\mu} + \underline{a} \cdot \langle \underline{E}_1(R) \rangle , \quad (4.23)$$

where  $\underline{m}'(R)$  is the appropriate  $R$ -dependent quantity. Using eqs. (4.3) and (4.22a) it clearly follows that

$$\underline{m}'(R) = \underline{m}' + \underline{a} \cdot \langle \Delta \underline{E}_1(R) \rangle , \quad (4.24a)$$

which we then write as

$$\underline{m}'(R) = \underline{m}' + \Delta \underline{p}(R) , \quad (4.24b)$$

where  $\Delta \underline{p}(R)$  is the average excess induced moment given by

$$\Delta \underline{p}(R) = \underline{a} \cdot \langle \Delta \underline{E}_1(R) \rangle . \quad (4.25)$$

In the present theory we will find it convenient to express  $\langle \Delta \underline{E}_1(R) \rangle$  in an intermolecular reference frame in which the  $z$ -axis is along the ion-solvent vector. Hence, instead of eq. (4.25) we use

$$\Delta \underline{p}(R) = \underline{a} \langle \Delta \underline{E}_1(R) \rangle . \quad (4.26)$$

where the average polarizability,  $\underline{a}$ , of a solvent molecule is defined by eq. (4.1b). We point out that for the water molecule  $\underline{a}$  is nearly spherically symmetric [164], and therefore eq. (4.1b) will be a very good approximation. Also, since the present theory will be used in conjunction with the SCMF approximation,  $\underline{m}'$  should be replaced everywhere with  $\underline{m}_e$ , the effective permanent dipole moment.

We now define the additional ion-solvent interaction term due to  $\Delta p(R)$  as

$$u_{is}^{\Delta p}(12) = -\Delta p(R) \cdot \langle \Delta E_{1I}(R) \rangle - \Delta p(R) \cdot \left[ \langle \Delta E_{1D}(R) \rangle + \langle \Delta E_{1Q}(R) \rangle \right] + \frac{1}{2} \Delta p(R) \cdot \langle \Delta E_1(R) \rangle . \quad (4.27)$$

The first term in eq. (4.27) is the interaction between the excess induced moment and the excess ion field felt by a solvent at a distance  $R$ . The second term takes into account the interaction between the excess moment and the surrounding solvents, while the last term in eq. (4.27) is simply the polarization term. Since eq. (4.26) ensures that  $\Delta p(R)$  and  $\langle \Delta E_1(R) \rangle$  will always be in the same direction, eq. (4.27) can be written in the form

$$u_{is}^{\Delta p}(R) = -\frac{1}{2} \Delta p(R) \langle \Delta E_1(R) \rangle . \quad (4.28)$$

Finally, combining eqs. (4.26) and (4.28) yields the expression

$$u_{is}^{\Delta p}(R) = -[\Delta p(R)]^2 / 2a . \quad (4.29)$$

It is interesting to note that  $u_{is}^{\Delta p}(R)$  is a spherically symmetric interaction which will always be attractive relative to infinite separation.

We now have only to determine expressions for each term of eq. (4.22b) contributing to  $\langle \Delta E_1(R) \rangle$ . However, even for the current simplified model, this is a non-trivial task. In the present theory we will consider only those contributions which can be more easily characterized and which require knowledge of only the pair correlation functions. These terms should exactly (at the mean field level) determine the long-range behaviour of  $\langle \Delta E_1(R) \rangle$ . Hence the RDMF theory, as presented here, will be most accurate at large  $R$ . Moreover, since we would expect the long-range behaviour of  $\langle \Delta E_1(R) \rangle$  to be more important for electrolyte solutions at infinite dilution or low concentration, the RDMF theory should provide the best results for these systems. We also point out that our approximation for  $\langle \Delta E_1(R) \rangle$  is not unique and that others may be possible, particularly if 3-body correlation functions were available.

Let us first examine the simplest case, that of  $\langle \Delta \underline{E}_{1I}(R) \rangle$ , the average excess local ion field at a distance  $R$  from an ion. We will identify contributions from three terms, the first term being the direct term,  $\langle \Delta \underline{E}_{1q}(R) \rangle$ , due to the charge on the ion. The other two terms,  $\langle \Delta \underline{E}_{1+}(R) \rangle$  and  $\langle \Delta \underline{E}_{1-}(R) \rangle$ , are essentially screening terms and are due to all other positive and negative ions in the system. Therefore we write

$$\langle \Delta \underline{E}_{1I}(R) \rangle = \langle \Delta \underline{E}_{1q}(R) \rangle + \langle \Delta \underline{E}_{1+}(R) \rangle + \langle \Delta \underline{E}_{1-}(R) \rangle . \quad (4.30a)$$

It is obvious that

$$\langle \Delta \underline{E}_{1q}(R) \rangle = q_i / r^2 , \quad (4.30b)$$

where  $q_i$  is the charge on the ion, which we have labelled  $i$ , and  $\langle \Delta \underline{E}_{1q}(R) \rangle$  will always be directed along the vector joining the ion  $i$  and the solvent at  $R$ .

In order to determine the two other terms of eq. (4.30a), we will first examine the average interaction between the dipole moment of a solvent particle at  $R$ , which we will call the *reference* particle (see Figure 4), and all other ions (*i.e.*, excluding  $q_i$ ). Now we know that because the solvent molecule has  $C_{2v}$  symmetry, the average orientation of the total dipole moment of the reference solvent will be in the direction of  $\langle \Delta \underline{E}_{1q}(R) \rangle$  (*i.e.*, along the ion-solvent vector) and all other orientations will average to zero. Thus, if we ignore fluctuations we can define

$$\begin{aligned} \underline{m}^\dagger(R) &= \underline{m}'(R) \langle \Phi_{00}^{011}; i_s(R) \rangle \\ &= \underline{m}'(R) \langle \cos \theta_{is}(R) \rangle \end{aligned} \quad (4.31)$$

as the average projection of  $\underline{m}'(R)$  onto the ion-solvent vector, where  $\langle \cos \theta_{is}(R) \rangle$  is given by eqs. (2.89a) and (2.89b) and the angle  $\theta_{is}$  is illustrated in Figure 3. Again, we stress that in the intermolecular reference frame this will be the only non-zero projection of  $\underline{m}'(R)$ . If we can obtain an expression for the interaction between  $\underline{m}^\dagger(R)$  and a spherical shell of ions at a distance  $r$  from  $q_i$ , then we have only to integrate (*i.e.*, sum over all such shells) to obtain an expression for the total interaction. In Figure 4 we have illustrated the problem being considered and have indicated all the variables used in the derivation outlined below.

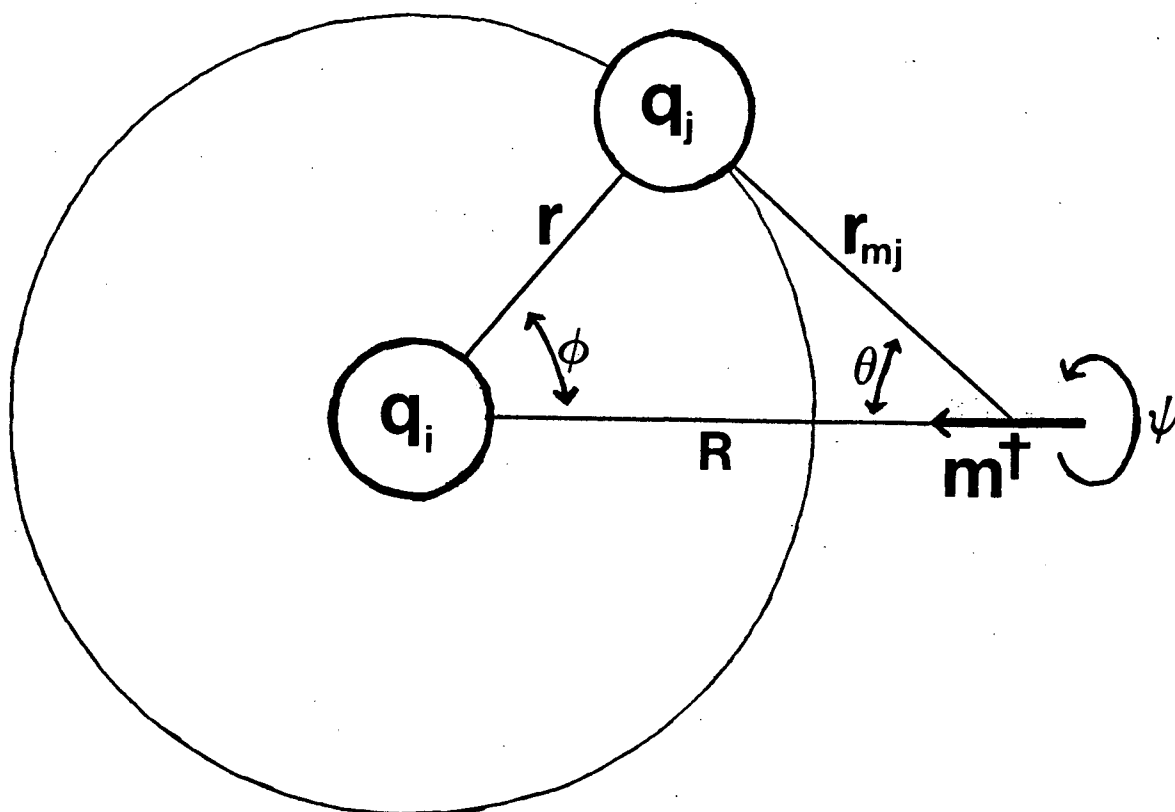


**Figure 4.** An illustration of the method used in determining  $\langle \Delta E_{1I}(R) \rangle$ . The case where  $q_i$  is a negative ion is shown. The dipole moment,  $m^\dagger$ , located at a distance  $R$  from the ion,  $q_i$ , is that of the reference solvent particle.

From eqs. (2.5) and (2.17) it is easy to show [79,81] that the interaction between  $\underline{m}^\dagger(R)$  and  $q_j$  is given by

$$u_{mj}(12) = \frac{m^\dagger(R) q_j}{r_{mj}^2} \Phi_{00}^{101}(12) , \quad (4.32)$$

when we take  $f^{mnl}$  as given by eq. (2.9a). Following the conventions given in Figures 3 and 4, and using an explicit form for the rotational invariant (see Appendix A of Ref. 81 or Appendix B of Ref. 61), we rewrite eq. (4.32) in the form

$$u_{mj}(12) = -\text{sign}(q_j) \left[ \frac{m^\dagger(R) q_j}{r_{mj}^2} \right] \cos \theta , \quad (4.33)$$

where the sign function equals 1 if  $q_j$  is positive and -1 if  $q_j$  is negative. From the law of cosines [165] we have the relationships

$$r_{mj}^2 = r^2 + R^2 - 2rR \cos \phi \quad (4.34a)$$

and

$$\cos \theta = \frac{R - r \cos \phi}{r_{mj}} , \quad (4.34b)$$

which, when substituted into eq. (4.33), yield

$$u_{mj}(R, r, \phi) = -\text{sign}(q_j) m^\dagger(R) q_j \frac{R - r \cos \phi}{[r^2 + R^2 - 2rR \cos \phi]^{\frac{3}{2}}} . \quad (4.35)$$

Then the average interaction energy,  $U_{mj}^{sh}(R, r)$ , between  $\underline{m}^\dagger(R)$  and the spherical shell of ions (positive or negative) at a distance  $r$  from  $q_j$  is given by

$$U_{mj}^{sh}(R, r) = \rho_j \int g_{sj}(R, r, \phi, \psi) u_{mj}(R, r, \phi) dA dr , \quad (4.36a)$$

in which the element of area

$$dA = r^2 \sin \phi d\phi d\psi . \quad (4.36b)$$

The limits of integration for  $d\psi$  are 0 to  $2\pi$  (a full revolution), while for  $d\phi$  they are  $\phi_m$  to  $\pi$ , where

$$\phi_m = \begin{cases} 0, & \text{if } |r-R| \geq d_{js} \\ \cos^{-1} \left[ \frac{r^2 + R^2 - d_{js}^2}{2rR} \right], & \text{if } |r-R| \leq d_{js} \end{cases} \quad (4.37)$$

guarantees that the ion  $q_i$  and the reference solvent do not interpenetrate.

Now, in principle, we do not know  $g_{sj}(R, r, \phi, \psi)$ . However, since we know that the distribution of ions must be uniform in the spherical shell (valid only when  $q_i$  is a spherically symmetric ion) and if we assume it to be independent of  $R$ , the position the reference solvent, then we can write

$$g_{sj}(R, r, \phi, \psi) = g_{ij}(r) , \quad (4.38)$$

where  $g_{ij}(r)$  is just the ion-ion radial distribution function. This approximation should become exact at large  $r$ . Inserting eqs. (4.35) and (4.38) into eq. (4.36a) and integrating over  $d\psi$ , one obtains

$$U_{mj}^{sh}(R, r) = -2\pi r^2 \rho_j g_{ij}(r) \text{sign}(q_i) q_j m^\dagger(R) dr \\ \times \int_{\phi_m}^{\pi} \frac{(R - r \cos \phi) \sin \phi}{[r^2 + R^2 - 2rR \cos \phi]^{\frac{3}{2}}} d\phi . \quad (4.39)$$

Then integrating eq. (4.39) over  $d\phi$  (using standard forms for the trigonometric integrals which may be found in tables [165]) and simplifying yields the expression

$$U_{mj}^{sh}(R, r) = -2\pi r^2 \rho_j g_{ij}(r) \text{sign}(q_i) q_j m^\dagger(R) \\ \times \left[ \frac{r - R \cos \phi}{R^2 [r^2 + R^2 - 2rR \cos \phi]^{\frac{1}{2}}} \right]_{\phi_m}^{\pi} dr . \quad (4.40)$$

If one carefully evaluates eq. (4.40) at its limits, one finds that

$$U_{mj}^{sh}(R, r) = 0 \quad \text{for } r \geq R + d_{js} , \quad (4.41a)$$

$$U_{mj}^{sh}(R, r) = -2\pi r^2 \rho_j g_{ij}(r) \text{sign}(q_i) \frac{q_j m_j^\dagger(R)}{R^2} \\ \times \left[ 1 + \frac{R^2 - r^2 - d_{js}^2}{2rd_{js}} \right] dr \quad \text{for } R-d_{js} \leq r \leq R+d_{js} , \quad (4.41b)$$

$$U_{mj}^{sh}(R, r) = -4\pi r^2 \rho_j g_{ij}(r) \text{sign}(q_i) \left[ \frac{q_j m_j^\dagger(R)}{R^2} \right] dr \\ \text{for } r \leq R-d_{js} . \quad (4.41c)$$

We remark that eqs. (4.41) are consistent with basic electrostatic theory [140] which states that from an internal point of view a spherical shell of charge is electrically nonexistent (*cf.* eq. (4.41a)); from an external point of view it is electrically equivalent to a point charge whose charge is equal to that contained in the shell (*cf.* eq. (4.41c) where  $N_j = 4\pi r^2 \rho_j g_{ij}(r) dr$ ).

The total average interaction energy,  $U_{mj}(R)$ , between  $\underline{m}^\dagger(R)$  and all other ions,  $q_j$ , in the system is found by simply integrating eqs. (4.41) over all values of  $r$ . The ions are not allowed to interpenetrate so we write

$$U_{mj}(R) = \int_{d_{ij}}^{\infty} U_{mj}^{sh}(R, r) , \quad (4.42)$$

and inserting eqs. (4.41) one obtains the necessary result

$$U_{mj}(R) = -4\pi \rho_j \text{sign}(q_i) \frac{q_j m_j^\dagger(R)}{R^2} \left[ \int_{d_{ij}}^{R-d_{js}} \left[ r^2 g_{ij}(r) \right] dr \right. \\ \left. + \frac{1}{2} \int_{R-d_{js}}^{R+d_{js}} \left[ r^2 g_{ij}(r) \left[ 1 + \frac{R^2 - r^2 - d_{js}^2}{2rd_{js}} \right] \right] dr \right] . \quad (4.43)$$

Now taking advantage of the fact that all other ions will be uniformly distributed in spherical shells about  $q_i$ , it clearly follows that  $\langle \Delta E_{1j}(R) \rangle$  ( $j = +$  or  $-$ ) will be non-zero only along  $\underline{m}^\dagger(R)$ , and consequently we have that

$$U_{mj}(R) = -m_j^\dagger(R) \langle \Delta E_{1j}(R) \rangle . \quad (4.44)$$

Using eqs. (4.43) and (4.44) one immediately obtains



$$\begin{aligned} \langle \Delta \underline{E}_{1j}(R) \rangle = & 4\pi \rho_j \text{sign}(q_i) \frac{q_j}{R^2} \left[ \int_{d_{ij}}^{R-d_{js}} r^2 g_{ij}(r) dr \right. \\ & \left. + \frac{1}{2} \int_{R-d_{js}}^{R+d_{js}} r^2 g_{ij}(r) \left[ 1 + \frac{R^2 - r^2 - d_{js}^2}{2rd_{js}} \right] dr \right], \quad (4.45) \end{aligned}$$

where  $j = +$  or  $-$ . To ensure that  $\langle \Delta \underline{E}_{1q}(R) \rangle$  has the same directional sense as  $\langle \Delta \underline{E}_{1j}(R) \rangle$ , we must multiply eq. (4.30b) by  $\text{sign}(q_i)$ . Equations (4.30) and (4.45) are combined to give the desired relationship

$$\begin{aligned} \langle \Delta \underline{E}_{1I}(R) \rangle = & \frac{\text{sign}(q_i)}{R^2} \left[ q_i + \sum_{j=+,-} \left[ 4\pi \rho_j q_j \int_{d_{ij}}^{R-d_{js}} r^2 g_{ij}(r) dr \right. \right. \\ & \left. \left. + \frac{1}{4d_{js}} \int_{R-d_{js}}^{R+d_{js}} r g_{ij}(r) [R^2 - (r-d_{js})^2] dr \right] \right], \quad (4.46) \end{aligned}$$

where  $\langle \Delta \underline{E}_{1I}(R) \rangle$  will always be directed along the ion-solvent vector.

We now turn our attention to the excess local dipole field,  $\langle \Delta \underline{E}_{1D}(R) \rangle$ . Let us picture an ion in a polar solvent of  $C_{2v}$  symmetry. We find that on average all the dipole moments point either directly at or directly away from the ion, depending upon the sign of the charge on the ion. Clearly, all dipoles in the same spherical shell (we shall refer to them as being lateral) will mutually repel one another. It is this contribution to the local dipole field due to the lateral dipole moments which we will examine.

We determine the lateral dipole field, and hence  $\langle \Delta \underline{E}_{1D}(R) \rangle$  in the present theory, in a manner quite similar to that employed for  $\langle \Delta \underline{E}_{1I}(R) \rangle$ . Again, it is only the average projections,  $\underline{m}^\dagger(r)$ , of the total dipole moments that need to be considered. In order to derive an expression for  $\langle \Delta \underline{E}_{1D}(R) \rangle$  we first examine the interaction between our reference dipole,  $\underline{m}^\dagger(R)$ , and all spherical shells of dipole moments,  $\underline{m}^\dagger(r)$ , at a distance  $r$  from the ion. In Figure 5 we have illustrated the situation being examined along with all the necessary variables.

From eq. (2.5) and (2.17b) we can show [67] that the interaction between  $\underline{m}^\dagger(r)$  and  $\underline{m}^\dagger(R)$  is given by

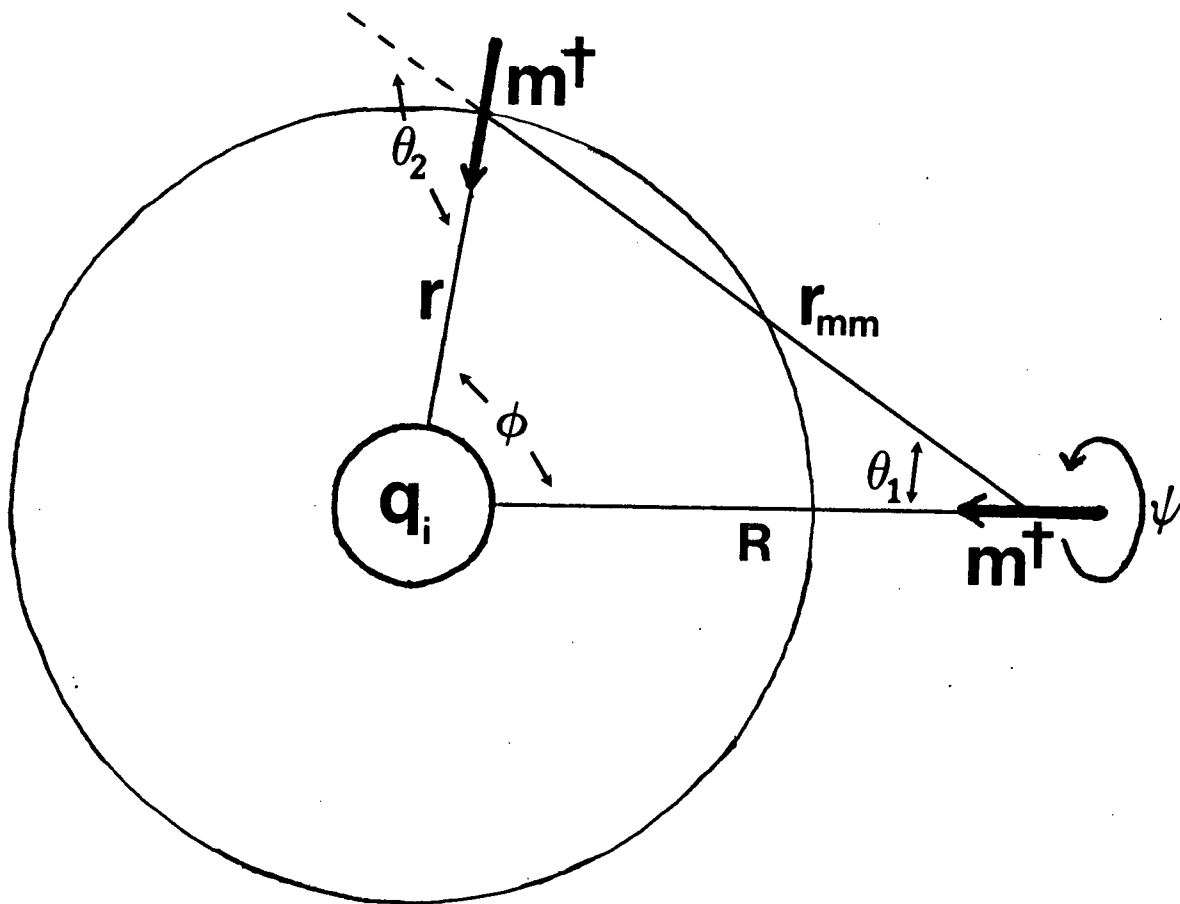


Figure 5. An illustration of the method used in determining  $\langle \Delta E_{1D}(R) \rangle$ . The case where  $q_i$  is a negative ion is shown.

$$u_{mm}(12) = \frac{-\underline{m}^\dagger(r)\underline{m}^\dagger(R)}{r_{mm}^3} \Phi_{00}^{112}(12) , \quad (4.47)$$

where we again take  $f^{mn1}$  as given by eq. (2.9a). The rotational invariant can be written [61,81] in the form

$$\Phi_{00}^{112}(12) = 2\cos\theta_1\cos\theta_2 - \sin\theta_1\sin\theta_2\cos(\phi_1-\phi_2) , \quad (4.48)$$

where  $\theta_1$  and  $\theta_2$  are the angles indicated in Figure 5 and  $\phi_1$  and  $\phi_2$  are the azimuthal angles. It is easy to see from Figure 5 that  $\phi_1$  and  $\phi_2$  must always be equal. Analogous to eqs. (4.34) we have the relationships

$$r_{mm}^2 = r^2 + R^2 - 2rR\cos\phi , \quad (4.49a)$$

$$\cos\theta_1 = \frac{R - r\cos\phi}{r_{mm}} \quad (4.49b)$$

and

$$\cos\theta_2 = \frac{R\cos\phi - r}{r_{mm}} . \quad (4.49c)$$

From the law of sines [165] it is easy to show that

$$\sin\theta_1 = \frac{r\sin\phi}{r_{mm}} \quad (4.49d)$$

and

$$\sin\theta_2 = \frac{R\sin\phi}{r_{mm}} . \quad (4.49e)$$

Substituting eqs. (4.49) into eq. (4.48) and combining this result with eq. (4.47) yields

$$u_{mm}(R, r, \phi) = \frac{\underline{m}^\dagger(r)\underline{m}^\dagger(R)}{r_{mm}^5} \left[ 3rR - 2(r^2+R^2)\cos\phi + rR\cos^2\phi \right] . \quad (4.50)$$

We note that this expression is invariant to  $\text{sign}(q_i)$  because both  $\underline{m}^\dagger(r)$  and  $\underline{m}^\dagger(R)$  will reverse direction if the charge on the ion  $i$  is reversed (*i.e.*,  $\theta_1 \rightarrow 180^\circ + \theta_1$ ,  $\theta_2 \rightarrow 180^\circ + \theta_2$ ).

The average lateral dipole-dipole interaction energy,  $U_{mm}^{\text{lat}}(R, r)$ , between  $\underline{m}^\dagger(R)$  and the spherical shell of dipoles at a distance  $r$  from the same ion will be given by

$$U_{mm}^{lat}(R, r) = \rho_s \int g_{ss}(R, r, \phi, \psi) u_{mm}(R, r, \phi) dA dr, \quad (4.51)$$

where  $dA$  is expressed in eq. (4.36b). The limits of integration are still 0 to  $2\pi$  for  $d\psi$  and  $\phi_m$  to  $\pi$  for  $d\phi$ , as was the case for  $\langle \Delta E_{1I}(R) \rangle$ , but now

$$\phi_m = \begin{cases} 0, & \text{if } |r-R| \geq d_s \\ \cos^{-1} \left[ \frac{r^2 + R^2 - d_s^2}{2rR} \right], & \text{if } |r-R| \leq d_s \end{cases}. \quad (4.52)$$

Again, as was the case for  $\langle \Delta E_{1I}(R) \rangle$ , we know that  $g_{ss}(R, r, \phi, \psi)$  is spherically symmetric (*i.e.*, the solvents are uniformly distributed in the shell). We will also assume it is independent of  $R$  and take

$$g_{ss}(R, r, \phi, \psi) = g_{is}(r) \equiv g_{00;is}^{000}(r). \quad (4.53)$$

Now substituting eqs. (4.50) and (4.53) into eq. (4.51) and integrating over  $d\phi$ , one obtains

$$U_{mm}^{lat}(R, r) = 2\pi r^2 \rho_s g_{is}(r) m^\dagger(r) m^\dagger(R) dr \times \int_{\phi_m}^{\pi} \frac{[3rR - 2(r^2 + R^2)\cos\phi + rR\cos^2\phi]\sin\phi}{[r^2 + R^2 - 2rR\cos\phi]^{\frac{5}{2}}} d\phi. \quad (4.54)$$

The integration of eq. (4.54) is non-trivial to perform, but after considerable manipulation (again making use of standard tables of trigonometric integrals [165]) it can be shown that

$$U_{mm}^{lat}(R, r) = 2\pi r^2 \rho_s g_{is}(r) m^\dagger(r) m^\dagger(R) \left[ \frac{1 - \cos^2\phi_m}{[r^2 + R^2 - 2rR\cos\phi]^{\frac{3}{2}}} \right] dr. \quad (4.55)$$

It then follows from eqs. (4.52) and (4.55) that

$$U_{mm}^{lat}(R, r) = 0 \quad \text{for } |r-R| \geq d_s \quad (4.56a)$$

and

$$U_{mm}^{\text{lat}}(R, r) = 2\pi r^2 \rho_s g_{is}(r) \frac{m^\dagger(r) m^\dagger(R)}{d_s^3} \left[ 1 - \left[ \frac{r^2 + R^2 - d_s^2}{2rR} \right]^2 \right] dr$$

for  $|r-R| \leq d_s$  . (4.56b)

Finally, the total average lateral dipole interaction energy,  $U_{mm}(R)$ , between  $\underline{m}^\dagger(R)$  and all other dipole moments is found by integrating eqs. (4.56) over all values of  $r$ , although only those shells for which  $|r-R| < d_s$  will contribute. We obtain the expression

$$U_{mm}(R) = \frac{\pi \rho_s m^\dagger(R)}{2R^2 d_s^3} \int_{R-d_s}^{R+d_s} \left[ m^\dagger(r) g_{is}(r) [(2rR)^2 - (r^2 + R^2 - d_s^2)^2] \right] dr . \quad (4.57)$$

Now taking advantage of the fact that the solvent distribution about the ion is independent of the angle, and because all the average projected moments,  $m^\dagger(r)$ , are directed along the ion-solvent vector, it must follow that the total average lateral dipole field will be in the direction of  $\underline{m}^\dagger(R)$ . All other components to the average field must average to zero. Thus, analogous to eq. (4.44) we write that

$$U_{mm}(R) = -m^\dagger(R) \langle \Delta E_{1D}(R) \rangle , \quad (4.58)$$

which when combined with eq. (4.57) yields

$$\langle \Delta E_{1D}(R) \rangle = \frac{\pi \rho_s}{2R^2 d_s^3} \int_{R-d_s}^{R+d_s} \left[ m^\dagger(r) g_{is}(r) [(r^2 + R^2 - d_s^2)^2 - (2rR)^2] \right] dr . \quad (4.59)$$

We point out that in eq. (4.59)  $\underline{m}^\dagger(R)$  will contain contributions due to both the bulk average dipole moment,  $\underline{m}'$ , and the average excess induced moment,  $\Delta p(R)$ . From eqs. (4.24b) and (4.31) we find that

$$m^\dagger(R) = m' \langle \cos \theta_{is}(R) \rangle + \Delta p(R) , \quad (4.60)$$

where we have taken advantage of the fact that  $\Delta p(R)$ , and hence  $\langle \Delta E_{1D}(R) \rangle$ , will be non-zero only along  $\underline{m}^\dagger(R)$ . This has already been shown to be the case for  $\langle \Delta E_{1I}(R) \rangle$  and  $\langle \Delta E_{1D}(R) \rangle$  in the present theory and below we find this to be also true for  $\langle \Delta E_{1Q}(R) \rangle$ . Inserting eq. (4.60) into eq. (4.59) and using eqs. (2.89) we obtain the relationship

$$\langle \Delta E_{1D}(R) \rangle = \frac{\pi \rho_s}{2R^2 d_s^3} \int_{R-d_s}^{R+d_s} \left[ \frac{m' h_{00}^{011}(r)}{3 \text{sign}(q_i)} + \Delta p(r) g_{is}(r) \right] \frac{dr}{[(r^2 + R^2 - d_s^2)^2 - (2rR)^2]} \quad (4.61)$$

which is the desired result. Inspection of eq. (4.61) reveals that two distinct contributions to  $\langle \Delta E_{1D}(R) \rangle$  can be identified, one due only to  $m'$ , and the other due to  $\Delta p(R)$ . This separation will prove useful in discussions below.

The excess local quadrupole field,  $\langle \Delta E_{1Q}(R) \rangle$ , is determined in a very similar fashion to that used for  $\langle \Delta E_{1D}(R) \rangle$ . We will again consider the contribution to  $\langle \Delta E_{1Q}(R) \rangle$  due to lateral fields. These lateral fields are a consequence of the average projections,  $\Theta_s^\dagger(r)$ , of the quadrupole moments of the solvent particles around the ion  $i$ . The projections  $\Theta_s^\dagger(r)$  are analogous to the projections  $m^\dagger(r)$  and will be defined below. We emphasize that this derivation applies strictly to square quadrupole moments as defined by eq. (2.22) and illustrated in Figure 2(a).

First let us define [67,72] the functions

$$\underline{\Phi}^{022}(12) = \Phi_{02}^{022}(\Omega_1, \Omega_2, \hat{r}) + \Phi_{0-2}^{022}(\Omega_1, \Omega_2, \hat{r}) \quad (4.62a)$$

and

$$\underline{\Phi}^{123}(12) = \Phi_{02}^{123}(\Omega_1, \Omega_2, \hat{r}) + \Phi_{0-2}^{123}(\Omega_1, \Omega_2, \hat{r}) \quad (4.62b)$$

which, if  $f^{mnl}$  is given by eq. (2.9a), can be written [81,166] in the explicit forms

$$\underline{\Phi}^{022}(12) = \sqrt{6} \left[ (\hat{x}_2 \cdot \hat{r}_{12})^2 - (\hat{y}_2 \cdot \hat{r}_{12})^2 \right] \quad (4.63a)$$

and

$$\begin{aligned} \underline{\Phi}^{123}(12) = \sqrt{6} \left[ 5 [(\hat{x}_2 \cdot \hat{r}_{12})^2 - (\hat{y}_2 \cdot \hat{r}_{12})^2] (\hat{z}_1 \cdot \hat{z}_2) \right. \\ \left. - 2 [(\hat{x}_2 \cdot \hat{z}_1)(\hat{x}_2 \cdot \hat{r}_{12}) - (\hat{y}_2 \cdot \hat{z}_1)(\hat{y}_2 \cdot \hat{r}_{12})] \right] \quad (4.63b) \end{aligned}$$

Then using the definition of the Euler angles  $\alpha, \beta, \gamma$  as well as the rotation matrix (see eq. (39)) of Ref. 166, it can be shown that

$$\underline{\Phi}^{022}(12) = \sqrt{6} \sin^2 \beta_2 \cos 2\gamma_2 \quad (4.64a)$$

and

$$\begin{aligned} \underline{\Phi}^{123}(12) = \sqrt{6} \left[ 3 \cos \beta_1 \sin^2 \beta_2 \cos 2\gamma_2 + 2 \sin \beta_1 \sin \beta_2 \right. \\ \left. \times [\cos \beta_2 \cos 2\gamma_2 \cos(a_1 - a_2) + \sin 2\gamma_2 \sin(a_1 - a_2)] \right] . \quad (4.64b) \end{aligned}$$

As in the case of  $\langle \Delta \underline{E}_{1D}(R) \rangle$ , we will determine the average interaction between all average projections,  $\underline{\Theta}_S^\dagger(r)$ , of the quadrupole moments in a spherical shell at a distance  $r$  from the ion  $q_i$  and the dipole moment  $\underline{m}^\dagger(R)$ . In Figure 6 we have tried to represent this geometrical problem, indicating the variables used in the following derivation. However, before we can examine the dipole-quadrupole interaction, we must first define  $\underline{\Theta}_S^\dagger(r)$ . From eqs. (2.5), (2.19c) and (4.64a) it follows that the ion-square quadrupole interaction [79,81] is given by

$$u_{i\Theta}(12) = \frac{q_i \Theta_S}{r^3} \sin^2 \beta_2 \cos 2\gamma_2 . \quad (4.65)$$

It is the most energetically favourable quadrupole orientation with respect to the ion  $i$  which is pictured in Figure 6(a). This orientation of the quadrupole moment is the only one that will not average to zero for molecules of  $C_{2v}$  symmetry and it is onto this orientation that we determine the average projection of the quadrupole moment. It is clear from eq. (4.65) that for  $\Theta_S$  positive, which is the case for a water-like solvent [72], this projection corresponds to

$$\beta_2^I = 90^\circ \quad (4.66a)$$

and

$$\cos 2\gamma_2^I = -\text{sign}(q_i) , \quad (4.66b)$$

where the superscript  $I$  indicates the angles as defined for the ion reference frame (see Figure 6(b)). We point out that  $u_{i\Theta}(12)$  is independent of  $a_2^I$  and therefore  $\underline{\Theta}_S^\dagger(r)$  is allowed to spin freely about the  $z_I$  axis. We can then write that

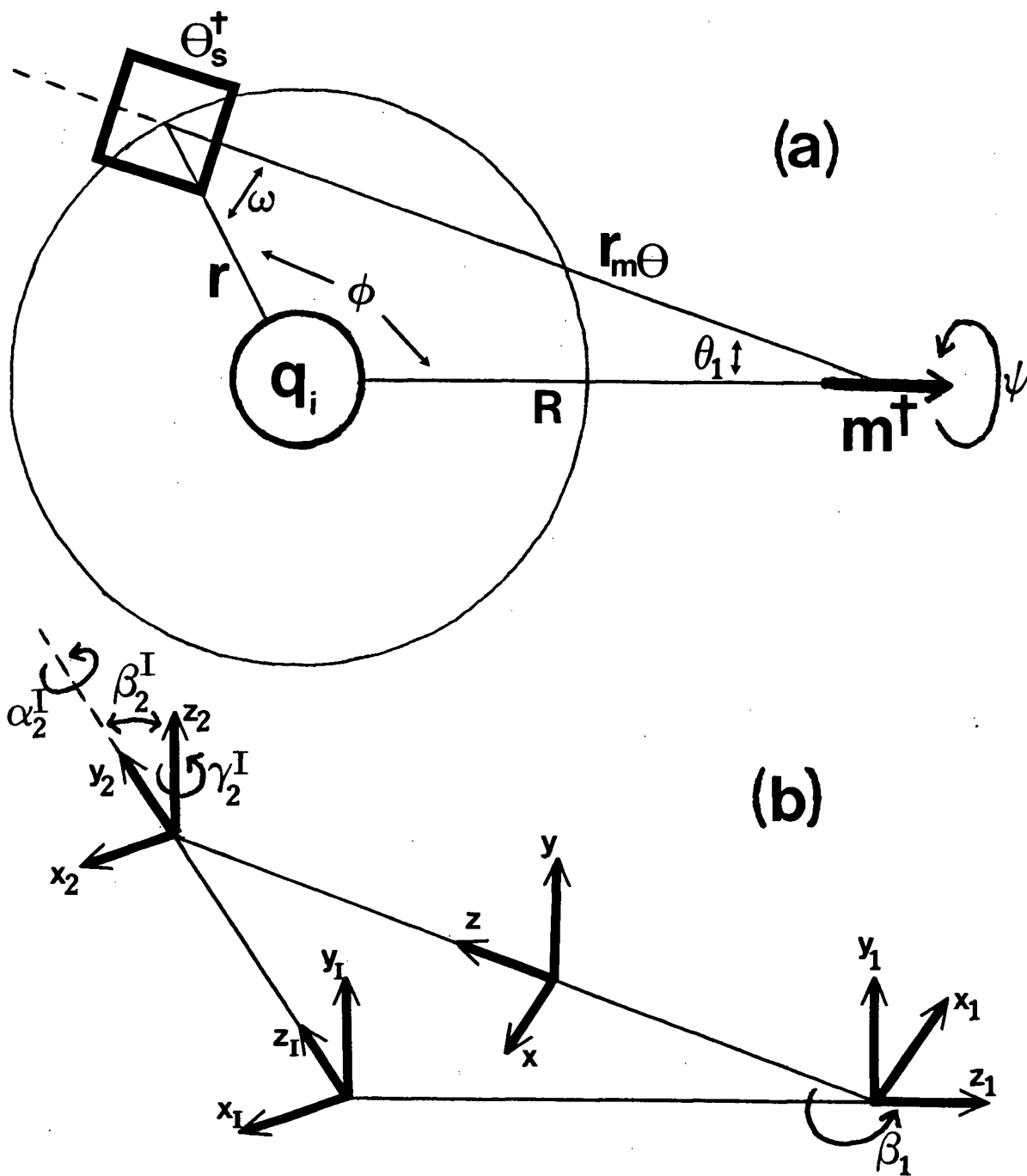


Figure 6. An illustration of the method used in determining  $\langle \Delta E_{1Q}(R) \rangle$ . The case where  $q_i$  is a positive ion is shown. For clarity the various reference frames and their rotations are separately given in (b).



$$\theta_s^\dagger(r) = \frac{-\theta_s}{\text{sign}(q_i)} \langle \Phi^{022}(r) \rangle, \quad (4.67a)$$

which, when combined with eqs. (4.62a) and (2.87) becomes

$$\theta_s^\dagger(r) = \frac{-\theta_s}{\text{sign}(q_i)} \frac{8h_{02;is}^{022}(r)}{5g_{00;is}^{000}(r)}. \quad (4.67b)$$

Now using eqs. (2.5), (2.17b), (2.19c) and (4.62b) we can show that the dipole-square quadrupole interaction,  $u_{m\theta}(12)$ , can be expressed [67,72] in the form

$$u_{m\theta}(12) = \frac{m^\dagger(R) \theta_s^\dagger(r)}{\sqrt{6} r_{m\theta}^4} \Phi^{123}(12). \quad (4.68)$$

However, the function  $\Phi^{123}(12)$ , as given by eq. (4.64b), is not expressed in terms of angles shown in Figure 6. Thus, before proceeding we must first write  $\Phi^{123}(12)$  in terms of these angles, i.e.,  $\beta_2^I$ ,  $\gamma_2^I$ ,  $\beta_1$  and  $\omega$ . We begin by expressing the unit vectors  $\hat{x}_2$ ,  $\hat{y}_2$  and  $\hat{z}_2$  in terms of the Euler angles  $\alpha_2^I$ ,  $\beta_2^I$  and  $\gamma_2^I$  associated with the ion reference frame (see Appendix C). Now in order to go from the ion reference frame to the frame  $(\hat{x}, \hat{y}, \hat{z})$ , we must rotate about the  $y_I$  axis by an angle  $\omega$  (see Figure 6(b)). Therefore we apply the rotation matrix [166]

$$\underline{R} = \begin{bmatrix} \cos\omega & 0 & -\sin\omega \\ 0 & 1 & 0 \\ \sin\omega & 0 & \cos\omega \end{bmatrix} \quad (4.69)$$

to the unit vectors  $\hat{x}_2$ ,  $\hat{y}_2$  and  $\hat{z}_2$ . We can also express  $\hat{x}_2$ ,  $\hat{y}_2$  and  $\hat{z}_2$  in terms of the Euler angles  $\alpha_2$ ,  $\beta_2$  and  $\gamma_2$ , as done in Appendix C. Equating the components of the two forms for  $\hat{x}_2$ ,  $\hat{y}_2$  and  $\hat{z}_2$  yields several relationships (given in Appendix C) between the two sets of Euler angles associated with the two different reference frames. We substitute these expressions into eq. (4.64b), for which we take  $\alpha_1=0$  (this follows from our choice of reference frame), and after considerable manipulation and simplification (see Appendix C) we obtain

$$\begin{aligned} \Phi^{123}_{(12)} = \sqrt{6} & \left[ 3\cos\beta_1 (\cos^2\omega - \sin^2 a_2^I \sin^2\omega) \right. \\ & \left. + 2\sin\beta_1 \sin\omega \cos\omega (1 + \sin^2 a_2^I) \right] \cos 2\gamma_2^I . \end{aligned} \quad (4.70)$$

Finally, we replace  $\beta_1$  by  $\theta_1$  and eliminate the  $\cos 2\gamma_2^I$  dependence in eq. (4.70) by noting that the products

$$\cos\beta_1 \cos 2\gamma_2^I = \cos\theta_1 \quad (4.71a)$$

and

$$\sin\beta_1 \cos 2\gamma_2^I = \sin\theta_1 \quad (4.71b)$$

are independent of the sign of  $q_i$ . Combining eqs. (4.68), (4.70) and (4.71) yields the necessary result

$$\begin{aligned} u_{m\Theta}^{(12)} = \frac{m^\dagger(R) \Theta_S^\dagger(r)}{r_{m\Theta}^4} & \left[ 3\cos\theta_1 (\cos^2\omega - \sin^2 a_2^I \sin^2\omega) \right. \\ & \left. + 2\sin\theta_1 \sin\omega \cos\omega (1 + \sin^2 a_2^I) \right] . \end{aligned} \quad (4.72)$$

We have already pointed out that the average projection of the quadrupole moment is allowed to spin freely about the  $z_I$  axis, and hence we cannot specify the  $a_2^I$  angle. However, we can remove the  $a_2^I$  dependence from eq. (4.72) by taking advantage of the fact that all angles,  $a_2^I$ , are equally probable (at the mean field level) and simply angle-averaging (integrating) over them. After performing this integration one has the result

$$\begin{aligned} u_{m\Theta}^{<a>(12)} = \frac{3m^\dagger(R) \Theta_S^\dagger(r)}{r_{m\Theta}^4} & \left[ \cos\theta_1 (\cos^2\omega - \frac{1}{2}\sin^2\omega) \right. \\ & \left. + \sin\theta_1 \sin\omega \cos\omega \right] . \end{aligned} \quad (4.73)$$

As in the case of  $\langle \Delta E_{1D}(R) \rangle$ , we employ relationships analogous to eqs. (4.49) in order to express functions of  $\theta_1$  and  $\omega$  as functions of  $r$ ,  $R$  and  $\phi$ , and consequently eq. (4.73) becomes

$$u_{m\Theta}^{<a>}(R, r, \phi) = \frac{3m^\dagger(R) \Theta_S^\dagger(r)}{r_{m\Theta}^7} \left[ 2r^2R - \frac{R^3}{2} - \left( \frac{5}{2}rR^2 + r^3 \right) \cos\phi + \left( r^2R + \frac{3}{2}R^3 \right) \cos^2\phi - \frac{rR^2}{2} \cos^3\phi \right] . \quad (4.74)$$

The average lateral quadrupole-dipole interaction energy,  $U_{m\Theta}^{\text{lat}}(R, r)$ , is again found by integrating over  $dA$ . Using the approximation (4.53) and integrating over  $d\psi$  one has

$$U_{m\Theta}^{\text{lat}}(R, r) = 6\pi r^2 \rho_S g_{iS}(r) \Theta_S^\dagger(r) m^\dagger(R) dr \times \int_{\phi_m}^{\pi} \frac{2r^2R - \frac{R^3}{2} - \left( \frac{5}{2}rR^2 + r^3 \right) \cos\phi + \left( r^2R + \frac{3}{2}R^3 \right) \cos^2\phi - \frac{rR^2}{2} \cos^3\phi}{[r^2 + R^2 - 2rR\cos\phi]^{\frac{7}{2}}} \sin\phi d\phi , \quad (4.75)$$

where  $\phi_m$  is given by eq. (4.52). Evaluating the integral over  $d\phi$  in eq. (4.75) requires a great deal of effort, but with the aid of tables of standard trigonometric integrals [165] and after much simplification the result can be written in the form

$$U_{m\Theta}^{\text{lat}}(R, r) = 3\pi r^2 \rho_S g_{iS}(r) \Theta_S^\dagger(r) m^\dagger(R) \times \left[ \frac{(r - R\cos\phi_m)(1 - \cos^2\phi_m)}{[r^2 + R^2 - 2rR\cos\phi]^{\frac{5}{2}}} \right] dr . \quad (4.76)$$

Applying eq. (4.52) immediately yields

$$U_{m\Theta}^{\text{lat}}(R, r) = 0 \quad \text{for } |r - R| \geq d_S \quad (4.77a)$$

and

$$U_{m\Theta}^{\text{lat}}(R, r) = 3\pi r^2 \rho_S g_{iS}(r) \frac{m^\dagger(R) \Theta_S^\dagger(r)}{d_S^5} \left[ 1 - \left[ \frac{r^2 + R^2 - d_S^2}{2rR} \right]^2 \right] \times \left[ \frac{r^2 - R^2 + d_S^2}{2r} \right] dr \quad \text{for } |r - R| \leq d_S . \quad (4.77b)$$

We remark that these expressions bear striking similarity to eqs. (4.55), the lateral dipole result.

The total average lateral quadrupole-dipole interaction energy is again found by integrating eqs. (4.77) over all values of  $r$  (*i.e.*, summing over shells). Explicitly, we obtain

$$U_{m\Theta}(R) = \frac{3\pi\rho_s m^\dagger(R)}{8R^2 d_s^5} \int_{R-d_s}^{R+d_s} \left[ \frac{\Theta_s^\dagger(r)}{r} g_{is}(r) \right. \\ \left. \times [(2rR)^2 - (r^2 + R^2 - d_s^2)^2] (r^2 - R^2 + d_s^2) \right] dr . \quad (4.78)$$

One can use arguments very similar to those used for  $\langle \Delta \underline{E}_{1D}(R) \rangle$  to show that  $\langle \Delta \underline{E}_{1Q}(R) \rangle$  will also only be non-zero in the direction of  $\underline{m}^\dagger(R)$ , so we write

$$U_{m\Theta}(R) = -m^\dagger(R) \langle \Delta \underline{E}_{1Q}(R) \rangle . \quad (4.79)$$

Finally, the combination of (4.67b), (4.78) and (4.79) gives the desired result

$$\langle \Delta \underline{E}_{1Q}(R) \rangle = \frac{3\pi\rho_s \Theta_s}{5 \text{sign}(q_i) R^2 d_s^5} \int_{R-d_s}^{R+d_s} \left[ \frac{h_{02;is}^{022}(r)}{r} \right. \\ \left. \times [(2rR)^2 - (r^2 + R^2 - d_s^2)^2] (r^2 - R^2 + d_s^2) \right] dr . \quad (4.80)$$

It is interesting to note that both  $\langle \Delta \underline{E}_{1D}(R) \rangle$  and  $\langle \Delta \underline{E}_{1Q}(R) \rangle$ , as given by eqs. (4.61) and (4.80), respectively, can be perceived as having an apparent  $1/R^2$  dependence. Thus, they can be viewed as additional screening terms, appearing to be the result of effective charges, analogous to the case for  $\langle \Delta \underline{E}_{1+}(R) \rangle$  and  $\langle \Delta \underline{E}_{1-}(R) \rangle$ .

We now have expressions for all three terms contributing to  $\langle \Delta \underline{E}_1(R) \rangle$ . Given the necessary projections of the correlation functions,  $\langle \Delta \underline{E}_{1I}(R) \rangle$  and  $\langle \Delta \underline{E}_{1Q}(R) \rangle$  can be evaluated directly using eqs. (4.46) and (4.80), respectively. However,  $\langle \Delta \underline{E}_{1D}(R) \rangle$ , as given by eq. (4.61), must be solved iteratively since it depends on the value of  $\Delta p(R)$ , which in turn depends upon  $\langle \Delta \underline{E}_{1D}(R) \rangle$ . Once the total excess local field,  $\langle \Delta \underline{E}_1(R) \rangle$ , has been determined, eqs. (4.26) and (4.29) will immediately give us the effective ion-solvent potential,  $u_{is}^{\Delta p}(R)$ , for the RDMF theory.

In the present study we employ the RHNC theory, as described in Chapter II, to determine the correlation functions for a solution. These

correlation functions can then be used in the RDMF theory to evaluate  $u_{1S}^{\Delta p}(R)$ , which in turn modifies the ion-solvent pair potential, and hence the correlation functions. As mentioned above, the RDMF theory must be solved in conjunction with the SCMF approximation. Therefore, for a given system we solve the SCMF/RDMF/RHNC theory in the following manner. For a fixed set of system parameters, including  $m_e$  and  $\underline{a}$ , the RHNC theory is solved numerically still using the iterative method outlined in section 5 of Chapter II, but now at each iterative cycle we update the current estimate for  $\Delta p(R)$ . In principle, this calculation must then be repeated for several values of the effective permanent dipole,  $m_e$ , to allow the self-consistent values of  $m'$ ,  $\underline{a}'$  and  $m_e$  to be evaluated using the SCMF approximation. We point out that at infinite dilution the value of  $m_e$  is just that of the pure solvent.

It follows from eq. (3.45) that because  $u_{1S}^{\Delta p}(R)$  is a spherically symmetric potential term it may make a contribution to the low concentration limiting behaviour of  $C_{1S}$ . In order to investigate this possibility we need to examine the large  $R$  and low concentration dependences of the terms contributing to  $\langle \Delta \underline{E}_1(R) \rangle$ .

First we will examine the large  $R$  behaviour of  $\langle \Delta \underline{E}_{1Q}(R) \rangle$ . It can be shown [61] that at  $\rho_2 = 0$

$$h_{02;is}^{022}(r) \rightarrow a/r^3 \quad \text{as } r \rightarrow \infty, \quad (4.81)$$

where  $a$  is some constant. If we then insert this form for  $h_{02;is}^{022}(r)$  into eq. (4.80) and integrate, one finds that the integral evaluates to an identity 0. Clearly, we then have that at infinite dilution

$$\langle \Delta \underline{E}_{1Q}(R) \rangle = 0 \quad \text{as } R \rightarrow \infty. \quad (4.82)$$

Therefore,  $\langle \Delta \underline{E}_{1Q}(R) \rangle$  has no long-range tail, becoming zero as soon as  $h_{02;is}^{022}(r)$  attains its large  $r$  behaviour, and consequently it cannot contribute to the low concentration limiting behaviour of  $u_{1S}^{\Delta p}(R)$ .

We now turn our attention to  $\langle \Delta \underline{E}_{1I}(R) \rangle$ . From eqs. (3.34) and (3.35a) we have that as  $r \rightarrow \infty$  and  $\kappa \rightarrow 0$ ,

$$g_{ij}(r) \rightarrow 1 - \left[ \frac{q_i q_j}{\epsilon kT} \right] \frac{e^{-\kappa r}}{r}, \quad (4.83)$$

where  $\kappa$  is given by eq. (3.35b). We insert eq. (4.83) into eq. (4.46) and expand and integrate (see Appendix B). Then collecting terms and applying the small  $\kappa$  limit yields

$$\langle \Delta E_{1I}(R) \rangle = \frac{\text{sign}(q_i)}{R^2} \left[ q_i + \sum_{j=+,-} \left[ 4\pi \rho_j q_j \left[ \frac{1}{3}(R^3 - d_{js}^3) + \frac{q_i q_j d_{ij}^2}{2\epsilon kT} \right] + \frac{q_i q_j}{\kappa \epsilon kT} [e^{-\kappa R(R+1/\kappa)} - 1/\kappa] \right] \right] . \quad (4.84)$$

If we now use eq. (3.35b) and charge neutrality, dropping any terms linear in  $\rho_2$ , we obtain the result

$$\langle \Delta E_{1I}(R) \rangle = \frac{|q_i|}{R^2} e^{-\kappa R(1+\kappa R)} , \quad (4.85)$$

which represents the  $R \rightarrow \infty$  and  $\kappa \rightarrow 0$  limiting behaviour of  $\langle \Delta E_{1I}(R) \rangle$ . We note that in the infinite dilution limit (*i.e.*,  $\kappa=0$ ) eq. (4.85) becomes

$$\langle \Delta E_{1I}(R) \rangle = \frac{|q_i|}{R^2} , \quad (4.86)$$

which is consistent with eq. (4.30).

In considering the low concentration limiting behaviour of  $\langle \Delta E_{1D}(R) \rangle$  we find it convenient to split  $\langle \Delta E_{1D}(R) \rangle$ , and hence eq. (4.61), into two parts;  $\langle \Delta E_{1m}(R) \rangle$  due only to  $m'$ , and  $\langle \Delta E_{1p}(R) \rangle$  directly dependent only upon  $\Delta p(R)$ . First we will examine  $\langle \Delta E_{1m}(R) \rangle$ . From eq. (3.47) it follows that as  $\rho_2 \rightarrow 0$  and  $R \rightarrow \infty$ ,

$$\langle \Delta E_{1m}(R) \rangle = \frac{|q_i|}{8R^2 d_s^3} \left[ \frac{\epsilon-1}{\epsilon} \right] \int_{R-d_s}^{R+d_s} \left[ (1+\kappa r) e^{-\kappa r} \times \left[ r^2 - 2(R^2 + d_s^2) + \frac{(R^2 - d_s^2)^2}{r^2} \right] \right] dr . \quad (4.87)$$

If one performs the integration in eq. (4.87) and collects terms (see Appendix B), then it can be shown that in the limit  $\kappa \rightarrow 0$  and  $R \rightarrow \infty$

$$\langle \Delta E_{1m}(R) \rangle = \frac{-2|q_i|}{3R^2} \left[ \frac{\epsilon-1}{\epsilon} \right] e^{-\kappa R(1+\kappa R)} . \quad (4.88)$$

We remark that eqs. (4.85) and (4.88) are very similar. It is clearly the case that at low concentration and long range nearly two thirds of the ion field will be cancelled by the lateral dipolar field due to  $m_e$  when the pure solvent dielectric constant,  $\epsilon$ , is large (as is the case for water). This is an obvious indication of how poor an approximation eq. (4.1a) is for aqueous electrolyte solutions.

In order to determine the long-range low concentration behaviour of  $\langle \Delta E_{1p}(R) \rangle$  we must know  $\Delta p(R)$ , but  $\Delta p(R)$  depends upon  $\langle \Delta E_1(R) \rangle$ , which in turn depends upon  $\langle \Delta E_{1p}(R) \rangle$ . To obtain a first approximation for  $\Delta p(R)$ , which we will designate as  $\Delta p^{(1)}(R)$ , we use eqs. (4.22b) and (4.26), combined with the results from eqs. (4.82), (4.85) and (4.88), which yield

$$\Delta p^{(1)}(R) = \frac{a |q_i|}{3R^2} \left[ \frac{\epsilon+2}{\epsilon} \right] e^{-\kappa R} (1+\kappa R) . \quad (4.89)$$

This result can then be substituted into the expression

$$\langle \Delta E_{1p}(R) \rangle = \frac{\pi \rho_s}{2R^2 d_s^3} \int_{R-d_s}^{R+d_s} \left[ \Delta p(r) [(r^2+R^2-d_s^2)^2 - (2rR)^2] \right] dr , \quad (4.90)$$

which follows from eq. (4.61) when  $g_{is}(r)=1$  (valid at large  $r$ ). After performing the necessary integration and simplifying (see Appendix B), one has that

$$\langle \Delta E_{1p}(R) \rangle^{(1)} = \frac{|q_i|}{3R^2} \left[ \frac{\epsilon+2}{\epsilon} \right] (-\xi) e^{-\kappa R} (1+\kappa R) , \quad (4.91a)$$

where

$$\xi = \frac{8\pi \rho_s a}{3} . \quad (4.91b)$$

We now combine this result with eqs. (4.82), (4.85), (4.88), (4.22b) and (4.26) to obtain a second estimate for  $\Delta p(R)$ , namely

$$\Delta p^{(2)}(R) = \frac{a |q_i|}{3R^2} \left[ \frac{\epsilon+2}{\epsilon} \right] e^{-\kappa R} (1+\kappa R) (1-\xi) . \quad (4.92)$$

By repeating the above procedure to obtain higher and higher order estimates of  $\Delta p(R)$ , it is possible to show that

$$\Delta p^{(\infty)}(R) = \frac{a|q_i|}{3R^2} \left[ \frac{\epsilon+2}{\epsilon} \right] e^{-\kappa R} (1+\kappa R) (1-\xi+\xi^2-\xi^3+\dots) . \quad (4.93)$$

For  $|\xi| < 1$  (i.e., for  $a\rho_s < 3/8\pi$ ), we recognize the last factor in eq. (4.93) as the Taylor series expansion for  $1/(1+\xi)$ . We note that for water at 25°C,  $\xi=0.403$ . Therefore, we have the self-consistent result

$$\Delta p(R) = \frac{a|q_i|}{(3+8\pi\rho_s a)R^2} \left[ \frac{\epsilon+2}{\epsilon} \right] e^{-\kappa R} (1+\kappa R) , \quad (4.94)$$

which will be valid only at long range and low concentration.

Let us now consider the average excess local field,  $\langle \Delta \underline{E}_1(R) \rangle$ , at infinite dilution (i.e.,  $\rho_2=0$ ) for the special case when the solvent is *polarizable* but *non-polar*. In such a case  $m'=0$ , and furthermore  $\langle \underline{E}_1 \rangle = \langle \Delta \underline{E}_{1m}(R) \rangle = 0$ . Starting with an initial guess for  $\langle \Delta \underline{E}_1(R) \rangle$  as given by eq. (4.86), and using eq. (4.90) in the same iterative scheme outlined above, we can show that for this system at large  $R$

$$\langle \Delta \underline{E}_1(R) \rangle = \frac{|q_i|}{R^2} \frac{3}{3+8\pi\rho_s a} . \quad (4.95)$$

Substituting the Clausius-Mosotti relationship [139],

$$\frac{\epsilon_\infty - 1}{\epsilon_\infty + 2} = \frac{4}{3}\pi\rho_s a , \quad (4.96a)$$

into eq. (4.95) immediately yields the relationship

$$\langle \Delta \underline{E}_1(R) \rangle = \frac{|q_i|}{R^2} \frac{\epsilon_\infty + 2}{3\epsilon_\infty} , \quad (4.96b)$$

where  $\epsilon_\infty$  is the high frequency dielectric constant due only to molecular polarizability. Pollock *et al.* [167] have also studied polarization effects in this system. They obtained exactly the same expression for the large  $R$  dependence of the average local field. Moreover, Pollock *et al.* [167] found that continuum theory predicted a different result. When the two expressions were compared with reported values for the average local field at large  $R$  obtained from computer simulation [167], eq. (4.96b) was found to give essentially exact results, while the continuum expression was only accurate for



small values of  $\rho_s a$ .

It is also interesting to examine the behaviour of  $\langle \Delta E_1(R) \rangle$  at infinite dilution when the solvent is *polar* but *not polarizable*. From eqs. (4.86) and (4.88) it is easily shown that at large R

$$\langle \Delta E_1(R) \rangle = \frac{|q_i|}{R^2} \frac{\epsilon+2}{3\epsilon} . \quad (4.97)$$

Curiously, eqs. (4.96b) and (4.97) are equivalent in form indicating that the field due to a charge will be *screened* to the same extent in either system provided that they have the same dielectric constant.

We point out that  $\Delta p(R)$ , as given by eq. (4.94), has that same large-R low concentration limiting behaviour as  $h_{00;iS}^{011}(r)$ , and thus we would expect it to affect the limiting behaviour of  $C_{iS}$ . Using eqs. (3.39b), (3.45), (4.29) and (4.94) it is again possible to show, after considerable manipulation (see Appendix B), that as  $\rho_2 \rightarrow 0$ ,

$$C_{iS}^{\Delta p} \rightarrow \frac{2\pi a \beta q_i^2}{(3+8\pi \rho_s a)^2} \left[ \frac{\epsilon+2}{\epsilon} \right]^2 \left( \frac{1}{d_{iS}} - \frac{3}{2}\kappa + \dots \right) , \quad (4.98)$$

where  $C_{iS}^{\Delta p}$  is the contribution to  $C_{iS}$  due only to  $u_{iS}^{\Delta p}(R)$  and  $\beta = 1/kT$ . If we now define  $S_C^{\Delta p}$  as being the contribution to the total limiting slope,  $S_C$ , of  $C_{iS}$  (as given in eq. (3.43)) due only to  $u_{iS}^{\Delta p}(R)$ , then combining eqs. (3.43) and (4.98) along with eq. (3.35c) yields

$$S_C^{\Delta p} = \frac{-12\pi a \Lambda \nu^{\frac{3}{2}}}{(3+8\pi \rho_s a)^2} \frac{(\epsilon+2)^2}{\epsilon} . \quad (4.99)$$

Furthermore, it follows from eq. (3.41) that if  $u_{iS}^{\Delta p}(R)$  make a contribution to the limiting slope of  $C_{iS}$ , then it must also influence the limiting behaviour of  $G_{+S} = G_{-S}$ . Therefore,  $u_{iS}^{\Delta p}(R)$  will affect the limiting laws of all thermodynamic properties of electrolyte solutions which have a dependence on ion-solvent correlations at low concentration (e.g.,  $\bar{V}_2$ ). We again emphasize that the value of  $S_C^{\Delta p}$  should be accurately given by eq. (4.99) since the long-range low concentration behaviour of  $\Delta p(R)$  predicted by the RDMF theory, i.e., eq. (4.94), should be an exact result at the mean field level.

## CHAPTER V

### RESULTS FOR WATER-LIKE MODELS

#### 1. Introduction

In Chapter II we have defined the water-like models we will investigate. We will report results obtained using the RHNC/SCMF theory which was described in Chapters II and IV. For the most part, this study will focus upon the full  $C_{2v}$  water model, with and without the octupole moment. We will find it convenient to refer to the  $C_{2v}$  model which includes only dipole and quadrupole moments as the  $C_{2v}$  *quadrupole* model, whereas the term  $C_{2v}$  *octupole* model will be used when the octupole has also been included. However, the *tetrahedral* model (*i.e.*, a model containing only a dipole and a square quadrupole) was also examined to allow comparison with previous work [67,168]. Moreover, this simplified model was employed extensively as the solvent in our study of model aqueous electrolyte solutions (as will be discussed in Chapter VI). It also proved useful in exploring the basis set dependence of the RHNC theory for models of non-linear symmetry. We will discuss basis sets and basis set dependence in section 2 of this chapter. We find that the basis set corresponding to  $n_{\max}=4$  represents a reasonable compromise between convergence and computational requirements. Hence, this basis set was used to obtain virtually all results reported in sections 3 and 4. In section 3 we will present results obtained for the multipolar hard-sphere models. A modified version of this model, which incorporates a soft spherical potential, will be examined in section 4. Our discussions will focus mainly on the structural and dielectric properties of the model systems being investigated.

In this study we have examined water-like models at several different temperatures and pressures. The temperature and pressure points at which calculations were done are given in Table II, along with the corresponding experimental densities. The points sample a relatively large portion of the phase diagram of liquid water and were chosen to correspond with those examined in previous work [67,168]. Of importance here is the fact that the dielectric constant has been measured [48,169,170] at all these points. We shall refer to points at 1 atm. or at vapour pressure as being at *normal*

**TABLE II.** Experimental densities of water for the temperatures and pressures examined in this study.

Temperature (°C)	Pressure	Density (g/ml)	
25	1 atm.	0.99707	[169]
90	1 atm.	0.9653	[48]
200	Vapour Press.	0.865	[48]
300	Vapour Press.	0.710	[48]
370	Vapour Press.	0.452	[170]
100	5000 bars	1.106	[170]
200	5000 bars	1.051	[170]
300	5000 bars	0.993	[170]
400	5000 bars	0.931	[170]

pressure, while those at 5000 bars shall be referred to as *high* pressure points.

In Chapter IV we have outlined how polarizability may be included in the present models through the SCMF approximation. Again, it is an experimental value of the polarizability tensor which we have used in the models. The individual components of the tensor were determined using the average polarizability,  $\alpha = 1.444 \times 10^{-24} \text{ cm}^3$ , reported by Eisenberg and Kauzmann [171] and the experimental results of Murphy [164] to find their relative values. The following values of the components of the polarizability tensor were obtained:

$$\alpha_{xx} = 1.501 \times 10^{-24} \text{ cm}^3,$$

$$\alpha_{yy} = 1.390 \times 10^{-24} \text{ cm}^3,$$

$$\alpha_{zz} = 1.442 \times 10^{-24} \text{ cm}^3.$$

This form for the tensor was employed in all SCMF calculations. We also note that the SCMF results we will report are those determined when the energies given by Simpson's rule integration of eq. (2.80) are used in the calculation. The dielectric constants we will give were determined through eqs. (2.93), again employing Simpson's rule to perform the required integration.

In our calculations, and in some of the following discussion, it is convenient to express all parameters in reduced units. The water-like fluids we shall consider can be totally characterized by the following reduced

parameters:

$$\rho^* = \rho d_s^3, \quad (5.1a)$$

$$d^* = d/d_s, \quad (5.1b)$$

$$\mu^* = (\beta \mu^2/d_s^3)^{1/2}, \quad (5.1c)$$

$$\theta^* = (\beta \theta^2/d_s^5)^{1/2}, \quad (5.1d)$$

$$\Omega^* = (\beta \Omega^2/d_s^7)^{1/2}, \quad (5.1e)$$

$$a^* = a/d_s^3, \quad (5.1f)$$

where  $\beta = 1/kT$  and  $d_s = 2.8\text{\AA}$  is the hard-sphere diameter of the water-like model. It clearly follows from eq. (5.1b) that  $d_s^* = 1$ .

## 2. Choice of Basis Set

In the present study it is important to first determine an HNC basis set which is computationally practical, yet gives reasonable convergence for the properties we shall consider. In Table III we have presented the number of unique projection terms which must be included in the HNC basis sets for both  $C_{2v}$  and tetrahedral models for  $n_{\max} = 2, 3, 4, 5, 6$ . In Table IV we have explicitly given the unique projections for  $n_{\max} = 2$  for both models. A set of

**TABLE III.** Numbers of unique projection terms required in HNC basis sets. Both tetrahedral and  $C_{2v}$  models are considered.

$n_{\max}$	Tetrahedral Model	$C_{2v}$ Model
2	12	19
3	29	49
4	74	130
5	144	262
6	286	532

TABLE IV. Projection terms included in  $n_{\max}=2$  basis sets.

Model	# of Unique Projections	Projections Included ( $mnl;\mu\nu$ )
Tetrahedral	12	(000;00),(022;00),(110;00),(112;00), (121;02),(123;02),(220;00),(220;22), (222;00),(222;22),(224;00),(224;22)
$C_{2v}$	19	all those above plus (011;00),(022;02),(121;00),(123;00), (220;02),(222;02),(224;02)

TABLE V. Maximum numbers of non-zero terms for any given projection in the HNC binary product. Values are given for each basis set included in Table III.

$n_{\max}$	Tetrahedral Model	$C_{2v}$ Model
2	28	48
3	150	225
4	1000	1800
5	3200	6200
6	12000	—

unique projections consists of all terms which cannot be related by some symmetry requirement of the model, *i.e.*, eqs. (2.11), (2.12), (2.14), or (2.23). It is obvious from Table III that the number of unique projections grows very rapidly as  $n_{\max}$  is increased, with the number of terms required by the tetrahedral model being slightly more than half the number needed by a general model of  $C_{2v}$  symmetry. As one might expect, the HNC basis sets for systems of linear symmetry consist of far fewer projections when  $n_{\max}$  is large (*e.g.*, 84 for  $n_{\max}=6$  [71,110]).

In Table V we have recorded the maximum number of non-zero terms in the HNC binary product, or double sum (*cf.* eq. (2.67)), that any given projection in a specific basis set can ever have. As we would expect, this number grows very rapidly as  $n_{\max}$  is increased since the total number of terms in the double sum will increase as the square of the number of

**TABLE VI.** CPU time required per iteration on an FPS 164 array processor. Times are given for each basis set included in Table III and are in CPU seconds. The values in parentheses are for calculations which limit the number of terms considered in the binary product (as discussed in the text).

$n_{\max}$	Tetrahedral Model	$C_{2v}$ Model
2	2.5	3.0
3	7.0	9.5
4	30	50
5	90(80)	(230)
6	470(330)	not attempted

projections in the basis set. However, inspection of the values given in Tables III and V immediately leads us to conclude that at least 85% of these terms are zero for a tetrahedral model, and this figure rises to 90% for a general model of  $C_{2v}$  symmetry.

Finally, in Table VI we report the times required for an FPS 164 array processor (*i.e.*, the CPU time required) to complete one full iteration of the RHNC theory (see section 5 of Chapter II). Values are given for each basis set considered in this study. Also included in the table are the times which result when *small* terms in the binary product are ignored. We see that for the largest basis set examined, the  $n_{\max}=6$  tetrahedral, there is a considerable time savings (~30%), although the amount of time saved becomes much smaller for smaller basis sets. Consequently, this truncation procedure was extensively used for calculations involving only the two largest basis sets (*i.e.*, the  $n_{\max}=6$  tetrahedral and the  $n_{\max}=5$   $C_{2v}$ ). It should also be noted that there was no detectable change observed in the solution sets obtained as a result of this additional truncation of the HNC binary product.

The basis set dependence of the RHNC results for the dielectric constant,  $\epsilon$ , the average energies and the contact value of the radial distribution function,  $g(r=d)$ , for a specific tetrahedral fluid is given in Table VII. The parameters of the model being examined were chosen to be similar to those of the water-like models at 25°C. It is obvious from Table VII that there is strong basis set dependence when going from  $n_{\max}=2$  to  $n_{\max}=3$  to  $n_{\max}=4$ . Fortunately, we find that there is only slight basis set dependence

**TABLE VII.** Basis set dependence of  $\epsilon$ , the average energies and  $g(r=d)$ . A tetrahedral fluid for which  $\rho^*=0.7317$ ,  $\mu^*=2.50$  and  $\Theta_s^*=0.94$  is considered.

$n_{\max}$	2	3	4	5	6
$\epsilon$	89.1	83.7	66.5	66.4	66.2
$-U_{DD}/NkT$	9.19	9.42	9.17	9.15	9.14
$-U_{DQ}/NkT$	5.93	6.49	7.01	7.06	7.07
$-U_{QQ}/NkT$	1.49	1.50	1.76	1.76	1.79
$g(r=d)$	10.14	11.24	11.95	12.07	12.16

with the  $n_{\max}=5$  and  $n_{\max}=6$  systems. For all the properties considered in Table VII, there is less than 2% difference between the  $n_{\max}=4$  and  $n_{\max}=6$  results. The basis set dependence we observe for this tetrahedral model is similar to that reported for models with dipoles and linear quadrupoles [71,110]. Considering the fact that 100, and sometimes more, iterations are required to converge a solution set for a given model system, the  $n_{\max}=4$  basis set would seem to be a reasonable compromise between computational requirements and accuracy. Therefore, the  $n_{\max}=4$  basis set was used exclusively to obtain all the results presented in sections 3 and 4.

One observation which can be made for the larger basis sets is that when given in Cartesian representation (*i.e.*, when  $f^{mnl}$  is given by eq. (2.9a))  $h_{\mu\nu}^{mnl}(r)$  becomes very small for large  $l$ , *e.g.*, for  $l \geq 7$  all contact values are less than  $10^{-3}$ . Thus one might expect that these basis sets could reasonably be truncated on  $l$ . Equation (2.48b) represents the required condition. Two calculations were done using the same tetrahedral model; one was  $n_{\max}=4$ ,  $l_{\max}=6$ , and the other was  $n_{\max}=4$ ,  $l_{\max}=4$ . In both cases the solution sets obtained were markedly different (in an unsystematic manner) from the solution with no truncation on  $l$ . Clearly, truncation of the basis set on  $l$  does not represent a viable approach for the models we are considering. Upon re-examination of the contact values of  $h_{\mu\nu}^{mnl}(r)$ , this time in Blum's [101-103] representation (*i.e.*, when  $f^{mnl}$  is given by eq. (2.9b)), we find that the values do not decrease for large  $l$ . Obviously, it is the  $1/l!$  factor in

the Cartesian representation of  $h_{\mu\nu}^{mn1}(r)$  which causes the large  $l$  terms for these systems to appear to become small.

Finally, we point out that partial basis set dependence (*i.e.*, for  $n_{\max}=2,3,4$ ) was determined for a  $C_{2v}$  quadrupole fluid at the same reduced density and with the same dipole moment as the above tetrahedral model. The reduced quadrupole moment was taken as being that of water at 25°C. As one would expect, we found behaviour very similar to that demonstrated by the tetrahedral model, as given in Table VII. The basis set dependence of a  $C_{2v}$  octupole fluid for  $n_{\max}=4$  and  $n_{\max}=5$  was also examined. We found a slightly stronger dependence (*e.g.*, about a 4% drop in  $\epsilon$  and a 2% increase in the magnitude of the total average energy) than was the case for the tetrahedral system. This is not a surprising result since we would expect the octupole moment to increase the magnitudes of the higher order projections, and hence increase their importance.

### 3. Results for Hard-Sphere Models

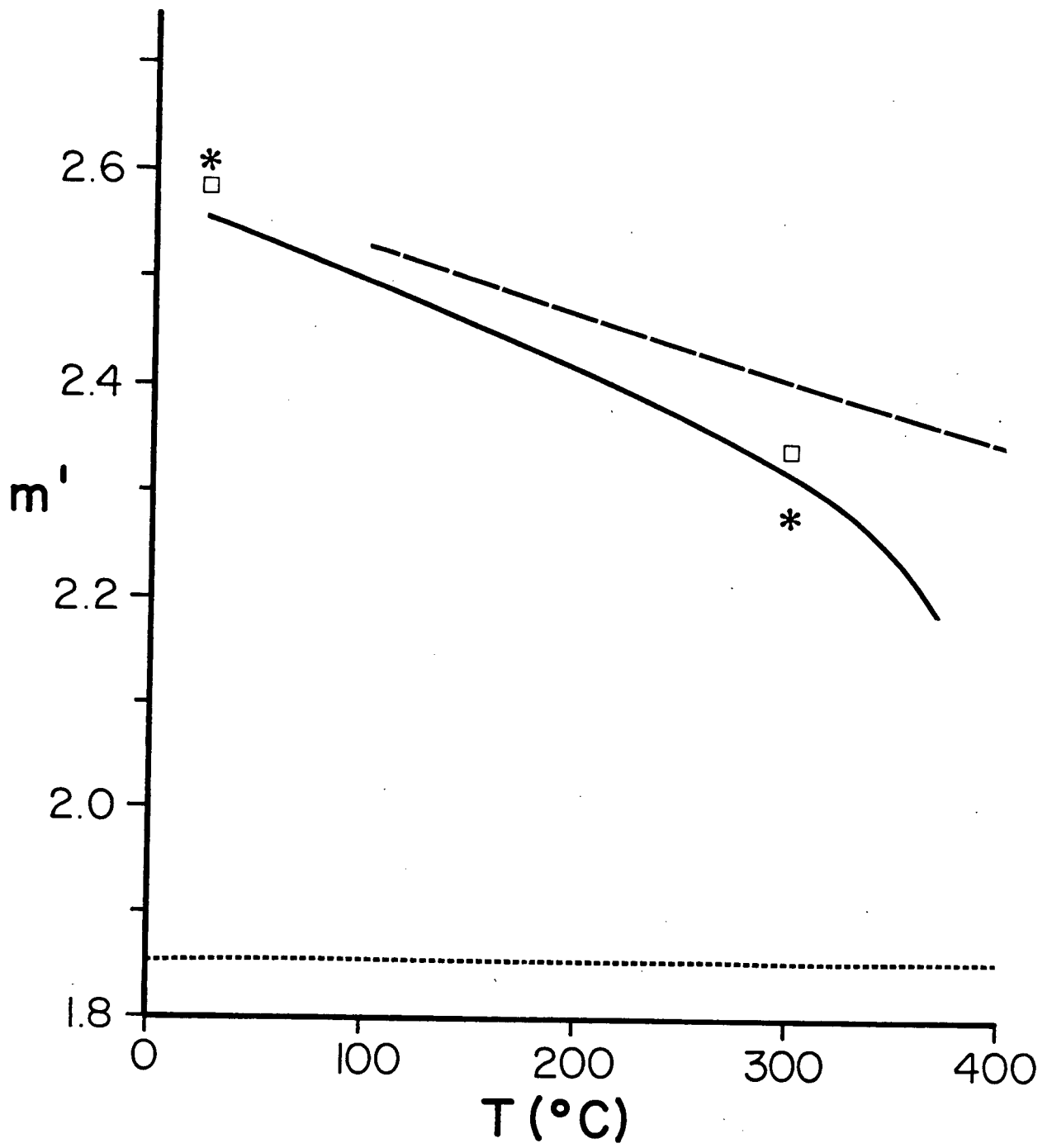
Calculations using the  $n_{\max}=4$  basis set were carried out at all the temperatures and pressures listed in Table II. The  $C_{2v}$  quadrupole model was studied at all points, while the  $C_{2v}$  octupole fluid was examined only at normal pressure at 25°C and 300°C. The calculation at 25°C was repeated with a tetrahedral model where  $\Theta_s^*=0.94$ , this value being consistent with previous work [67,72,168].

The average dipole moments,  $m'$ , as determined with the SCMF approximation, are shown in Figure 7. Not surprisingly, we find that  $m'$  decreases with increasing temperature, but increases with increasing pressure. Yet, even at high temperature the value of  $m'$  is still well above that of the permanent dipole moment of water. The addition of the octupole moment is found to cause only a slight increase in the average dipole moment. The results obtained here are in striking agreement with previous work [67,168] in which the tetrahedral model was examined over the same temperature and pressure ranges. However, these earlier studies [67,168] employed the RLHNC instead of the RHNC theory. In the present study, we found that the tetrahedral fluid at 25°C gave values for  $m'$  almost identical to those



Figure 7.

The mean dipole moment of water-like particles as a function of temperature and pressure. The values of the moments are in Debyes. The solid and dashed lines are the SCMF results for the  $C_{2v}$  quadrupole model at normal and high pressure, respectively. The dotted line represents the permanent dipole moment of water. The open squares are values obtained for  $C_{2v}$  octupole fluids at normal pressure, while the stars represent SCMF results at the same points for the soft  $C_{2v}$  model discussed in the next section.



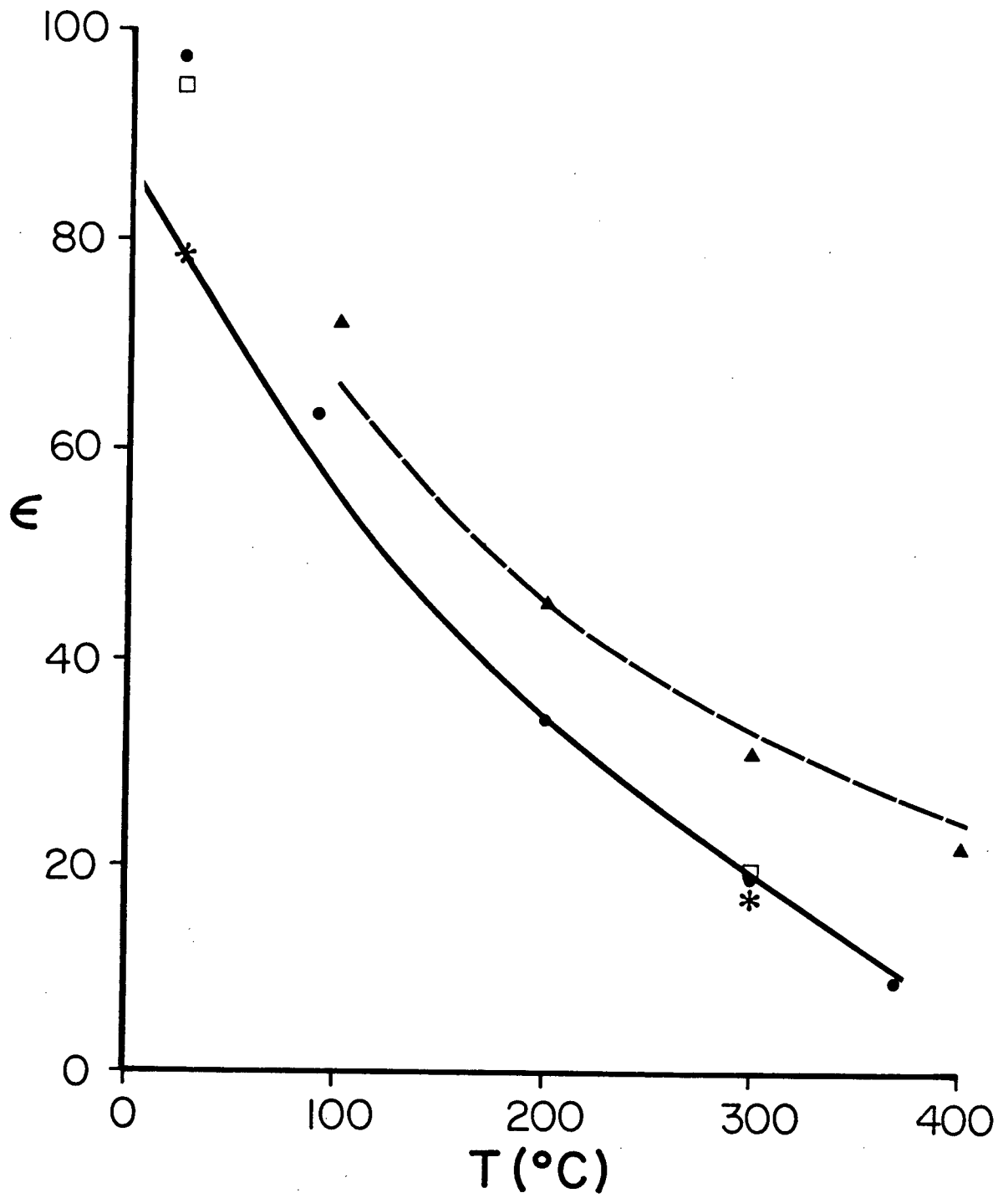
obtained for the  $C_{2v}$  quadrupole system. The average dipole moments we determine at 25°C compare very well with values that have been calculated for ice [172] or reported for another polarizable water-like model [37].

The dielectric constants obtained for the polarizable systems being investigated here are shown in Figure 8. We find that at higher temperatures, *i.e.*, > 100°C, the simple hard-sphere models we are considering give results which are in good agreement with experimental data, both at normal and high pressure. At lower temperatures, however, we find that the hard-sphere models consistently overestimate  $\epsilon$ . We remark that this was not the case in earlier RLHNC studies of the tetrahedral model [67], where good agreement with experiment was found even at 25°C. Using the RHNC theory, we obtain  $\epsilon=105$  for the tetrahedral fluid considered in Ref. 67 (we remark that this value is larger than the value,  $\epsilon=97.4$ , found for the  $C_{2v}$  quadrupole fluid), even though the effective dipole moment was essentially the same. The RHNC is usually the more accurate theory, therefore we would expect it to give the better estimate of the dielectric constant for this model system. Later in this section we will show that the packing structure (*i.e.*, the radial distribution function) predicted by the RHNC theory for the present hard-sphere models at 25°C is quite different from that of real water. At higher temperatures, both real water and our model fluids become less structured, and hence the structural differences become less significant. The fact that we obtain good agreement with experiment for  $\epsilon$  at higher temperatures but not at lower temperatures strongly suggests that the unique packing structure of water at low temperature, *i.e.*, 25°C, affects its dielectric properties. This hypothesis will be examined in detail in section 4.

The importance of polarizability in the present water-like fluids can be easily demonstrated. If we ignore polarizability and take the effective dipole moment to be simply the gas phase value, then we obtain  $\epsilon=28.4$  for the  $C_{2v}$  quadrupole fluid at 25°C. It is also interesting to point out that the MCY [49] and TIP4P [41] models, two popular water-like models, have recently been shown [45,46] to give dielectric constants of 34 and 53, respectively, at 20°C. Both models are non-polarizable and have dipole moments of about 2.2D. In comparison with these results, those obtained here at 25°C for our polarizable hard-sphere fluids appear more respectable.

Figure 8.

The dielectric constants of water and of water-like models as functions of temperature and pressure. The dots and triangles are SCMF results for  $C_{2v}$  quadrupole fluids at normal and high pressure, respectively. The open squares and stars refer to the same models as in Figure 7. The solid and dashed lines represent experimental values [48,169,170] at normal and high pressure, respectively.



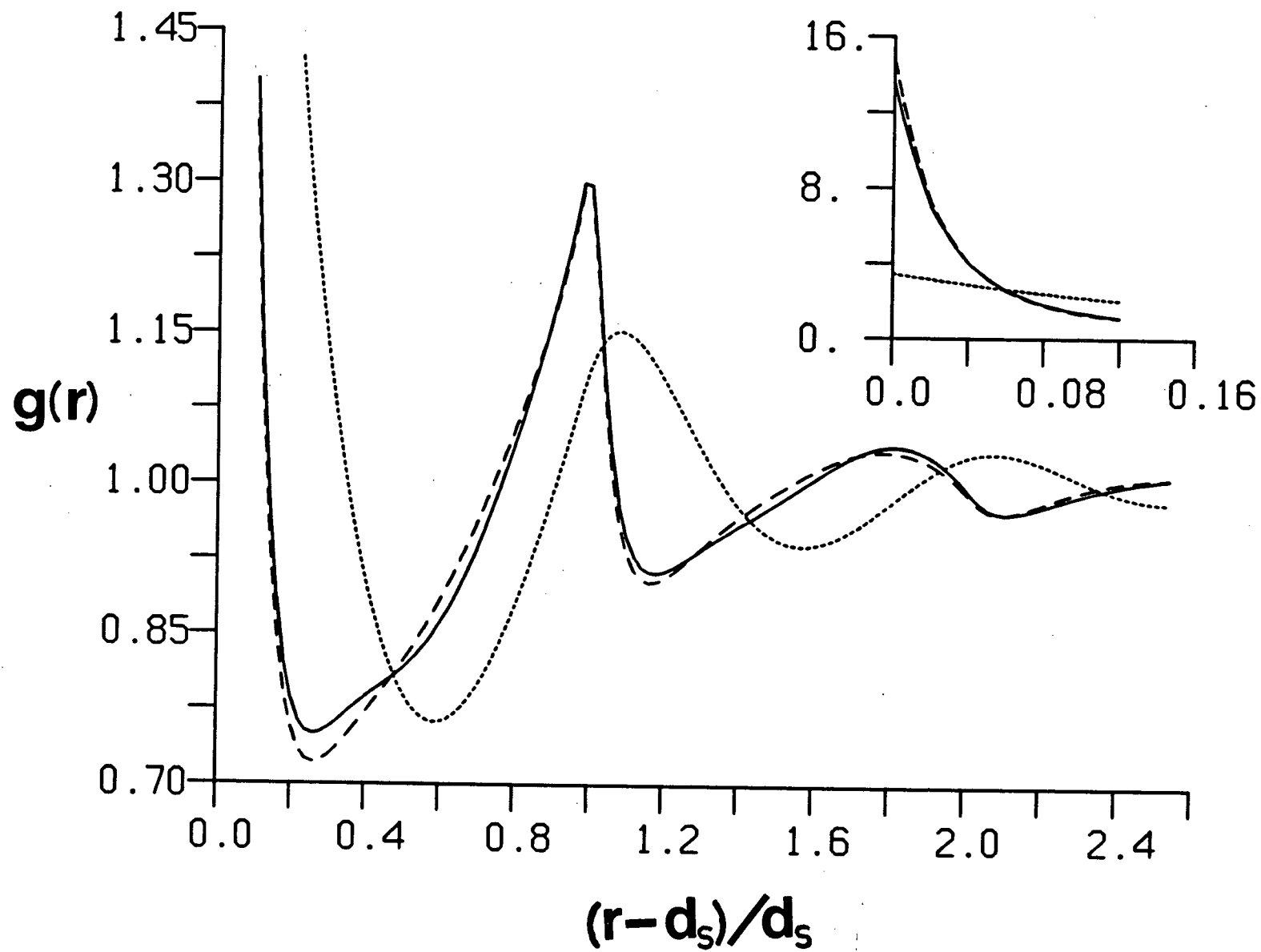
In general, we find that addition of the octupole moment to the  $C_{2v}$  quadrupole model causes a noticeable drop in  $\epsilon$  for a fixed dipole moment. We have also found (see Figure 7) that the addition of the octupole moment to the model results in a larger average dipole moment, which should give rise to a larger dielectric constant. We find that the two effects tend to cancel one another. Consequently, in Figure 8 we see that the  $C_{2v}$  quadrupole and  $C_{2v}$  octupole fluids give quite similar dielectric constants.

The total average configurational energies,  $U_{TOT}/NkT$ , were computed for these polarizable systems using eq. (4.20). At 25°C the tetrahedral, the  $C_{2v}$  quadrupole and the  $C_{2v}$  octupole fluids give values of -16.4, -16.8 and -18.1, respectively. These compare well with the experimental value [41] of -16.7. This agreement is perhaps quite fortuitous since we might expect some of the terms which we have ignored in the potential (e.g., dispersion and short-range repulsive terms) to make fairly large contributions to the energy. We remark that the RLHNC result [67] of -16.9 for the tetrahedral fluid at 25°C is again close to the value given by the RHNC theory.

The radial distribution function,  $g(r)=g_{00}^{000}(r)$ , obtained for the  $C_{2v}$  quadrupole and the  $C_{2v}$  octupole fluids at 25°C are shown in Figure 9. Both systems have the same effective dipole moment,  $m_e^*=2.75$ , and hence any differences in structure are due solely to the influence of the octupole moment. We point out that this value of  $m_e^*$  is very close to the SCMF results of 2.74 and 2.77 for the polarizable  $C_{2v}$  quadrupole and  $C_{2v}$  octupole fluids, respectively. Also shown in Figure 9 is the radial distribution function of the hard-sphere reference system (which would also be the RLHNC result for  $g(r)$ ). The effects of the strong multipolar interactions are clearly evident. For the two multipolar fluids, the contact value of  $g(r)$  has increased dramatically from the hard-sphere value, while the position of the first minimum has moved inward. The result is a very sharp first peak in  $g(r)$ , as is evident in Figure 9. The second peak has also sharpened and shifted inward for both multipolar systems. However, its maximum still occurs at a separation of about  $2d_s$ , whereas for real water the maximum in the second peak appears at about  $1.65d_s$ , corresponding to the *tetrahedral* distance [121,122]. If we compute the coordination numbers,

Figure 9.

Radial distribution functions for water-like fluids at 25°C. The solid and dashed lines are RHNC results for the  $C_{2v}$  quadrupole and the  $C_{2v}$  octupole models, respectively, when  $m_e^* = 2.75$ . The dotted line represents the hard-sphere radial distribution function for that density.





$$CN = 4\pi\rho_s \int_{d_s}^R r^2 g(r) dr , \quad (5.2)$$

where  $R$  represents the separation corresponding to the first minimum of the integrand, we find that both the  $C_{2v}$  models give values of about 5.7 at 25°C. Again, these do not compare well with the result for water at 25°C, where  $CN \approx 4.5$  [122]. Thus, even accounting for the structural effects of the unrealistic repulsive cores of the  $C_{2v}$  models, the RHNC results for  $g(r)$  for these two fluids are still quite different from that of real water.

The effects of the addition of the octupole moment to the  $C_{2v}$  quadrupole model can also be seen in Figure 9. As might be expected, the contact peak of  $g(r)$  becomes somewhat steeper due to the extra terms in the multipole potential. The maximum in the second peak shows virtually no change; however, a small shoulder on the second peak has developed at the tetrahedral distance. Moreover, the third and fourth peaks appear to be shifted slightly inward. Clearly, the octupole moment does influence the packing structure in a desirable way, but the magnitude of its effects are still relatively small.

In an attempt to try and improve our results for the radial distribution function, we also examined the effects of increasing the values of the quadrupole and octupole moments. We found that increasing the quadrupole and octupole by 15% and 50%, respectively, produces very little change in the RHNC result for  $g(r)$  except to generate an even steeper contact peak. Therefore, at least within the RHNC theory, hard-sphere models containing only the low order multipole moments of water appear unable to give a tetrahedral structure similar to that of water.

In Figures 10-16 we have shown some of the projections of the pair correlation functions of the  $C_{2v}$  quadrupole and  $C_{2v}$  octupole fluids. The projections which have been plotted are all those which contain potential terms for both models, as well as  $h_{00}^{110}(r)$ . We remark that these projections represent only a small subset of the total number of unique projections in the HNC basis set used in the calculations. Most of the correlation functions are at least moderately affected by the addition of the octupole moment to the  $C_{2v}$  quadrupole model;  $h_{00}^{123}(r)$  and  $h_{00}^{224}(r)$  change markedly, while  $h_{02}^{123}(r)$

Figure 10.

The projection  $h_{00}^{110}(r)$ . The solid and dashed lines represent RHNC results for the  $C_{2v}$  quadrupole and the  $C_{2v}$  octupole models, respectively, at 25°C and  $m_e^*=2.75$ .

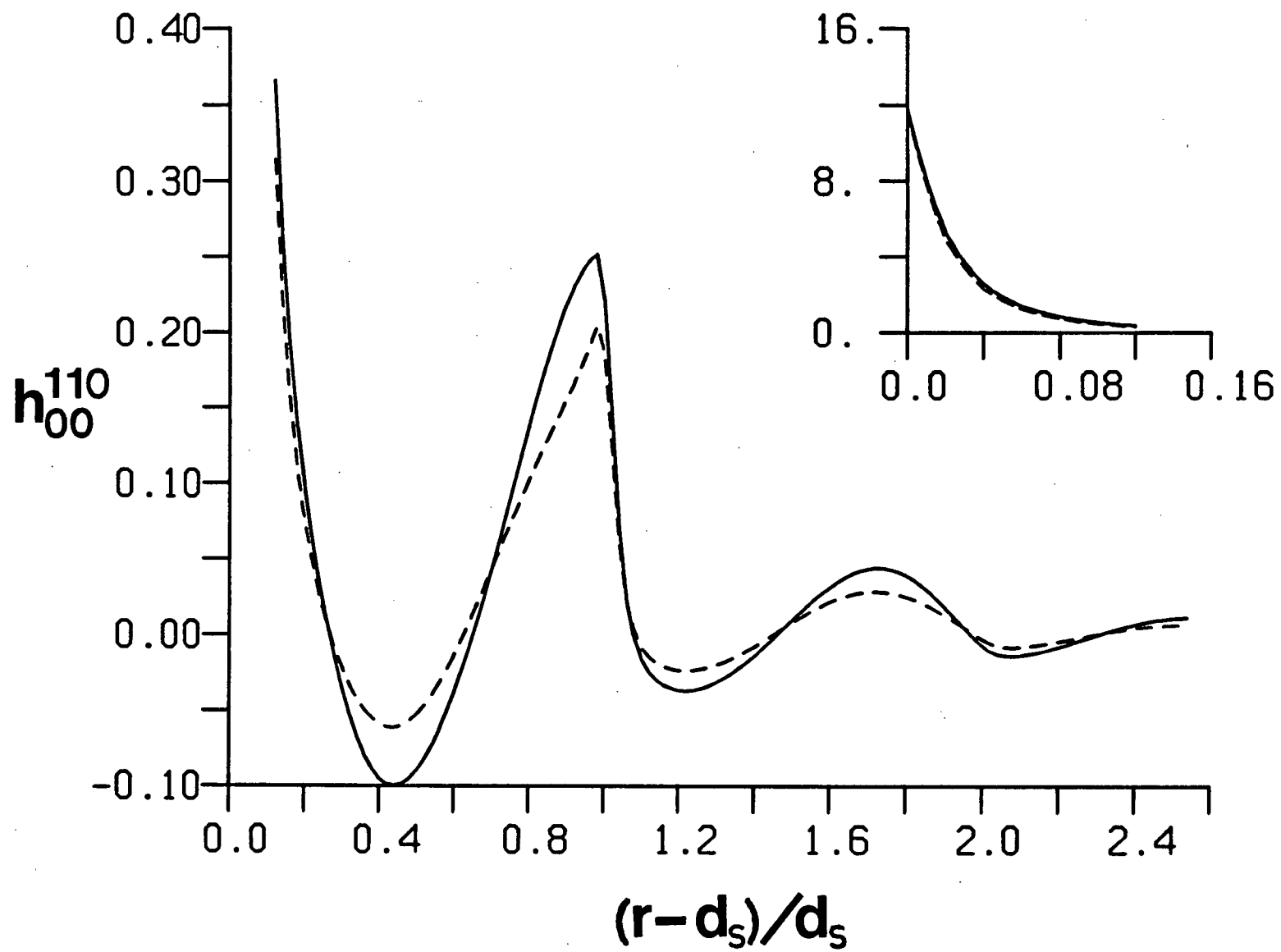


Figure 11.

The projection  $h_{00}^{112}(r)$ . The curves are defined as in Figure 10.

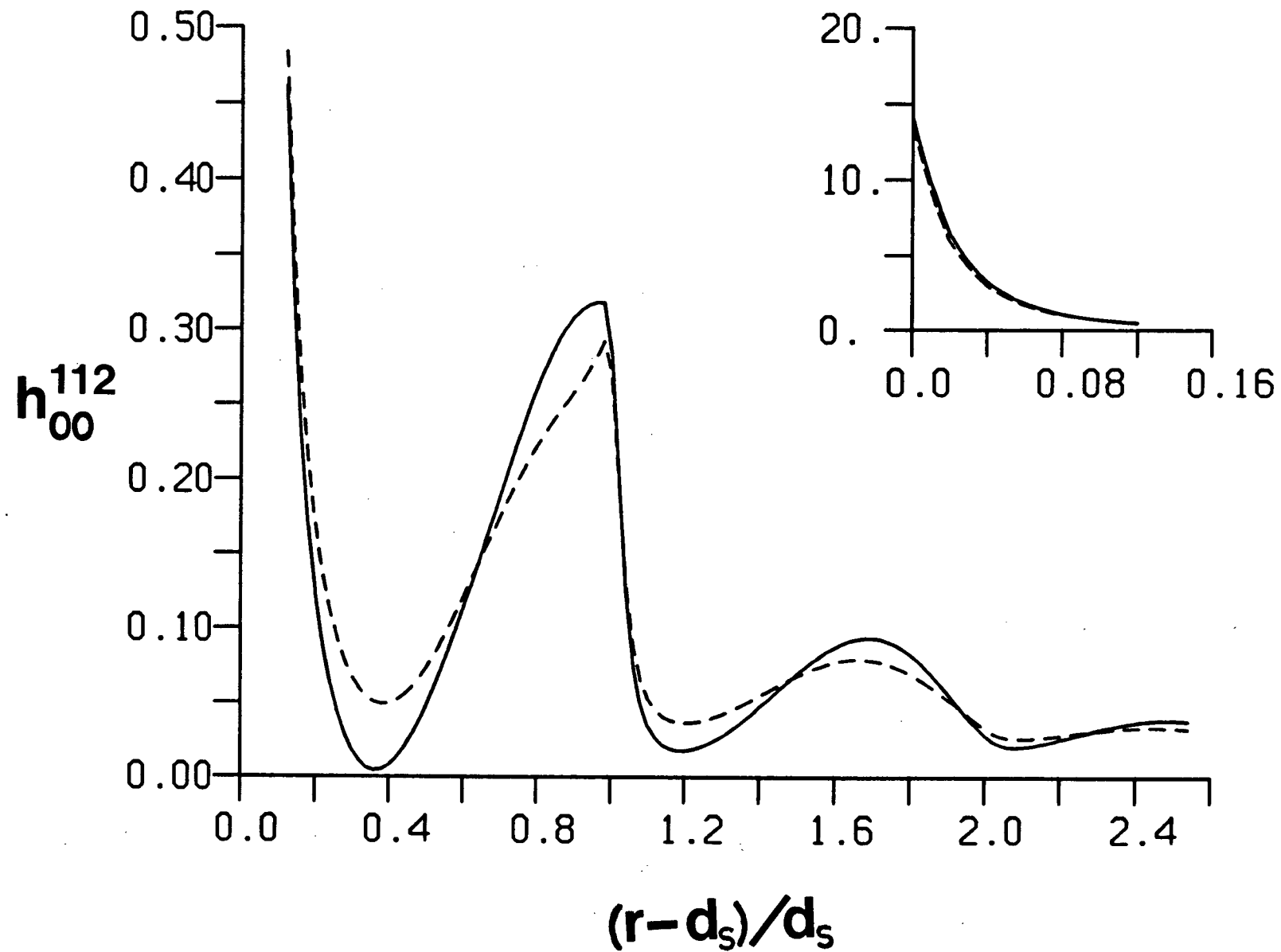


Figure 12.

The projection  $h_{00}^{123}(r)$ . The curves are defined as in Figure 10.

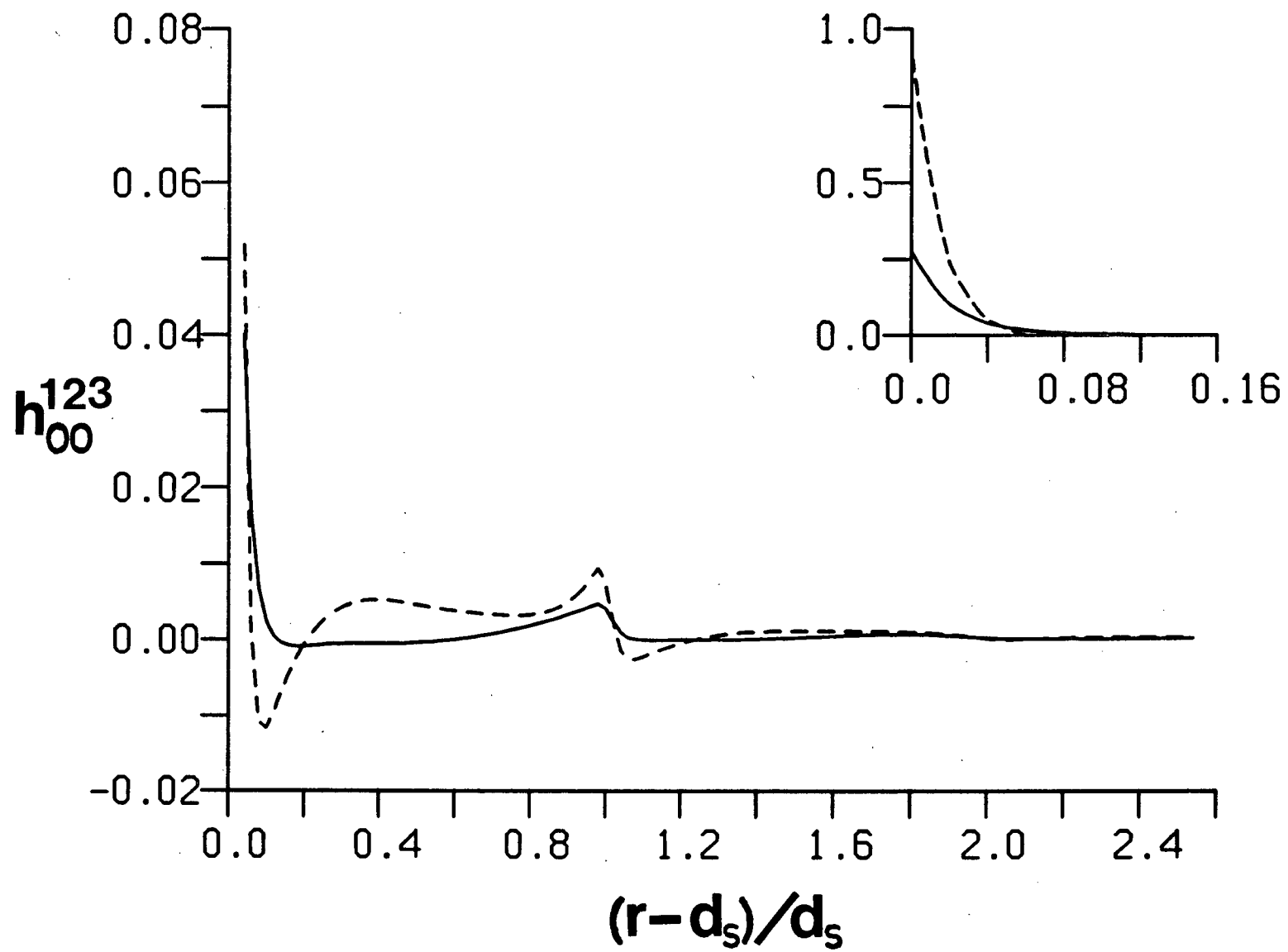


Figure 13.

The projection  $h_{02}^{123}(r)$ . The curves are defined as in Figure 10.



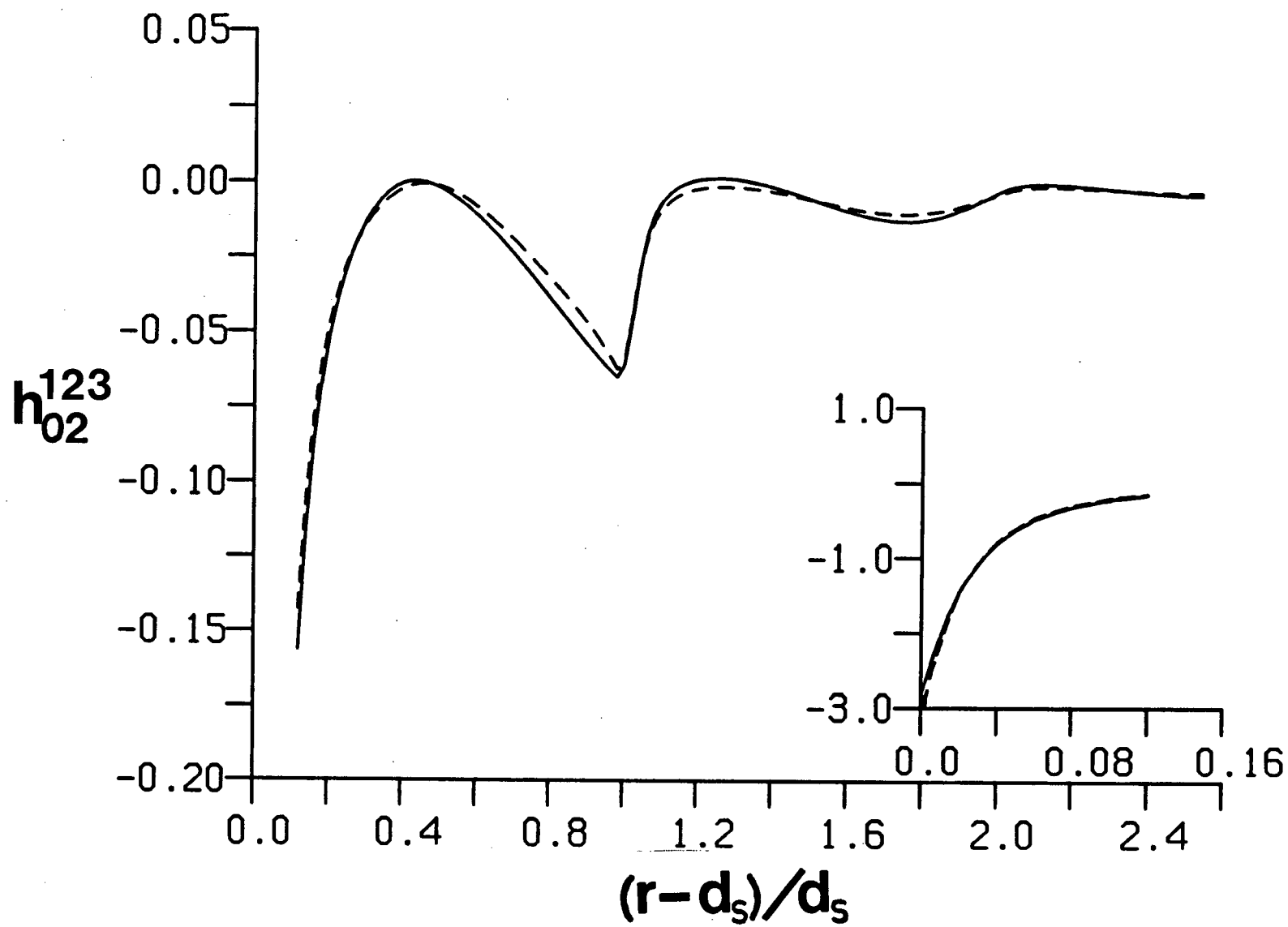


Figure 14.

The projection  $h_{00}^{224}(r)$ . The curves are defined as in Figure 10.

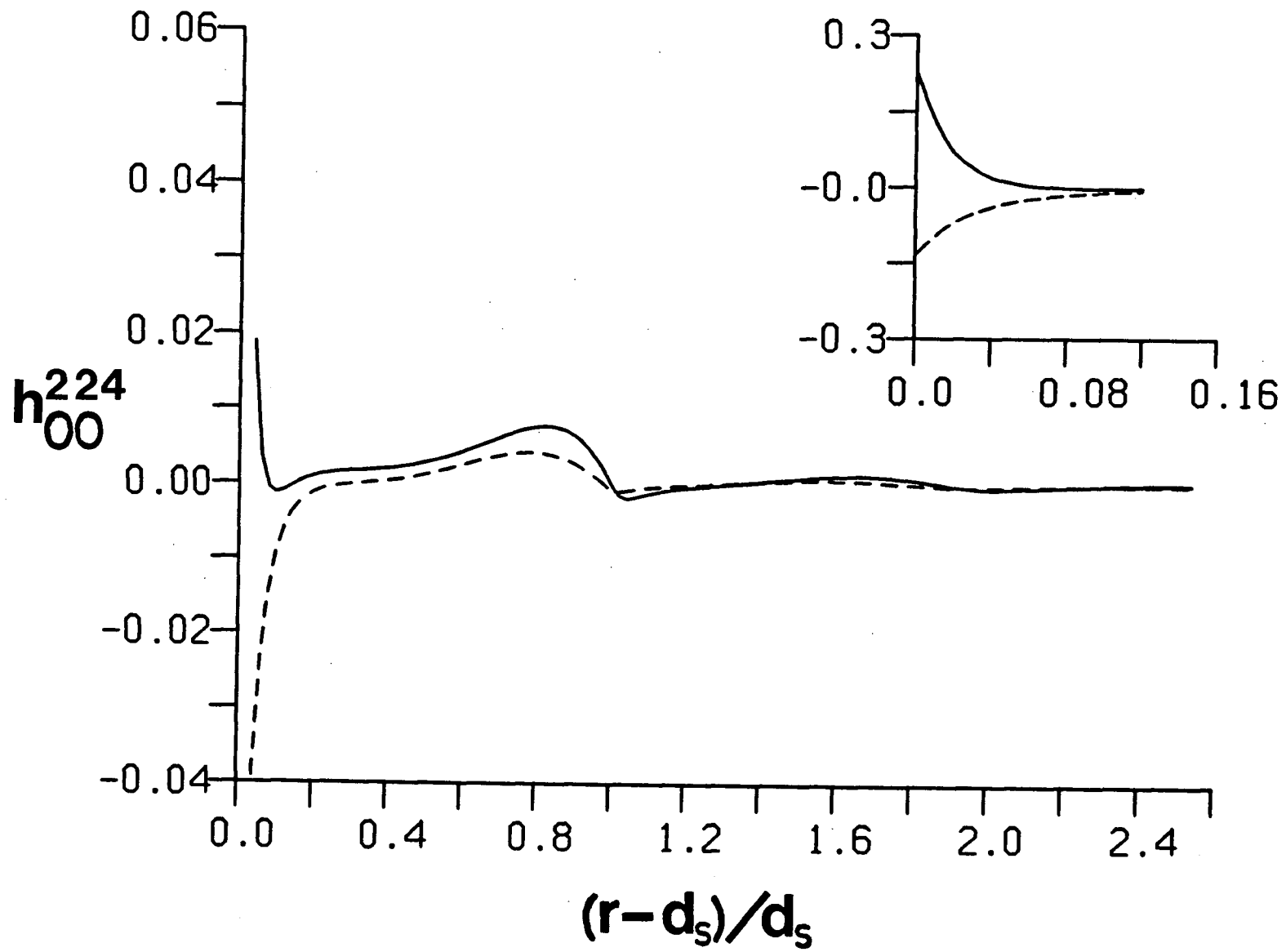


Figure 15.

The projection  $h_{02}^{224}(r)$ . The curves are defined as in Figure 10.

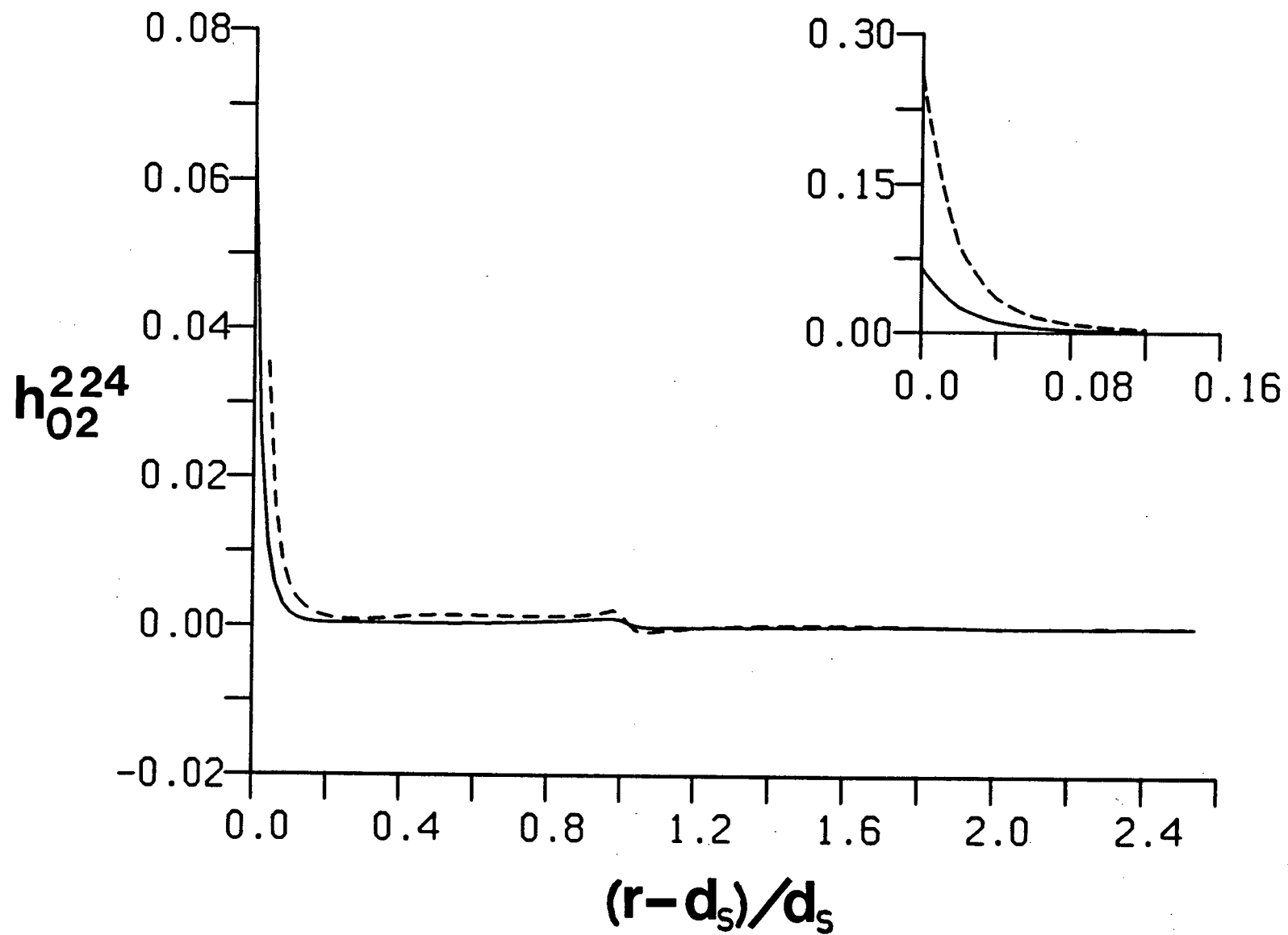
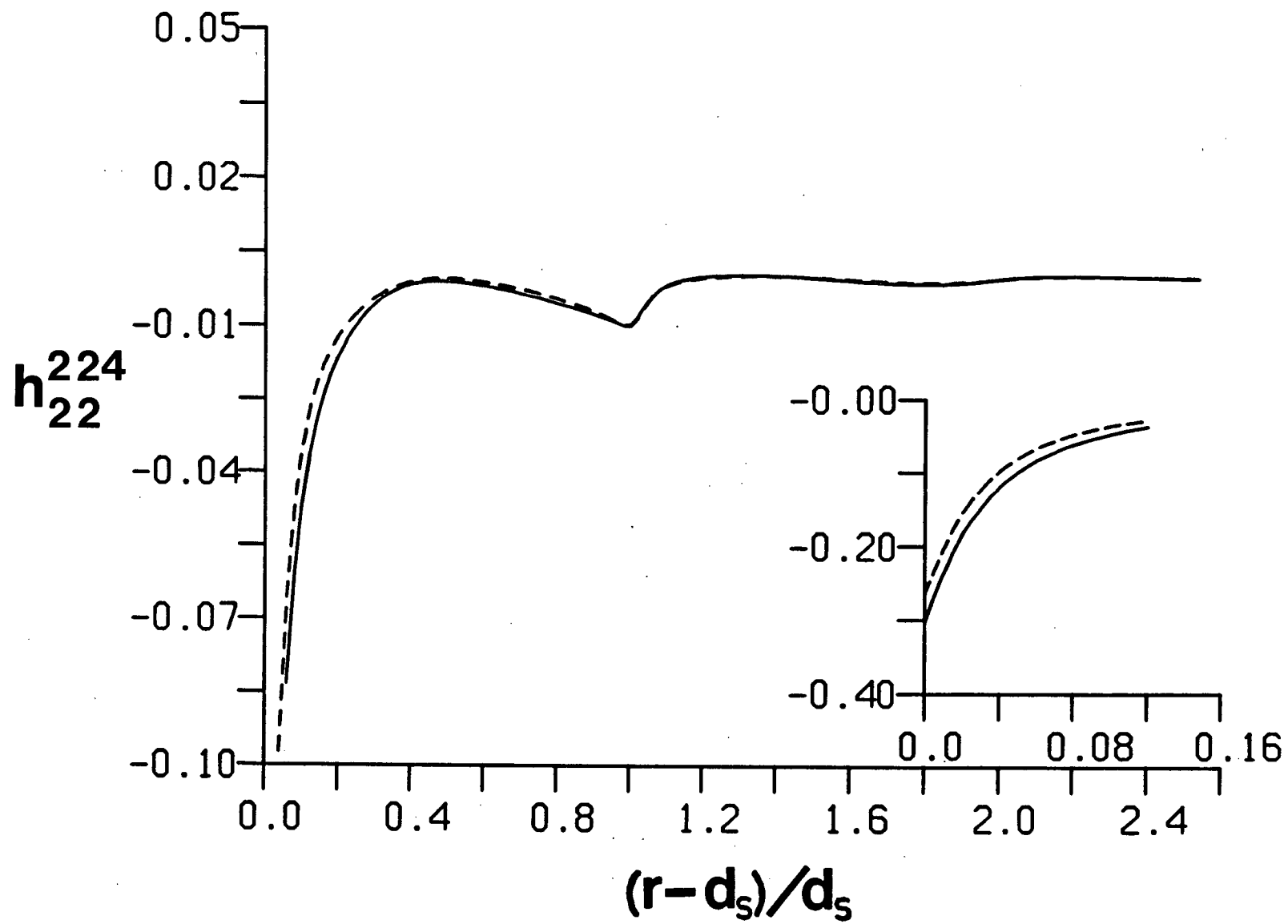


Figure 16.

The projection  $h_{22}^{224}(r)$ . The curves are defined as in Figure 10.



and  $h_{22}^{224}(r)$  appear to be the least affected. However, we find that there is no systematic variation in the correlation functions since each represents a different angle dependence. The dipole-dipole correlations, as given by  $h_{00}^{110}(r)$  and  $h_{00}^{112}(r)$ , are of particular interest. In both cases we find that the correlation functions become less structured with the addition of the octupole moment. This is consistent with the observed drop in the dielectric constant and the decrease in the average dipole-dipole energy. Clearly, the octupole forces act to disrupt the dipolar structure within the fluid. This is, of course, also true of the quadrupole [67].

Before concluding this discussion of results for hard-sphere water-like fluids, we point out that because of its simplicity, the tetrahedral model was used extensively in our study of model aqueous electrolyte solutions (as will be discussed in Chapter VI). It is obvious from Tables III and VI that this solvent model reduces the computational resources required to solve the RHNC theory. This becomes an important consideration in the case of electrolyte solutions, particularly at low concentration where a much larger number of points is required in the numerical grid. In previous studies [67,72,79-81] in which the tetrahedral model was employed, the parameter  $\Theta_s$  was somewhat arbitrarily set to the value of  $2.50 \times 10^{-26}$  esu cm<sup>2</sup>. In the present study, we have found that this value of the square quadrupole moment underestimates the effect of the full quadrupole tensor of water. However, we do find that  $\Theta_s = 2.57 \times 10^{-26}$  esu cm<sup>2</sup> (which is just slightly larger than half the sum of the magnitudes of  $\Theta_{xx}$  and  $\Theta_{yy}$ ) works very well as an *effective* square quadrupole moment. In this case the tetrahedral and  $C_{2v}$  quadrupole models give almost identical results for all average properties, including the dielectric constant and average energies. The radial distribution functions appear indistinguishable. Thus, this value of the square quadrupole moment was used in the tetrahedral solvent model employed in our study of aqueous electrolyte solutions.



#### 4. Results for Soft Models

In the previous section we have found that for hard-sphere water-like fluids, the RHNC results for  $\epsilon$  do not agree well with experiment at lower temperatures, *i.e.*,  $< 100^\circ\text{C}$ . We have speculated that this discrepancy might be due to the fact that the structure, *i.e.*, the radial distribution function, of these model systems is quite different from that of real water. In this section we will show how the *correct* structure can be obtained by modifying only the spherical potential (*i.e.*, by making the model soft). We will then examine the dielectric properties of this new model.

First, let us define an empirical short-range potential

$$u_{\text{SR}}(r) = \tau \left[ A e^{ar} + B e^{br} + C e^{cx^2} + D e^{dy^4} \right], \quad (5.3a)$$

where

$$x = r - x_0 \quad (5.3b)$$

and

$$y = r - y_0. \quad (5.3c)$$

This potential was added to the  $C_{2v}$  octupole model as a spherically symmetric term and the hard-sphere diameter was reduced to  $0.92d_s$ . The parameters  $a$ ,  $b$ ,  $c$  and  $d$  were empirically assigned the values  $-10d_s^{-1}$ ,  $-40d_s^{-1}$ ,  $-35d_s^{-2}$  and  $-700d_s^{-4}$ , respectively.  $\tau$  was taken as  $1.34 \times 10^{-13}$  ergs per molecule, while  $x_0 = 1.16d_s$  and  $y_0 = 1.65d_s$ . In Table VIII the values of  $A$ ,  $B$ ,  $C$  and  $D$  used to generate three different forms of  $u_{\text{SR}}(r)$  are given. These will prove useful in examining the effects of turning on, or off, certain parts of the potential. In Figure 17 we have shown the three forms of the potential

TABLE VIII. Parameters for  $u_{\text{SR}}(r)$ .

Potential	A	B	C	D
$u_{\text{SR}}^{(1)}(r)$	40000	$1 \times 10^{15}$	0	0
$u_{\text{SR}}^{(2)}(r)$	40000	$1 \times 10^{15}$	0.18	0
$u_{\text{SR}}^{(3)}(r)$	40000	$1 \times 10^{15}$	0.18	-0.08

Figure 17.

Soft potentials at 25°C. The solid, dotted and dashed lines represent the potentials  $\beta u_{SR}^{(3)}(r)$ ,  $\beta u_{SR}^{(2)}(r)$  and  $\beta u_{SR}^{(1)}(r)$ , respectively, where the forms of these potentials are defined by the parameters given in Table VIII.

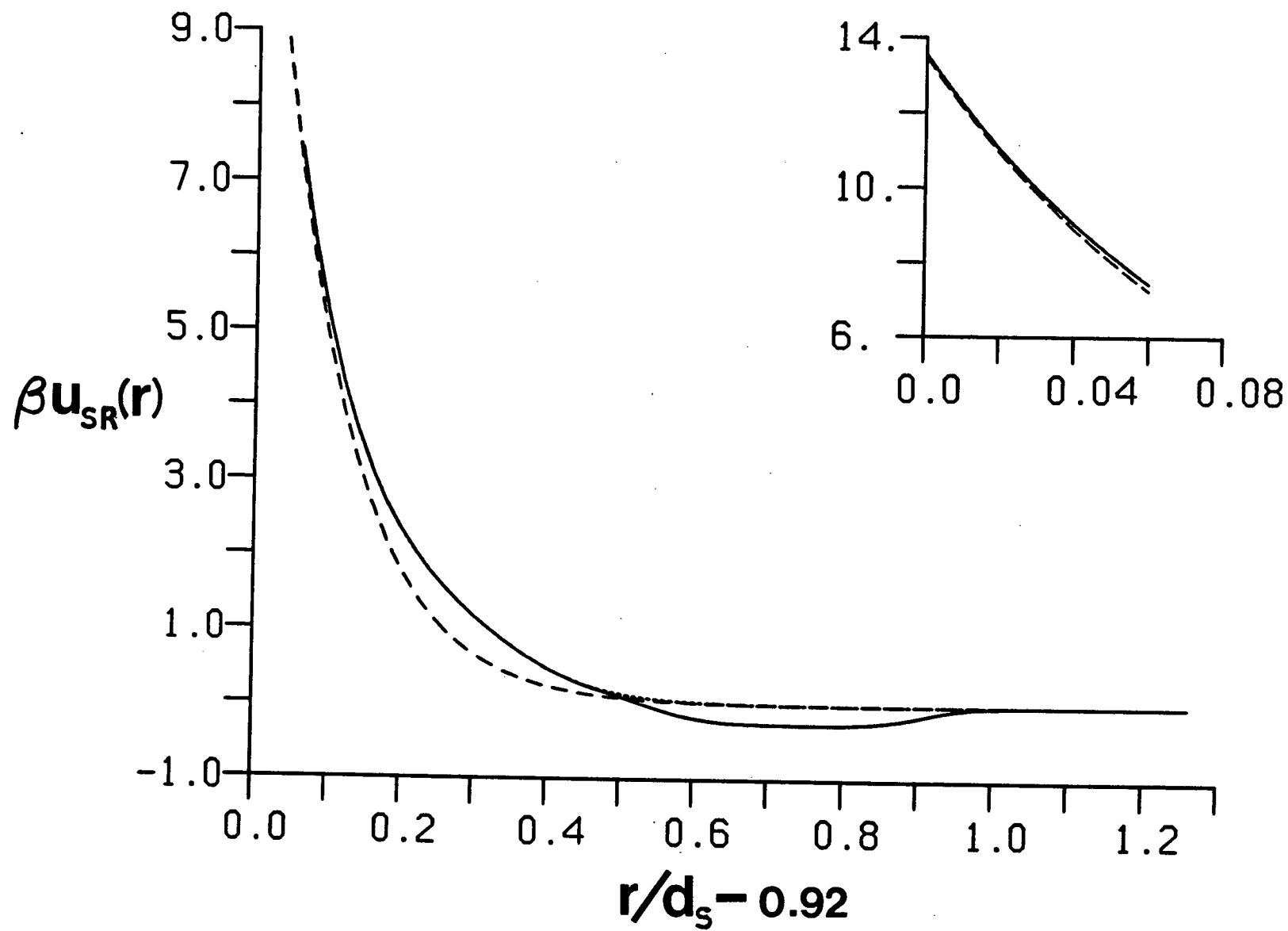
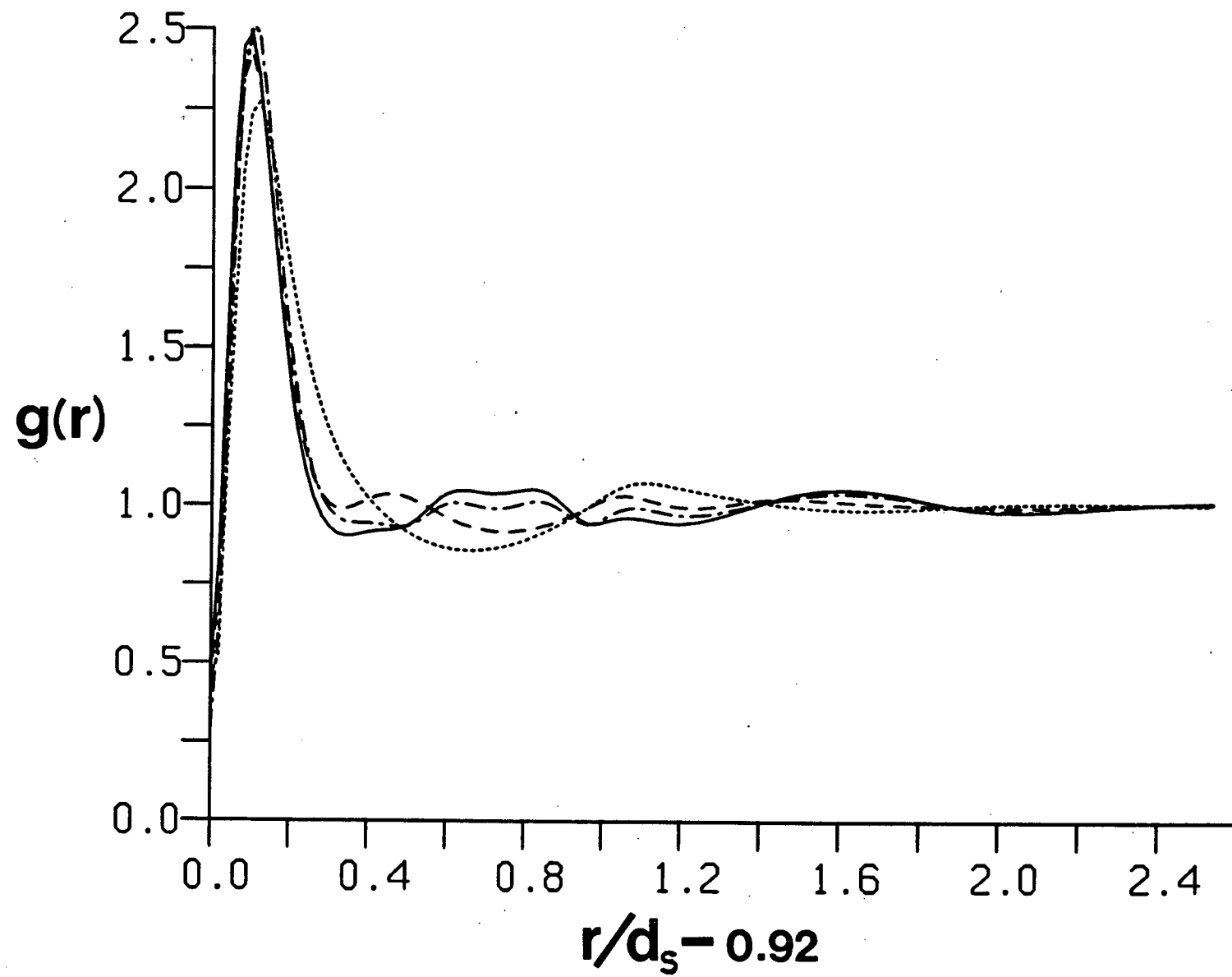


Figure 18.

Radial distribution functions for soft water-like models at 25°C and  $m_e^* = 2.75$ . The solid, dashed and dotted lines are RHNC results for the models employing  $\beta u_{SR}^{(3)}(r)$ ,  $\beta u_{SR}^{(2)}(r)$  and  $\beta u_{SR}^{(1)}(r)$ , respectively. The dash-dot line represents  $g(r)$  for the model system using  $\beta u_{SR}^{(3)}(r)$  but with no octupole moment.



which we will investigate at 25°C. We point out that  $\beta u_{SR}^{(2)}(r)$  may be hard to detect because it is indistinguishable from  $\beta u_{SR}^{(3)}(r)$  for  $r < 1.35d_s$  and  $\beta u_{SR}^{(1)}(r)$  for  $r > 1.45d_s$ . It is clear from Figure 17 that these potentials are simple smooth functions.

In Figure 18 we have shown RHNC results for the radial distribution function for 4 different soft water-like models 25°C. The dependence upon the various terms in the soft potential, as well as upon the octupole moment can be seen. We find that when a simple soft potential like  $\beta u_{SR}^{(1)}(r)$  is employed, the first peak in  $g(r)$  becomes quite broad, its maximum being less than 2.5. This is consistent with results which have been reported [121] for water at 25°C. However, the first minimum in  $g(r)$  appears approximately where the second peak should be. Moreover, the coordination number is somewhere within the range 6-8, depending upon where we stop the integration in eq. (5.2). In order to correct the position of the first minimum and to reduce the CN, another repulsive term is added to the spherical potential, *i.e.*, we use  $\beta u_{SR}^{(2)}(r)$ . The first minimum in  $g(r)$  now appears in about the correct position and CN=4.7 which is close to that of real water. However, the radial distribution function still has a minimum at about  $r = 1.7d_s$  with small peaks on either side. These two small peaks are drawn into a single peak centred at  $r = 1.65d_s$  with the additional attractive term contained in  $\beta u_{SR}^{(3)}(r)$ . We also see from Figure 18 that if the octupole moment is not included in the model, then  $g(r)$  is clearly affected. The most significant of the effects is the drop in the second peak at the tetrahedral distance. This would seem to indicate that the octupole moment is important in stabilizing the tetrahedral structure. In the discussion below we shall refer to the water-like model which utilizes  $u_{SR}^{(3)}(r)$  and includes the octupole moment as the *soft*  $C_{2v}$  model.

The radial distribution functions of the soft  $C_{2v}$  and of the  $C_{2v}$  octupole fluids at 25°C are compared with the experimental  $g(r)$  of Narten and Levy [121] in Figure 19. The RHNC result for the soft  $C_{2v}$  model is in good agreement with the experimental curve, while that of the  $C_{2v}$  octupole fluid is clearly in very poor agreement. In Figure 20 the structure factors,  $S(k)$ , of the two model systems are again compared with the experimental result of Narten and Levy [121]. In general, the partial structure factor is defined [13] by

Figure 19.

Radial distribution functions of water and of water-like fluids at 25°C and  $m_e^* = 2.75$ . The solid and dashed lines are RHNC results for the soft  $C_{2v}$  and the  $C_{2v}$  octupole model systems, respectively. The dotted line is the experimental result of Narten and Levy [121]. We note that most of the contact peak for the  $C_{2v}$  octupole model does not appear on the plot.

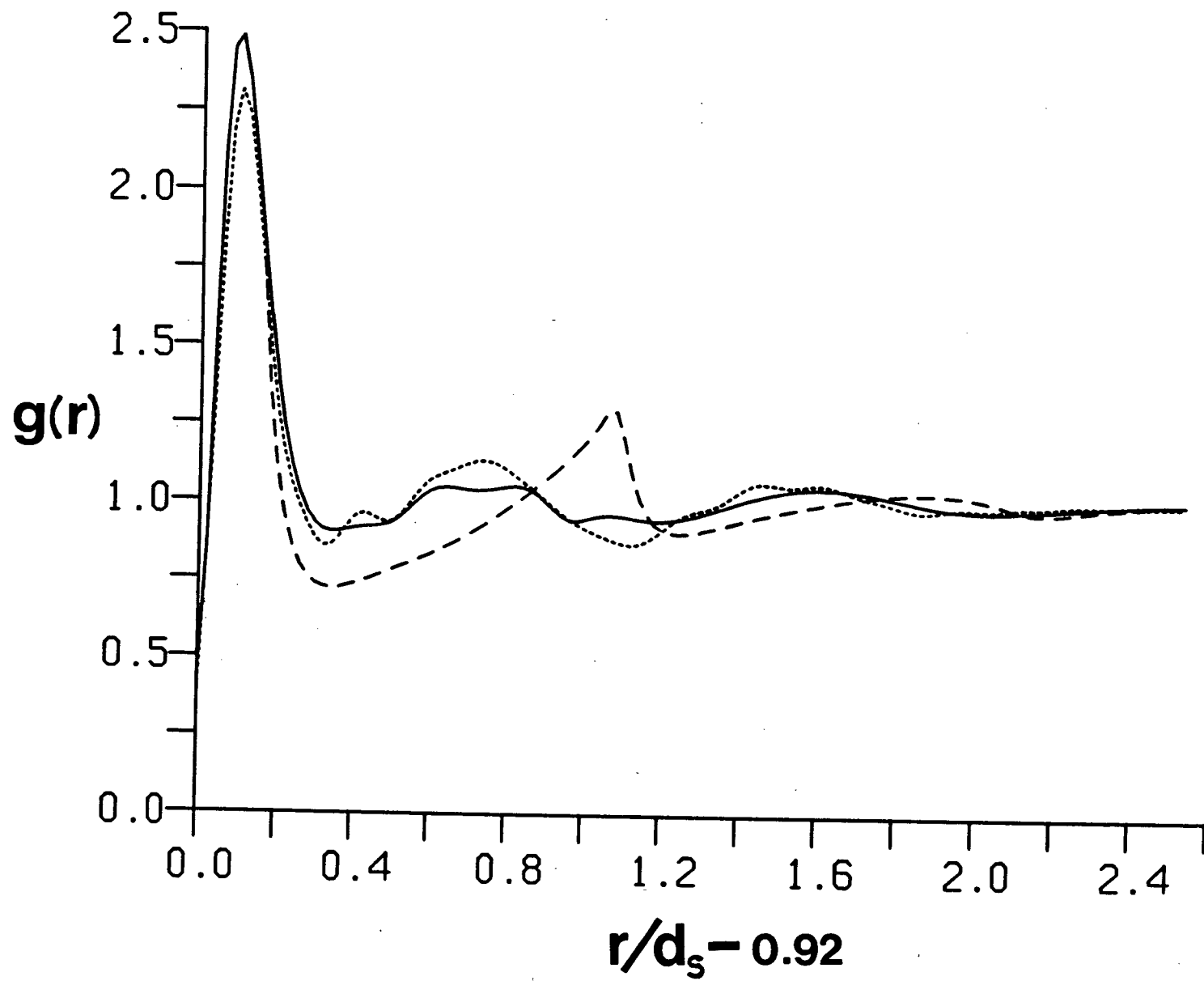
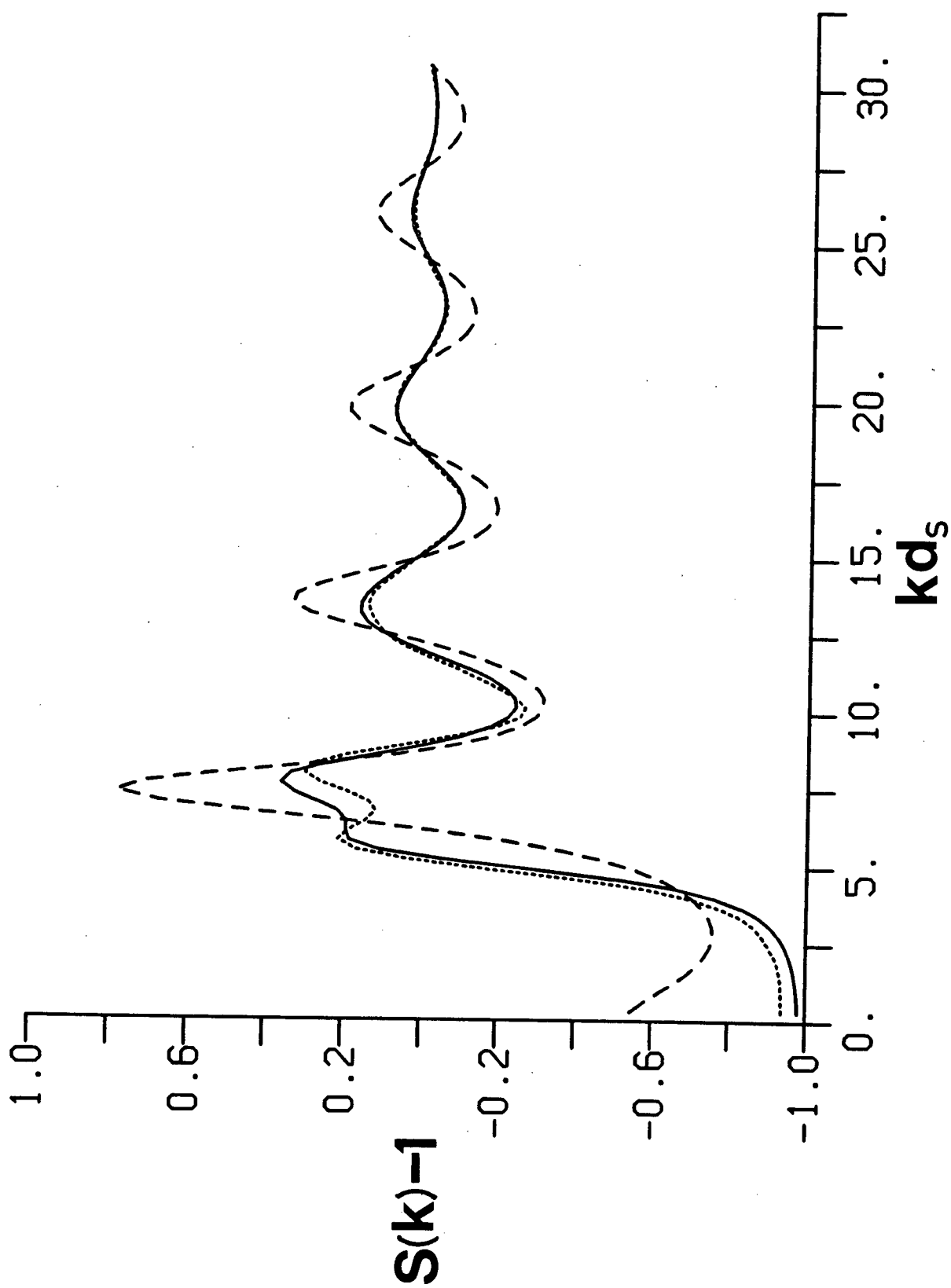




Figure 20.

Structure factors of water and of water-like fluids at 25°C and  $m_e^* = 2.75$ . The curves are as in Figure 19.



$$S_{\alpha\beta}(k) = 1 + \frac{4\pi\rho}{k} \int_0^{\infty} r (g_{\alpha\beta}(r)-1) \sin kr \, dr , \quad (5.4)$$

Clearly, the soft  $C_{2v}$  model is again in good agreement with experiment. The  $S(k)$  of the  $C_{2v}$  octupole fluid does not show the characteristic split peak evident in the experimental curve and its amplitude of oscillation is too large. We stress that the only difference between the  $C_{2v}$  octupole and the soft  $C_{2v}$  models is the addition of the spherical potential,  $u_{SR}^{(3)}(r)$ . However, what is not entirely clear is whether  $u_{SR}^{(3)}(r)$  is simply correcting for inadequacies in the hard-sphere model, or whether it is also compensating for a deficiency in the RHNC theory. Very recent work [173] suggests that part of the problem may actually lie with the RHNC theory.

Full RHNC/SCMF calculations were then done at 25°C and 300°C using the soft  $C_{2v}$  model. The resulting average dipole moments and dielectric constants are shown in Figures 7 and 8, respectively. At 25°C the average dipole moment is slightly larger than the  $C_{2v}$  octupole result, while at 300°C the opposite is found. Of most importance here is the fact that the dielectric constants obtained at both temperatures are in very good agreement with experiment. Thus, it would appear that the unique packing structure of water at low temperature does influence its dielectric properties.

Again, we emphasize that there is nothing unique about our choice of a soft potential, *i.e.*,  $u_{SR}^{(3)}(r)$ . Our purpose was merely to show that the experimental structure for water at 25°C could be fit with a simple multipolar model by adjusting the soft spherical potential.

## CHAPTER VI

### RESULTS FOR MODEL AQUEOUS ELECTROLYTE SOLUTIONS

#### 1. Introduction

In this study we have investigated model electrolyte solutions consisting of a single salt dissolved in one of the water-like solvents described in Chapter V. The vast majority of the solutions examined (virtually all those at finite concentration) utilize the tetrahedral solvent model because of its simplicity, as described in Chapters II and V. Also, in Chapter V we have shown that when the full quadrupole tensor of water is replaced by an effective square quadrupole moment, the properties of the pure water-like solvent remain essentially unchanged. The ions are treated simply as charged hard spheres, as discussed in Chapter II. Only univalent ions were considered; their hard-sphere diameters are given in Table I. All the model solutions investigated were at 25°C.

Model aqueous electrolyte solutions of this type had been previously studied at infinite dilution with the RLHNC theory [79-81]. As an extension of this earlier work [79-81], we began the present study by first attempting to examine the same model solutions, again using the RLHNC, but now at finite concentration. We found that although the RLHNC theory appears to give reasonable results for ion-ion potentials of mean force at infinite dilution, it does not work well for model aqueous electrolyte solutions at finite concentration. Small ions appear to be quite insoluble (*e.g.*, for KCl we were able to obtain numerical solutions only up to a concentration of 0.125M), while larger ions appear to be quite soluble (*e.g.*, for CsI we were able to reach a concentration of 2M with no apparent difficulties). Clearly, this behaviour is not consistent with what is observed for real aqueous solutions of the alkali halides [169]. This unrealistic behaviour of the RLHNC theory is largely due to the fact that the RLHNC closure allows no direct coupling between anisotropic terms in the pair potential and the radial distribution function, as discussed in Chapter II. Consequently, we find that in the RLHNC theory the degree of solvation of an ion (*i.e.*, the packing of the solvent around the ion) is determined almost exclusively by the hard-sphere packing structure. Obviously then, we would not expect the RLHNC theory to give

good results where there are strong interactions between the ion and the solvent, as is the case for aqueous electrolyte solutions.

The reference QHNC theory [63] was also briefly examined for the same model for aqueous electrolyte solutions. The ion solvation, particularly for smaller ions, was found to greatly improve (*i.e.*, the contact values of  $g_{is}(r)$  increased sharply). Furthermore, this change in the degree of solvation had a strong influence upon not only the thermodynamic properties of the solution, but also the ion-ion structure (*i.e.*,  $g_{ij}(r)$ ). These results clearly showed the sensitivity of these systems and indicated that a very accurate theory would be required in order to obtain accurate results for the present models. Therefore, in the remainder of this Chapter essentially all the results reported for model electrolyte solutions were obtained using the RHNC theory, as described in Chapter II.

The HNC basis set dependence of the properties of interest in this study was examined. The particular case of a model KCl solution at 0.5M was considered. As was the case for the pure solvent, strong basis set dependence was observed for all properties when going from  $n_{\max}=2$  to  $n_{\max}=3$  to  $n_{\max}=4$ . Fortunately, we again found only slight basis set dependence for almost all results when going to  $n_{\max}=5$  (*e.g.*, the constant volume derivative of the activity coefficient increased by about 1%). Of the properties examined,  $\bar{V}_2$  showed the greatest sensitivity, increasing 2.6 cc/mole. We remark that the  $n_{\max}=5$  calculation was pushing our computational resources to their limit, and hence the  $n_{\max}=6$  calculation was not even attempted. Thus, the  $n_{\max}=4$  HNC basis set (now containing 95 unique projections) was used exclusively to obtain all other results reported in this chapter.

In this study we have examined several model aqueous electrolyte solutions (employing the tetrahedral water-like solvent) over a range of concentrations, including infinite dilution, as given in Table IX. (We remark that the molarity concentration scale has been used universally throughout this chapter.) Aqueous solutions of alkali halides have received the most attention, although three other salts have also been considered. In order to mimic the constant pressure conditions under which most real electrolyte solutions are studied, we have used the experimental densities [174,175] of the real systems whenever possible in our model calculations. For both MBr and M'I we have

**TABLE IX.** Model aqueous electrolyte solutions studied. Those concentrations given in parentheses are for solutions which are beyond the solubility limit of their real counterparts. The concentrations indicated with a star represent those beyond which numerical solutions could not be obtained.

Salt	Concentration (moles/litre)
LiF	0
LiCl	0*
NaCl	0, 0.025, 0.05, 0.075, 0.1, 0.25, 0.5, 0.75, 1.0, 1.5, 2.0, 3.0, 4.0, (6.0), (8.0), (12.0), (16.0)
KCl	0, 0.025, 0.05, 0.075, 0.1, 0.15, 0.25, 0.5, 0.75, 1.0, 1.5, 2.0, 3.0, 4.0
CsI	0, 0.025, 0.05, 0.075, 0.1, 0.15, 0.25, 0.5, 0.75, 1.0, 1.5, 2.0, 2.5, (3.0), (4.0), (6.0), (9.0), (9.1)*
MBr	0, 0.025, 0.05, 0.075, 0.1, 0.25, 0.5, 0.6, 0.7, 0.75, 0.8, 0.85, 0.9, 1.0
M'I	0, 0.025, 0.05, 0.075, 0.1, 0.25, 0.5, 0.6, 0.65, 0.7, 0.725, 0.74*
EqEq	0, 0.025, 0.05, 0.075, 0.1, 0.25, 0.5

employed the density data of a  $(C_2H_5)_4NBr$  solution [175]. We point out that MBr and M'I have the same value of  $\bar{d}_{+-}$  (as given by eq. (2.24b)). In the discussions below we will use  $\bar{d}_{+-}$  as measure of the *ion size* of a salt. For the EqEq solutions we have employed the densities of aqueous NaCl since both salts again have the same value of  $\bar{d}_{+-}$ . Thus, results from model EqEq and NaCl solutions, as well as from MBr and M'I solutions, can be compared in order to examine the effects of ion asymmetry.

In the present study we found that the RHNC theory could be solved for our model NaCl and CsI solutions at concentrations above the solubility limits of their real counterparts, as indicated in Table IX. For example, we were still able to study our model NaCl solution at a concentration of 16M, which corresponds to the mole fractions  $x_1=0.25$  and  $x_s=0.50$ ! Densities for these systems were obtained by extrapolating the experimental results. We point out that for the salts M'I and CsI there were concentrations beyond

which we were numerically unable to solve the RHNC theory (also indicated in Table IX). The behaviour of these solutions near these points will be discussed below. It is obvious from Table IX that for the most part the alkali halides are very soluble in the tetrahedral solvent. An apparent exception to this rule appears to be LiCl. However, the difficulties encountered with LiCl may quite possibly be numerical in origin. In order to reach a finite (but low) concentration of a given salt, a numerical solution set for that same salt at infinite dilution always served as the initial guess (input) into the RHNC theory. For all the other salts investigated (*i.e.*, those given in Table IX) this scheme worked well. Unfortunately, because of the extreme behaviour demonstrated by Li<sup>+</sup> at infinite dilution (as described below), this method may not be applicable to model solutions of Li<sup>+</sup> salts.

The solvent models we have considered in this study are polarizable. Hence, a full SCMF calculation (as outlined in Chapter IV) would be required, in principle, at every concentration for each solution we wish to investigate. Of course, for a solution at infinite dilution all properties of the solvent, including its effective dipole moment, remain unchanged from those of the pure solvent. A full SCMF calculation was carried out on a KCl solution at 2.0M. We found that even at this relatively high concentration the average local electric field in the bulk (as given by the SCMF theory) changed by less than 1% from the pure solvent value. Consequently, the effective dipole moment obtained,  $m_e^* = 2.734$ , differs from the pure tetrahedral solvent result by less than 0.25%. If we define the quantity

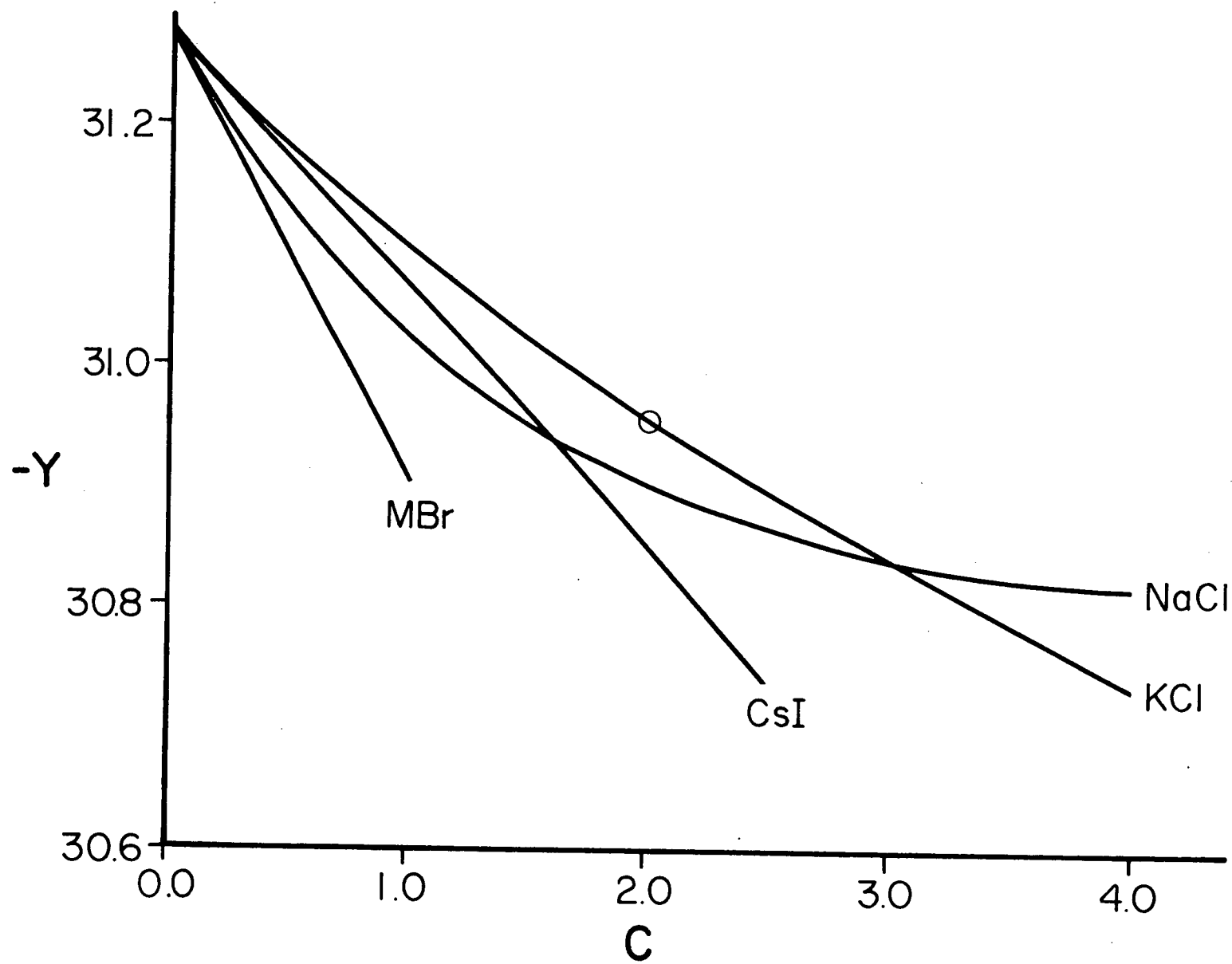
$$Y = \frac{U_{DD}^e}{2N_s kT} + \frac{U_{DQ}^e}{N_s kT} + \frac{U_{ID}^e}{N_s kT}, \quad (6.1)$$

then it clearly follows from eqs. (4.12) and (4.19) that within the SCMF theory  $Y$  will be related to the average local field in the bulk. In Figure 21 we have shown  $Y$  for several solutions which were examined using  $m_e^* = 2.74$ , the pure solvent value. The value of  $Y$  obtained for a 2.0M KCl solution has also been clearly indicated. It is obvious from Figure 21 that even at concentrations of 4.0M, we would still expect the average local field in the bulk to remain very close to the pure solvent result. Thus, at least for the current models within the SCMF approximation, it would appear that as the concentration of an electrolyte solution is increased, the decrease in the solvent contribution to

Figure 21.

The concentration dependence of  $\gamma$ . Results are given for four salts in the tetrahedral solvent for which  $m_e^* = 2.74$ . The point indicated with a circle represents a 2.0M KCl solution. Its significance is discussed in the text.





the average local electric field is almost exactly compensated by an increased contribution from the ions. Therefore, to a very good approximation, the effective dipole moment of the pure tetrahedral solvent can be taken as being independent of salt concentration. This is what was done in the present study, and hence all finite concentration results presented in this chapter were determined using  $m_e^* = 2.74$ . Moreover, the solvent model then becomes equivalent to a non-polarizable model with a permanent dipole moment equal to  $m_e$ . It should also be noted that not performing a full SCMF calculation at each concentration for every solution represents a substantial reduction (by at least a factor of three) in the total number of computations required.

In Chapter IV we have introduced the RDMF theory which allows us to examine the average local field experienced by a solvent particle as a function of its separation from an ion. The effects of treating the polarization of the solvent at this level will be examined in section 5, where we will present results obtained at infinite dilution and at low concentration.

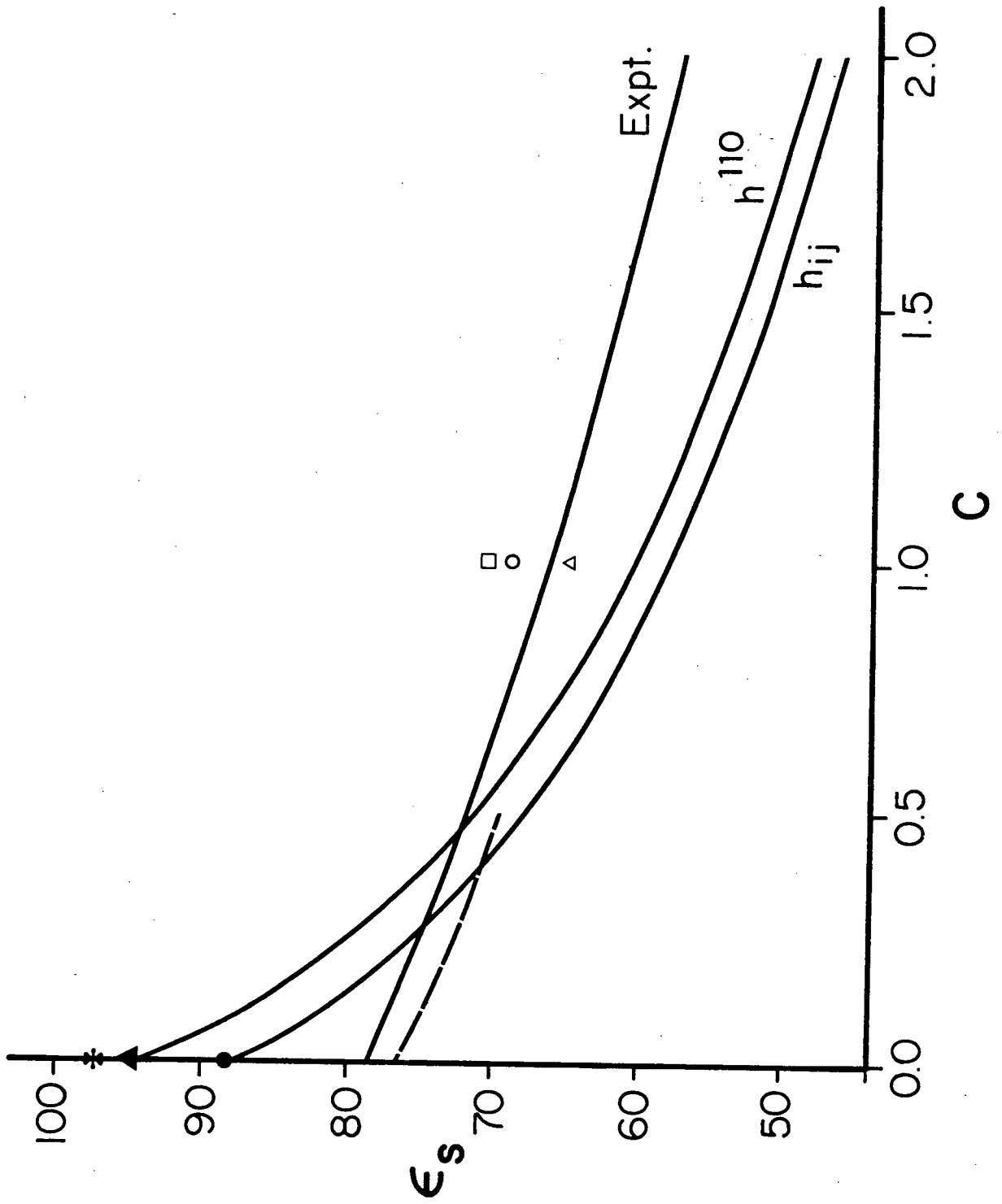
All the results for model aqueous electrolyte solutions reported in sections 2 through 5 were determined using the tetrahedral solvent model with  $m_e = 2.605D$ . In section 6 we will consider model electrolyte solutions at infinite dilution which employ several different solvent models, including the nonpolarizable tetrahedral solvent (*i.e.*,  $m_e = \mu = 1.855D$ ), as well as the  $C_{2v}$  quadrupole and  $C_{2v}$  octupole solvents described in Chapter V. Particular attention will be paid to the effects the different water-like solvents have upon ion-solvent and ion-ion structure.

## 2. Dielectric Properties

The equilibrium dielectric constants,  $\epsilon_s$ , of our model electrolyte solutions were determined using eqs. (2.95), (2.96) and (2.97). In principle, these three formulas should all yield the same value for  $\epsilon_s$ . However, in Figure 22 we see that numerically the agreement is not exact. We find that eqs. (2.95) and (2.96) give results which are essentially in mutual agreement and which extrapolate to an infinite dilution value that is consistent with those calculated for the pure solvent. The dielectric constants determined from eqs. (2.97) are consistently smaller (by about 5%) than those obtained from the

Figure 22.

Comparing theoretical and experimental values for the dielectric constant of aqueous KCl solutions. The lines labelled with  $h^{110}$  and  $h_{ij}$  represent RHNC results for model solutions calculated from eqs. (2.96) and (2.97), respectively, employing Simpson's rule for the required integrations. At finite concentration  $\epsilon_s$  as given by eqs. (2.95) fall very close to the  $h^{110}$  curve. The star and the solid triangle are values for the pure tetrahedral solvent ( $m_e^*=2.74$ ) obtained from eqs. (2.93) using Simpson's rule and from eqs. (2.95) using trapezoidal rule, respectively, while the dot is the pure solvent dielectric constant obtained from the limiting slope of  $\rho_2 G_{+-}$ . The experimental line represents the results of Behret *et al.* [176] for aqueous KCl, while the open square, circle and triangle are measurements of Harris and O'Konski [177], Giese *et al.* [178] and Haggis *et al.* [179], respectively. The dashed line is  $\epsilon_s$  for a model CsI solution studied with the RLHNC theory.



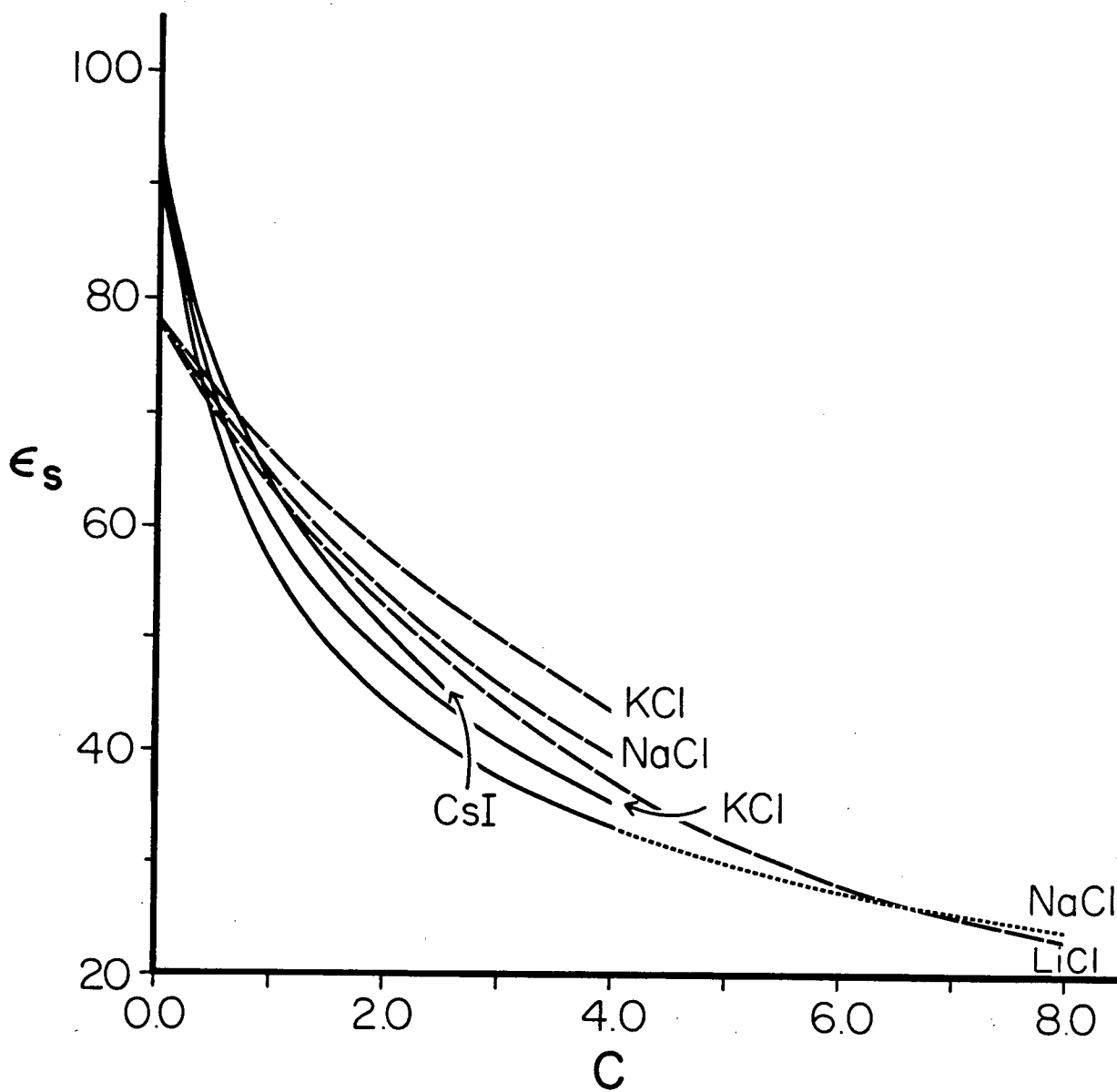
other two routes and extrapolate to a value lower than those found for the pure solvent. This extrapolated value does, however, agree very well with the pure solvent dielectric constant,  $\epsilon = 88.3$ , which is consistent with all limiting law behaviour reported in section 3. Unfortunately, this discrepancy appears to be due to the lack of numerical accuracy in the Hankel transforms, with the limiting factors being the FFT and the numerical grid width employed,  $\Delta r = 0.02$ . (We remark that for solution systems with smaller values of the electrostatic parameters the agreement between the various routes to  $\epsilon_s$  is much better.) In Figure 22 we see that the discrepancy between the various routes to the dielectric constant is comparable to the variation found between typical experimental results. Moreover, the qualitative behaviour of  $\epsilon_s$  for our model solutions is independent of the route used to determine it. The dielectric constants we will report below were all obtained from eq. (2.96).

Also included in Figure 22 are RLHNC results for  $\epsilon_s$  for a model CsI solution. This theoretical curve is very similar to the experimental curve for KCl. We note that the dielectric properties of aqueous KCl and CsI solutions are quite similar at concentrations below 1M [176,180]. Thus, as with the pure solvent, the RLHNC values (when they can be obtained) for the dielectric constants of the model aqueous electrolyte solutions being considered here are in surprisingly good agreement with experiment. Unfortunately, the RLHNC results are probably less accurate than those for the RHNC for the present models.

In Figure 23 we have compared experimental values of the dielectric constants with those determined in the present study for model aqueous electrolyte solutions. We find that at low concentration the RHNC results for  $\epsilon_s$  are consistently larger than those of experiment. This is simply a consequence of the fact that the pure tetrahedral solvent has a larger dielectric constant than does pure water. We also observe in Figure 23 that for our model solutions the limiting slopes for  $\epsilon_s$  are steeper than those found for their real counterparts. Again, the larger value of  $\epsilon$  for the pure solvent can partially account for this discrepancy since the limiting slope depends upon  $\epsilon$  [79]. At higher concentrations (*i.e.*,  $>1M$ ) the results for our model electrolyte solutions appear to be in qualitative agreement with experiment. Even at very high concentration (*i.e.*, 8.0M) our model NaCl solution has very similar behaviour to that of a real LiCl solution. For our

**Figure 23.**

The dielectric constants of real and of model aqueous electrolyte solutions as functions of concentration. The solid lines are RHNC results for model solutions of NaCl, KCl and CsI, while the dashed lines represent the experimental values [176] for LiCl, NaCl and KCl. The dotted portion of the model NaCl curve indicates the concentrations for which extrapolated values of the density were used.



model solutions  $\epsilon_s$  decreases more slowly with  $c$  for larger ions, which is also consistent with what is observed experimentally. Thus, the dielectric properties of our model aqueous electrolyte solutions are in reasonable qualitative agreement with experiment.

### 3. Thermodynamic Properties

First we will examine the average energies of the model electrolyte solutions being investigated in this study. The average energies of the effective systems were calculated using eqs. (2.80) and (2.81). In principle, in order to determine the total average energies of the polarizable systems within the SCMF approximation, we must employ eq. (4.20) which we can rewrite as

$$U_{TOT} = U_{TOT}^e + U_{POL} , \quad (6.2)$$

where  $U_{POL}$  is the total polarization energy. However, we have already found that to a very good approximation  $\langle E_1 \rangle^e$  (and hence  $U_{POL}$ ) is independent of salt concentration and we have taken  $m_e$  to be constant. Therefore, in the present study the energies we will report are those of the effective system (when applicable), since those of the polarizable system are very closely related, never differing by more than an additive constant or multiplicative factor.

In Figure 24 we have shown the average total ion-ion energies per ion for model NaCl, KCl and MBr solutions along with the limiting slope given by eq. (3.75). The ion-ion energies of all three solutions increase in magnitude with increasing concentration and approach their limiting behaviour at low concentration (*i.e.*,  $<0.1M$ ). At higher concentration we find that KCl has the most negative values, although for all the salts examined the average ion-ion energies are always smaller in magnitude than those predicted by the limiting law relationship (*i.e.*, eq. (3.75)). We remark that the CsI line, which has not been included in Figure 24, lies between the KCl and NaCl curves. For solutions of both larger and smaller ions than KCl (*e.g.*, NaCl and MBr), it can be seen that the average ion-ion energies deviate more quickly from the limiting law.



Figure 24.

Average total ion-ion energies per ion as functions of square root concentration. The solid lines are RHNC results for three of the model electrolyte solutions studied, while the dashed line represents the limiting slope determined from eq. (3.75) using  $\epsilon=88.3$ . We point out that it is the negative energies which have been plotted.

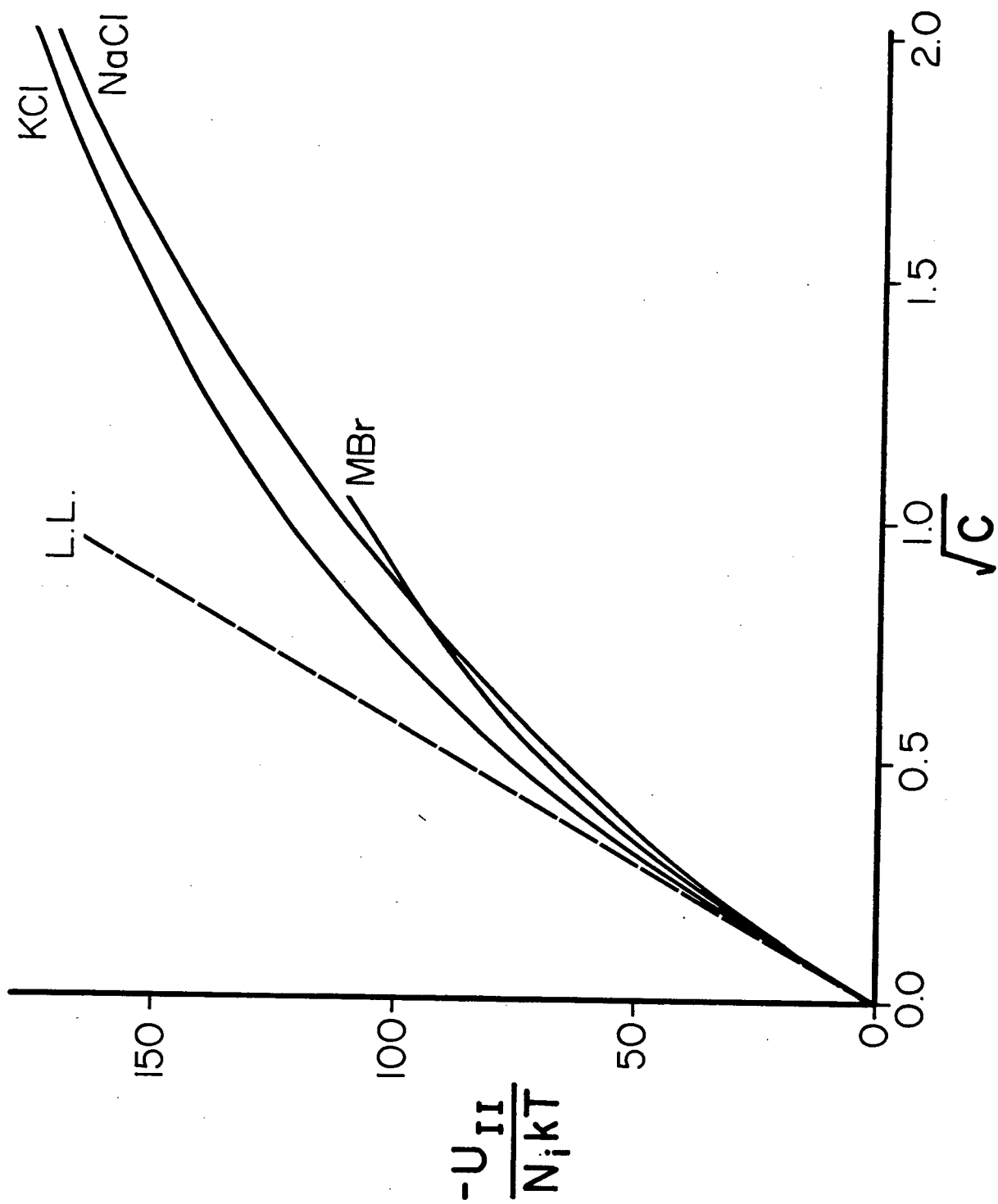
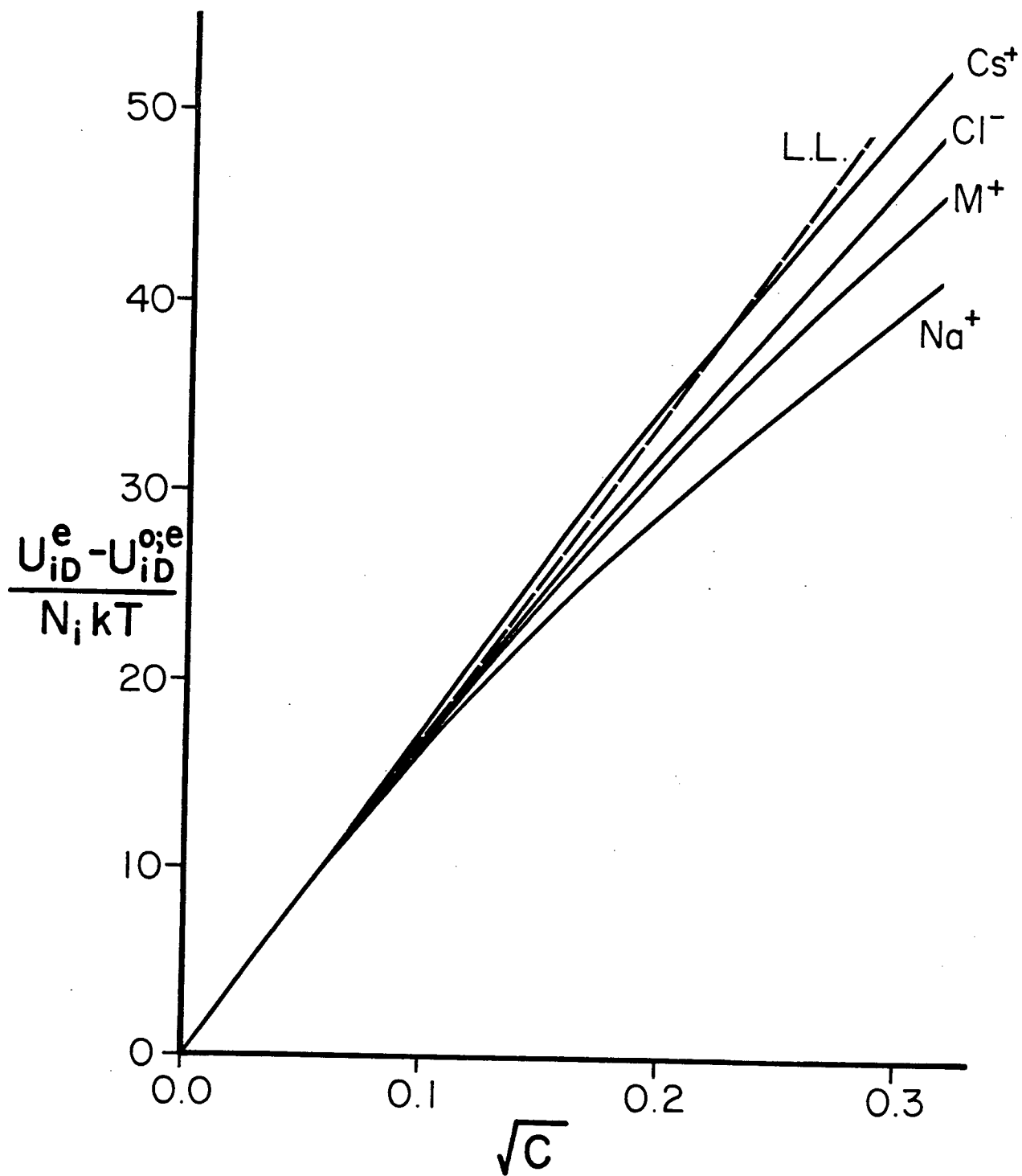


Figure 25.

Average ion-dipole energies per ion as functions of square root concentration. The solid lines are RHNC results for four of the ions being investigated,  $\text{Na}^+$  and  $\text{Cl}^-$  of NaCl,  $\text{Cs}^+$  of CsI and  $\text{M}^+$  of MBr. The dashed line represents the limiting slope determined from eq. (3.76) employing  $\epsilon = 88.3$ . For ease of comparison the infinite dilution values (which are negative) have been subtracted from all the energies. We also point out that it is the energies of the effective systems which have been plotted.



The average ion-dipole energies per ion for four of the ions considered in the present study have been plotted in Figure 25. Only the low concentration behaviour has been illustrated. It can be clearly seen from Figure 25 that at very low concentration (*i.e.*,  $<0.025\text{M}$ ) the ion-dipole energies do take on the limiting law dependence given by eq. (3.76). We find that as the concentration is increased the energies become more negative than those predicted by the limiting law, although for  $\text{Cs}^+$  we observe that for a small range of concentrations the values are more positive than the values given by eq. (3.76). Again, it is the smallest and the largest ions considered in Figure 25 which deviate most rapidly from the limiting slope. It should be pointed out that unlike the ion-dipole energies, the average ion-quadrupole energies per ion show a non-universal (*i.e.*, a different slope for ions of different size) linear dependence upon  $c$  at low salt concentration.

In Figure 26 we have plotted the average ion-solvent energies, again per ion, for four of the model aqueous electrolyte solutions we have examined. As we would expect, the energies become more negative (*i.e.*, increase in magnitude) as ion size is decreased, but decrease in magnitude quite rapidly as the concentration is increased. At low concentration the ion-solvent energies become linear in  $\sqrt{c}$  because of the dominant ion-dipole term. Counter-ion effects can also be seen in Figure 26. For  $\text{Cl}^-$  at moderate concentration (*i.e.*,  $0.25\text{M}$  to  $0.75\text{M}$ ) we find that the ion-solvent energies are more negative when  $\text{Na}^+$ , rather than  $\text{K}^+$ , is the counter-ion. This would seem to indicate that  $\text{Na}^+$  is more effective than  $\text{K}^+$  at disrupting the solvent structure, thus allowing the solvent to interact more strongly with a  $\text{Cl}^-$  ion at these concentrations. At higher concentrations (*i.e.*,  $>1.0\text{M}$ ) the converse is true. In these solutions the ions will on average be closer together, and hence the preferential solvation of the  $\text{Na}^+$  ion (as will be discussed in more detail in section 4) is at the expense of the  $\text{Cl}^-$  ion. Counter-ion effects can also be examined by comparing the  $\text{Cs}^+$  and  $\text{Br}^-$  curves in Figure 26. These two ions will be solvated symmetrically by the tetrahedral solvent. In this case we find that at moderate concentrations the  $\text{Br}^-$  ion, which is paired with the larger  $\text{M}^+$  ion, has the more negative energy.

The average solvent-solvent energies per solvent for model  $\text{NaCl}$ ,  $\text{KCl}$  and  $\text{CsI}$  solutions are shown in Figure 27. It can be seen that with increasing concentration the solvent-solvent energy decreases in magnitude. The most

Figure 26.

Average ion-solvent energies per ion as functions of square root concentration. The solid, dashed, dash-dot and dotted lines are RHNC results for model solutions of NaCl, KCl, CsI and MBr, respectively. Each line has been labelled with its appropriate ion. It is the energies of the effective systems which have been illustrated.

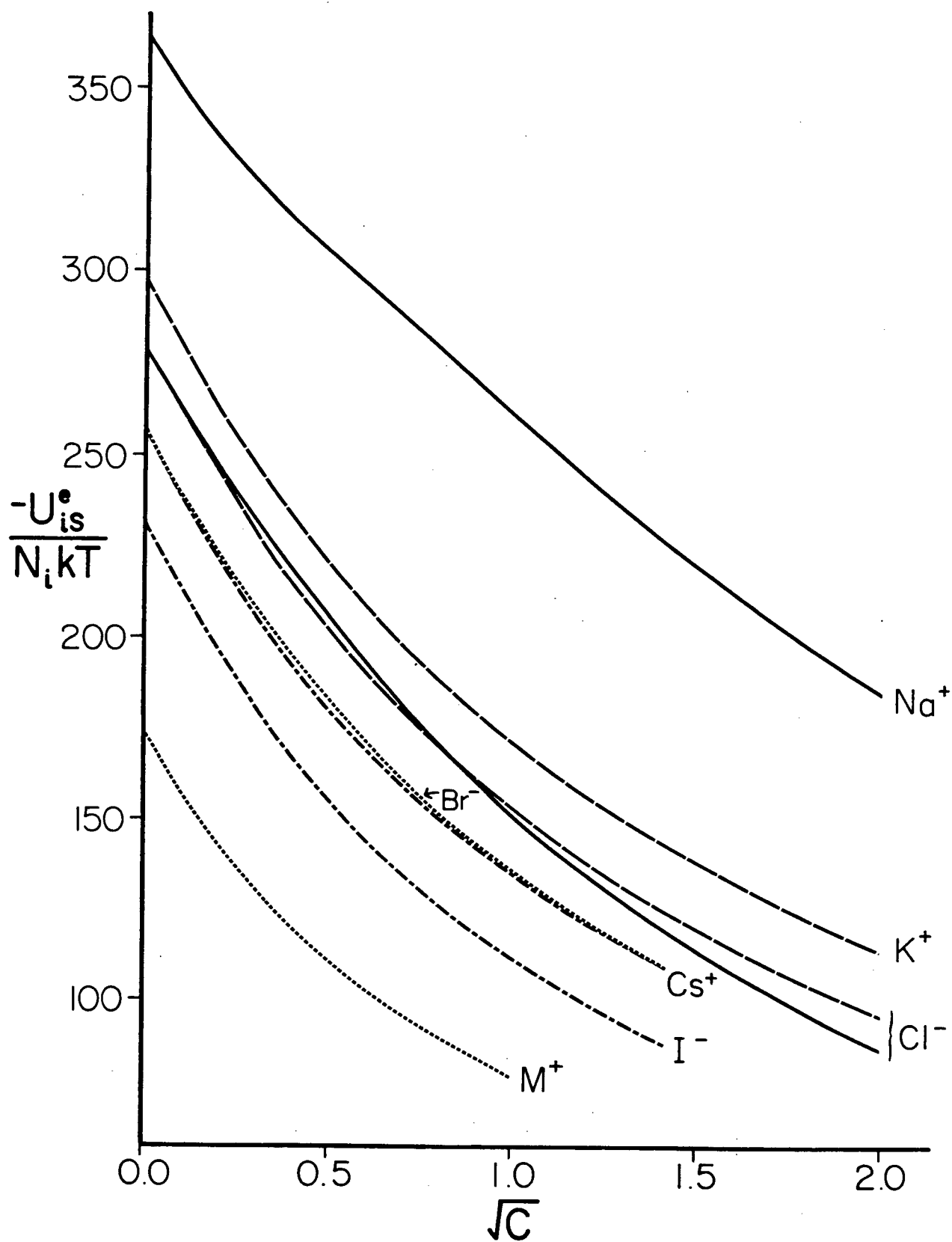
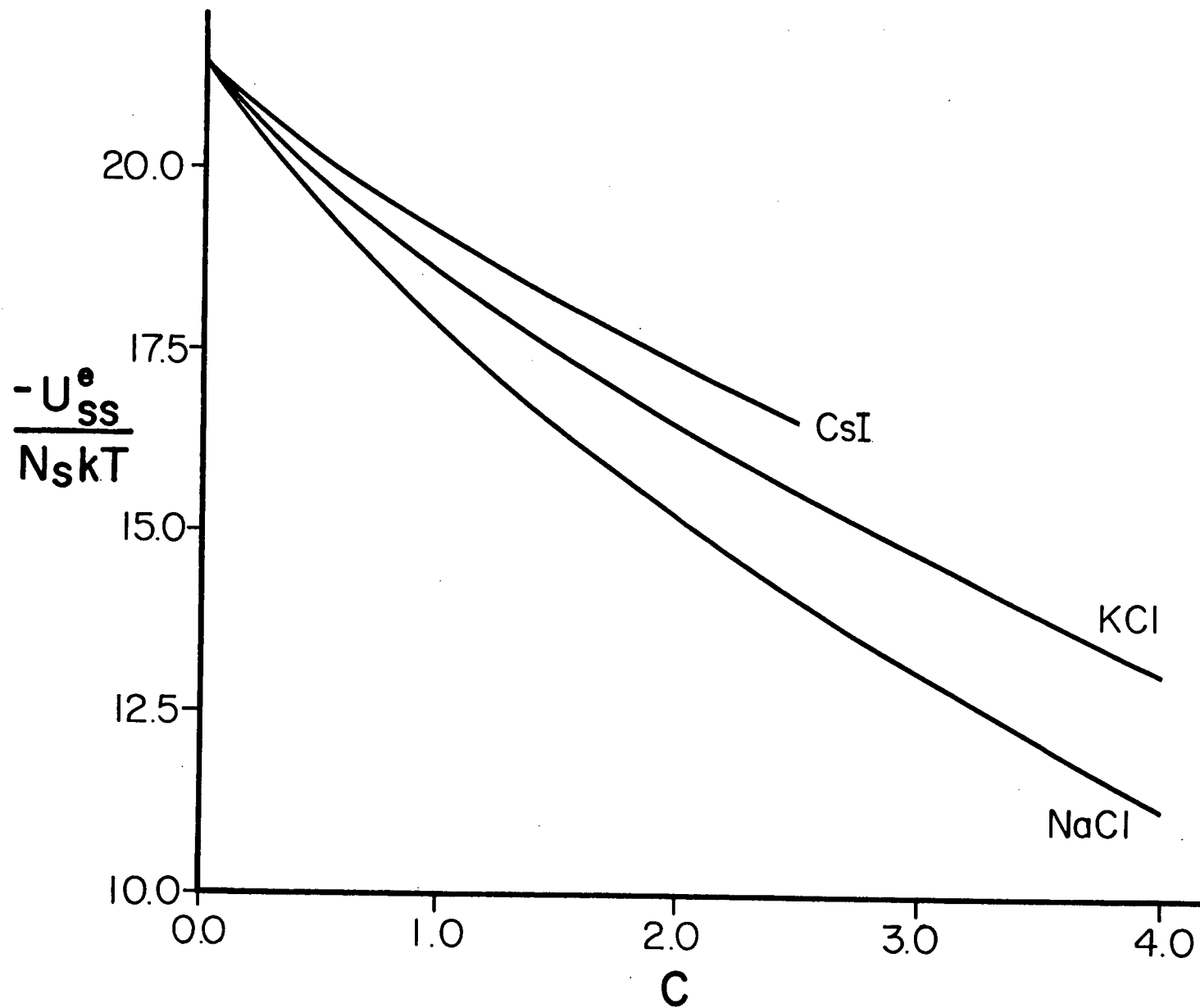


**Figure 27.**

Average solvent-solvent energies per solvent as functions of concentration. RHNC results for three of the model aqueous electrolyte solutions considered in this study have been illustrated. The energies shown are those of the effective systems.





rapid decrease is observed for NaCl, the slowest for CsI. This clearly indicates that small ions are more effective at disrupting the solvent structure. We note that the average energies for a MBr solution, which have not been included in Figure 27, are almost indistinguishable from those of CsI, being only slightly more negative at lower concentrations.

The total average energies for four of the model solutions investigated in this study are shown in Figure 28. We find that for all the solutions examined, the total energy becomes more negative (*i.e.*, increases in magnitude) as the concentration is increased. Furthermore, with smaller ions the rate of increase in magnitude of the total energy is more rapid. We also observe from Figure 28 that to a good approximation the total average energies have a linear dependence upon  $c$ , even at higher concentrations. This is a somewhat surprising result since Figures 24, 26 and 27 would indicate that the average ion-ion, ion-solvent and solvent-solvent contributions to the total average energy are not linear in concentration. Clearly then, the non-linear contributions to the total energies must cancel one another to a large degree. In Chapter III (*cf.* eqs. (3.76) and (3.77)) we have observed some cancellation of this type for the total average ion-dipole energy and average dipole-dipole energy in the low concentration limit (only when  $\epsilon$  is large). What is not clear is why the apparent linearity in the total average energy should persist over such a large concentration range (evident to at least 4M). However, this linearity is consistent with what is observed experimentally for the heats of dilutions of at least some strong electrolytes [174].

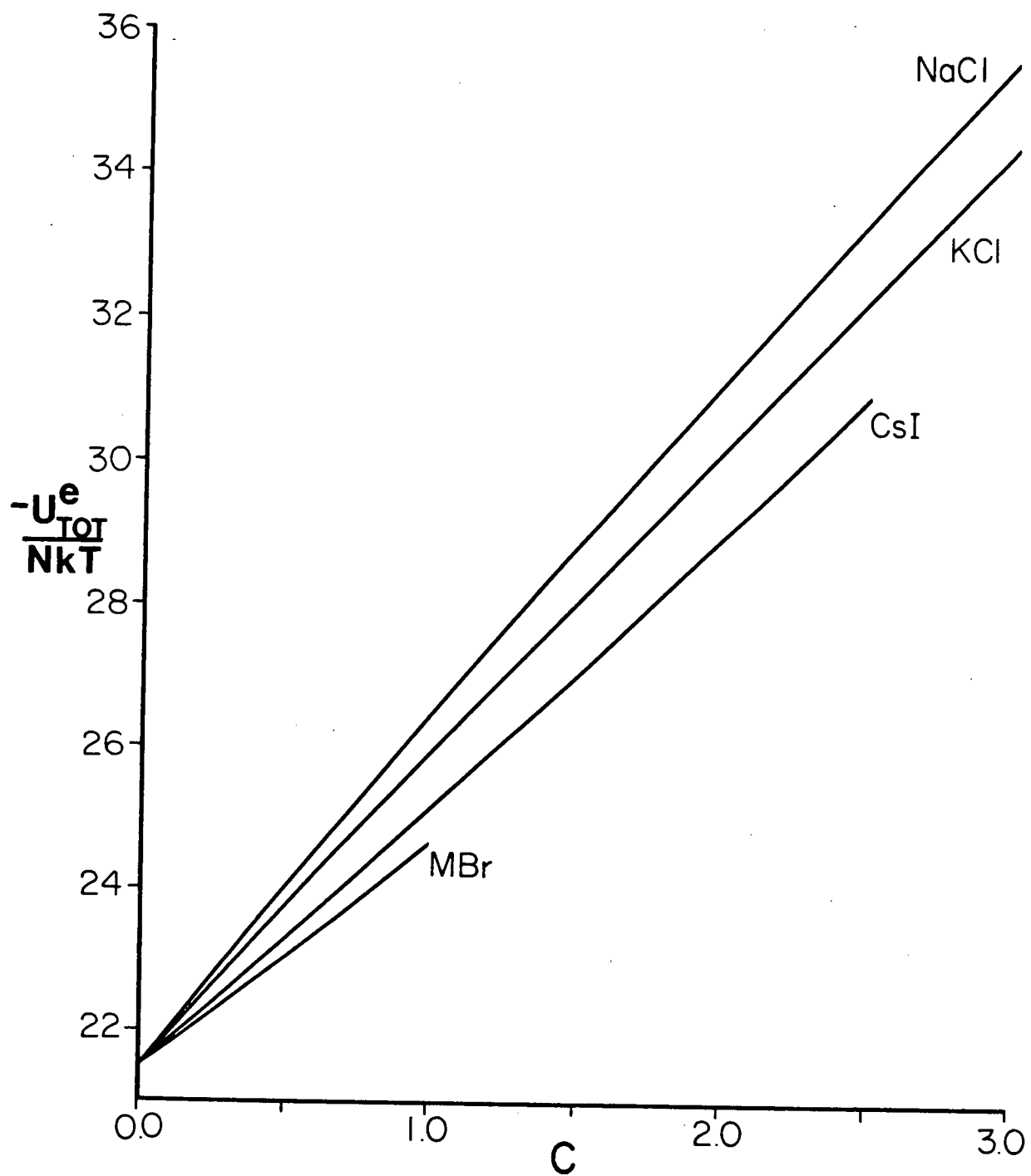
The pressures of our model solutions were calculated to RHNC level accuracy using the pressure equation (2.82). We find that even at 1.0M the calculated pressures have changed by less than 10% from the pure solvent value. Hence, constant pressure conditions appear to have been approximately maintained for our model electrolyte solutions. We again point out that we have used the experimental densities in our model calculations in order to mimic real constant pressure conditions.

From our discussion in Chapter III we know that at finite concentration  $h_{a\beta}(r)$  ( $a, \beta = +, -, s$ ) are all screened at large  $r$  and so we can write

$$h_{a\beta}(r) = \frac{a_{a\beta}}{r} e^{-\kappa r}, \quad (6.3)$$

**Figure 28.**

Total average energies as functions of concentration. The four curves shown represent RHNC results for model NaCl, KCl, CsI and MBr solutions. We note that it is the energies of the effective systems which have been plotted.

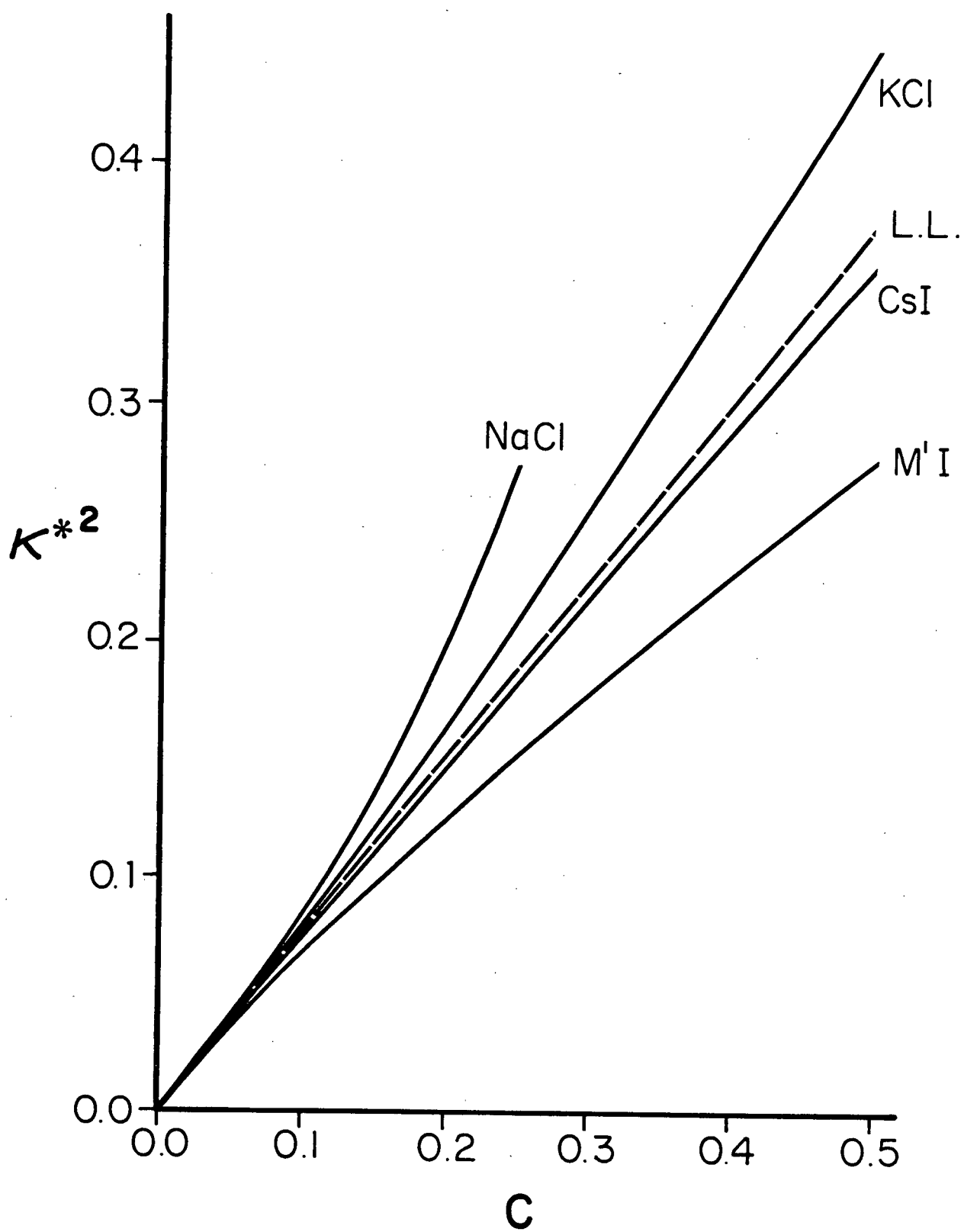


where  $a_{\alpha\beta}$  is a constant dependent upon the parameters of the system. The screening parameter,  $\kappa$ , is given by eq. (3.35c) at very low concentration. By fitting the long-range tails of  $h_{\alpha\beta}(r)$  to the functional form given by eq. (6.3), we have obtained numerical values for  $\kappa$  for the model aqueous electrolyte solutions we have examined. Values for  $\kappa^* = \kappa d_s$  were determined from each of the functions  $h_{++}(r)$ ,  $h_{--}(r)$ ,  $h_{+-}(r)$ ,  $h_{+s}(r)$  and  $h_{-s}(r)$ , as well as from  $h_{00;ss}^{110}(r)$ . For most of the solutions investigated the long-range tail of  $h_{ss}(r)$  was very small because of its  $\rho_2^2$  dependence (cf. eq. (3.42c)), and hence was not used to calculate an additional value of  $\kappa^*$ . The six values that were obtained were always in very good agreement at concentrations less than 0.5M. At concentrations higher than 0.5M the numerical fits usually became too difficult to perform as the long-range tails became shorter ranged (*i.e.*, they were decaying faster because  $\kappa$  was increasing).

In Figure 29 we have shown results for  $\kappa^{*2}$  determined in the present study. At very low concentration we find that the calculated screening parameters approach the limiting law given by eq. (3.35c). Both positive (tend toward larger values) and negative (tend toward smaller values) deviations from the limiting law can be seen in Figure 29. Of the solutions studied,  $\kappa^{*2}$  increases most rapidly with concentration for NaCl. For both NaCl and KCl solutions the values of  $\kappa^{*2}$  are consistently larger than those given by eq. (3.35c), indicating that for these solutions the long-range tails of  $h_{\alpha\beta}(r)$  are shorter ranged (*i.e.*, they are screened more quickly) than those predicted by the limiting law. The smallest values of  $\kappa^{*2}$  were obtained for M'l, these values always being smaller than those given by eq. (3.35c). Thus the long-range tails of  $h_{\alpha\beta}(r)$  for the M'l solution are longer ranged (*i.e.*, they are screened more slowly) than those predicted by the limiting law. We remark that for M'l  $h_{\alpha\beta}(r)$  were sufficiently long ranged so as to enable us to determine values for the screening parameter up to 0.74M (which is the highest concentration studied for this solution). Over the concentration range 0.6M to 0.7M we discover that  $\kappa^{*2}$  stops increasing and remains approximately constant. For concentrations above 0.7M  $\kappa^{*2}$  actually begins to decrease with increasing  $c$ . We also find that at these concentrations the long-range tails of  $h_{++}(r)$  and  $h_{--}(r)$  actually change sign and become positive, indicating an apparent long-range attraction between like ions. This behaviour would seem to contradict the usual notions of ionic screening and of ionic interaction

**Figure 29.**

The square of the Debye screening parameter as a function of concentration. The solid lines are results for four of the model aqueous electrolyte solutions studied. The dashed line represents the limiting law as given by eq. (3.35c) when  $\epsilon=88,3$  is used.



within solution. Clearly, solvent effects (in addition to those described by the dielectric constant) are making significant contributions to the long-range ion-ion correlations in the M'l solution. We will discuss these solvent effects in greater detail below. From Figure 29 it can be seen that for the CsI solution the screening parameters are just slightly smaller than those given by eq. (3.35c). It should also be pointed out that the values of  $\kappa^{\star 2}$  for MBr and EqEq solutions, which have not been included in Figure 29, lie very close to the KCl curve. Therefore, we find that the behaviour of  $\kappa$  depends not only upon the ion size (*i.e.*, the value of  $d_{+-}$ ), but also upon the size asymmetry of the two ions. At a given concentration the value of  $\kappa$  decreases within increasing ion size, but increases with increasing asymmetry.

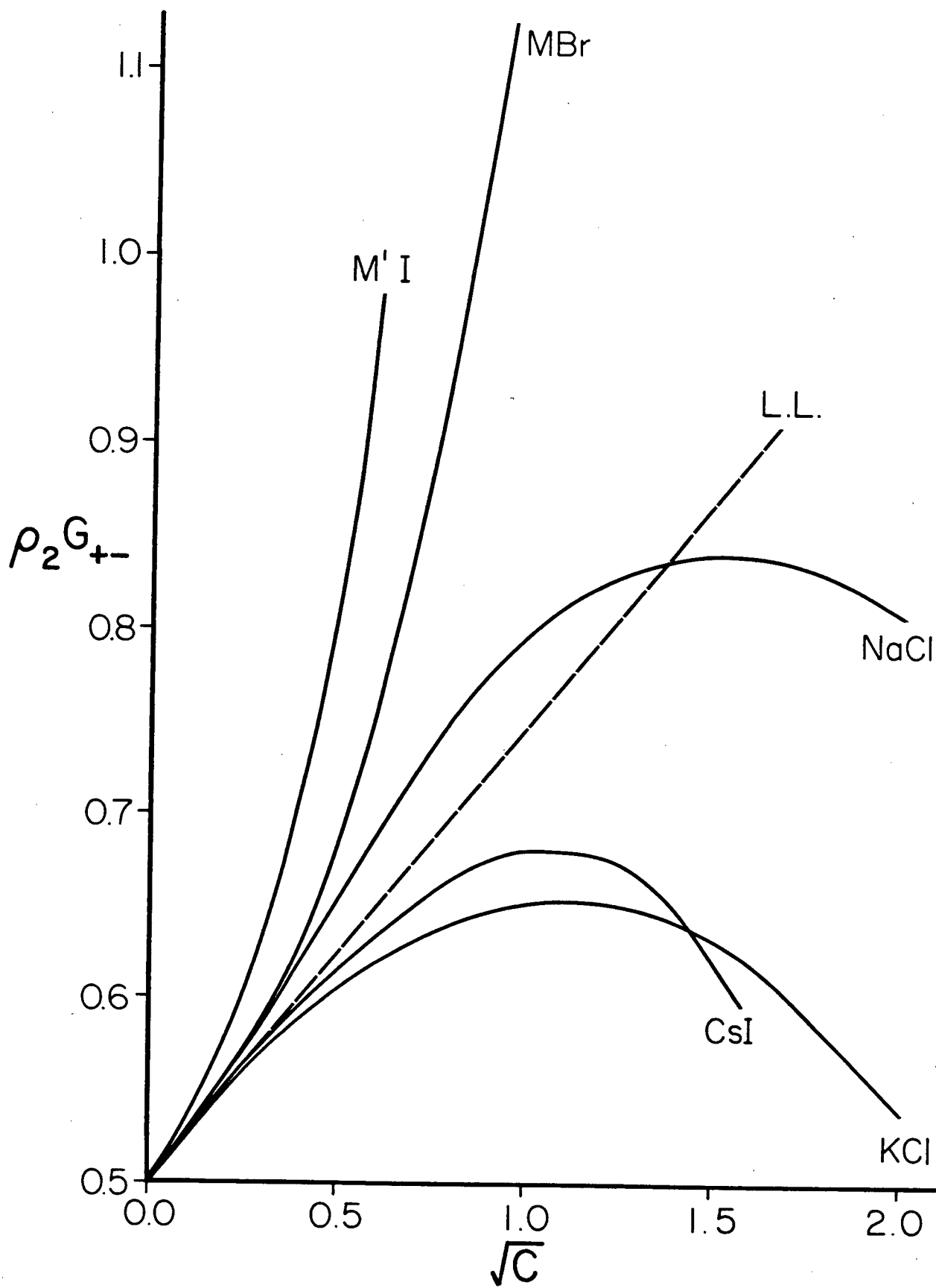
In order to make use of the thermodynamic expressions given in Chapter III, we must first determine values for  $G_{a\beta}$  by evaluating eq. (3.1a). We will also examine  $C_{IS}$  as defined by eqs. (3.43) and (3.39b). The required integrations were performed using the trapezoidal rule because all the Fourier transforms in our calculations were evaluated with trapezoidal rule and  $G_{a\beta}$  and  $C_{a\beta}$  represent the  $k \rightarrow 0$  limits of these transforms. Care was taken in computing the contributions to  $G_{a\beta}$  due to the long-range tails of  $h_{a\beta}(r)$ , particularly at low concentration. These contributions were determined analytically whenever the long-range tail of  $h_{a\beta}(r)$  was successfully fit to eq. (6.3). Finally, we remark that numerically the charge neutrality conditions given by eqs. (3.5c) and (3.5d) were always satisfied to a reasonable level of accuracy (*e.g.*, at 0.1M to within 0.01%, while at 4.0M to within 0.1%).

First we will examine our results for  $G_{+-}$ . It is clear from eq. (3.36a) that  $G_{+-}$  will diverge as  $\rho_2 \rightarrow 0$ . Thus, in Figure 30 we have plotted the product  $\rho_2 G_{+-}$  which remains finite in the  $\rho_2 \rightarrow 0$  limit and has a limiting value of  $1/\nu = 0.5$  for all the model solutions we have investigated. At low concentration the values of  $\rho_2 G_{+-}$  always approach the limiting law, although the results for M'l deviate very rapidly from limiting behaviour. At low concentration the M'l, MBr and NaCl solutions all demonstrated what we shall refer to as *super limiting-law* behaviour, that is  $\rho_2 G_{+-}$  increases more rapidly with  $\sqrt{c}$  than predicted by the limiting law. For NaCl the  $\rho_2 G_{+-}$  curve does eventually cross the line representing the limiting slope at a concentration of about 2.0M. For M'l  $\rho_2 G_{+-}$  appears to show divergent behaviour. It increases very rapidly with  $\sqrt{c}$ , reaching a value of 2.55 (not shown in Figure 30) at



Figure 30.

The product  $\rho_2 G_{+-}$  as a function of square root concentration. The solid lines represent results for five of the model aqueous electrolyte solutions considered in this study. The dashed line is the limiting slope determined from eqs. (3.36) using  $\epsilon = 88.3$ .



0.74M. The values of  $\rho_2 G_{+-}$  also increase rapidly with increasing concentration for the MBr solution, however, they do not appear to be diverging. We find that at the highest concentrations studied for MBr the rate of increase appears to have become constant. For KCl the values of  $\rho_2 G_{+-}$  are always smaller than those given by eq. (3.36). We see in Figure 30 that the CsI curve initially follows the limiting law quite closely, then turns down quite sharply at a concentration of about 1M. We note that the results for the EqEq solution (not included in Figure 30) are only just slightly larger than those for NaCl. Thus, the behaviour of  $\rho_2 G_{+-}$  appears to have no simple dependence upon ion size or asymmetry. Furthermore, we observe super limiting-law behaviour for both large and small ions.

It is interesting to point out that at low (but still finite) concentration the values of  $\rho_2 G_{+-}$  are not entirely determined by the long-range behaviour of  $h_{+-}(r)$ , at least for some of the solutions investigated here. We find that although both NaCl and MBr solutions show super limiting-law behaviour for  $\rho_2 G_{+-}$ , their values of  $\kappa$  would predict the opposite to be true (although for MBr the long-range tails of  $h_{\alpha\beta}(r)$  do show some of the same peculiar behaviour found for an M'l solution). The apparent divergent behaviour of  $\rho_2 G_{+-}$  for M'l is, however, consistent with the fact that its value for  $\kappa$  increases relatively slowly and then actually begins to decrease with increasing concentration. Consequently, even at relatively low concentration the short-range ion-ion structure can play an important role in determining the behaviour of  $\rho_2 G_{+-}$ . Moreover, this short-range ion-ion structure will depend strongly upon the details of the ion solvation, and hence upon the nature of the solvent itself.

In Figure 31 we have considered the quantity  $C_{IS}$  as defined by eq. (3.43). At very low concentration we find that our numerical results do agree with the limiting slope,  $S_c$ , determined from eq. (3.48). There does, however, appear to be a slight discrepancy between  $C_{IS}^0$ , the infinite dilution value, and the value obtain from the extrapolation of  $C_{IS}$  to infinite dilution. This discrepancy is easily accounted for by the difference in numerical accuracy of the different calculations involved. We also observe from Figure 31 that, for the most part, the larger the ions the more rapidly  $C_{IS}$  deviates from its limiting behaviour.

Figure 31.

$C_{IS}$  as a function of square root concentration. For ease of comparison we have plotted the difference between the infinite dilution value,  $C_{IS}^0$ , and  $C_{IS}$  itself. The solid lines are RHNC results for five of the solutions examined in the present study. The dashed line represents the limiting slope,  $S_c$ , determined using  $\epsilon = 88.3$  in eq. (3.48).

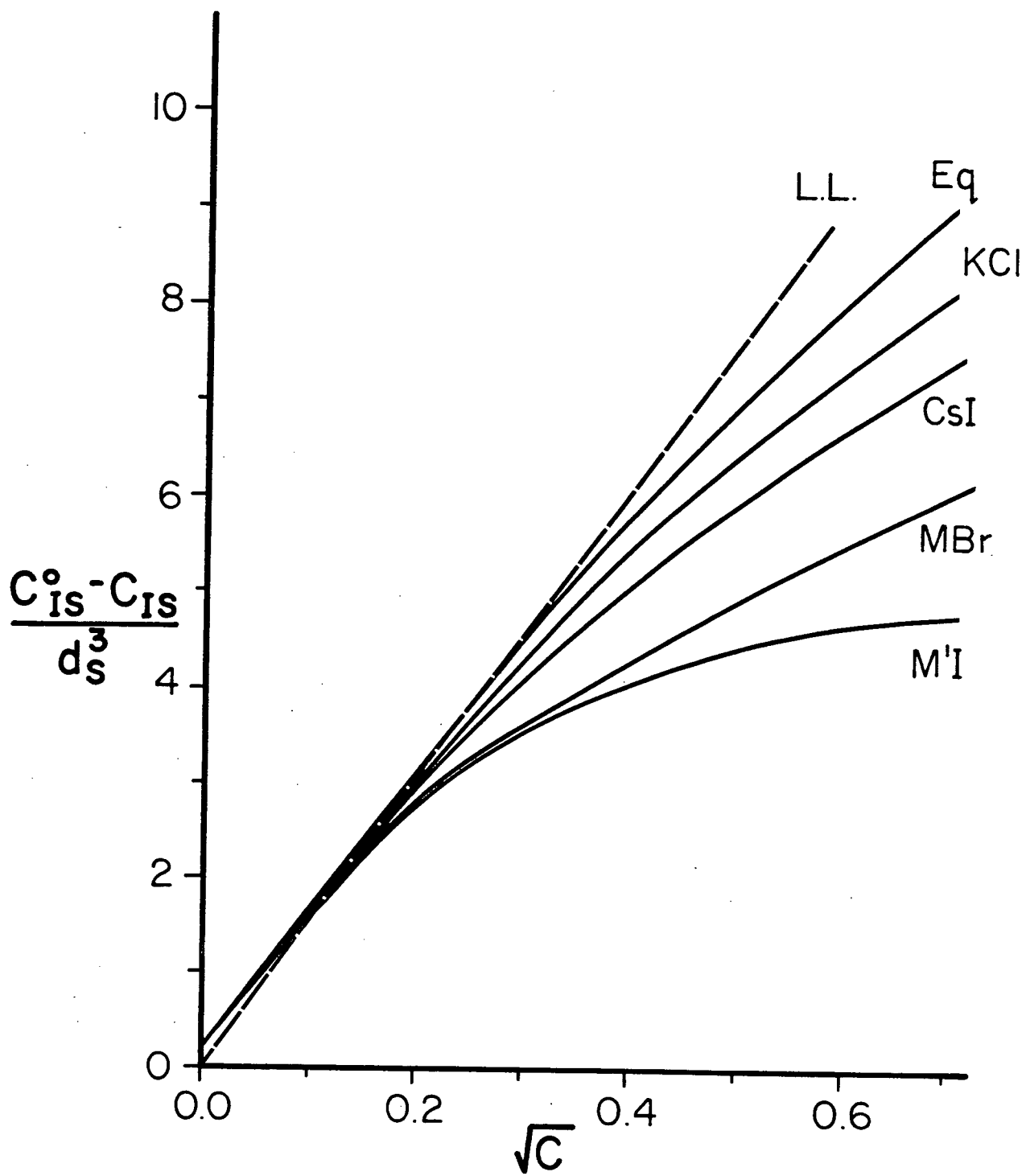
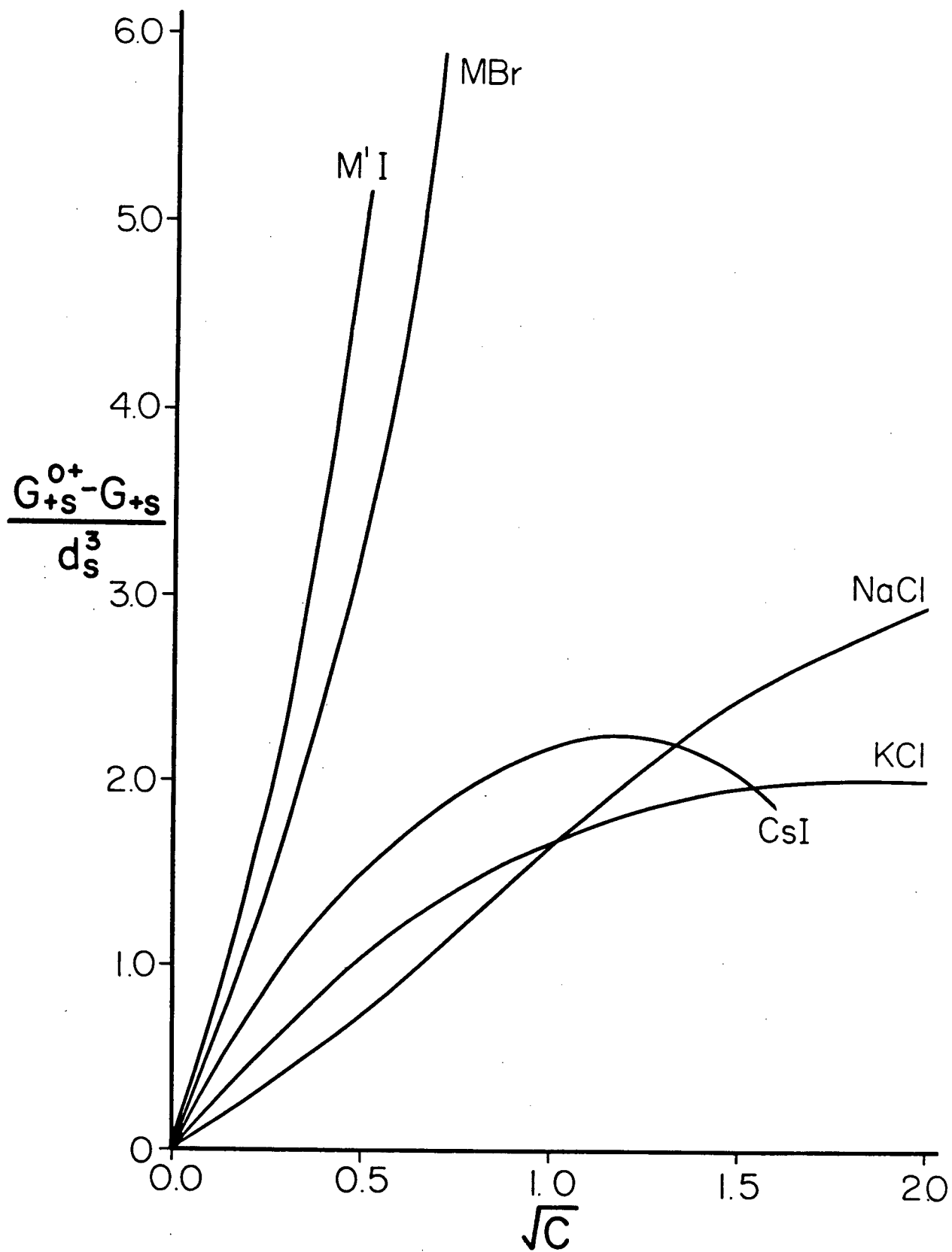


Figure 32.

$G_{+S}$  as a function of square root concentration. The difference between the limiting value  $G_{+S}^{0+}$  (as defined by eq. (3.49b)) and  $G_{+S}$  has been plotted for ease of comparison. RHNC results for model NaCl, KCl, CsI, MBr and M'I solutions have been included.



The dependence of  $G_{+s} = G_{-s}$  upon  $\sqrt{c}$  for five model electrolyte solutions has been illustrated in Figure 32. At very low concentration  $G_{+s}$  appears to be a linear function of  $\sqrt{c}$ , although the limiting slope for each solution is clearly different. Both of these observations are consistent with eq. (3.49a). At higher concentrations we find  $G_{+s}$  demonstrates a variety of behaviours, with no simple relationship to ion size or asymmetry being indicated. For example,  $G_{+s}$  is a monotonic decreasing function for NaCl, while for CsI it actually begins to increase and crosses the NaCl curve at a concentration of about 1.5M. For the M'I and MBr solutions  $G_{+s}$  decreases rapidly, and in fact appears to be diverging for M'I. The apparent divergent behaviour of  $G_{+s}$  for the M'I solution is an expected result. This is because in Figure 30 we have already found that  $\rho_2 G_{+-}$  appears to diverge for M'I and from eq. (3.41) we know that  $G_{+s}$  depends upon the product  $\rho_2 G_{+-}$ .

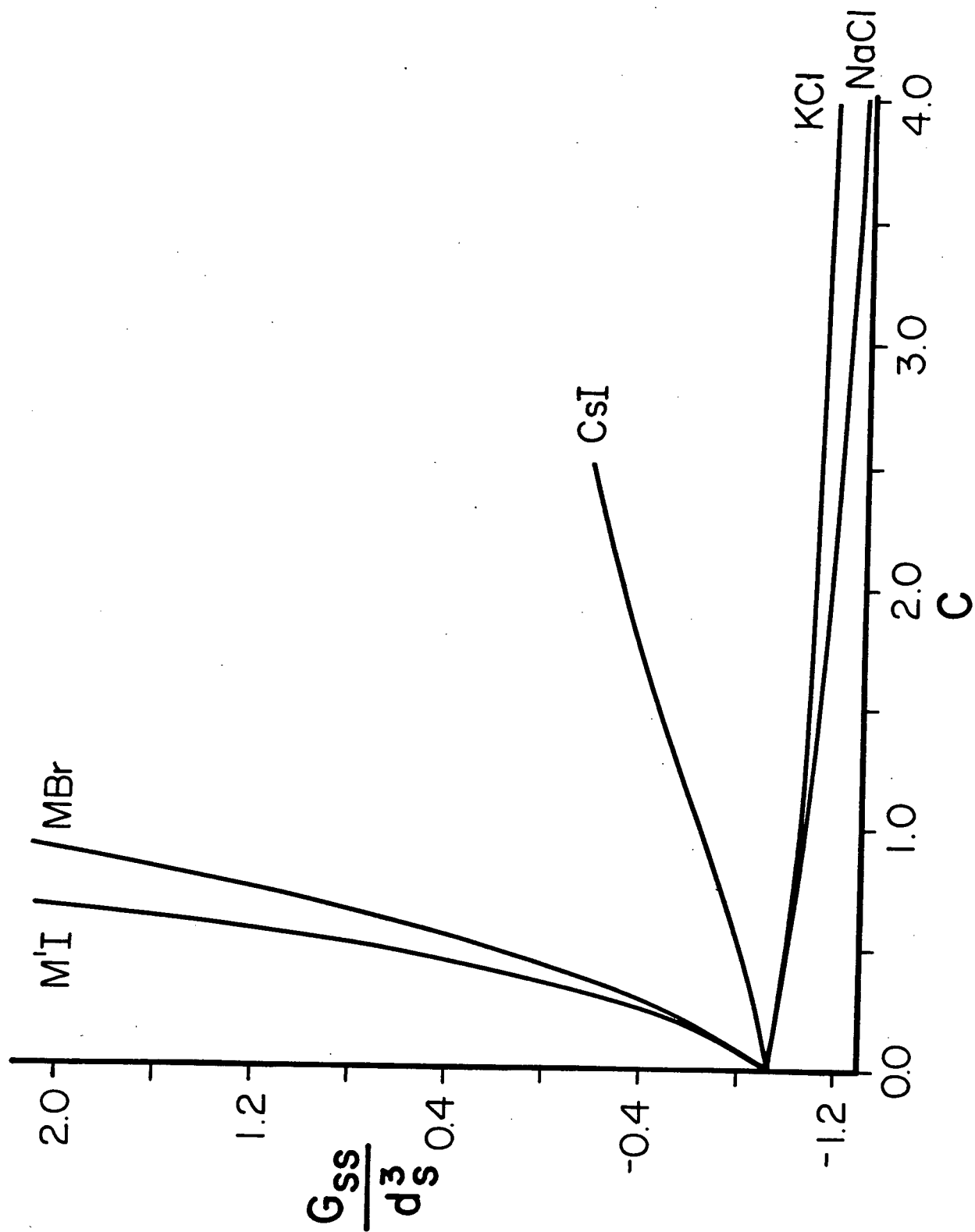
In Figure 33 we have shown results for  $G_{ss}$  obtained for model NaCl, KCl, CsI, MBr and M'I solutions. At very low concentration we find that  $G_{ss}$  has a linear dependence on  $c$ , which is consistent with eq. (3.54). We see from Figure 33 that  $G_{ss}$  is a monotonic decreasing function for the NaCl and KCl solutions, while for CsI, MBr and M'I it strictly increases with increasing concentration. The slope of the curves for  $G_{ss}$  appears to increase with increasing ion size, becoming very large for MBr and M'I. Again, we observe that  $G_{ss}$  appears to diverge for the M'I solution as the concentration approaches 0.74M (where  $G_{ss}$  has a value of  $4.08d_s^3$ ). We remark that this behaviour is consistent with eq. (3.53) and the apparent divergent nature of  $G_{+s}$  observed for M'I in Figure 32.

Before proceeding, it should be pointed out that divergent behaviour in  $\rho_2 G_{+-}$ ,  $G_{+s}$  and  $G_{ss}$  was also demonstrated by our CsI solution at a concentration of about 9M. For this solution the magnitudes of  $\rho_2 G_{+-}$ ,  $G_{+s}$  and  $G_{ss}$  were found to increase sharply with  $c$  for concentrations above 8.5M. As indicated in Table IX, we were only able to reach a concentration of 9.1M, above which we could not obtain numerical solutions for the RHNC theory. Although the values of  $\rho_2 G_{+-}$ ,  $G_{+s}$  and  $G_{ss}$  also increase very rapidly with  $c$  for the MBr solution, they do not appear to diverge (at least for the concentrations examined) like those of the M'I solution. Consequently, for MBr we were able to reach a concentration of 1.0M with no apparent difficulties. It is interesting to note that for the two salts MBr and M'I,  $d_{+-}$  (i.e., the ion



Figure 33.

$G_{SS}$  as a function of salt concentration. We have shown RHNC results for five of the model aqueous electrolyte solutions examined in this study.



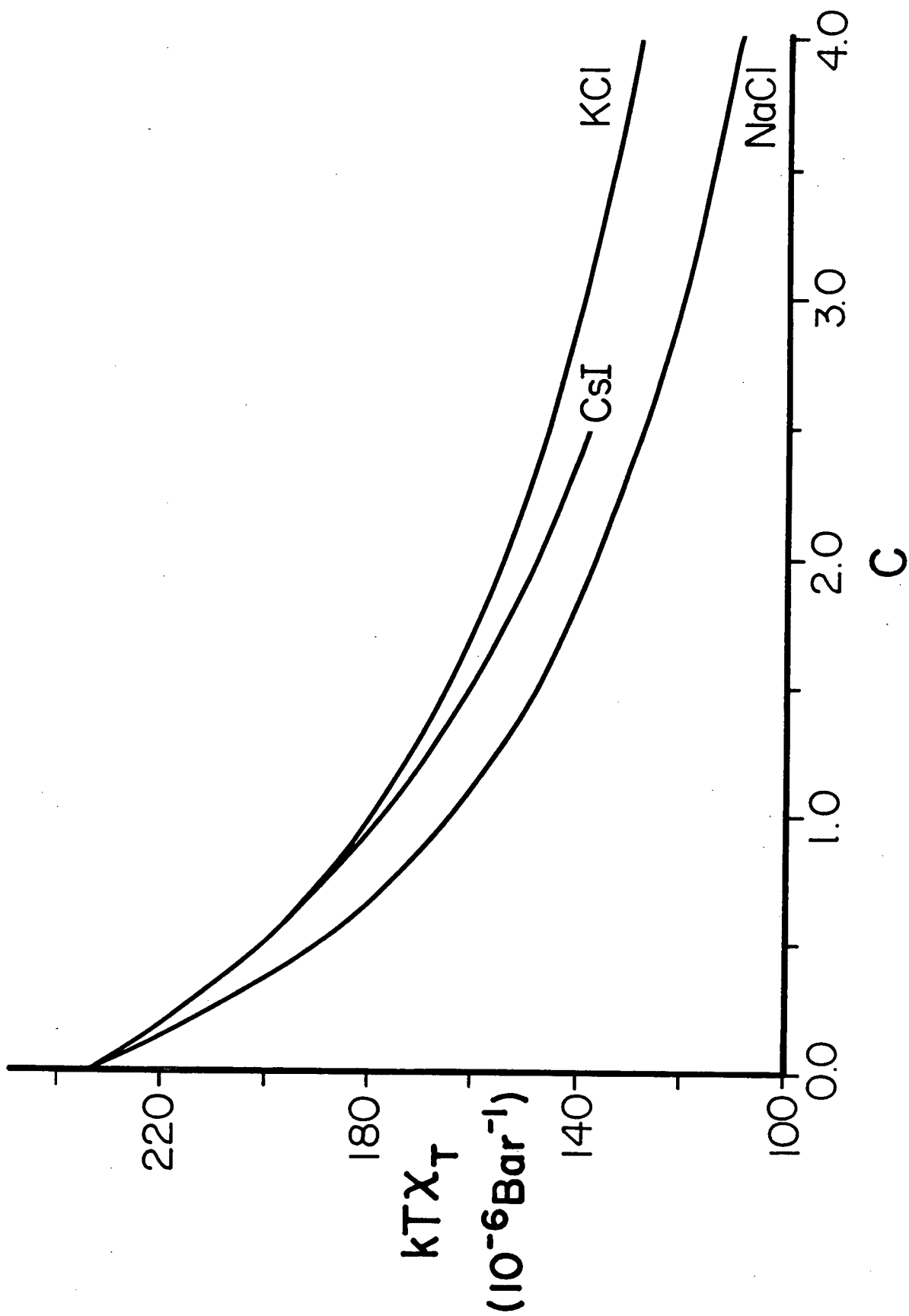
size) is the same. These two salts differ only in the size asymmetry of their respective ions which clearly has a large effect.

The divergent behaviour demonstrated by the CsI and M'I solutions appears to come through the OZ equation (see eq. (3.37)) but the actual sources remain unclear. The physical significance of this behaviour is also not entirely clear. However, if we examine the long-range tails of  $h_{a\beta}(r)$  we find that the values are positive for  $a\beta = ++, --, +-, ss$  and negative for  $a\beta = +s, -s$  (*i.e.*, at long range like species attract, unlike repel). Thus, it appears as though these solutions may be preparing to undergo a phase separation (*e.g.*, salt precipitation) as  $\rho_2 G_{+-}$ ,  $G_{+s}$  and  $G_{ss}$  begin to diverge. For MBr somewhat similar but more exotic behaviour can be seen in the long-range tails of  $h_{a\beta}(r)$ . There we find that the magnitude of  $h_{++}(r)$  is consistently must larger than that of  $h_{--}(r)$  at long range. Moreover, the long-range tails of  $h_{a\beta}(r)$  are not exclusively positive or negative (*i.e.*, repulsive or attractive), but rather show long regions (the order of 5 to  $10d_s$ ) over which the functions appear monotonic, separated by intervals of rapid changes in sign. Again, we stress that the solvent must be playing a major role in determining the behaviour of the CsI, M'I and MBr solutions. Clearly, these systems and their behaviour require more detailed study.

Now having determined the  $G_{a\beta}$  for our model aqueous electrolyte solutions we can use the expressions given in Chapter III to calculate some of their thermodynamic properties. First we shall consider the isothermal compressibility,  $\chi_T$ . In Figure 34 we have plotted  $kT\chi_T$  as obtained from eq. (3.20) for the NaCl, KCl, and CsI solutions. Results for the three remaining solutions which were studied at finite concentration were determined but are not included in Figure 34. We find that the isothermal compressibility of the pure tetrahedral solvent does not compare well with the result for real water at 25°C,  $kT\chi_T = 45.7 \times 10^{-6} \text{Bar}^{-1}$  [169]. At low concentration the values of  $\chi_T$  show a linear dependence upon  $c$  in accordance with eq. (3.74). As is observed experimentally [6,181], the compressibilities of our model solutions decrease with increasing concentration, although the rates of decrease are several times larger than those of the real solutions. From Figure 34 we see that  $\chi_T$  decreases more rapidly for NaCl than for KCl which is consistent with experiment [181]. However, contrary to what is found experimentally [6], we find that  $\chi_T$  decreases more rapidly for CsI than for KCl. Finally, we point

Figure 34.

Isothermal compressibility as a function of concentration. Results for the three model alkali halide solutions considered in this study are shown. The values were obtained from eq. (3.20).



out that the isothermal compressibility of the M'I solution (not included in Figure 34) shows none of the divergent behaviour demonstrated by  $G_{a\beta}$ , but rather forms a smooth curve which would lie just above the KCl result. Clearly, the apparent divergences in the  $G_{a\beta}$  for M'I must cancel in the expression for  $\chi_T$  (cf. eq. (3.20)).

The partial molar volume of the solvent was determined using eq. (3.16) and results for several model solutions are shown in Figure 35. At low concentration we find that  $\bar{V}_s$  becomes linear in concentration, as predicted by eq. (3.73). We observe that  $\bar{V}_s$  increases with increasing concentration for NaCl and KCl, but decreases with increasing concentration for CsI and MBr. In Chapter III we have concluded from eq. (3.73) that the behaviour of  $\bar{V}_s$  (i.e., whether it increases or decreases with  $c$ ), at least at low concentration, will be determined by  $\bar{V}_2^0$ . For all the solutions examined here we find this to be true (values for  $\bar{V}_2^0$  can be easily computed from the results for  $\bar{V}_i^0$  given below in Table XI).

The partial molar volumes of four of the salts examined in the present study are shown in Figure 36. At very low concentration we find that the partial molar volumes of all the salts studied obey the HNC limiting law given by eq. (3.63). In Figure 36 we see that with increasing ion size  $\bar{V}_2$  deviates more rapidly from limiting law behaviour. For the CsI and MBr solutions the slopes of the curves for  $\bar{V}_2$  actually change sign and  $\bar{V}_2$  begins to decrease with increasing concentration. We also observe that once the curves for  $\bar{V}_2$  for these two solutions have turned over, they again appear to become linear in  $\sqrt{c}$ . This behaviour (i.e., the negative slope together with an apparent linearity in  $\sqrt{c}$ ) for  $\bar{V}_2$  has been found experimentally for some solutions, particularly those of tetraalkylammonium salts [182]. In the past there has been considerable debate in the literature [183] as to whether or not the partial molar volumes of these tetraalkylammonium salts do in fact obey the universal limiting law predicted by Debye-Hückel theory [6]. For many of the tetraalkylammonium salts  $\bar{V}_2$  appears to turn over at very low concentration, as is the case here for MBr. Consequently, it becomes very difficult to obtain experimental results [184] of sufficient accuracy at low enough concentration in order to demonstrate that the limiting law does still hold for these salts. Fortunately, for our model solutions we are able to perform calculations at infinite dilution. Thus, unlike experiment, we know the value of  $\bar{V}_2^0$  for a

**Figure 35.**

Partial molar volume of the solvent as a function of concentration. Results obtained from eq. (3.16) for model NaCl, KCl, CsI and MBr solutions have been included.

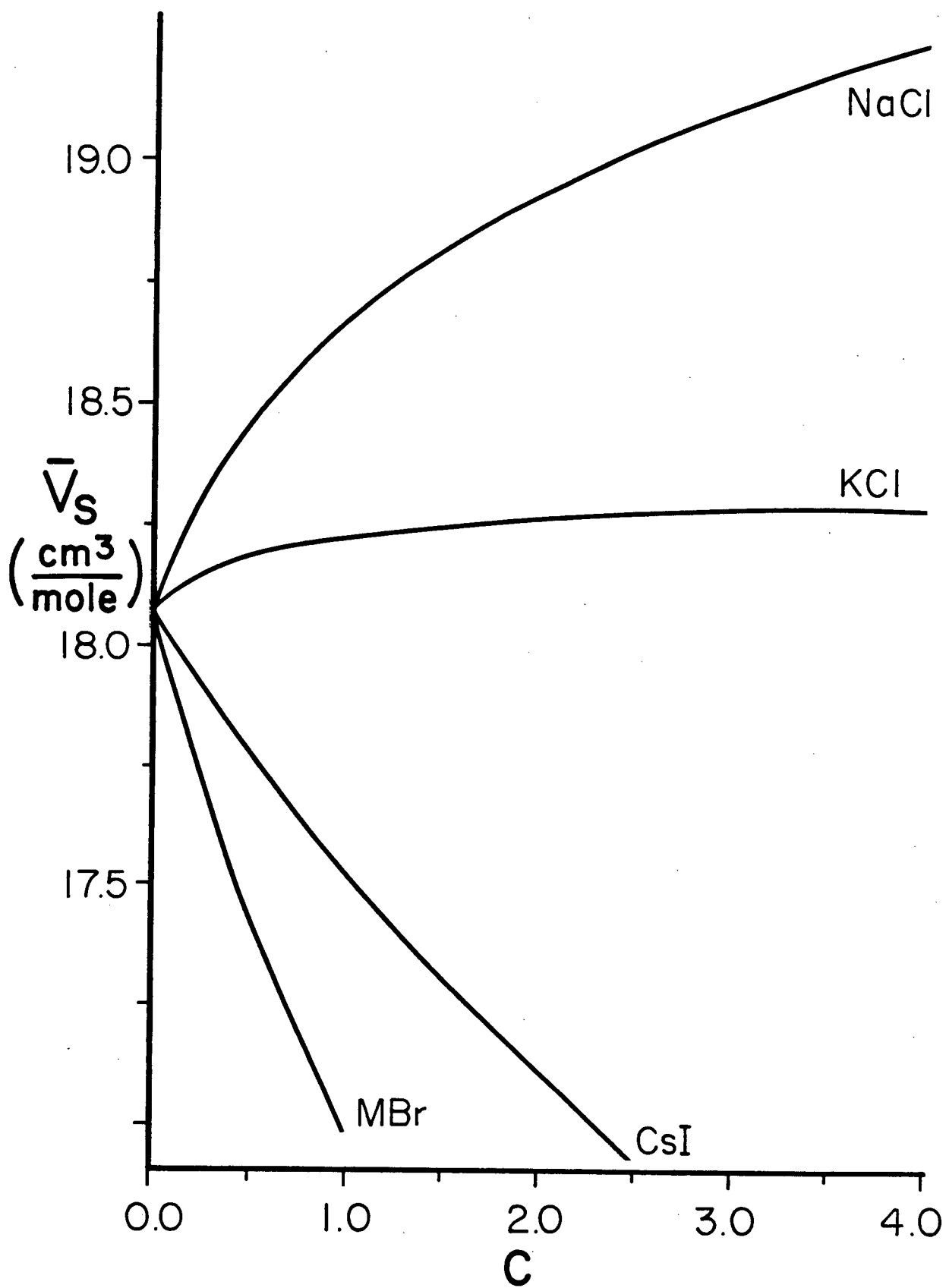
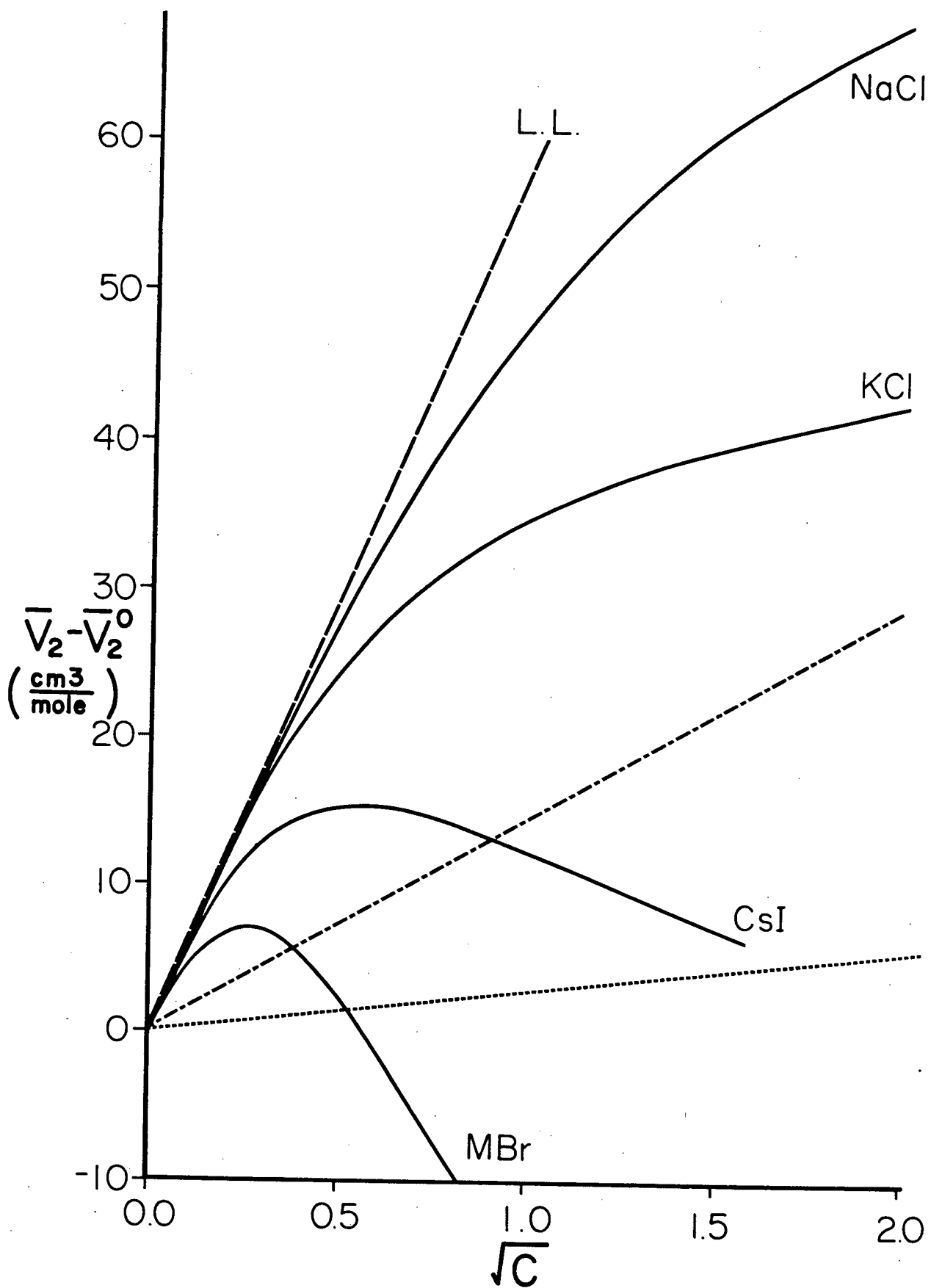




Figure 36.

Partial molar volume of the solute as a function of square root concentration. The solid lines represent results obtained from eq. (3.15) for model NaCl, KCl, CsI and MBr solutions. For ease of comparison we report the differences between  $\bar{V}_2$  and its infinite dilution value,  $\bar{V}_2^0$ . The dashed line is the limiting slope,  $S_V$ , determined from eq. (3.65) using  $\epsilon=88.3$  and  $S_c$  as given by eq. (3.48). The dotted line is the limiting slope,  $S_V^r$ , for real 1:1 aqueous electrolyte solutions at 25°C [6], while the dash-dot line is the *corrected* limiting slope which results from the multiplication of  $S_V^r$  by the ratio  $\chi_T^0(\text{tetrahedral solvent}) / \chi_T^0(\text{real water})$ .



given salt, and hence for salts such as MBr there can be no ambiguity about the low concentration behaviour of  $\bar{V}_2$ .

It is obvious from Figure 36 that  $\bar{V}_2$  shows much larger variation with concentration for our model aqueous electrolyte solutions than for their real counterparts. The limiting slope determined for our model solutions is approximately 20 times larger than that of real aqueous solutions at 25°C. A factor of about 5 can be immediately accounted for by the difference in the isothermal compressibilities of the two solvents. A *corrected* limiting slope for the real solutions which takes this difference into account has been included in Figure 36. However, this corrected slope is still much smaller than that of our model solutions. In Chapter III it was shown that for a given solvent model the HNC theory overestimates  $S_c$ , and hence does not give accurate results for  $S_v$ . We also recall that thermodynamics [6] provides us with an alternative route for determining  $S_v$ , cf. eq. (3.66). Numerically we can obtain an approximate value for  $(\partial \ln \epsilon / \partial P)_T$  for the tetrahedral solvent by repeating the pure solvent calculation at one or two slightly higher densities. The isothermal compressibility can then be used to determine the corresponding pressure changes. This procedure was carried out and the results obtained indicate that the HNC theory overestimates  $S_c$  for the tetrahedral solvent by about an order of magnitude! This error is more than sufficient to move the limiting slope reported in Figure 36 for the tetrahedral solvent to a position below that of the corrected limiting slope for water at 25°C. This reduction of  $S_v$  for the tetrahedral solvent is a desirable result since in Chapter IV we have shown that the RDMF makes an additional contribution to  $S_c$  which will increase  $S_v$ . We will discuss the effects of the RDMF in detail in section 5.

The constant pressure derivatives of the logarithms of the mean molarity activity coefficients were determined in the present study using eq. (3.30b). Integrating these values directly in order to obtain  $\ln \gamma_{\pm}$  (we note that here the constant pressure derivatives are the appropriate values to integrate since we have chosen to mimic constant pressure conditions) would prove very difficult, however, because of the singularity in the derivative at  $\rho_2=0$ . We deal with this problem in a manner very similar to that used by Rasaiah and Friedman [151]. The singularity is conveniently removed by subtracting the

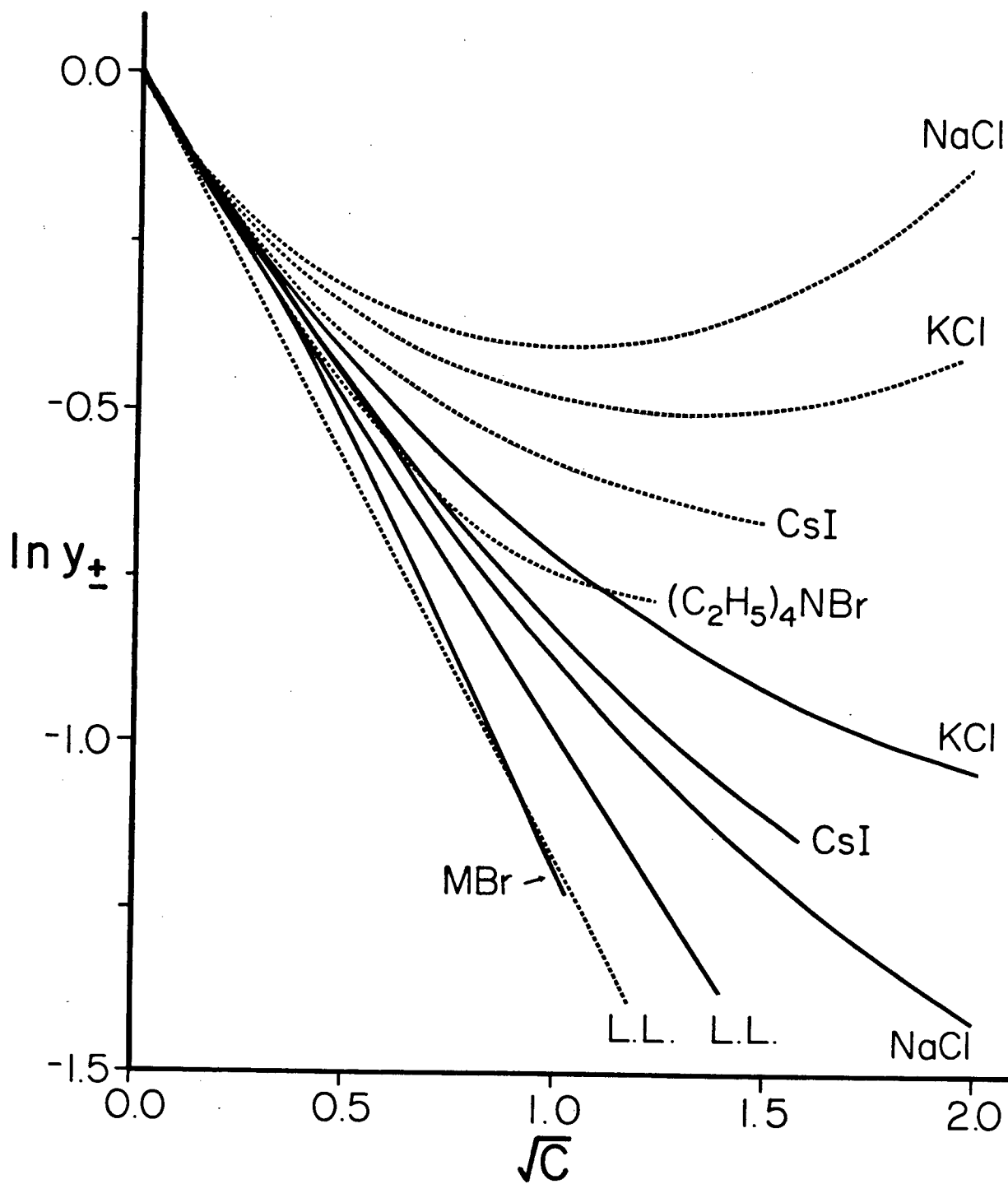
limiting law for the derivative of  $\ln \gamma_{\pm}$  (as given by eq. (3.56)) from  $(\partial \ln \gamma_{\pm} / \partial \rho_2)_P$ . The resulting difference function is smooth and equals zero at  $\rho_2 = 0$ , and hence can be easily integrated. We then simply add on the value of  $\ln \gamma_{\pm}$  given by the Debye-Hückel limiting law. All the values for  $\ln \gamma_{\pm}$  which we shall report were calculated in this fashion.

In Figure 37 we have compared the values of  $\ln \gamma_{\pm}$  obtained for our model aqueous electrolyte solutions with those of real solutions. We point out that the limiting law slopes of the model and of the real solutions differ slightly because of the difference in the dielectric constants of their respective solvents. From Figure 37 we observe that in general  $\ln \gamma_{\pm}$  deviates much more slowly from limiting law behaviour for the model electrolyte solutions being considered here than it does for their real counterparts. If we compare results for the real and model alkali halides, we find that  $\ln \gamma_{\pm}$  turns up much more quickly for the real solutions. Like the experimental curves,  $\ln \gamma_{\pm}$  for our model KCl solution turns up more rapidly than does the model CsI curve. However, unlike experiment, we find that our results for  $\ln \gamma_{\pm}$  for NaCl are consistently less than those of both CsI and KCl.

Also included in Figure 37 are the measured values of  $\ln \gamma_{\pm}$  for an aqueous solution of  $\text{Et}_4\text{NBr}$  which would seem to be a reasonable counterpart for the current MBr system. We see that for MBr  $\ln \gamma_{\pm}$  is always smaller than for the model alkali halides. Similar behaviour can be observed for  $\text{Et}_4\text{NBr}$  with respect to the real alkali halides. Unlike  $\text{Et}_4\text{NBr}$ , however, the values of  $\ln \gamma_{\pm}$  for MBr are always less than those given by the Debye-Hückel limiting law. For  $\ln \gamma_{\pm}$  we shall refer to this as *super Debye-Hückel* behaviour. We remark that for M'I (results for it have not been included in Figure 37)  $\ln \gamma_{\pm}$  decreases even more rapidly than for MBr. Super Debye-Hückel behaviour has been observed experimentally for some tetraalkylammonium salts (*e.g.*,  $\text{Pr}_4\text{NI}$  and  $\text{Et}_4\text{NI}$  [186]) and has been interpreted [5,186] as being a consequence of the hydrophobic natures of these relatively large ions. Furthermore, it has been hypothesized [5,186] that in aqueous solution there will be an attractive force (due to the solvent) between two such large hydrophobic ions. In the present study we have seen strong evidence for long-range attractive forces between both like and unlike ions in our model M'I solution (and to a lesser degree for MBr), as was discussed earlier. Clearly, many of the properties exhibited by the M'I and MBr solutions

Figure 37.

$\ln \gamma_{\pm}$  as a function of square root concentration. The solid lines represent RHNC results for four of the model solutions investigated in this study. The dotted lines are experimental results [185,186] for several 1:1 aqueous electrolyte solutions at 25°C. The limiting law slopes (labelled with L.L.) have also been included for both the model and real solutions.



are consistent with what is observed experimentally for aqueous solutions of tetraalkylammonium salts.

It is obvious from eq. (3.30b) that the constant pressure derivatives of  $\ln \gamma_{\pm}$  depend upon both  $G_{+-}$  and  $G_{+S}$ . If we ignore  $G_{+S}$  in eq. (3.30b), then it immediately follows that super limiting-law behaviour for  $\rho_2 G_{+-}$  implies super Debye-Hückel behaviour for  $\ln \gamma_{\pm}$ . In Figure 30 we have found that NaCl, MBr and M'I all show super limiting-law behaviour, although in Figure 37 we see that only the MBr and M'I curves are super Debye-Hückel. For our model MBr and M'I solutions  $G_{+S}$  is always negative. We note that this negative value for  $G_{+S}$  will tend to decrease the value of  $(\partial \ln \gamma_{\pm} / \partial \rho_2)_P$ , and hence will emphasize super Debye-Hückel behaviour. For our model NaCl solution  $G_{+S}$  is positive (up to a concentration of 3.0M), and consequently will tend to increase  $\ln \gamma_{\pm}$ . We find that even though  $G_{+S}$  is generally much smaller than  $G_{+-}$  for NaCl (about 40 times smaller at 1.0M), the effect of  $G_{+S}$  is sufficiently large to cause  $\ln \gamma_{\pm}$  to turn up from the Debye-Hückel limiting law. Unfortunately, the values of  $G_{+S}$  are not large enough to move the NaCl curve for  $\ln \gamma_{\pm}$  above those of CsI and KCl. Clearly, however, the values of  $G_{+S}$  (which depend upon the solvent structure around an ion) can have a strong influence upon results for  $\ln \gamma_{\pm}$  even at very low concentration.

Let us now return again to Figure 30. What we would like to determine is whether or not a real aqueous solution of NaCl (or any alkali halide for that matter) shows super limiting-law behaviour for  $\rho_2 G_{+-}$ . Obviously, the mean activity coefficient does not represent a convenient means of investigating this. However, if we examine eq. (3.33), we immediately see that the derivative of the osmotic pressure depends only upon the reciprocal of  $\rho_2 G_{+-}$ . Unfortunately, osmotic pressure measurements for aqueous electrolyte solutions are difficult to perform and have received relatively little attention [7]. On the other hand measurements of the osmotic coefficients (as defined in eq. (3.58)) for aqueous electrolyte solutions have received a great deal of attention [6,7] and numerous tables of values are available [6,7,185]. We note that a general thermodynamic relationship between the activity and osmotic coefficients [6,7] does exist. Unfortunately, the simple relationship between  $\Pi$  and  $\phi$  given in eq. (3.61) holds only in the limit  $\rho_2 \rightarrow 0$ , and consequently cannot be used to deduce the behaviour of  $\Pi$  from that of  $\phi$  at finite concentration. Equation (3.58) can be employed at finite concentration if the

behaviour of  $\bar{V}_s$  is known, although this expression is still only an approximate one. We point out that the derivative of the osmotic pressure in eq. (3.33) is not only at constant temperature, but also at constant solvent chemical potential. In our model calculations  $\mu_s$  has been allowed to vary with concentration (experimentally,  $\mu_s$  would normally be held fixed at the pure solvent value), and hence our derivative of  $\Pi$  will reflect this fact. Therefore, no definitive answer can currently be given as to whether or not the present results for  $\rho_2 G_{+-}$  for a model NaCl solution are consistent with those of its real counterpart. Experimental values for  $\phi$  for aqueous solutions of NaCl at 25°C would suggest that this is not the case unless some of the discrepancies mentioned above make large contributions to  $(\partial\Pi/\partial\rho_2)$ . However, we point out that the present results for NaCl may provide some explanation for the unconventional behaviour demonstrated by other aqueous solutions of small ions, *e.g.*, the cation order reversal for  $\gamma_{\pm}$  and  $\phi$  for fluoride salts [6]. We again emphasize that osmotic pressure measurements would provide a very simple and direct route for obtaining information about ion-ion structure in electrolyte solutions.

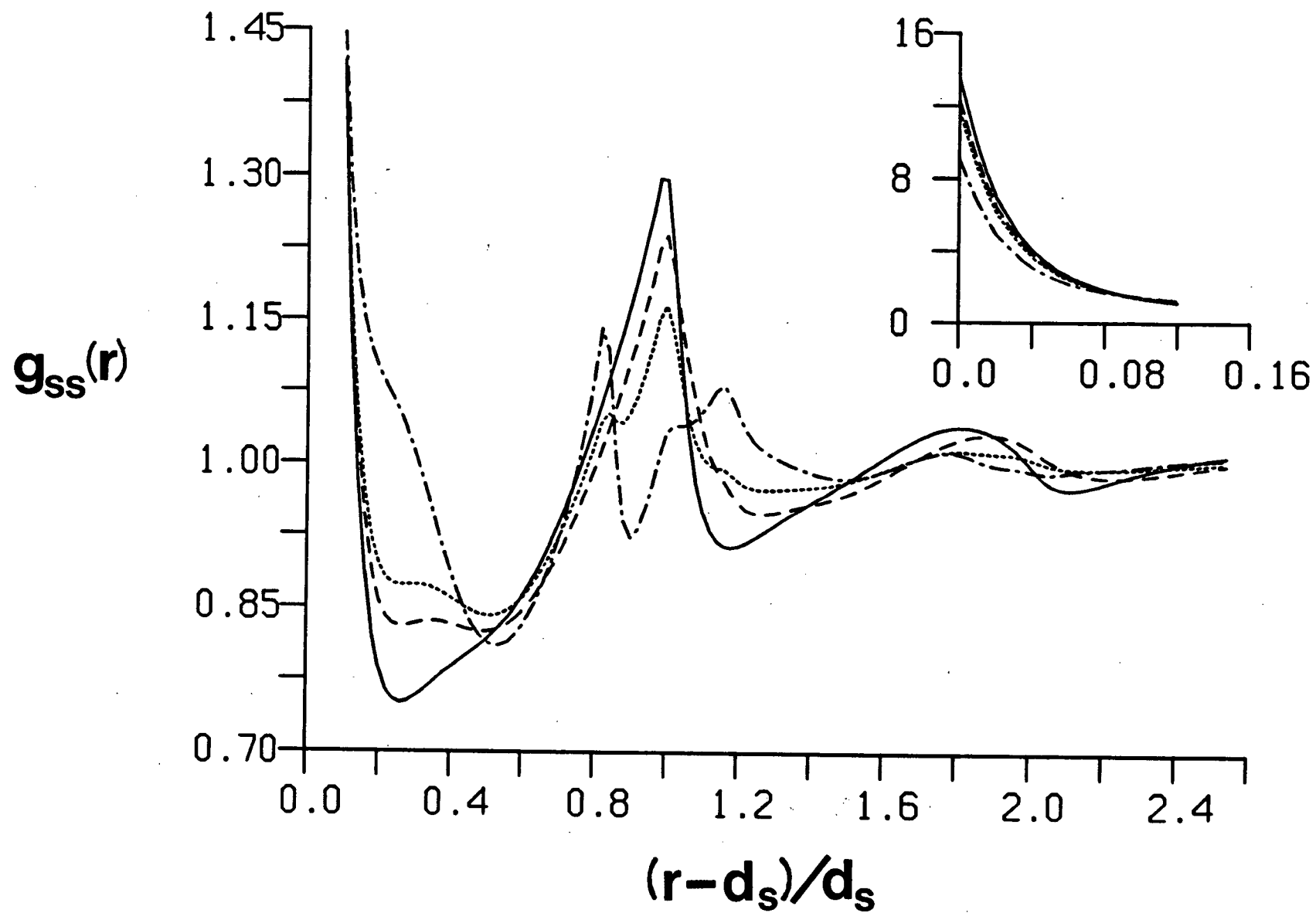
#### 4. Structural Properties

First we shall consider the solvent-solvent structure of our model aqueous electrolyte solutions. In Figure 38 we have plotted the solvent-solvent radial distribution functions of model KCl and NaCl solutions at 4.0M and 4.0M and 12M, respectively, along with  $g_{ss}(r)$  for the pure tetrahedral solvent at 25°C. We find that the solvent-solvent packing structure in both solutions at 4.0M still resembles that of the pure solvent, although the presence of the ions at this concentration is having an obvious influence. The solvent structure generally appears to be dampened, that is to say, the peaks in  $g_{ss}(r)$  have become smaller and the wells are not as deep. It is also evident from Figure 38 that NaCl is more effective than KCl at disrupting the solvent-solvent packing structure. If we now examine  $g_{ss}(r)$  for NaCl at 12M we see that the solvent structure has changed dramatically from that of the pure solvent. The contact value of  $g_{ss}(r)$  has decreased substantially and the position of the first minimum has shifted outward. The second neighbor peak, which was originally centred at  $r=2d_s$  for the pure solvent, now appears as



Figure 38.

Solvent-solvent radial distribution functions of the pure solvent and of several model electrolyte solutions. The solid line is the radial distribution function of the pure tetrahedral solvent at 25°C, while the dashed line represents  $g_{ss}(r)$  for a model KCl solution at a concentration of 4.0M. The dotted and dash-dot lines are results for model NaCl solutions at 4.0M and 12M, respectively.



three distinct peaks at  $r \approx 1.8d_s$ ,  $2d_s$  and  $2.15d_s$  for 12M NaCl. The smallest of these peaks (the one at  $r=2d_s$ ) is what remains of the second neighbor peak of the pure solvent. The two remaining peaks appear at separations which correspond to solvent particles separated by either a  $\text{Na}^+$  or  $\text{Cl}^-$  ion. The  $\text{Na}^+$  peak is the sharper of the two which would suggest that the solvents surrounding a  $\text{Na}^+$  ion are more rigidly held in position. The present results for  $g_{ss}(r)$  clearly indicate that for 12M NaCl a vast majority of the solvent particles in the model solution are directly involved in ion solvation (*i.e.*, comprise the first solvation shell). Finally, we point out that small peaks at  $r=1.85d_s$  and  $2.15d_s$  can already be seen in  $g_{ss}(r)$  for a model NaCl solution at 4.0M.

In the present study the quantity  $\langle \cos \theta_{ss}(r) \rangle = \Phi_{00;ss}^{110}(r)$ , where  $\theta_{ss}$  is just the angle between the two dipole vectors of two solvent particles, can be determined using eq. (2.87). Results for  $\langle \cos \theta_{ss}(r) \rangle$  for the pure tetrahedral solvent and for model NaCl and CsI solutions at 4.0M are shown in Figure 39. We find that  $\langle \cos \theta_{ss}(r) \rangle$  shows oscillatory behaviour similar to that of  $g_{ss}(r)$ . Again, the presence of the ions in solution is found to disrupt solvent-solvent correlations, in this case dipole-dipole correlations. From Figure 39 we observe that NaCl is much more effective than CsI at disrupting the dipolar correlations between solvent particles. If we examine  $\langle \cos \theta_{ss}(r) \rangle$  for NaCl and CsI more closely, drops in the values of the functions can be seen at separations corresponding to the diameters of the ions present. Hence, these features of  $\langle \cos \theta_{ss}(r) \rangle$  appear to be due to the opposing (*i.e.*,  $\theta_{ss}=180^\circ$ ) dipole moments of two solvent particles separated by a single ion.

Next we shall examine the ion-solvent structure of our model aqueous electrolyte solutions. The ion-solvent radial distribution functions at infinite dilution for three of the ions considered in this study (spanning a large range of ion size) have been compared in Figure 40. The dependence of  $g_{is}(r)$  upon ion size is much as we might expect. For small ions  $g_{is}(r)$  is more structured (*i.e.*, the contact and all subsequent peaks become larger and the first and all subsequent minima grow deeper). As shown in Figure 40,  $g_{is}(r)$  for  $\text{Na}^+$  has a very large contact value which then very quickly drops to a deep minimum at a reduced separation (*i.e.*,  $r-d_{is}$ ) of  $0.2d_s$ . This would indicate that the first shell of solvent particles around a  $\text{Na}^+$  ion is held in

Figure 39.

$\langle \cos \theta_{SS}(r) \rangle$  for the pure solvent and for model electrolyte solutions. The solid line is  $\langle \cos \theta_{SS}(r) \rangle$  determined for the pure tetrahedral solvent at 25°C, while the dashed and dotted lines represent results for model NaCl and CsI solutions, respectively, at a concentration of 4.0M.

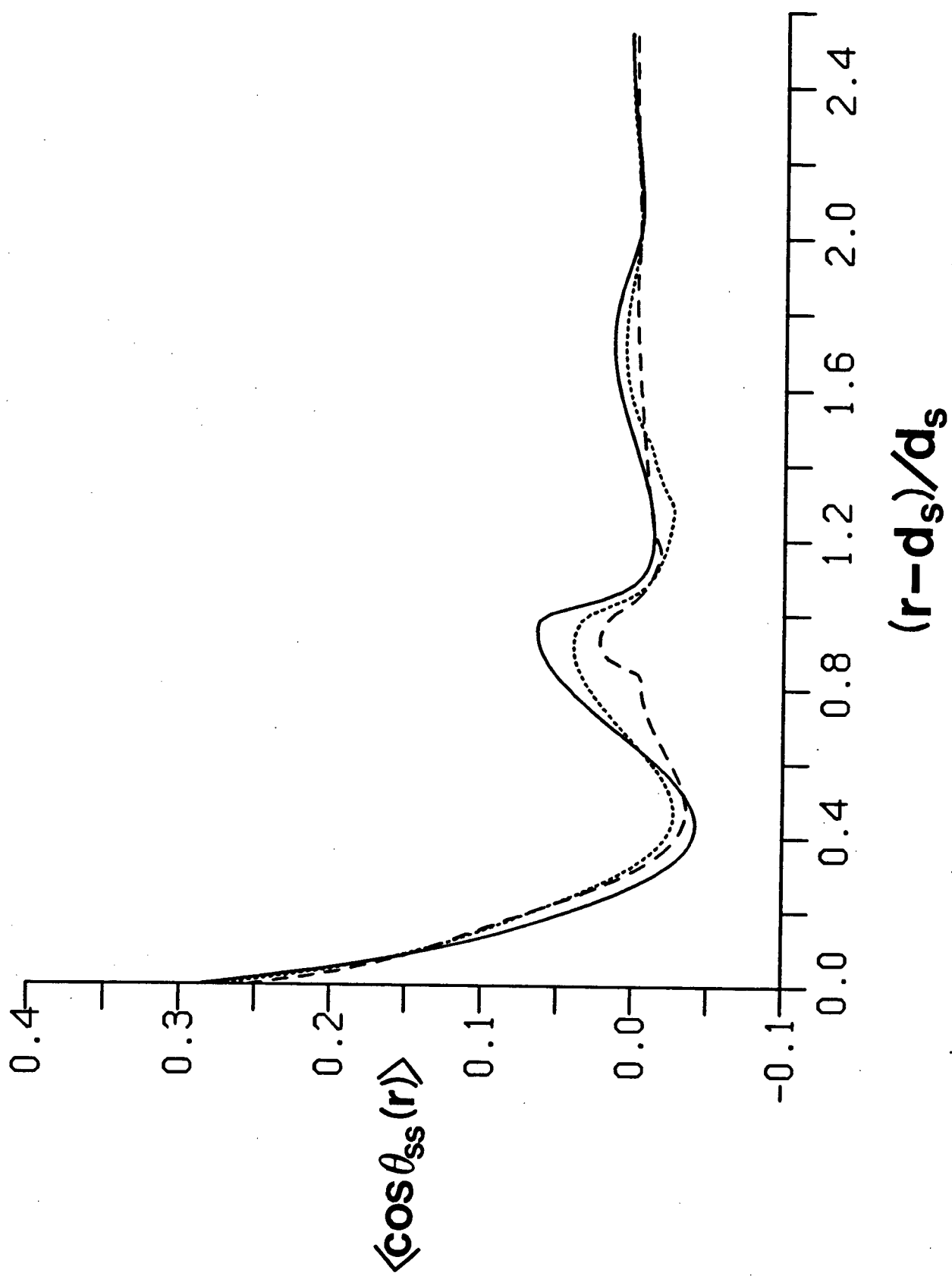
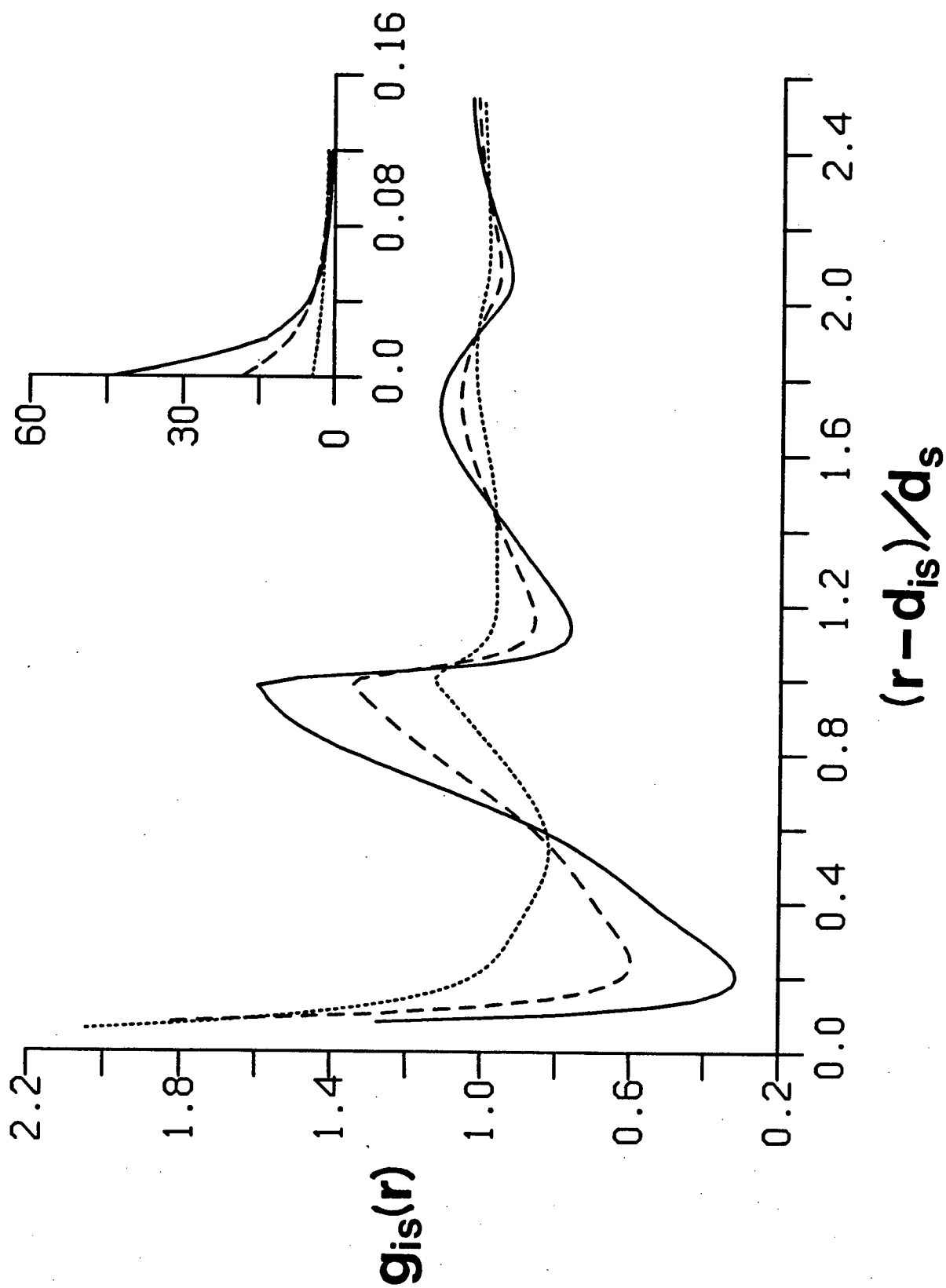


Figure 40.

Ion-solvent radial distribution functions at infinite dilution. The solid, dashed and dotted lines are results obtained in the present study for  $\text{Na}^+$ ,  $\text{Cl}^-$  and  $\text{M}^+$ , respectively.



very tightly. For large ions such as  $M^+$ , the contact value of  $g_{iS}(r)$  is much smaller. The first minimum is also much shallower and has moved out to  $r - d_{iS} = 0.5d_S$  (which is also the position of the hard-sphere minimum). Thus, the first solvation shell of a  $M^+$  ion appears to be held relatively loosely. As in the case of the pure tetrahedral solvent, the positions of the peaks in  $g_{iS}(r)$  are found to be strongly dictated by the hard-sphere packing of the solvent around the ions. The second peak always has its maximum at a reduced separation of one solvent diameter. However, we see in Figure 40 that at least for the smaller  $Na^+$  and  $Cl^-$  ions this second peak is distorted towards smaller separations so that the average reduced separation of the second solvation shell is slightly less than one solvent diameter.

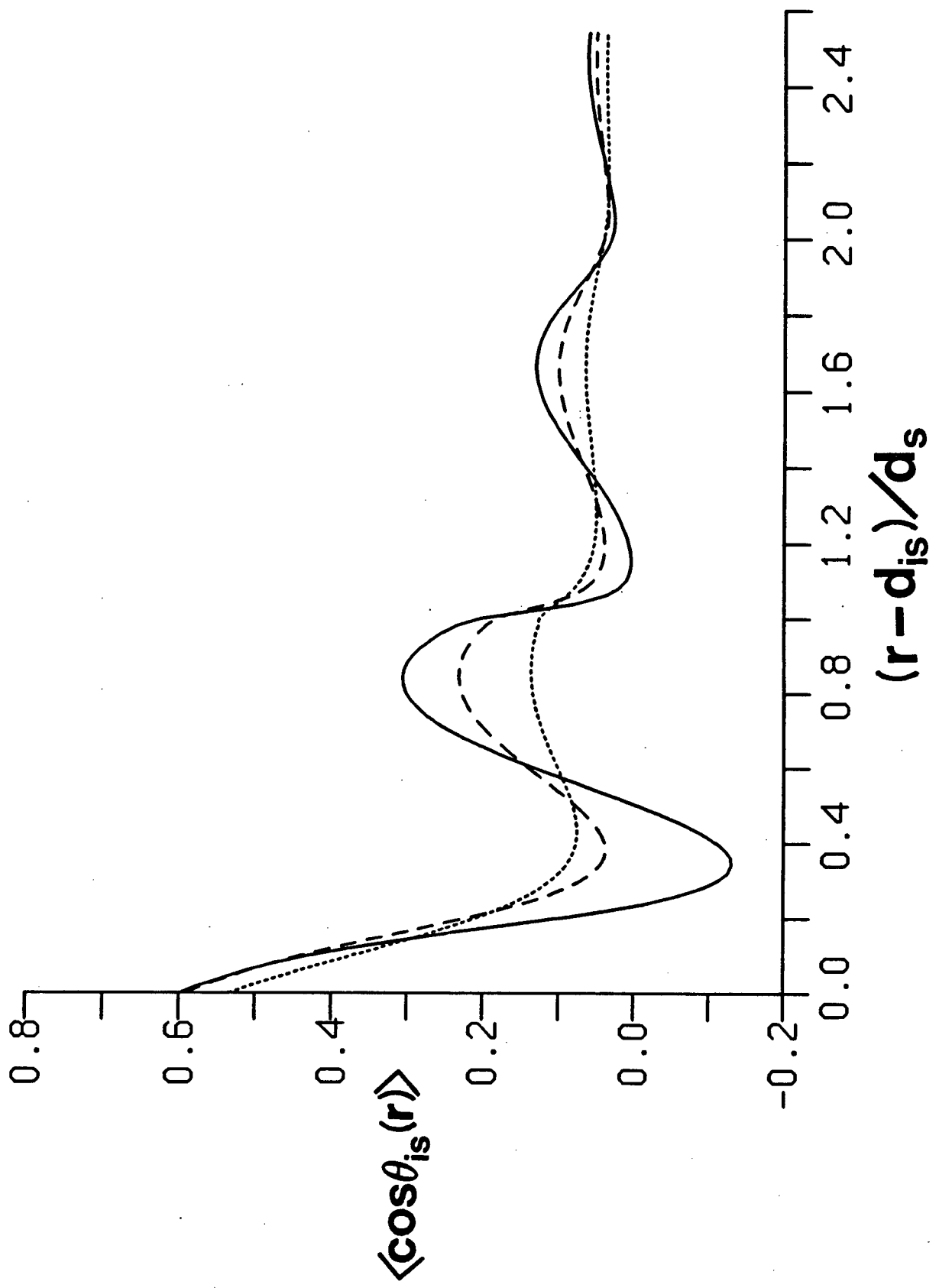
The coordination numbers of the ions (*i.e.*, the numbers of solvents in the first solvation shell) can be determined using eq. (5.2). We remark that for small ions such as  $Na^+$  the CN is reasonably well defined because the first minimum of  $g_{iS}(r)$  is so deep. However, for larger ions such as  $M^+$  it becomes much less obvious at what point to stop integrating in eq. (5.2) (*i.e.*, the first solvation shell becomes more poorly defined). For both the  $Na^+$  and  $Cl^-$  we find  $CN \approx 7.5$ , while for  $M^+$  the CN is somewhere in the range of 10 to 15. For  $M^+$  the value of its CN appears reasonable because of its large size. The CN for  $Na^+$  is somewhat larger than the values usually reported by computer simulation studies [50,51,53,54,58],  $CN = 5.4-7.3$ , although for  $Cl^-$  the agreement is better,  $CN = 5.6-8.4$ . Neutron diffraction studies [13,16] a high concentration report a coordination number of about 5.8 for  $Cl^-$ .

In the present study we have also examined the values of  $\langle \cos \theta_{iS}(r) \rangle$  obtained from eq. (2.89a), where the angle  $\theta_{iS}$  is defined in Figure 3. Infinite dilution results for this function are given in Figure 41 for the  $Na^+$ ,  $Cl^-$  and  $M^+$  ions. (We again note that positive values of  $\langle \cos \theta_{iS}(r) \rangle$  represent favourable dipole orientations with respect to the ion, while negative values indicate unfavourable ones.) The oscillatory behaviour demonstrated by  $\langle \cos \theta_{iS}(r) \rangle$  is similar to that of  $g_{iS}(r)$ , although the positions of the first minima and second maxima do not coincide exactly with those of  $g_{iS}(r)$ . As in the case of  $g_{iS}(r)$ , we find that the structural features of  $\langle \cos \theta_{iS}(r) \rangle$  are generally more distinct for smaller ions. From Figure 41 we see that for both the  $Cl^-$  and  $M^+$  ions, the average dipole orientation of the solvent is favourable at all separations from the ion. However, for  $Na^+$  the average



Figure 41.

$\langle \cos \theta_{is}(r) \rangle$  at infinite dilution. The lines are as defined in Figure 40.



dipole orientation actually becomes unfavourable for a small range of separations around  $r-d_{is}=0.35d_s$ . We observe that the contact value of  $\langle \cos\theta_{is}(r) \rangle$  does not show strong ion size dependence. Nevertheless, if we were to compute  $\langle \cos\theta_{is} \rangle$  for the first solvation shell,  $\text{Na}^+$  gives a much larger result than does  $\text{M}^+$  since far more of the solvents in the first solvation shell of  $\text{Na}^+$  are at or very near contact. It is interesting to point out that if we use the contact values of  $\langle \cos\theta_{is}(r) \rangle$  in order to compute an  $\langle \theta_{is} \rangle$  at contact (*i.e.*, assuming the distributions are very narrow), we obtain an angle of approximately  $54^\circ$ , which is essentially half of the tetrahedral angle. This value compares favourably with results from computer simulations [50,53,58] and from diffraction experiments [13].

In Figure 42 we have plotted  $g_{is}(r)$  for a  $\text{Cl}^-$  ion at infinite dilution and for several model electrolyte solutions at finite concentration. We immediately observe that at finite concentration the packing of the solvent around a  $\text{Cl}^-$  ion is affected by the presence of other ions in the system, particularly at high concentration. As in the case of  $g_{ss}(r)$ , we see from Figure 42 that the structural features of  $g_{is}(r)$  become dampened at finite concentration (*e.g.*, the contact peak drops and the first minimum becomes shallower). Comparing  $g_{is}(r)$  for NaCl and KCl at 4.0M we find that  $g_{is}(r)$  has changed most markedly from its infinite dilution result for NaCl. This would again suggest that smaller ions, in this case  $\text{Na}^+$ , are more effective than ions of moderate size, such as  $\text{K}^+$ , at disrupting the solvent structure. For NaCl at 12M,  $g_{is}(r)$  for  $\text{Cl}^-$  bears surprisingly little resemblance to the infinite dilution result. The first minimum has been displaced outward, while the second neighbor peak has split into two distinct peaks. The smaller of the two is what remains of the peak due to the second solvation shell of a  $\text{Cl}^-$  ion. Clearly, at this concentration the  $\text{Cl}^-$  ion appears to have only a single solvation shell. The larger peak at a reduced separation of about  $0.8d_s$  corresponds to the arrangement where the counter-ion is situated in between the  $\text{Cl}^-$  ion and the solvent. This feature is also evident, though much smaller, for both the NaCl and KCl solutions at 4.0M. If we compute the CN of a  $\text{Cl}^-$  ion in our 12M NaCl solution, we obtain a value of 5.5 which is in good agreement with experimental estimates [13]. Moreover, for this same solution we find that the CN of a  $\text{Na}^+$  ion is approximately 4, which represents a considerable drop from its infinite dilution value. Therefore, in the present model of a 12M NaCl solution a  $\text{Na}^+$  ion has fewer solvents in its first

Figure 42.

Ion-solvent radial distribution function for  $\text{Cl}^-$ . The solid line is the infinite dilution result, while the dashed line represents  $g_{is}(r)$  for  $\text{Cl}^-$  in a model KCl solution at a concentration of 4.0M. The dotted and dash-dot lines are results for model NaCl solutions at 4.0M and 12M, respectively.

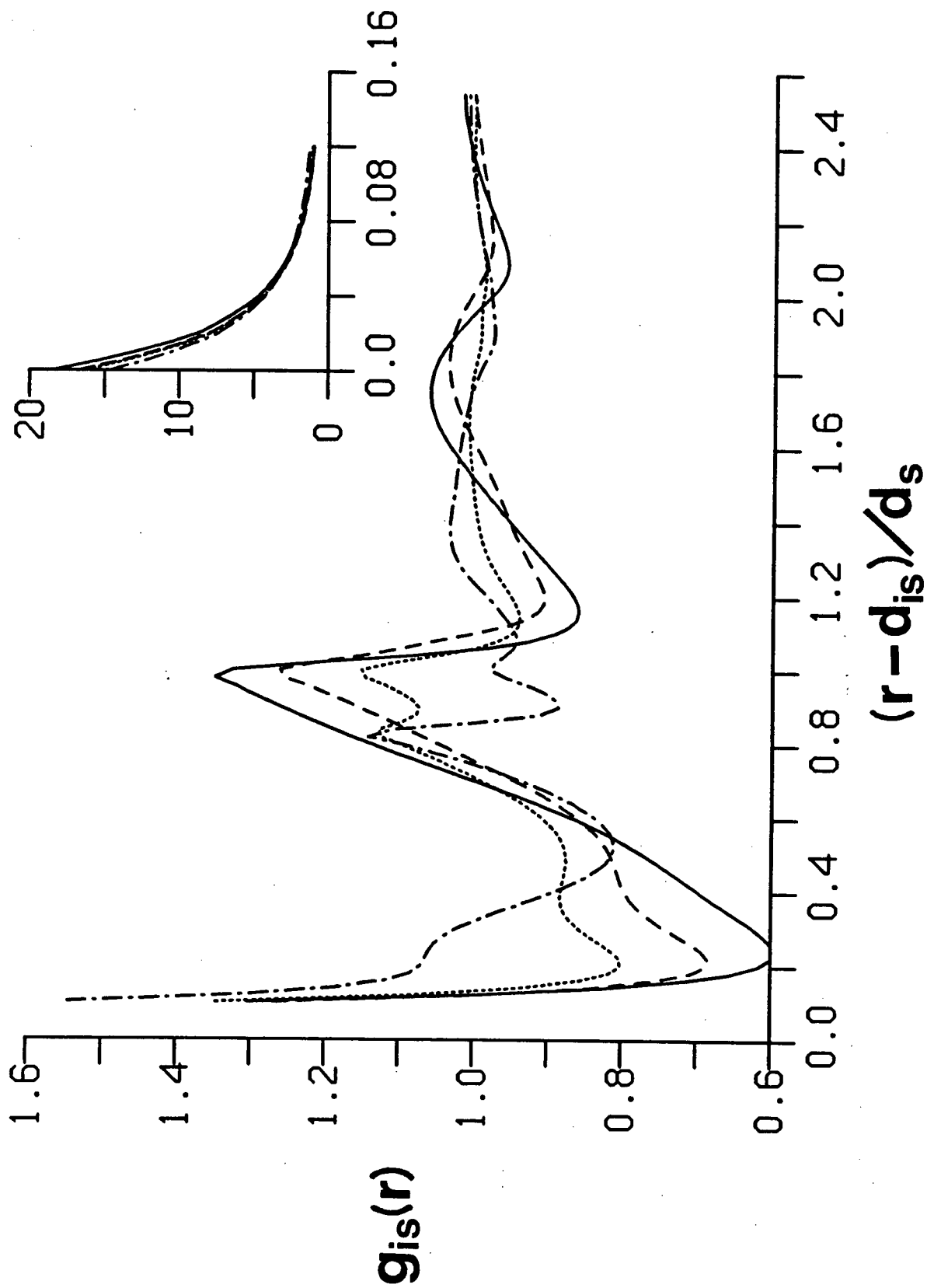
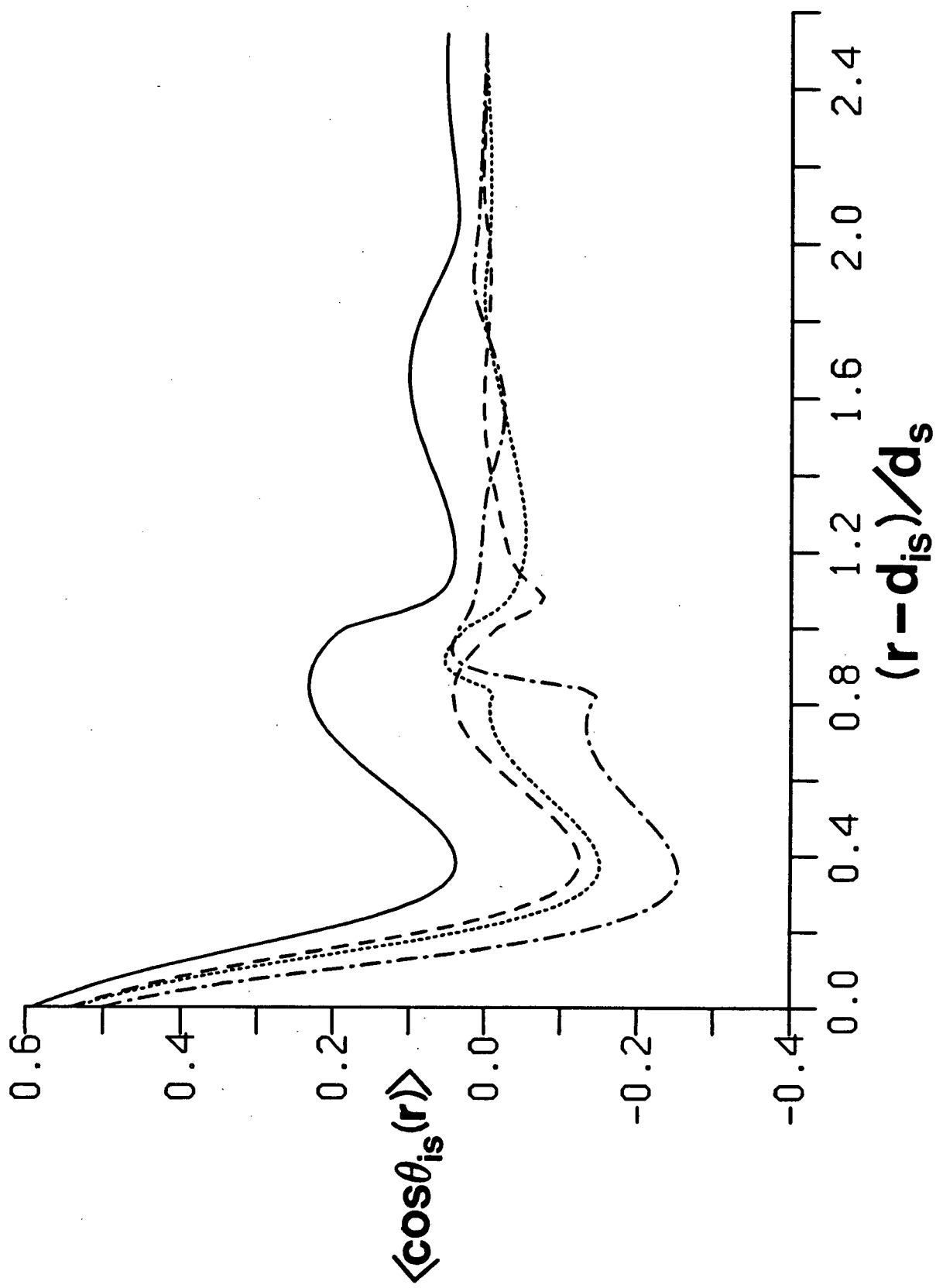


Figure 43.

$\langle \cos \theta_{is}(r) \rangle$  of  $\text{Cl}^-$ . The lines are as defined in Figure 42.



solvation shell than does a  $\text{Cl}^-$  ion, even though the  $\text{Na}^+$  ion interacts more strongly with each of the solvent particles than does the  $\text{Cl}^-$  ion.

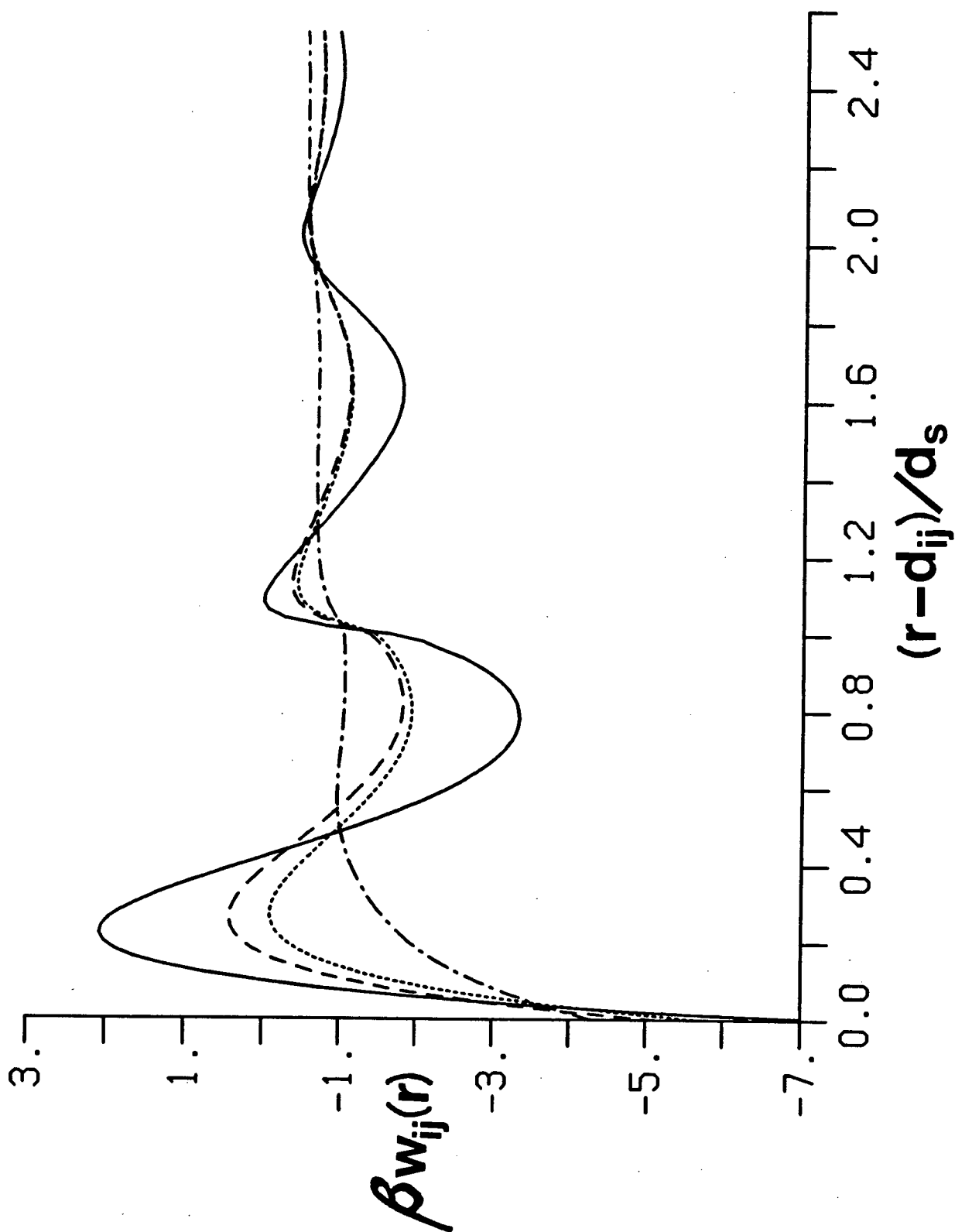
We have also calculated  $\langle \cos\theta_{is}(r) \rangle$  for the solvent particles surrounding a  $\text{Cl}^-$  ion. In Figure 43 we have shown  $\langle \cos\theta_{is}(r) \rangle$  at infinite dilution along with results for NaCl and KCl solutions at 4.0M and a NaCl solution at 12M. We observe that the contact value of  $\langle \cos\theta_{is}(r) \rangle$  demonstrates only slight concentration dependence and almost no counter-ion dependence (even at 4.0M), which is again consistent with experiment [13,16]. At infinite dilution  $\langle \cos\theta_{is}(r) \rangle$  for a  $\text{Cl}^-$  ion is always positive, indicating that the average dipole orientation is always favourable with respect to the ion, although the degree of dipole alignment varies with separation as shown by the oscillatory behaviour of  $\langle \cos\theta_{is}(r) \rangle$ . At a concentration of 4.0M the ion-dipole correlations become highly screened. We see in Figure 43 that at 4.0M  $\langle \cos\theta_{is}(r) \rangle$  now oscillates about zero (except near contact) indicating ranges of favourable as well as ranges of unfavourable dipole orientation. Comparing the two curves at 4.0M we observe that  $\langle \cos\theta_{is}(r) \rangle$  is generally more negative for NaCl than for KCl. This again implies that smaller ions such as  $\text{Na}^+$  are more effective at disrupting the ordering of the solvent around a  $\text{Cl}^-$  ion. At 12M the shape of the curve for  $\langle \cos\theta_{is}(r) \rangle$  has changed markedly from the infinite dilution result. Strong dipole counter-alignment is evident over a large range of separations, starting at  $r - d_{is} \approx 0.2d_s$  and persisting until  $0.9d_s$ . A sharp drop in the value of  $\langle \cos\theta_{is}(r) \rangle$  can be seen at a reduced separation of about  $0.85d_s$ , corresponding to the  $\text{Na}^+$  peak identified in  $g_{is}(r)$ . The NaCl and KCl solutions at 4.0M show similar but smaller drops in  $\langle \cos\theta_{is}(r) \rangle$  at separations corresponding to the arrangement where the counter-ion is situated in between the  $\text{Cl}^-$  ion and the solvent.

We will now turn our attention to the ion-ion structure of our model aqueous electrolyte solutions. First we shall consider the potentials of mean force at infinite dilution for pairs of oppositely charged ions. In Figure 44 we have plotted results for  $\beta w_{ij}(r)$  for LiF, NaCl, EtEq and MBr. For small ion pairs (e.g., LiF) we find that  $w_{ij}(r)$  is very structured at short range, obviously depending very strongly upon the molecular nature of the solvent. For larger pairs of ions (e.g., MBr)  $w_{ij}(r)$  becomes a much less structured function with much smaller oscillations. Thus, for large ion pairs  $w_{ij}(r)$  takes on its long-range asymptotic behaviour, as given by eq. (2.99), very quickly



Figure 44.

Potentials of mean force at infinite dilution for several pairs of oppositely charged ions. The solid, dashed, dotted and dash-dot lines represent results for LiF, NaCl, EqEq and MBr, respectively, in the tetrahedral solvent.



(i.e., within one or two solvent diameters), while for smaller pairs of ions  $w_{ij}(r)$  takes three or four solvent diameters before approaching its asymptotic form. From Figure 44 we see that at contact the magnitude of  $w_{ij}(r)$  increases slightly for smaller ion pairs, although  $w_{ij}(r)$  rises much more quickly from its contact value for pairs of small ions. If we compute the numbers of contact or near contact ion pairs for these salts (excluding LiF) at some low but finite concentration (e.g., 0.1M), we find that MBr has by far the largest number ( $\sim 0.26$ ) and NaCl the least ( $\sim 0.04$ ). In Figure 44 we observe that the first maximum of  $w_{ij}(r)$  increases with decreasing ion size but appears at approximately the same reduced separation for all ion pairs except MBr. For both LiF and NaCl this first maximum actually becomes positive (i.e.,  $w_{ij}(r)$  is repulsive with respect to infinite separation). We note that this behaviour is consistent with that observed by Pettitt and Rossky [82] for  $w_{ij}(r)$  for small ion pairs.

In Figure 44 we see that the second minimum in  $w_{ij}(r)$  for LiF is very deep and broad and is centred at a reduced separation of only  $0.8\bar{d}_s$ . For NaCl and EqEq the second minimum in  $w_{ij}(r)$  is very similar to that of LiF only not as deep, while for MBr it has become very shallow and has its minimum value at one solvent diameter. The situation where a solvent particle separates two oppositely charged ions is a very favourable dipolar configuration [79,81], and hence would be expected to become more important for larger ions with the present solvent model (because of the short-range nature of the ion-quadrupole interaction with respect to the ion-dipole interaction). The solvent-separated ion pair is also favoured by the hard-sphere packing of the solvent. The fact that the second minima in  $w_{ij}(r)$  for LiF, NaCl and EqEq all appear at  $r - \bar{d}_{ij} < \bar{d}_s$ , indicates that a solvent bridging structure (where the ions might be located near the tetrahedral corners of the solvent particle) is more stable than the solvent-separated geometry for smaller pairs of ions in the tetrahedral solvent. Clearly, the quadrupole moment must be playing an crucial role in stabilizing this bridging structure. Similar results were again reported by Pettitt and Rossky [82].

The effects of ion size asymmetry upon ion solvation can also be seen in Figure 44 by comparing  $w_{ij}(r)$  for NaCl and EqEq. We have previously noted that  $\bar{d}_{+-}$  is the same for both of these salts. We find that  $w_{ij}(r)$  is always more positive (i.e., less attractive) for NaCl than for EqEq. Obviously

increased ion asymmetry improves solvation for the present model. This observation differs from previous RLHNC results [81] for the same solution model which showed essentially no dependence upon ion size asymmetry.

If we compare the present RHNC results for  $w_{ij}(r)$  with those obtained from the RLHNC theory [80,81] using the same models, we find rather poor agreement, as might be expected from our earlier discussions. For both theories  $w_{ij}(r)$  shows the same basic oscillatory behaviour and positioning of the peaks. However, for small ion pairs such as LiF, the RHNC result for  $w_{ij}(r)$  is generally more structured (*i.e.*, has larger oscillations) than that of the RLHNC. The RLHNC also predicts much more negative contact values for  $w_{ij}(r)$  (for LiF the RLHNC gives about  $-12kT$ ) clearly indicating that the RHNC provides much better solvation of small ions. For larger ions the agreement improves only slightly, with the RHNC result for  $w_{ij}(r)$  now being less structured than that of the RLHNC. We note that this rather poor qualitative agreement between the RHNC and RLHNC results for  $w_{ij}(r)$  can not be explained simply in terms of the difference in the pure solvent dielectric constants obtained from the two theories.

The concentration dependence of  $g_{+-}(r)$  has been shown in Figure 45. The particular case of a model KCl solution has been considered. We observe that  $g_{+-}(r)$  for KCl has a fairly simple concentration dependence; as the concentration is increased (at least up to 4.0M)  $g_{+-}(r)$  essentially shows only screening effects. With increasing concentration  $g_{+-}(r)$  is shifted downward and the magnitude of the oscillations decreases, although the shape is essentially retained. Most of the other solutions investigated in this study show the same simple concentration dependence. The one major exception is the M'l solution (and to a much lesser degree the MBr case). In the previous section we have discussed how the long-range tail of  $g_{+-}(r)$  grows with increasing concentration for M'l. In Figure 46 we have plotted  $g_{+-}(r)$  for the M'l solution at three of the concentrations studied, including the highest concentration we were able to reach, specifically 0.74M. At short range we see the same concentration dependence found for KCl. At long range the tail of  $g_{+-}(r)$  drops when going from 0.1M to 0.5M, but then clearly increases again when going to 0.74M.

Before proceeding, let us return to Figure 30 and the super limiting-law behaviour demonstrated by NaCl for  $\rho_2 G_{+-}$ . If we examine  $g_{+-}(r)$  for NaCl

**Figure 45.**

Concentration dependence of  $g_{+-}(r)$  for KCl. The solid, dashed and dotted lines are results for model KCl solutions at 0.1M, 1.0M and 4.0M, respectively.

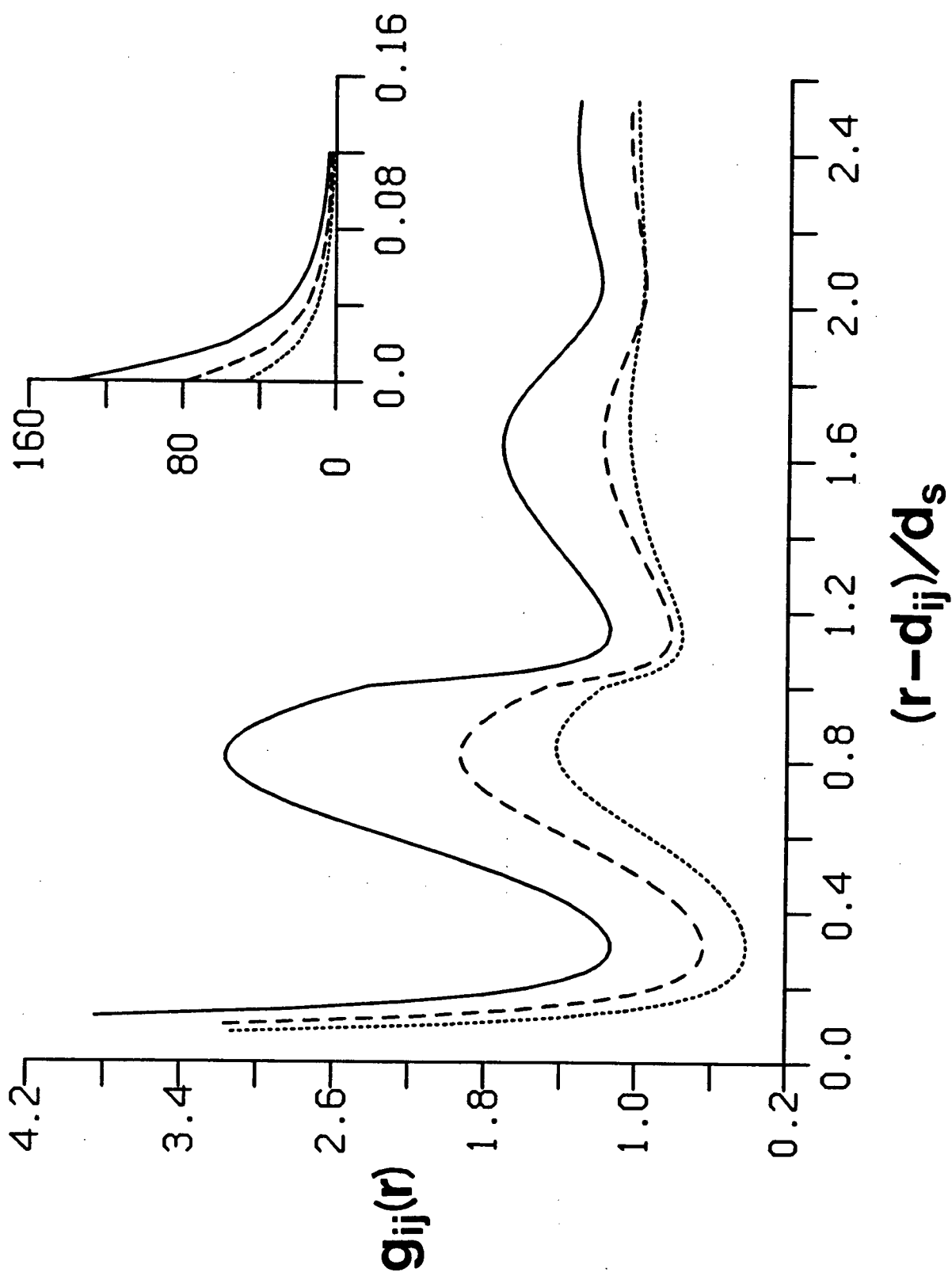
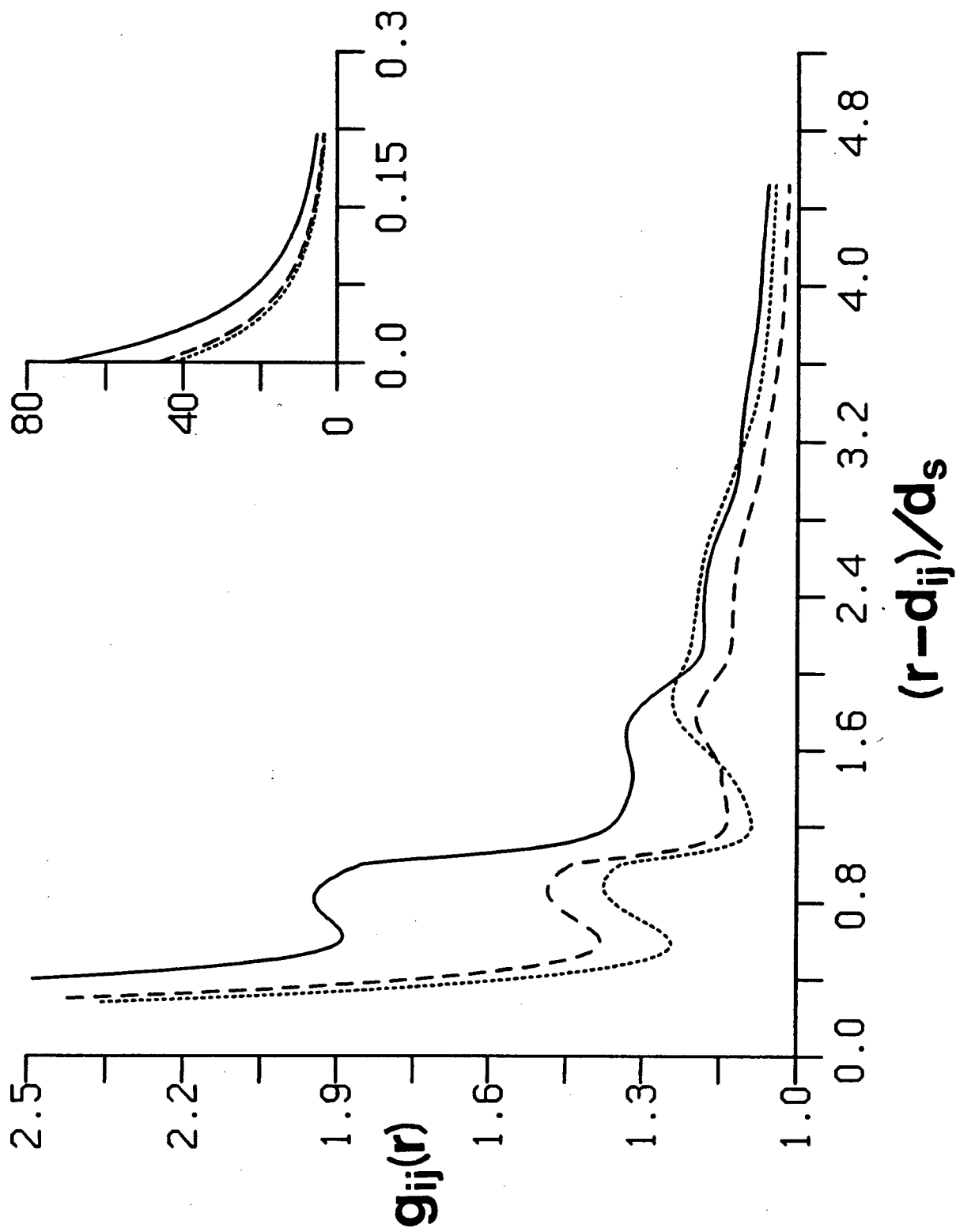


Figure 46.

Concentration dependence of  $g_{+-}(r)$  for M'I. The solid, dashed and dotted lines are results for model M'I solutions at 0.1M, 0.5M and 0.74M, respectively.



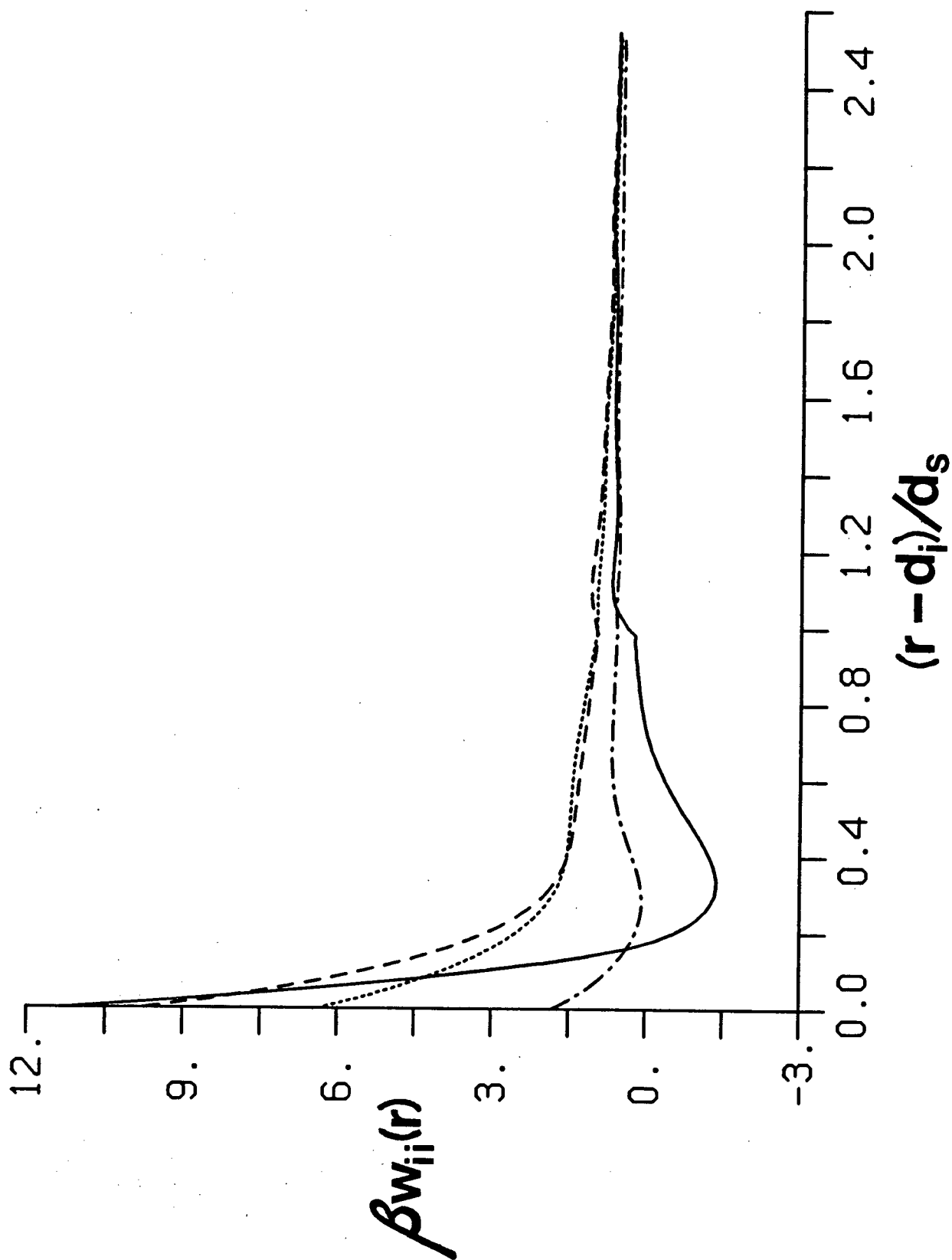


we find that it shows very similar behaviour and concentration dependence to that observed for model KCl solutions (see Figure 45). No obvious anomaly appears in  $g_{+-}(r)$  for our model NaCl solutions which might explain its super limiting-law behaviour. However, we shall see below that  $g_{++}(r)$  does show some unexpected behaviour and we know from the charge neutrality conditions (cf. eq. (3.5c)) that  $G_{+-}$  and  $G_{++}$  are inextricably linked to one another. Therefore, the super limiting-law dependence demonstrated by NaCl for  $\rho_2 G_{+-}$  may in fact be more a manifestation of the unconventional behaviour of its  $\text{Na}^+/\text{Na}^+$  radial distribution function.

Now let us turn our attention to like-ion correlations in our model electrolyte solutions. We have shown  $\beta w_{ii}(r)$  for  $\text{Na}^+$ ,  $\text{K}^+$ ,  $\text{I}^-$  and  $\text{M}^+$  ions at infinite dilution in Figure 47. We again remark that for the present ion and solvent models, ions equal in size but opposite in charge will be solvated equivalently (i.e.,  $w_{+-}(r) = w_{-+}(r)$ ). The ion size dependence of  $w_{ii}(r)$  is found to be not as simple as that of  $w_{ij}(r)$ . For the four ions considered in Figure 47 we observe that the contact value of  $w_{ii}(r)$  increases with decreasing ion size (although this is not the case for  $\text{Li}^+$ , see Figure 61). For ions only slightly larger than the solvent (e.g.,  $\text{K}^+$  and  $\text{I}^-$ )  $w_{ii}(r)$  is a surprisingly featureless function which decreases rapidly from its contact value to almost immediately take on its long-range asymptotic behaviour (as given by eq. (2.99)). As ion size is increased  $w_{ii}(r)$  clearly becomes less repulsive, particularly near contact, due in part to the decreasing coulombic repulsion. For  $\text{M}^+$ ,  $w_{ii}(r)$  actually has a local minimum very near contact (at a reduced separation of about  $0.25d_s$ ) which must be a result of the solvent forcing two such large and somewhat hydrophobic ions closer together. However, it is the behaviour of  $w_{ii}(r)$  for ions smaller than the solvent which appears the most striking. We see in Figure 47 that for  $\text{Na}^+$   $w_{ii}(r)$  decreases very rapidly from its contact value to a very broad well with its minimum at  $r - d_i \approx 0.3d_s$ . This minimum in  $w_{ii}(r)$  is in fact negative, that is, it is attractive with respect to infinite separation. Clearly, strong solvent forces must be present to overcome the strong coulombic repulsion between two such small ions at small separations. We find that this well grows (i.e., becomes deeper and extends to longer range) as the ion size is decreased (see Figure 61). In Figure 26 we have also found that the solvent is drawn in much more tightly to smaller ions. Together, these observations would suggest that ions which

Figure 47.

Potentials of mean force at infinite dilution for several pairs of like ions. The solid, dashed, dotted and dash-dot lines are results for  $\text{Na}^+/\text{Na}^+$ ,  $\text{K}^+/\text{K}^+$ ,  $\text{I}^-/\text{I}^-$  and  $\text{M}^+/\text{M}^+$  pairs, respectively, in the tetrahedral solvent.



interact very strongly with the solvent will show a minimum in  $w_{ii}(r)$  at small separations (*i.e.*, the solvent prefers to solvate these ions as a divalent pair). We will discuss this feature in  $w_{ii}(r)$  and its relationship with the ion-solvent interaction in section 5 and again in more detail in section 6.

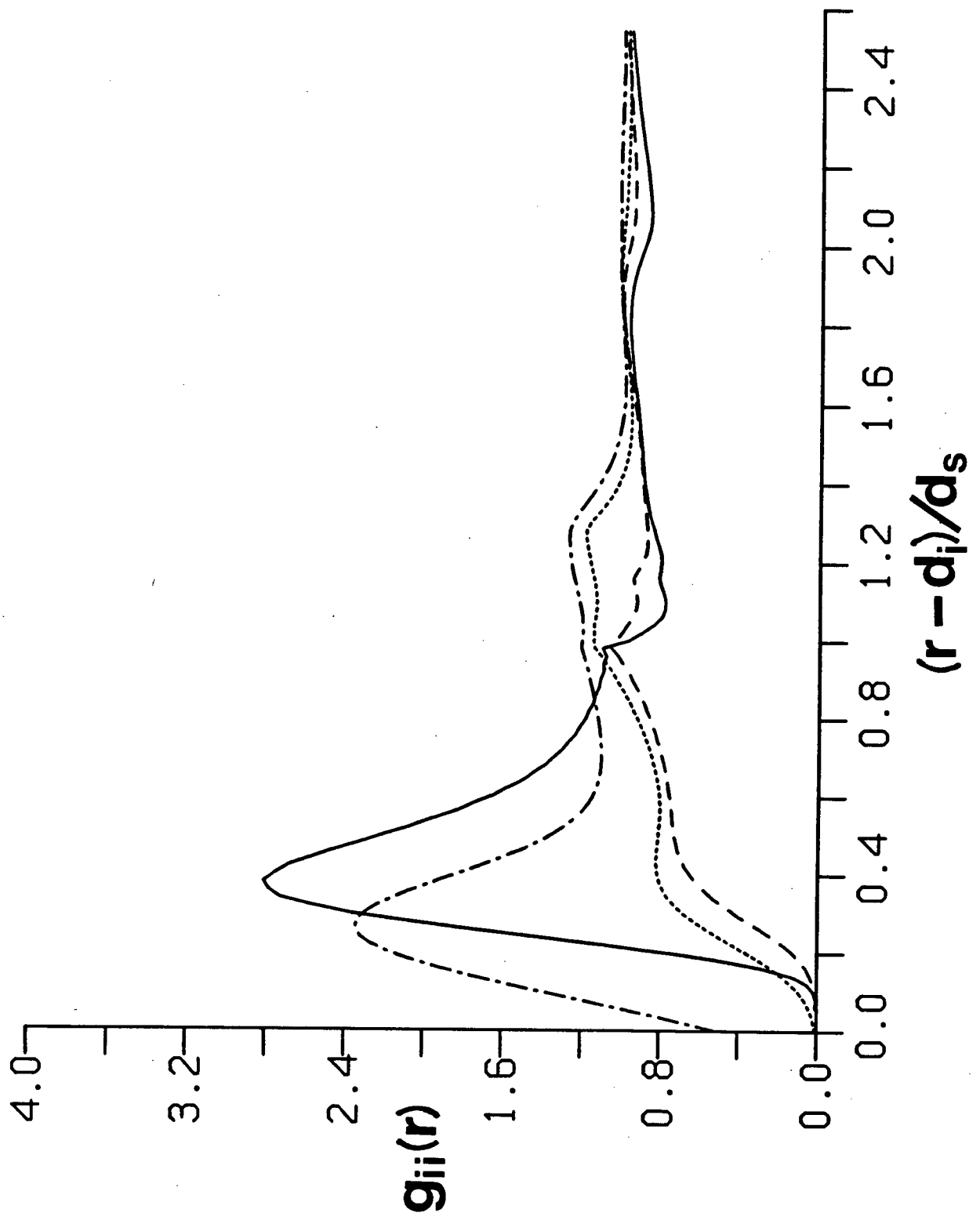
At this point we should say that although the present RHNC results for  $w_{ii}(r)$  may not be exact, we do believe that they are qualitatively correct for the present models. Pettitt and Rossky [82], using more complicated models and a related integral equation theory (RISM), obtained similar results for  $w_{ii}(r)$  for small anions (*i.e.*,  $F^-$  and  $Cl^-$ ). Clearly what is now needed are exact computer simulation results for these models in order to test the present theories.

Comparing the present RHNC results for  $w_{ii}(r)$  with those obtained for the same models from the RLHNC theory [80,81], we again find poor agreement. Generally the RLHNC results for  $w_{ii}(r)$  have an oscillatory behaviour similar to that of  $w_{ij}(r)$  (only inverted), while the functions determined in the present study show virtually no oscillations. Both theories do predict an attractive well in  $w_{ii}(r)$  at small separations for small ions, although in the RHNC this feature is much larger. For large ions the RLHNC theory shows larger hydrophobic effects (*i.e.*, for an ion twice the size of the solvent  $w_{ii}(r)$  is actually negative at contact). Again, the differences we see in  $w_{ii}(r)$  for the two theories can not be explained simply in terms of the difference in  $\epsilon$ .

In Figure 48 we have examined finite concentration results for  $g_{ii}(r)$  for the same four ions considered in Figure 47. Included in Figure 48 are the like-ion radial distribution functions of  $Na^+$ ,  $K^+$ ,  $I^-$  and  $M^+$  in 1.0M solutions of NaCl, KCl, CsI and MBr, respectively. We observe that even at a concentration of 1.0M much of the behaviour demonstrated by  $g_{ii}(r)$  for these ions still closely resembles that predicted by the potentials of mean force at infinite dilution. For both  $K^+$  and  $I^-$   $g_{ii}(r)$  starts at zero at contact and then rises slowly to a value of 1.0, showing only a few relatively small structural features. For  $M^+$   $g_{ii}(r)$  has a contact value of 0.5 and rises quickly to a maximum of 2.5 at a reduced separation of  $0.25d_s$ . This first peak in  $g_{ii}(r)$  for  $M^+$  is found to grow with increasing concentration, probably due simply to increased ionic screening. In Figure 48 we see that although  $g_{ii}(r)$  for  $Na^+$  starts out at zero at contact, it also rises quickly to a large peak with a

Figure 48.

$g_{ii}(r)$  for several ions in model electrolyte solutions at 1.0M. The solid, dashed, dotted and dash-dot lines are  $g_{ii}(r)$  for  $\text{Na}^+$  in a NaCl solution,  $\text{K}^+$  in a KCl solution,  $\text{I}^-$  in a CsI solution and  $\text{M}^+$  in a MBr solution, respectively.



maximum at  $r-d_i=0.4d_s$ . The value of  $g_{ii}(r)$  then remains larger than 1.0 until  $r-d_i=d_s$  (*i.e.*, until a single solvent can just fit in between the two  $\text{Na}^+$  ions), at which point  $g_{ii}(r)$  drops sharply below 1.0. We point out that the situation where a single solvent is between two ions of the same charge is energetically unfavourable. At very low concentration the first peak in  $g_{ii}(r)$  for  $\text{Na}^+$  is found to increase slightly with increasing concentration but reaches a maximum at about 0.1M (where it has a maximum value of about 5.0). As the concentration is increased above 0.1M, the peak then decreases and shifts slightly outward. It continues to decrease up to a concentration of about 4.0M, after which it shows relatively little change. Peaks due to ion triples can also be identified in Figure 48 (*e.g.*, for  $\text{I}^-$  and  $\text{M}^+$  at a reduced separation of  $1.3d_s$ ). Although the ion-triples peak is quite large for the CsI and MBr solutions, we find that it becomes much smaller for KCl and NaCl solutions.

The concentration and counter-ion dependence of the like-ion radial distribution function for  $\text{Cl}^-$  has been shown in Figure 49. Solutions of NaCl at 0.1M, 4.0M and 12M, as well as KCl at 4.0M, have been included in Figure 49. At 0.1M we see that from contact  $g_{ii}(r)$  rises slowly with increasing ion separation, while at higher concentration  $g_{ii}(r)$  rises much more quickly. Much of this effect can be interpreted as resulting from simple ionic screening. We point out that for NaCl and KCl solutions at 0.1M the curves for  $g_{ii}(r)$  for  $\text{Cl}^-$  are almost indistinguishable. However, at 4.0M the  $\text{Cl}^-/\text{Cl}^-$  radial distribution function shows definite counter-ion dependence, as can be seen from Figure 49. Of course, the peak due to ion triples appears at a larger separation for KCl than it does for NaCl. If we shift our attention to smaller separations, we observe that both NaCl and KCl have a peak in  $g_{ii}(r)$  for  $\text{Cl}^-$  at a reduced separation of about  $0.4d_s$ . This peak appears to grow with increasing concentration, although more quickly for NaCl than for KCl. For the 12M NaCl solution this peak has become quite large, indicating a relative high probability of finding two  $\text{Cl}^-$  ions close together. It should be noted that this peak must be due to different effects than the peak found in  $g_{ii}(r)$  for  $\text{Na}^+$ , since there the peak decreases with increasing concentration. The structure responsible for the peak in the  $\text{Cl}^-/\text{Cl}^-$  radial distribution function is not obvious; however, one possibility is an arrangement where a single solvent acts as a bridge between two  $\text{Cl}^-$  ions and the same cation. This structure is consistent with the fact that the peak is larger for NaCl than

Figure 49.

$g_{ii}(r)$  for  $\text{Cl}^-$  for several model electrolyte solutions. The solid, dashed and dash-dot lines represent results for NaCl solutions at 12M, 4.0M and 0.1M, respectively. The dotted line is  $g_{ii}(r)$  for  $\text{Cl}^-$  in a 4.0M KCl solution.



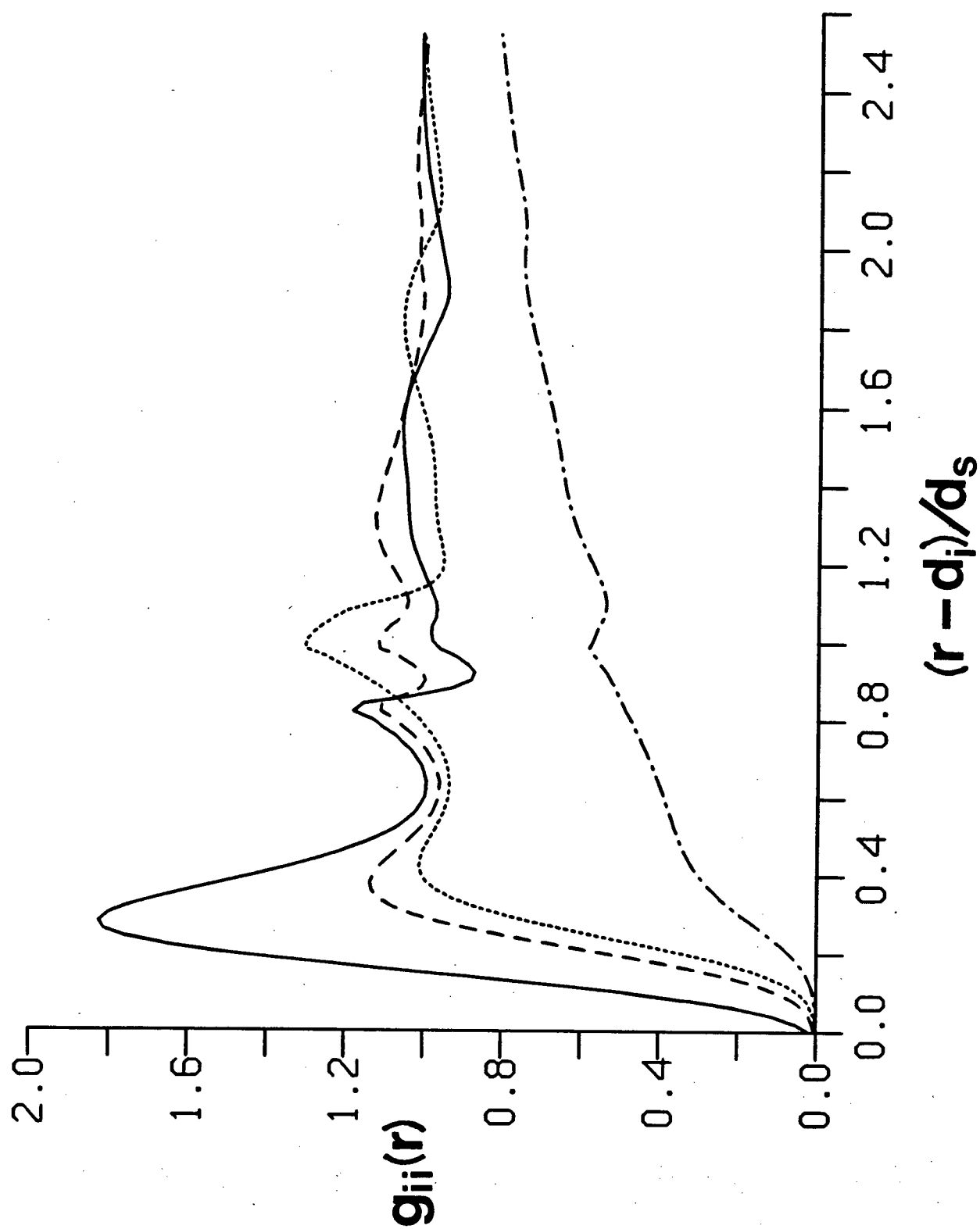
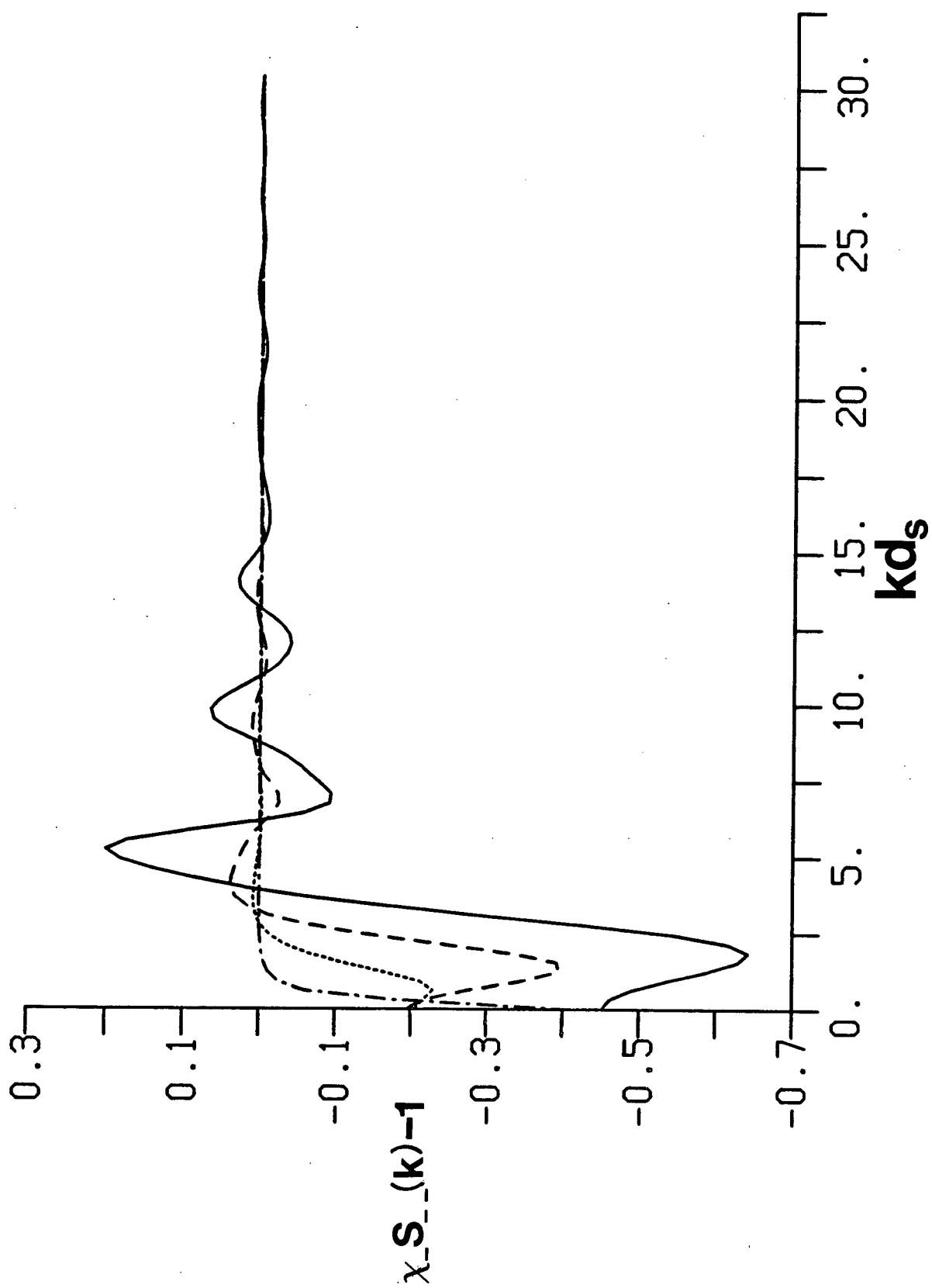


Figure 50.

Cl<sup>-</sup>/Cl<sup>-</sup> partial structure factors for model NaCl solutions. The solid, dashed, dotted and dash-dot lines are results for model NaCl solutions at 12M, 4.0M, 1.0M and 0.1M, respectively. We point out that the partial structure factor has been multiplied by the mole fraction,  $x_{-}$ , of Cl<sup>-</sup> ions.



KCl, since  $g_{+-}(r)$  would indicate that NaCl has a larger number of solvent-separated unlike ion pairs. This structure also predicts the correct concentration behaviour for the peak.

Finally, in Figure 50 we have plotted the  $\text{Cl}^-/\text{Cl}^-$  partial structure factor, as given by eq. (5.4), for a model NaCl solution at several concentrations. It is obvious from Figure 50 that at low concentration  $S_{--}(k)$  is dominated by its small  $k$  dependence, and hence by the long-range behaviour of  $g_{--}(r)$ . As the concentration is increased we observe structure appearing in  $S_{--}(k)$  at larger  $k$  values. If we compare the  $\text{Cl}^-/\text{Cl}^-$  partial structure factor of our model 12M NaCl solution with an experimental result from 14.9 molal LiCl in  $\text{D}_2\text{O}$  obtained by neutron scattering (see Figure 27 of Ref. 13), we find that they are qualitatively similar.

## 5. Effects of Including the RDMF

Heretofore, the results reported in this chapter have been for model aqueous electrolyte solutions which incorporate a non-polarizable solvent with a permanent dipole moment equal to the effective dipole moment,  $m_e$ , of the pure tetrahedral solvent. We have shown in section 1 that within the SCMF theory the average local electric field in the bulk is constant (to a very good approximation) for the model solutions being examined in this study. Consequently, the model solutions considered in sections 2, 3 and 4 of this chapter are effective systems within the SCMF theory corresponding to model electrolyte solutions which incorporate a polarizable water-like solvent. In this section we will examine the effects of treating the polarization of the solvent at the level of the RDMF theory, as described in Chapter IV. We emphasize that up to this point only the bulk average fields in our model aqueous electrolyte solutions have been considered.

We would expect the RDMF theory to be most accurate at infinite dilution and at low concentration. Hence, we have repeated calculations for model solutions which include the RDMF only for concentrations at or below 0.1M. The  $\text{Na}^+$ ,  $\text{K}^+$ ,  $\text{Cs}^+$ ,  $\text{M}^+$ ,  $\text{Cl}^-$ ,  $\text{Br}^-$ , and  $\text{I}^-$  ions were all studied at infinite dilution, while solutions of NaCl and CsI were investigated at finite concentration (*i.e.*, for  $c \leq 0.1\text{M}$ ). It was found that at the low (but finite)

concentrations examined, the inclusion of the RDMF had a negligible ( $\sim 0.1\%$  at 0.1M) effect upon the average local fields of the bulk. Therefore, as was done in all previously reported calculations, the effective dipole moment of the pure tetrahedral solvent was used in all model calculations reported in this section.

First we shall consider the additional ion-solvent interaction term,  $u_{is}^{\Delta p}(r)$ , as determined using eq. (4.29). In Figure 51 we have compared the values of  $u_{is}^{\Delta p}(r)$  given by the RDMF theory for a  $\text{Na}^+$  ion at infinite dilution with those obtained from eq. (4.1c). We recall that eq. (4.1c) considers only the two-body problem of a single polarizable solvent particle at a distance  $r$  from an ion, and hence represents the low density limit. It can be seen from Figure 51 that the RDMF theory predicts values for the additional ion-solvent interaction which are much smaller than those determined from eq. (4.1c). Clearly, the lateral solvent fields are having a very large effect upon  $u_{is}^{\Delta p}(r)$ , even at smaller separations. In Chapter IV we have shown that at long range the RDMF result for  $u_{is}^{\Delta p}(r)$  is essentially  $1/9$  that of  $u_{qp}(r)$  (when  $\epsilon$  is large). From Figure 51 we observe that for  $\text{Na}^+$   $u_{qp}(r)$  is about six times larger than  $u_{is}^{\Delta p}(r)$  at contact. We note that a similar result was found for all the ions investigated. The contact value of  $u_{is}^{\Delta p}(r)$  for  $\text{Na}^+$  corresponds to  $\Delta p(r=d_{is})=0.425D$ . We find that  $u_{is}^{\Delta p}(r)$  drops rapidly from contact, almost reaching zero at a reduced separation of  $0.5d_s$ , then increases slightly to a small peak at  $r-d_{is}=0.9d_s$ . None of the other ions examined here showed such a peak, although for virtually all these ions  $u_{is}^{\Delta p}(r)$  did flatten in the range  $0.4d_s < r-d_{is} < d_s$ . Beyond one solvent diameter  $u_{is}^{\Delta p}(r)$  was found to rapidly approach its long-range limiting behaviour.

The additional attraction between an ion and a solvent due to the RDMF was found to be relatively small at short range when compared with the electrostatic terms of the ion-solvent potential. Very little change in  $g_{is}(r)$  due to  $u_{is}^{\Delta p}(r)$  was observed, although close inspection reveals a very slight increase in  $g_{is}(r)$  at almost all separations.

In Figure 52 and 53 we have shown the effects of  $u_{is}^{\Delta p}(r)$  upon unlike ion potentials of mean force at infinite dilution for NaCl and MBr, respectively. We find that, in general, the addition of the RDMF improves ion solvation. This would seem consistent with the fact that the ion-solvent interaction has been increased slightly. For NaCl we observe that  $w_{ij}(r)$  has

Figure 51.

Additional ion-solvent interaction term due to  $\Delta p(r)$  for a  $\text{Na}^+$  ion at infinite dilution. The solid line represents  $u_{qp}(r)$  as given by eq. (4.1c), while the dashed line is  $u_{is}^{\Delta p}(r)$  obtained using the RDMF theory.

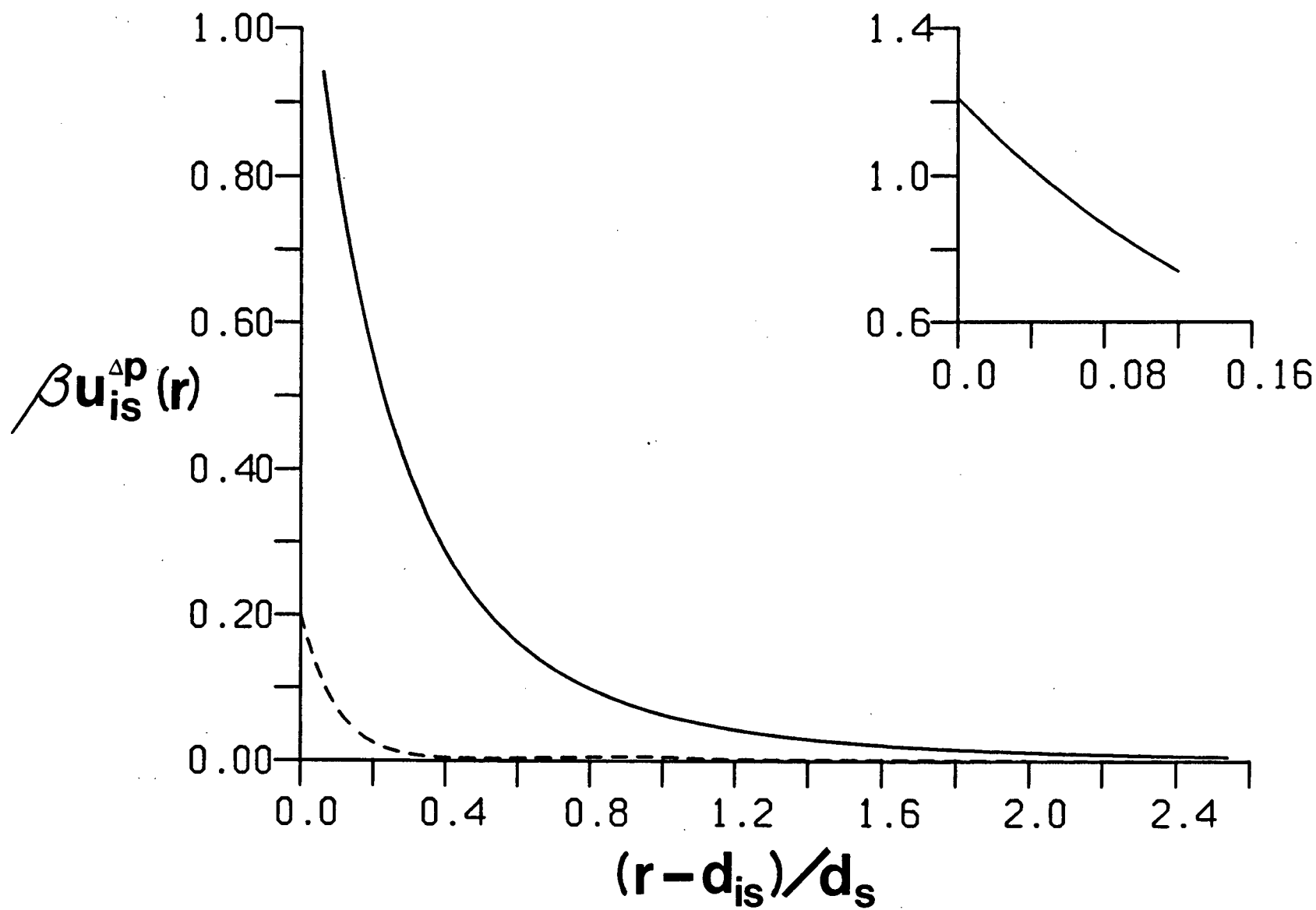


Figure 52.

Effect of the RDMF upon  $w_{ij}(r)$  for NaCl. The solid line is  $\beta w_{ij}(r)$  for NaCl in the tetrahedral solvent at 25°C when  $u_{is}^{\Delta p}(r) = 0$ , while the dashed line represents the result when  $u_{is}^{\Delta p}(r)$  is given by the RDMF theory.



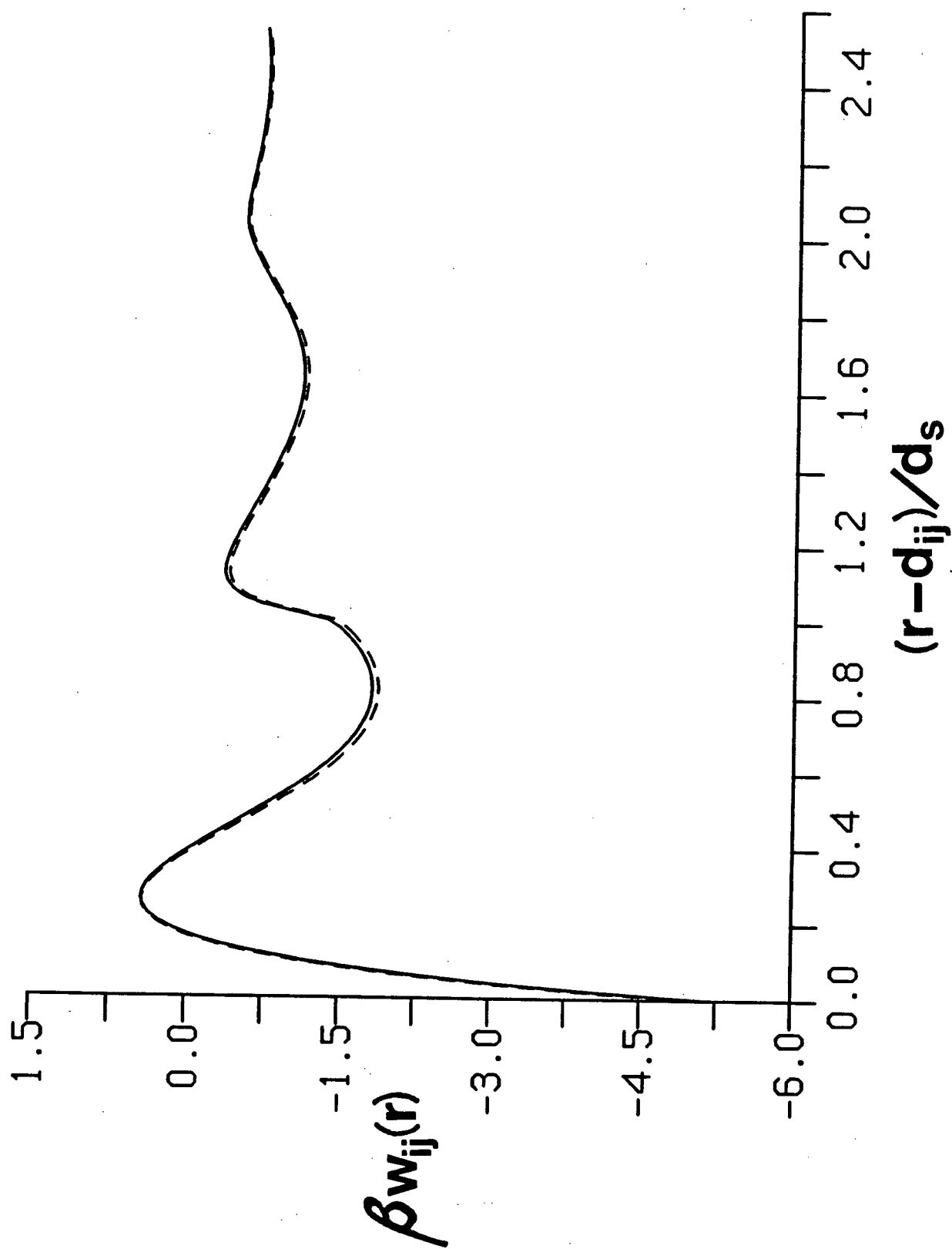
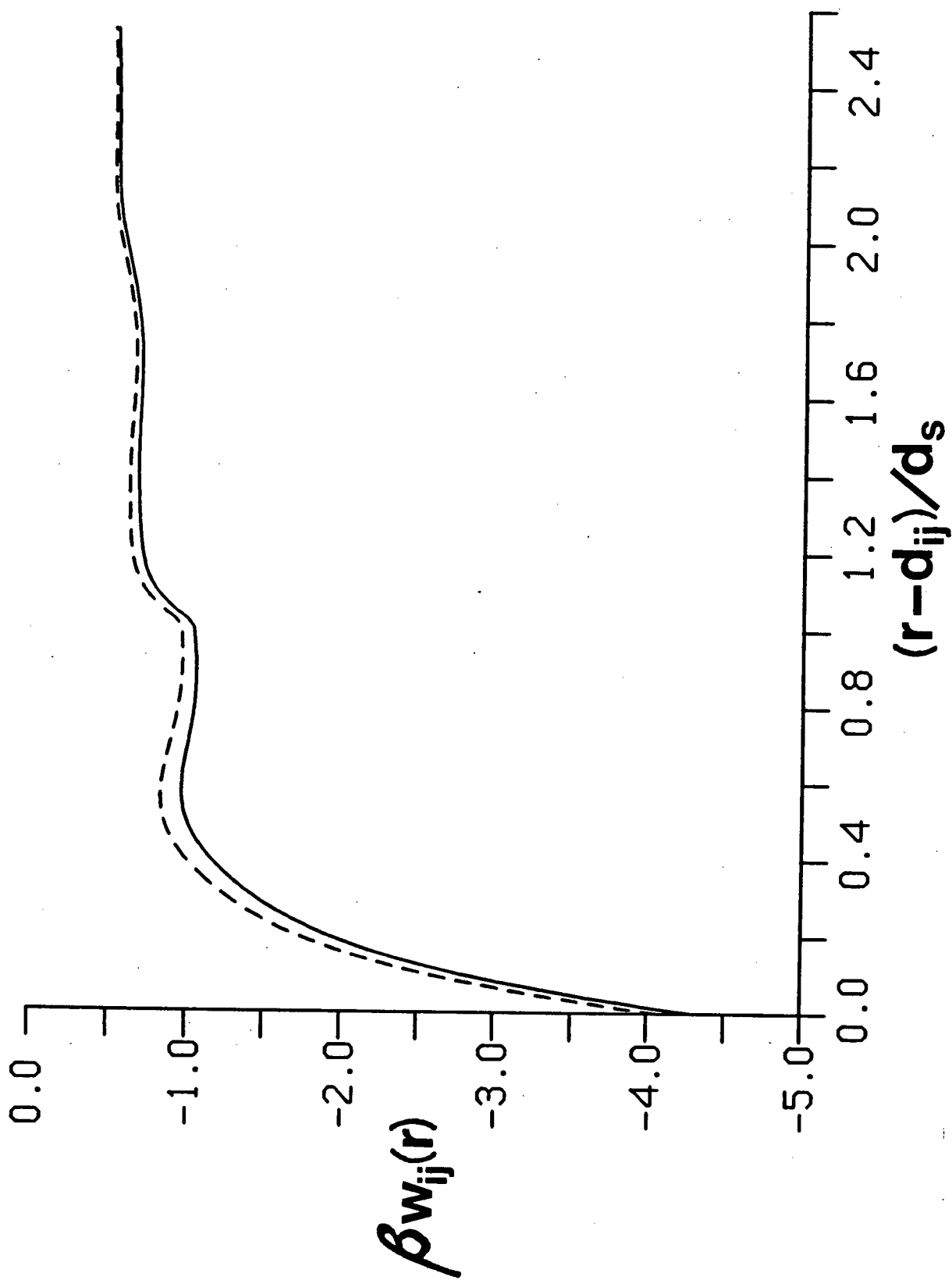


Figure 53.

Effect of the RDMF upon  $w_{ij}(r)$  for MBr. As in Figure 52, the solid line is for  $u_{is}^{\Delta p}(r)=0$ , while the dashed line is the RDMF result.



become slightly more positive near contact with the addition of  $u_{is}^{\Delta p}(r)$ , although it then becomes more negative at the solvent separated distance and beyond, as can be seen in Figure 52. For MBr the addition of  $u_{is}^{\Delta p}(r)$  shifts  $w_{ij}(r)$  to more positive values at all separations. Comparing the results in Figures 52 and 53 we discover that the RDMF appears to have a relatively larger effect upon  $w_{ij}(r)$  for larger ions, in this case MBr. In very recent work using McMillan-Mayer level theory, Pettitt and Rossky [82] have shown that some thermodynamic properties of model aqueous electrolyte solutions (in particular that of  $\phi$ ) are extremely sensitive to small changes in  $w_{ij}(r)$ . Thus, we would expect the shifts in  $w_{ij}(r)$  due to  $u_{is}^{\Delta p}(r)$  observed here for NaCl and MBr to result in significant changes in the activity coefficients of these two solutions at finite concentration.

The effects of the RDMF upon the like-ion potentials of mean force at infinite dilution for  $\text{Na}^+$  and  $\text{M}^+$  are shown in Figures 54 and 55, respectively. Here we find that small and large ions show opposite effects. For  $\text{M}^+$  we observe that the addition of  $u_{is}^{\Delta p}(r)$  shifts  $w_{ii}(r)$  to more positive values at all separations, indicating improved solvation. This behaviour is consistent with the proposed hydrophobic nature of these large ions; the increased ion-solvent interaction would be expected to reduce the hydrophobic effects, and consequently improve the solvation. For  $\text{Na}^+$  we see in Figure 54 that the addition of  $u_{is}^{\Delta p}(r)$  shifts  $w_{ii}(r)$  to more negative values at all separations. In section 3 we have proposed that the negative wells in  $w_{ii}(r)$  for small ions are a result of their very strong interaction with the solvent. Thus, if the ion-solvent interaction is increased we would expect the well in  $w_{ii}(r)$  to grow deeper. This is in fact what is observed in Figure 54.

In Chapter IV we have shown that  $u_{is}^{\Delta p}(r)$  will contribute to  $C_{IS}$  (cf. eq. (4.98)) and have derived an expression (cf. eq. (4.99)) for its contribution,  $S_c^{\Delta p}$ , to the limiting slope. The low concentration behaviour of  $C_{IS}$  for model NaCl and CsI solutions with and without the RDMF have been compared in Figure 56. At very low concentration we find that our numerical results do approach their respective limiting laws. It is obvious from Figure 56 that  $S_c^{\Delta p}$  makes an appreciable contribution to the limiting behaviour of  $C_{IS}$ , almost doubling the total limiting slope. Clearly then,  $u_{is}^{\Delta p}(r)$  can be expected to significantly affect the limiting laws of all thermodynamic properties of electrolyte solutions which depend upon ion-solvent correlations. We remark

Figure 54.

Effect of the RDMF upon  $w_{ii}(r)$  for  $\text{Na}^+$ . The solid line is  $\beta w_{ii}(r)$  for a  $\text{Na}^+$  ion in the tetrahedral solvent at  $25^\circ\text{C}$  when  $u_{is}^{\Delta p}(r)=0$ , while the dashed line represents the result when  $u_{is}^{\Delta p}(r)$  is given by the RDMF theory.

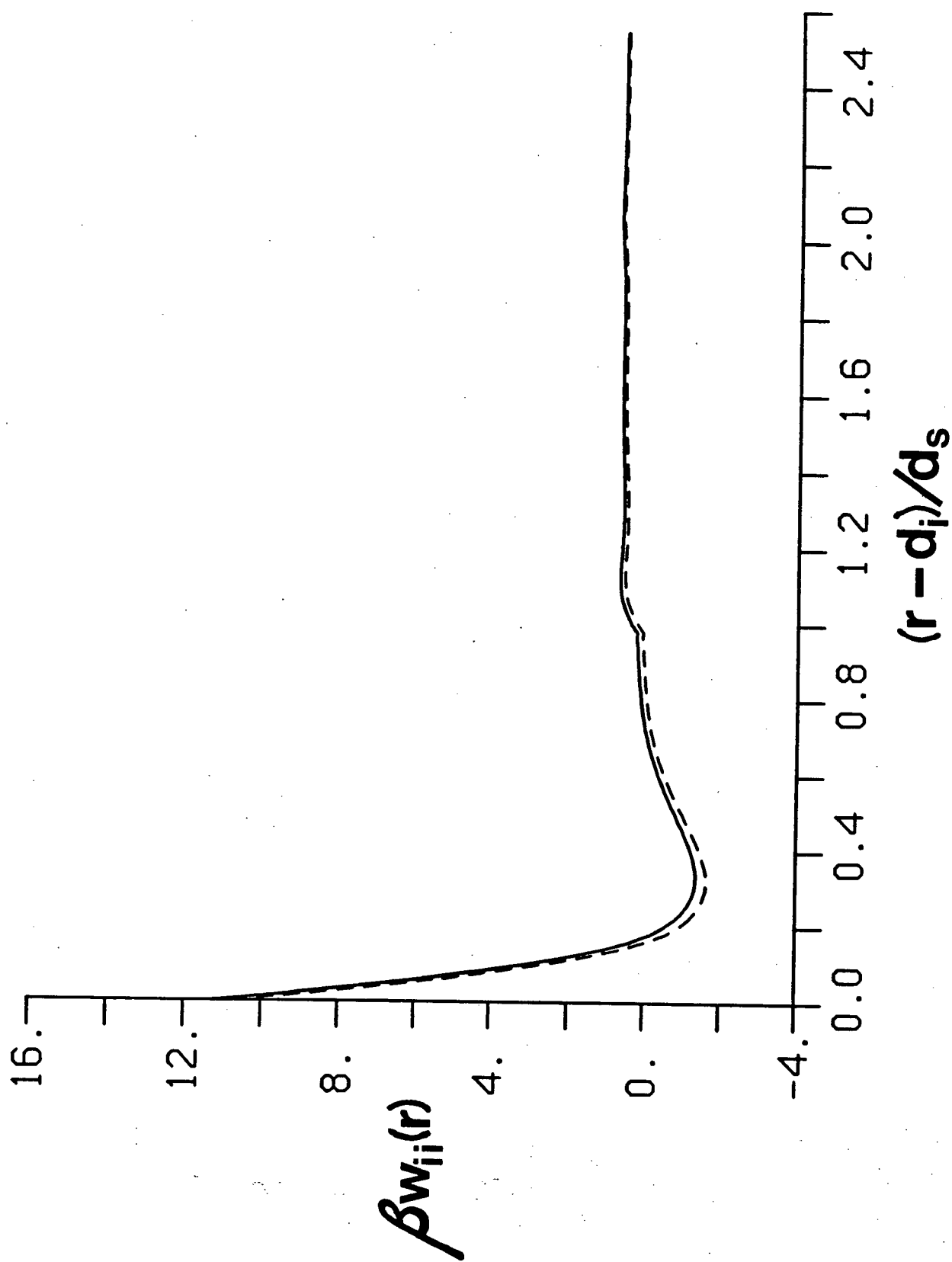


Figure 55.

Effect of the RDMF upon  $w_{ii}(r)$  for  $M^+$ . As in Figure 54, the solid line is for  $u_{is}^{\Delta p}(r)=0$ , while the dashed line is the RDMF result.

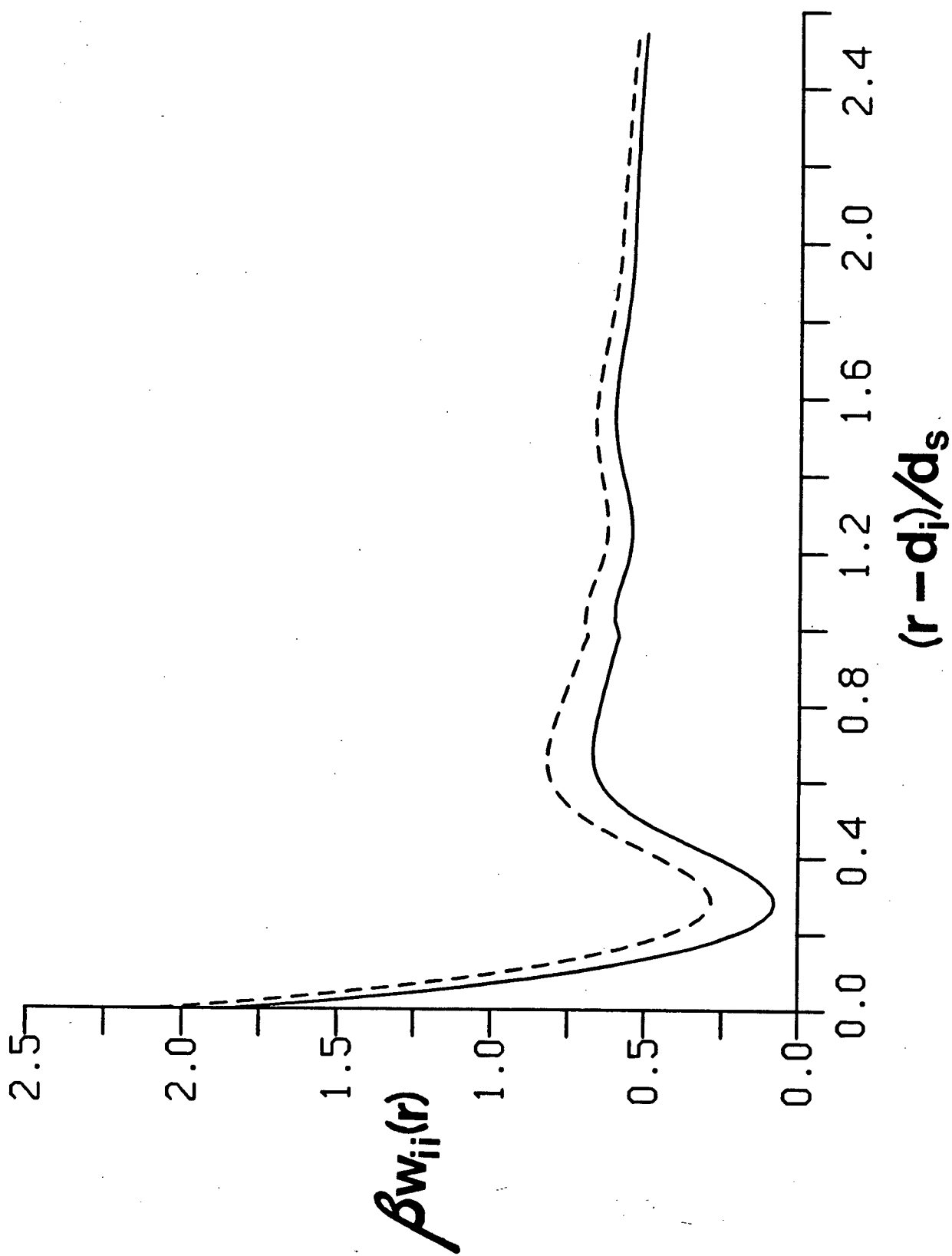
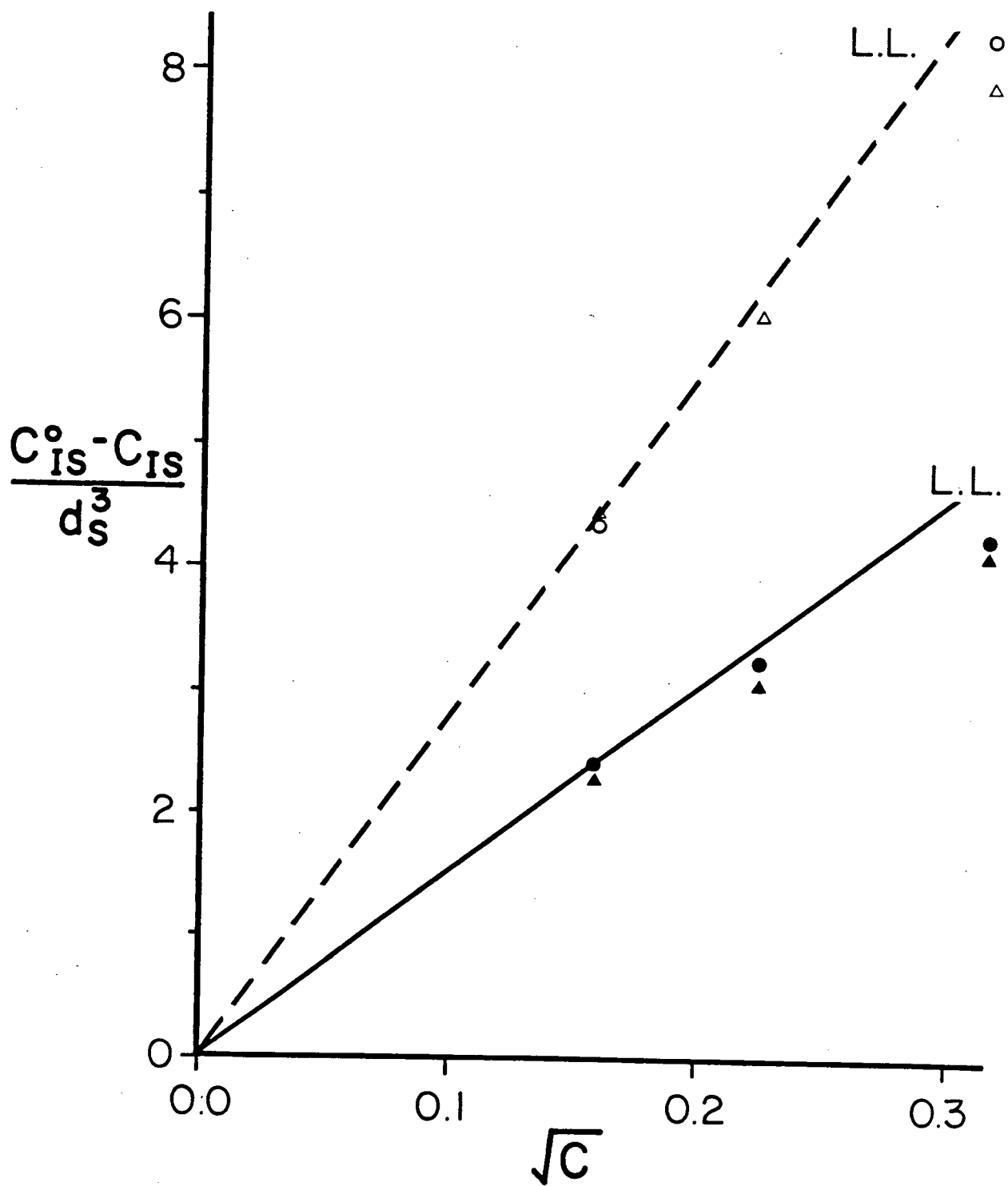




Figure 56.

Effect of the RDMF upon  $C_{IS}$ . For ease of comparison we have plotted the difference between the infinite dilution value,  $C_{IS}^0$ , and  $C_{IS}$  itself. The dots and solid triangles are RHNC results for model CsI and NaCl solutions, respectively, when  $u_{IS}^{\Delta p}(r) = 0$ . The open circles and triangles are results for model CsI and NaCl solutions, respectively, when  $u_{IS}^{\Delta p}(r)$  is given by the RDMF theory. The solid line is the limiting slope,  $S_c$ , determined using eq. (3.48) and  $\epsilon = 88.3$ . The dashed line represents the sum of  $S_c$  and  $S_c^{\Delta p}$  where the latter is given by eq. (4.99).



that the limiting values,  $C_{IS}^0$ , are also increased dramatically by the RDMF. Therefore, even though  $u_{IS}^{\Delta p}(r)$  appears as a relatively small term in the ion-solvent pair potential, its long-range  $1/r^4$  dependence and the fact that it is a spherically symmetric term allow it to have a relatively large effect upon many thermodynamic properties of electrolyte solutions.

As mentioned above, model NaCl and CsI solutions which included the RDMF were studied at low concentration. The average energies of these solutions remained virtually unchanged from the earlier  $u_{IS}^{\Delta p}(r)=0$  results. Quantities such as the dielectric constant and  $\kappa$  were also only slightly affected. As we would expect from our earlier discussion, the derivatives of  $\ln \gamma_{\pm}$  showed great sensitivity to the addition of the RDMF, even at the low concentrations examined. For CsI the derivative was found to increase (become smaller in magnitude) by about 20% at 0.1M, while for NaCl it decreased by approximately 10%.

From our discussion in Chapter IV it would seem obvious that the partial molecular volume of the solute should be particularly sensitive to the inclusion of the RDMF. Their infinite dilution values show strong dependence. For example, for CsI  $\bar{V}_2^0 = 75.6$  cc/mole when  $u_{IS}^{\Delta p}(r)=0$ , while  $\bar{V}_2^0 = 44.9$  cc/mole with the RDMF turned on. We find that the limiting slope of  $\bar{V}_2$  (see Figure 36) is almost doubled due to a similar increase in  $S_c$ . Unfortunately, even if we totally ignore the HNC contribution to  $S_c$  and use only  $S_c^{\Delta p}$  in determining  $S_v$ , we discover that the theoretical limiting slope still exceeds the real result by more than a factor of three, even after correcting for the difference in the compressibilities of the tetrahedral solvent and real water. Thus, it would appear that eq. (4.99) does not represent an exact result and that the RDMF theory is still only approximate, even in the limits  $\rho_2 \rightarrow 0$  and  $r \rightarrow \infty$ . What is not clear is why this should be the case. In Chapter IV we have shown that at infinite dilution the RDMF result for the average local field at long range (cf. eq. (4.96b)) is equivalent to the expression of Pollock *et al.* [167] for the special case when the solvent is polarizable but non-polar. A very similar expression (cf. eq. (4.97)) was obtained for the case when the solvent is polar but non-polarizable. However, since there are no computer simulation results available for the latter system, the accuracy of eq. (4.97) is not known. One of the most likely sources of error in the RDMF theory would seem to be that aspect of our mean field approach in which we

assume that only the average dipole moments directed towards the ion need be considered. One might also expect the three-body correlations (e.g., dipole-dipole-ion) to be important in determining the average excess local field. Moreover, since  $u_{iS}^{\Delta p}(r)$  (and hence  $C_{IS}$ ) depends upon  $\langle \Delta E_1(R) \rangle^2$ , small errors in the average excess local field will have a relatively large influence upon  $C_{IS}$ , and consequently upon its limiting slope.

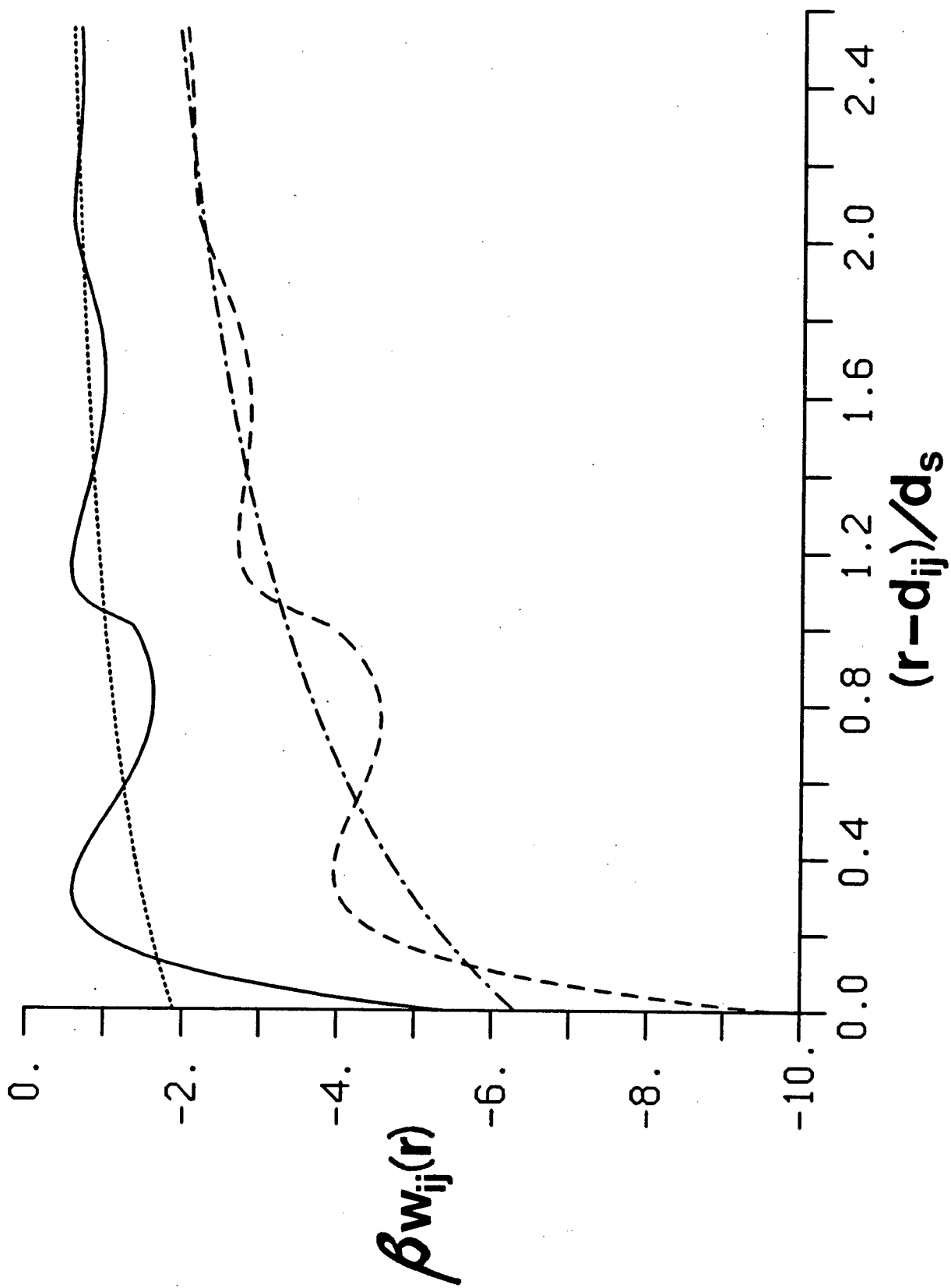
## 6. Results Obtained Employing Different Solvents

All results reported in the previous four sections were obtained using the tetrahedral solvent model (described in Chapter V) with an effective permanent dipole moment  $m_e = 2.605D$  and an effective square quadrupole moment  $\Theta_s = 2.57B$ . Model aqueous electrolyte solutions employing three different but closely related solvent models were also studied, with essentially all calculations being carried out at infinite dilution. In this section we will compare these results with those reported earlier in this chapter.

First we shall examine the effect of totally ignoring the polarizability of the solvent and taking its permanent dipole moment as being  $1.855D$ , which is the gas phase value for water [118]. This nonpolarizable tetrahedral solvent has a dielectric constant of  $28.4$  (as reported in Chapter V), while for the polarizable model  $\epsilon = 97.4$ . In Figure 57 we have compared  $w_{ij}(r)$  for KCl in the polarizable and nonpolarizable tetrahedral solvents. Also included in Figure 57 are the primitive model potentials of mean force. Clearly, the results for the two solutions differ markedly. We find much better solvation of the ions in the polarizable solvent,  $w_{ij}(r)$  being shifted to much more negative values for the nonpolarizable solvent. Closer inspection reveals that the potentials of mean force have very similar oscillatory behaviour about their respective long-range asymptotic limits. Thus, most of the dissimilarity seen in  $w_{ij}(r)$  for the two solvent models comes through the difference between their dielectric constants. Nevertheless, we would expect model solutions utilizing the nonpolarizable tetrahedral solvent to have thermodynamic properties which differ dramatically (for the most part) from those reported in section 3 for solutions employing the polarizable tetrahedral solvent.

Figure 57.

Potentials of mean force at infinite dilution for KCl in polarizable and nonpolarizable tetrahedral solvents. The solid and dashed lines are RHNC results for  $w_{ij}(r)$  determined for polarizable and nonpolarizable tetrahedral solvent models, respectively. The dotted and dash-dot lines represent their respective primitive model functions obtained from eq. (2.99) using the dielectric constants given in the text.



We have also investigated the effects of using the full quadrupole tensor of water in the solvent model. In the tetrahedral solvent model it has been replaced with an effective square quadrupole moment (as discussed in Chapter V). Calculations were carried out at infinite dilution for several different ions in the  $C_{2v}$  quadrupole solvent. A single computation was also performed at 0.5M for a model KCl solution. We note that the effective dipole moment and the dielectric constant of the  $C_{2v}$  quadrupole solvent are the same as for the tetrahedral solvent. As we would expect, the solvation of the ions equal in size but opposite in charge (e.g.,  $\text{Eq}^+/\text{Eq}^-$  and  $\text{Na}^+/\text{F}^-$ ) was no longer symmetric, with positive ions receiving a slight preference because of the negative  $zz$  component of the quadrupole tensor. Only slight changes were noticed in the ion-solvent and ion-ion structure due to the generalization of the quadrupole moment of the water-like solvent, this effect being a great deal smaller than that observed from the addition of the octupole moment to the solvent model, as discussed below. At 0.5M the thermodynamic properties of the model KCl solution were found to be very similar (differing by less than 1% in almost all cases) to those of the same solution with the tetrahedral solvent. Thus, the small  $zz$  component of the quadrupole tensor of water appears to have relatively little influence upon ion solvation and upon the thermodynamic properties of model aqueous electrolyte solutions.

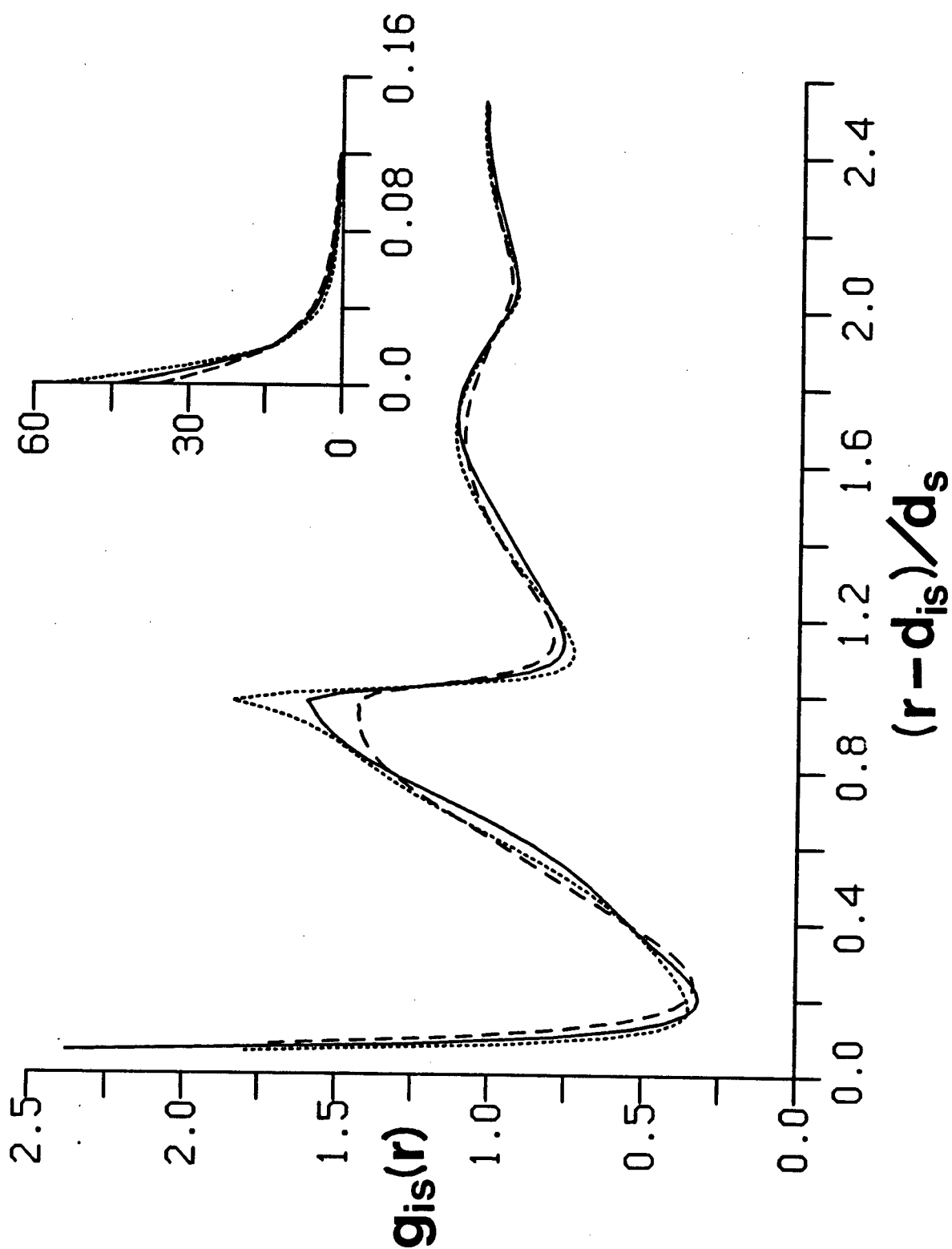
Finally, we will consider the effects of the addition of the octupole moment of water to the  $C_{2v}$  quadrupole solvent. In particular we shall examine its effect upon ion solvation and upon thermodynamic properties of model aqueous electrolyte solutions. The  $C_{2v}$  octupole solvent (as discussed in Chapter V) has an effective dipole moment of  $m_e = 2.634D$  and a dielectric constant of 94.9, both values being very close to those of the tetrahedral solvent. The  $\text{Li}^+$ ,  $\text{Na}^+$ ,  $\text{Eq}^+$ ,  $\text{K}^+$ ,  $\text{Cs}^+$ ,  $\text{F}^-$ ,  $\text{Eq}^-$ ,  $\text{Cl}^-$  and  $\text{I}^-$  ions were all studied at infinite dilution in the  $C_{2v}$  octupole solvent.

First, let us examine the changes in the ion-solvent structure. In Figure 58 we have plotted  $g_{is}(r)$  for  $\text{Na}^+$  and  $\text{F}^-$  ions in the  $C_{2v}$  octupole solvent along with  $g_{is}(r)$  for a  $\text{Na}^+$  ion (or equivalently, for a  $\text{F}^-$  ion) in the tetrahedral solvent. In the  $C_{2v}$  octupole solvent both ions show a slight increase in the occurrence of tetrahedral packing of the solvent about the ions, as indicated in Figure 58 by the increase in  $g_{is}(r)$  at a reduced separation of about  $0.65d_s$ . This is not a surprising result since the addition

Figure 58.

Ion-solvent radial distribution functions at infinite dilution for the tetrahedral and  $C_{2v}$  octupole solvents. The solid line is  $g_{1s}(r)$  for a  $Na^+$  (or  $F^-$ ) ion in the tetrahedral solvent. The dashed and dotted lines represent results for a  $Na^+$  and a  $F^-$  ion, respectively, in the  $C_{2v}$  octupole solvent.





of the octupole moment was found in Chapter V to stabilize tetrahedral packing within the pure solvent. In Figure 58 we see that the contact peak in  $g_{is}(r)$  for a  $F^-$  ion in the  $C_{2v}$  octupole solvent is sharper than for a  $F^-$  (or  $Na^+$ ) ion in the tetrahedral solvent, which in turn is sharper than for a  $Na^+$  ion in the  $C_{2v}$  octupole solvent. A similar observation can be made for the second peaks in  $g_{is}(r)$ . Beyond the second peak we observe that in the  $C_{2v}$  octupole solvent the amplitude of the oscillatory structure in  $g_{is}(r)$  remains larger for  $F^-$  than for  $Na^+$ . Thus, the solvation shell structure appears to be more clearly defined for a  $F^-$  ion than for a  $Na^+$  ion in the  $C_{2v}$  octupole solvent. Moreover, we find that in general for ions of equal size the anion is always preferentially solvated over the cation. The influence of the octupole moment, and hence the asymmetry in solvation, is found to decrease with increasing ion size because of the short-range nature of the ion-octupole interaction (with respect to that of the ion-dipole).

In Figure 59 we have compared  $\langle \cos\theta_{is}(r) \rangle$  for  $Na^+$  and  $F^-$  ions in the  $C_{2v}$  octupole and tetrahedral solvents. It can be seen from Figure 59 that the average orientation of the dipole moments of the solvent particles around these small ions is strongly influenced by the presence of the octupole moment in the solvent model. In the  $C_{2v}$  octupole solvent, we find a general decrease in the oscillatory structure of  $\langle \cos\theta_{is}(r) \rangle$ , particularly for  $Na^+$ , indicating an apparent decrease in dipolar structure. The positions and shapes of the peaks in  $\langle \cos\theta_{is}(r) \rangle$ , particularly for  $F^-$ , are obviously affected by the presence of the octupole moment in the solvent model. From Figure 59 we observe that in the  $C_{2v}$  octupole solvent the contact values of  $\langle \cos\theta_{is}(r) \rangle$  have dropped relative to the tetrahedral solvent results for both  $F^-$  and  $Na^+$  ions. However, if we examine the standard deviation of  $\cos\theta_{is}(r)$  as determined from eq. (2.91)), we find that for  $F^-$  the standard deviation,  $\sigma$ , is significantly smaller (by about 20%) in the  $C_{2v}$  octupole solvent, indicating a narrower distribution of angles. In the case of  $Na^+$ ,  $\sigma$  actually increases slightly from its value in the tetrahedral solvent. Evidently, the effect of the octupole moment is such that the orientation of the solvent, at least near contact, has become more directionally specific for anions than for cations of the same size. All the effects reported here for  $Na^+$  and  $F^-$  ions were also observed for larger cations and anions, although the influence of the octupole moment is again found to decrease with increasing ion size.

Figure 59.

$\langle \cos \theta_{iS}(r) \rangle$  at infinite dilution for the tetrahedral and  $C_{2v}$  octupole solvents.  
The lines are as defined in Figure 58.

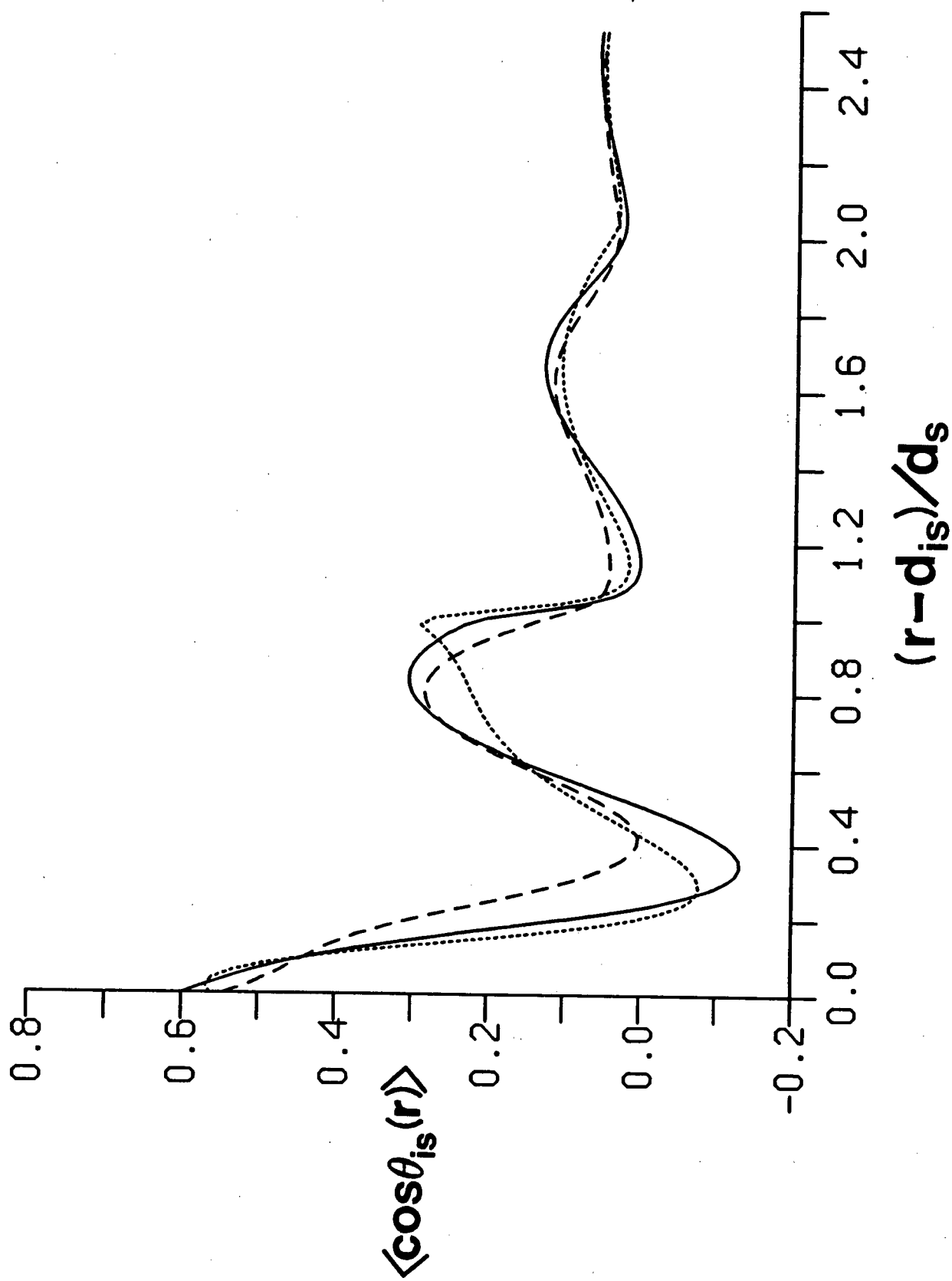
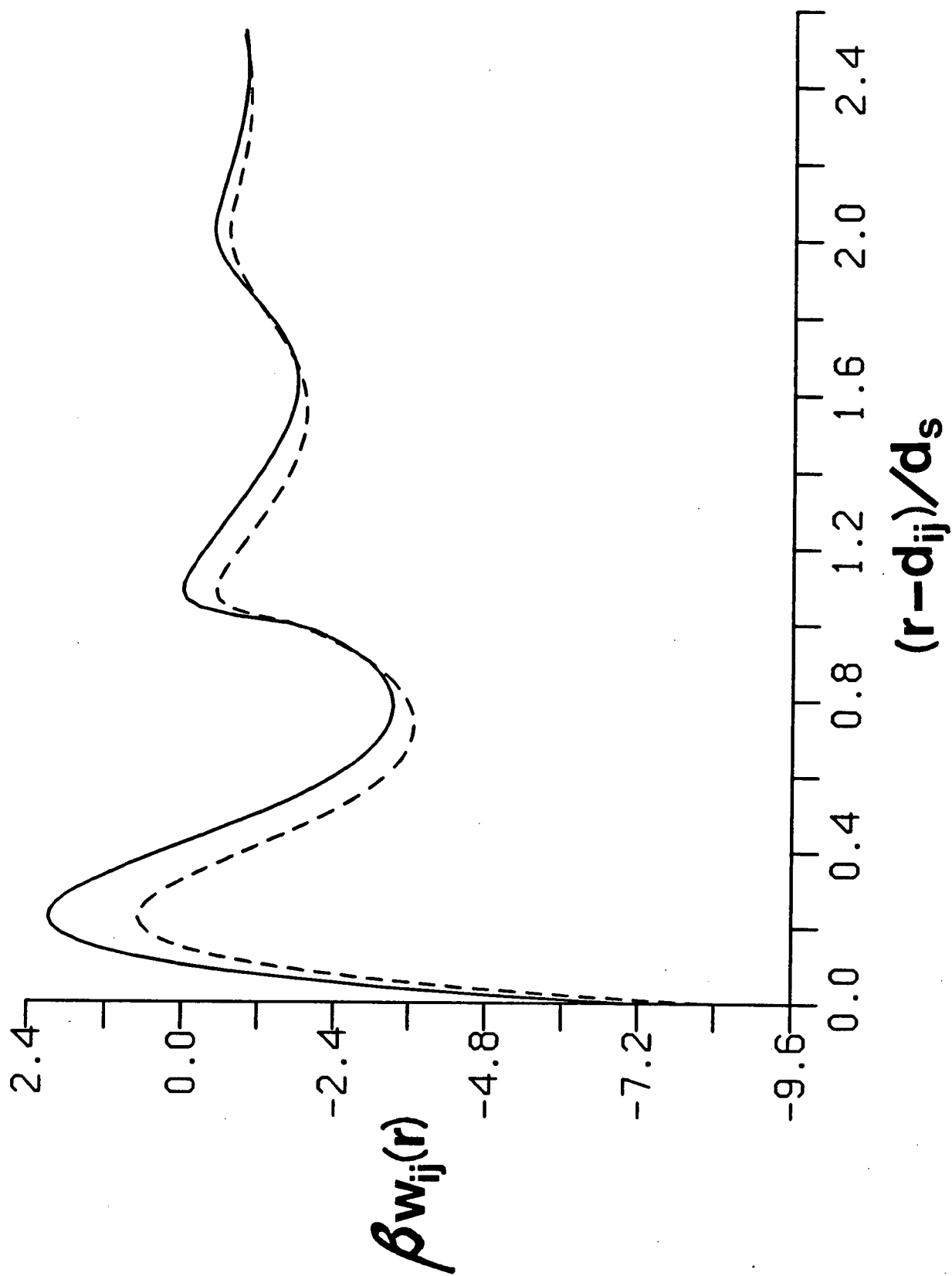


Figure 60.

Potentials of mean force at infinite dilution for LiF in the  $C_{2v}$  octupole and tetrahedral solvents. The solid and dashed lines are RHNC results for the tetrahedral and  $C_{2v}$  octupole solvents, respectively.



Let us now consider the sensitivity of the ion-ion structure to the presence of the octupole moment in the solvent model. The potentials of mean force at infinite dilution for LiF in both tetrahedral and  $C_{2v}$  octupole solvents have been compared in Figure 60. We observe that for LiF  $w_{ij}(r)$  is generally more negative (including the contact peak and the first maximum) in the  $C_{2v}$  octupole solvent. From Figure 60 we see that the second minimum of  $w_{ij}(r)$  is shifted still further inward. Its minimum is now at a reduced separation of about  $0.75d_s$ , indicating an increased preference for the solvent bridging structure for this small pair of ions in the  $C_{2v}$  octupole solvent. We again recall the work of Pettitt and Rossky [82] in which it was shown that small changes in  $w_{ij}(r)$  can result in large changes in some thermodynamic properties (in particular  $\phi$ ) of model aqueous electrolyte solutions. Clearly then, we might expect  $\ln \gamma_{\pm}$  for a LiF (or even NaCl) solution to show dramatically different concentration dependence when the tetrahedral solvent is replaced by the  $C_{2v}$  octupole solvent. It should also be pointed out that for larger ion pairs the difference between the  $C_{2v}$  octupole and tetrahedral results for  $w_{ij}(r)$  is much smaller.

The like-ion potentials of mean force for  $Li^+$  and  $F^-$  ions in both the  $C_{2v}$  octupole and tetrahedral solvents have been shown in Figure 61. Here we observe quite dramatic effects due to the addition of the octupole moment to the solvent model. For  $Li^+$  we find that  $w_{ii}(r)$  becomes much more repulsive at contact and the huge attractive well found with the tetrahedral solvent becomes much shallower in the  $C_{2v}$  octupole solvent. In Figure 61 we see that the converse is true in the case of  $F^-$ . As discussed above, the behaviour of  $w_{ii}(r)$  at short range seems to be closely related to the degree of solvation of that ion (*i.e.*, how tightly the solvent is held to the ion and consequently how well defined the solvation shell structure is). Thus, for  $F^-$  in the  $C_{2v}$  octupole solvent the contact peak in  $g_{is}(r)$  becomes sharper (see Figure 58) and the attractive well in  $w_{ii}(r)$  grows deeper, while for  $Li^+$  the opposite relationship is true. However, we emphasize here that it may well be the long-range changes in the ion-solvent structure, also evident in Figure 58, which have the largest influence upon the short-range behaviour of  $w_{ii}(r)$ . Once again, we note that the effects of the octupole moment upon  $w_{ii}(r)$  are most pronounced for small ions.

Figure 61.

Like-ion potentials of mean force at infinite dilution for  $\text{Li}^+$  and  $\text{F}^-$  in the  $\text{C}_{2v}$  octupole and tetrahedral solvents. The solid and dotted lines are RHNC results for  $\text{Li}^+/\text{Li}^+$  and  $\text{F}^-/\text{F}^-$ , respectively, in the tetrahedral solvent. The dashed and dash-dot lines represent  $\beta w_{ii}(\mathbf{r})$  for  $\text{Li}^+$  and  $\text{F}^-$ , respectively, in the  $\text{C}_{2v}$  octupole solvent.



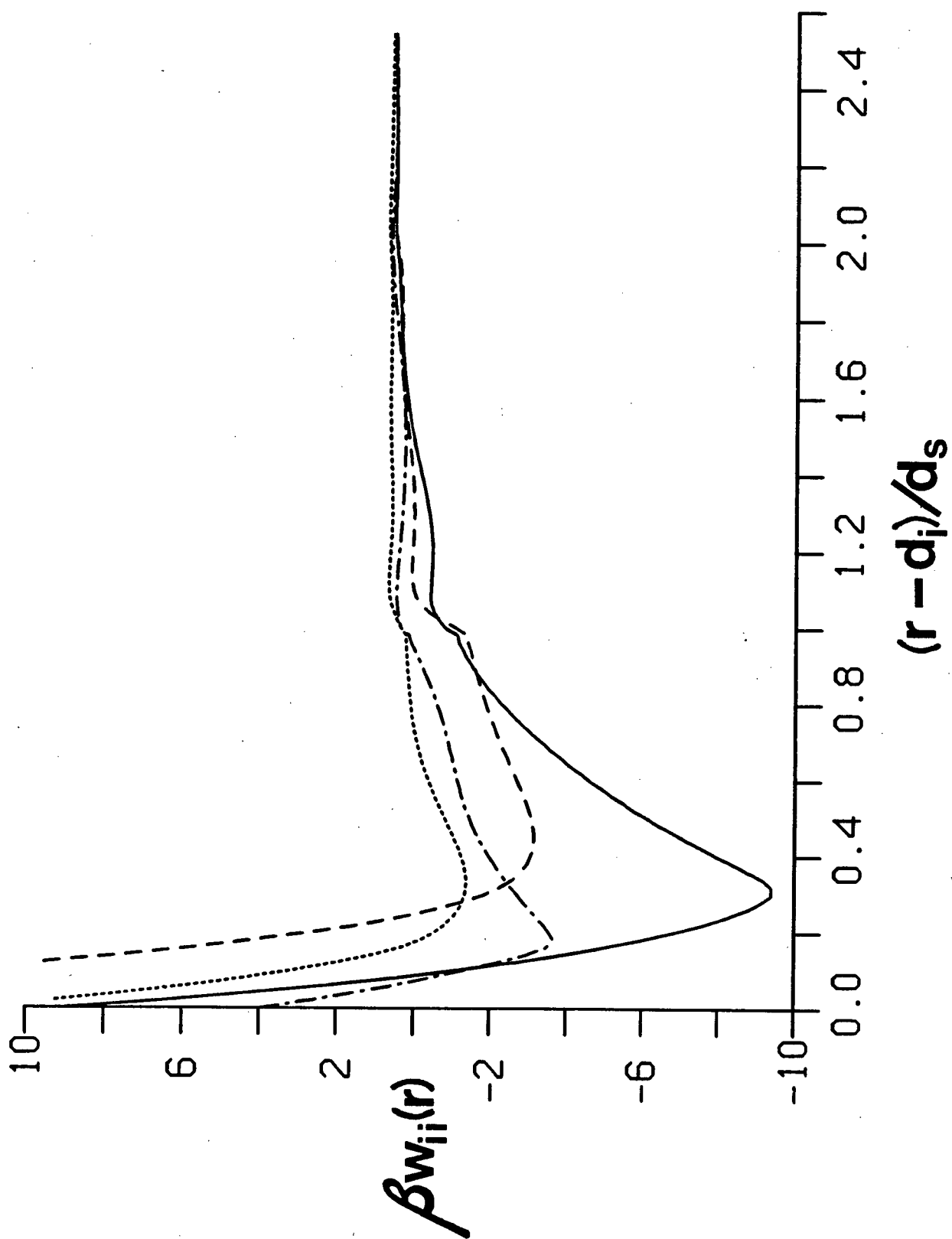


**TABLE X.** Average ion-solvent energies per ion at infinite dilution. Results for the  $C_{2v}$  octupole and tetrahedral solvents are compared. The values given are in kT units and are those of the effective systems.

ION	Tetrahedral Solvent	$C_{2v}$ Octupole Solvent
Li <sup>+</sup>	-424.1	-393.5
Na <sup>+</sup>	-363.8	-342.1
Eq <sup>+</sup>	-316.2	-301.7
K <sup>+</sup>	-296.4	-284.7
Cs <sup>+</sup>	-255.8	-249.6
F <sup>-</sup>	-363.8	-394.7
Eq <sup>-</sup>	-316.2	-336.5
Cl <sup>-</sup>	-278.7	-291.7
I <sup>-</sup>	-230.5	-235.1

We will now examine the influence that the octupole moment has upon some of the thermodynamic properties of electrolyte solutions at infinite dilution. The average ion-solvent energies per ion at infinite dilution are given in Table X, where results for several ions in both the tetrahedral and  $C_{2v}$  octupole solvents have been included. We find that the addition of the octupole moment to the solvent model has a fairly large effect upon the average ion-solvent energies. As we would expect from our previous discussions,  $U_{is}/N_i$  is more positive (*i.e.*, smaller in magnitude) for a cation in the  $C_{2v}$  octupole solvent than for the same cation in the tetrahedral solvent, while the converse is true for anions. Hence, if we consider two ions of the same size which are equal and opposite in charge (*e.g.*, Eq<sup>+</sup>/Eq<sup>-</sup> or Na<sup>+</sup>/F<sup>-</sup>), we find that the anion interacts more strongly with the  $C_{2v}$  octupole solvent than does the cation. We also observe from Table X that this asymmetry in solvation is largest for the smallest ions.

If we examine the individual ion-dipole, ion-quadrupole and ion-octupole contributions to the ion-solvent energy for any of the ions listed in Table X, we again find some interesting results. For anions in the  $C_{2v}$  octupole solvent the ion-octupole energy is negative and the ion-dipole and ion-quadrupole energies have decreased (*i.e.*, increased in magnitude) with respect to their values in the tetrahedral solvent. For cations in the  $C_{2v}$  octupole solvent, however, the ion-octupole energy is positive (indicating a net

average repulsion between the ion and the octupole moment) and the ion-dipole and ion-quadrupole energies have become less negative. Clearly, when a  $C_{2v}$  octupole solvent particle interacts with a positive ion, none of the most favourable dipole and quadrupole orientations correspond to favourable orientations of the octupole moment with respect to the ion. We note that the magnitude of the ion-octupole energy is always less than 5% of the total ion-solvent energy for all the ions listed in Table X.

Finally, let us focus upon the partial molar volume. In Chapter III we have shown that at infinite dilution  $\bar{V}_2^0$  can be split into two independent terms (of course this is not the case at finite concentration). Comparing eqs. (3.12) and (3.64a) we immediately have

$$\bar{V}_i^0 = kT\chi_T^0(1 - \rho_S C_{iS}^0) , \quad (6.4)$$

where  $\bar{V}_i^0$  is an individual ionic partial molecular volume. Then using eq. (6.4) we have calculated values for  $\bar{V}_i^0$  for several ions at infinite dilution in both the  $C_{2v}$  octupole and tetrahedral solvents. These values for  $\bar{V}_i^0$  have been recorded in Table XI along with experimental results for ions in real water. It is immediately obvious from Table XI that the trends in the present results are much larger than those of experiment. If we re-examine eq. (6.4), we see that  $\bar{V}_i^0$  depends upon the isothermal compressibility,  $\chi_T^0$ , of the pure solvent. We have reported earlier (in section 3) that  $\chi_T^0$  for the tetrahedral solvent is five times larger than that of water at 25°C. For the  $C_{2v}$  octupole solvent  $\chi_T^0$  is 50% larger still. Thus, in order to allow a more reasonable comparison (*i.e.*, one which does not depend upon the differences in  $\chi_T^0$ ) between both sets of theoretical results and those of experiment, we compute *corrected* values for  $\bar{V}_i^0$  using only the isothermal compressibility of real water in eq. (6.4). These corrected values for  $\bar{V}_i^0$  are also given in Table XI.

It can be clearly seen from Table XI that the octupole moment has a very large effect upon individual ionic partial molar volumes. We find that  $\bar{V}_i^0$  is much smaller (*i.e.*, more negative) for a cation in the  $C_{2v}$  octupole solvent than for the same cation in the tetrahedral solvent, while the converse relationship holds for anions. Moreover, for two ions equal in size and equal and opposite in charge (*i.e.*,  $Eq^+/Eq^-$  or  $Na^+/F^-$ ) there is a dramatic difference between their respective values of  $\bar{V}_i^0$  in the  $C_{2v}$  octupole solvent, with the anion always having the larger value (*i.e.*, appearing as though it is larger in

**TABLE XI.** Individual ionic partial molar volumes at infinite dilution. Results for the tetrahedral and  $C_{2v}$  octupole solvents are compared with those for real water at 25°C. The experimental partial molar volumes are from Table 6 on page 376 of Ref. 5. The value given in parentheses are corrected results as discussed in the text. All values for  $\bar{V}_i^0$  are given in cc/mole.

ION	Tetrahedral Solvent	$C_{2v}$ Octupole Solvent	Expt.
Li <sup>+</sup>	-103.1 (-20.0)	-226.5 (-29.3)	-11.2
Na <sup>+</sup>	-62.7 (-12.2)	-177.5 (-22.9)	-7.4
Eq <sup>+</sup>	-29.8 (-5.8)	-136.1 (-17.6)	—
K <sup>+</sup>	-14.5 (-2.8)	-116.6 (-15.1)	3.4
Cs <sup>+</sup>	22.6 (4.4)	-68.3 (-8.8)	15.5
F <sup>-</sup>	-62.7 (-12.2)	-2.0 (-0.3)	3.3
Eq <sup>-</sup>	-29.8 (-5.8)	46.0 (5.9)	—
Cl <sup>-</sup>	0.3 (0.1)	87.9 (11.4)	23.7
I <sup>-</sup>	53.0 (10.3)	158.5 (20.5)	41.4

solution). Clearly, for ions of the same size any dissimilarity in  $\bar{V}_i^0$  must be totally due to differences in their *apparent electrostriction* [5] of the solvent (that is to the total volume change or compression of the solvent due to the presence of the ion). Now one might expect that the electrostriction of the solvent should be proportional to the average interaction between the ion and the solvent. Consequently, we would then expect that the larger the magnitude of the average ion-solvent energy, the greater the degree of electrostriction, and hence the smaller  $\bar{V}_i^0$  should be. Unfortunately, this deduction is contradicted by the values in Tables X and XI. Let us try another approach. One view currently held for electrostriction [5] suggests that most of the effect occurs very near an ion, which for small univalent ions usually implies just the first solvation shell. If we re-examine Figure 58 we observe that the first solvation shell of a F<sup>-</sup> ion in the  $C_{2v}$  octupole solvent is held in more tightly (*i.e.*, experiences greater electrostriction) than is the first solvation shell of a Na<sup>+</sup> ion. Furthermore, if we compute coordination numbers for the Na<sup>+</sup> and F<sup>-</sup> ions (using eq. (5.2)), we find that in the  $C_{2v}$  octupole solvent it is the F<sup>-</sup> ion which has a slightly larger number of solvents in its first solvation shell. Again, we would conclude that the anion, in this case F<sup>-</sup>, should have the smaller value of  $\bar{V}_i^0$ , but again this would be contrary to the results in Table XI. In our discussion of Figure 58 we had mentioned apparent

differences in  $g_{iS}(r)$  at longer range for  $F^-$  and  $Na^+$  ions in the  $C_{2v}$  octupole solvent. Together, the above observations would strongly suggest that it is these changes in the long-range packing structure of the solvent around the ions which accounts for most of the gross dissimilarities in  $\bar{V}_i^0$  seen in Table XI for ions of equal size. Clearly then, the long-range ion-solvent structure (apart from the long-range ion-dipole correlations which give rise to  $S_V$ ) appears to be an important factor in determining the values of ionic partial molar volumes, at least for the model aqueous electrolyte solutions being considered in this study.

We conclude this discussion by noting that the ionic charge and size dependence of  $\bar{V}_i^0$ , as shown in Table XI, for ions in the  $C_{2v}$  octupole solvent is consistent with the experimental results given.

## CHAPTER VII

### CONCLUSIONS

In this thesis we have examined the structural, thermodynamic and dielectric properties of model aqueous electrolyte solutions which explicitly include the solvent as a molecular species. The dielectric and structural properties of the water-like solvents employed in this study were also investigated. The ion and solvent models used were simple ones incorporating known microscopic (molecular) properties with no freely adjustable parameters. We have considered only univalent ions, primarily focusing upon the alkali halides, and hence have modelled these ions simply as charged hard spheres. Ionic crystal radii were used to determine the hard-sphere diameters. The water-like solvent models were also treated as hard spheres into which measured values of the low-order multipole moments and polarizability tensor of water were included.

Our model systems were studied using integral equation methods, the RHNC theory [68] being employed almost exclusively. In order to apply the RHNC theory, it had to be first generalized for a multi-component system. In our generalization of the OZ equation we have examined the simplifications which result when all the species present in the system have at least  $C_{2v}$  symmetry. A computer program which uses general forms of the multipole potential and the OZ and RHNC equations was written and then used to generate all the results presented in this thesis, both for the pure solvent and for the solution systems.

In this study we have exploited the formalism of Kirkwood and Buff [104] in order to derive general relationships between integrals over  $h_{\alpha\beta}(r)$  and certain thermodynamic properties of electrolyte solutions. The usual Kirkwood-Buff expressions can not be applied directly because application of the charge neutrality conditions leads to indeterminate results for the thermodynamic quantities. By defining  $k$ -dependent analogs of the Kirkwood-Buff equations and taking the appropriate  $k \rightarrow 0$  limits analytically, we were able to obtain exact determinate expressions. These relationships are directly applicable to real systems since the system we have considered

incorporates the solvent as a true molecular species. Although we have reported results for a two-component salt/solvent system only, the method we have used is general and can easily be applied to more complicated systems.

The low concentration limiting behaviour of our thermodynamic expressions was also examined and compared with the macroscopic results obtained through Debye-Hückel theory [6]. Not surprisingly, the exact Debye-Hückel limiting law for  $\ln \gamma_{\pm}$  was extracted from the molecular theory. Moreover, the microscopic limiting law for  $\bar{V}_2$  was found to be functionally equivalent to the macroscopic expression. However, when the HNC approximation for the limiting slope of  $\bar{V}_2$  is compared with the exact macroscopic result, we discover that the HNC theory is rather inaccurate for this quantity. For the model aqueous electrolyte solutions we have considered, the HNC theory appears to overestimate the limiting slope for  $\bar{V}_2$  by about an order of magnitude.

In the present study we have described two levels of theory with which electrolyte solutions containing a polarizable solvent may be examined. The first of these is the SCMF approximation [67] in which the many-body problem of polarization is reduced (by ignoring fluctuations) to a problem involving an effective pairwise additive potential. In this thesis we have shown how the SCMF approximation can be applied to the present electrolyte solution model in order to determine the average total dipole moment of the solvent at finite salt concentration. We have also developed a second and more detailed level of formalism, the RDMF theory, which allows us to examine the average local electric field experienced by a solvent at a distance  $R$  from an ion. The RDMF theory is a mean field approach (like the SCMF approximation) and gives rise to an effective spherical potential between an ion and the solvent particles around it. Furthermore, this spherical potential was shown to have an effect upon the limiting laws of those thermodynamic properties which depend upon ion-solvent correlations at low concentration.

It should again be emphasized that most of the formalisms developed in this thesis are general and could be used with relative ease in the investigation of other systems besides the model aqueous electrolyte solutions considered in the present study. More general models for both the ions and the solvent could be examined, *e.g.*, where both the solvent and the ions possess more complicated short-range potentials and have higher multipole

moments. Solutions of more than one salt with ions of several different charges could be easily studied. We point out that the general form of the RHNC theory presented in this thesis could, in principle, be applied to any multi-component system characterized by angle-dependent pair potentials.

Several closely related water-like solvents were examined in this study using the RHNC theory. The HNC basis set dependence for these models was observed to be quite similar to that previously reported [71,110] for hard-sphere models with dipoles and linear quadrupoles. Model systems for liquid water were investigated over a large range of temperatures and pressures. These systems were found to have dielectric constants which agree well with experimental values, particularly at higher temperature. The RHNC results for the distribution functions of our water-like fluids are in rather poor agreement with experiment, particularly at low temperature. However, we were able to obtain the *correct* structure for liquid water at 25°C through the simple addition of a spherical potential to the hard-sphere model. Moreover, the addition of this soft potential also improved the low temperature dielectric properties of our water-like model. The octupole moment was shown to have relatively little effect upon the dielectric constant, although it was found to have a somewhat larger effect upon the structure within the model fluid systems.

Virtually all of the model aqueous electrolyte solutions we have investigated at finite concentration employed a polarizable solvent model with only dipole and square quadrupole moments. For these solutions and within the SCMF approximation, the average local electric field in the bulk was shown to be essentially independent of salt concentration, and hence the average total dipole moment of the solvent was taken to be a constant. The equilibrium dielectric constants obtained for these model solutions are in qualitative agreement with the experimental values for the dielectric constants of aqueous electrolyte solutions, particularly at higher concentrations. We also point out that all the microscopic limiting law expressions derived in this study were confirmed by our numerical results at low concentration.

Our relatively simple model for aqueous electrolyte solutions demonstrated a remarkable diversity of behaviour through simply varying the hard-sphere diameters of the ions. Pairs of smaller ions, such as NaCl, were found to be extremely soluble, whereas pairs of larger ions, such as M'I, were



relatively insoluble. Moreover, ion solvation and many thermodynamic properties were shown to be quite sensitive to the ion size asymmetry of a salt. The ion size dependence of several thermodynamic quantities was examined, including the isothermal compressibility, the partial molar volumes and the mean activity coefficient. Some of the behaviour observed is consistent with that demonstrated by real aqueous electrolyte solutions, *e.g.*, the slope of  $\bar{V}_2$  was found to change sign at very low concentration for solutions of large ions. Some of the behaviour observed disagreed with experimental results, *e.g.*, the values for  $\ln \gamma_{\pm}$  for our model NaCl solutions were less than those of CsI and KCl. However, even in the case of the NaCl system, the results reported in this study may provide some insight into unusual behaviour exhibited by other aqueous electrolyte solutions. We find that for thermodynamic properties such as the mean activity coefficient, both ion-solvent and short-range ion-ion structure can have a large influence, even at relatively low concentration.

In this study we have made a detailed investigation of the ion-ion, ion-solvent and solvent-solvent structure within our model solutions. Smaller ions were found to disrupt the solvent-solvent structure to a much greater degree than larger ions, although this effect only became obvious at higher concentrations. As we might expect, the solvation structure around an ion becomes more clearly defined as the size of the ion decreases, although both concentration and counter-ion effects were observed. Near contact the ion-solvent structure showed little counter-ion dependence, yet strong dependence was found in the second solvation shell, particularly at higher concentrations. The molecular nature of the solvent was seen to have a very strong influence on the short-range ion-ion structure for both like and unlike ion pairs. This was especially true in the case of either very small or very large ions. For the most part, the concentration dependence of the ion-ion correlations was dominated by simple ionic screening effects, although some counter-ion dependence was demonstrated by like-ion correlations at higher concentrations. Finally, we remark that previous RLHNC results using the same models at infinite dilution were found to be in rather poor agreement with the present results.

The effects of the RDMF theory were examined for several model aqueous electrolyte solutions at infinite dilution and at low concentration. The

electric field due to the ionic charge was shown to be substantially reduced by the lateral solvent fields, even at small separations. Consequently, the RDMF had only a small effect upon the short-range ion-solvent structure, although it appeared to have a larger impact on ion-ion correlations. As expected, the RDMF was observed to have a large influence upon some thermodynamic quantities, most notably  $\bar{V}_2$ . However, at least for some quantities the RDMF theory turns out to be relatively inaccurate, even in the long-range and low concentration limits. For example, the RDMF contribution to the limiting slope for  $\bar{V}_2$  exceeds the known macroscopic result for real aqueous electrolyte solutions. Nevertheless, we have been able to clearly demonstrate the importance of polarization in determining the structural and thermodynamic properties of electrolyte solutions. Obviously, further study of these polarization effects is warranted.

Whereas ion solvation was found to be relatively insensitive to the small  $zz$  component of the quadrupole tensor of water, the addition of the octupole moment to our water-like solvent model was shown to have a large impact. The octupole moment was found to have a particularly large effect upon  $g_{ii}(r)$ . The individual ionic partial molar volumes at infinite dilution demonstrated extreme sensitivity to the details of how an ion is solvated. Furthermore, the present results strongly suggest that the long-range ion-solvent packing structure is very important in determining the values of  $\bar{V}_i^0$ .

Several suggestions for further study have been made immediately above or in earlier discussions in this thesis. The very interesting behaviour exhibited by our solutions of larger ions clearly requires more detailed investigation. Our examination of the influence of the octupole moment of water upon ion solvation and thermodynamic properties needs to be extended both to higher moments (*e.g.*, hexadecapole) and to finite concentration. Ions with higher charges (*e.g.*, divalent) and with low order multipole moments (*e.g.*,  $\text{CN}^-$ ) should also be investigated. In this study we have considered model aqueous electrolyte solutions only at  $25^\circ\text{C}$ . Clearly, the temperature dependence of these systems should be examined, particularly at relatively high temperatures where the present models would be expected to work much better. The results presented in this thesis can very easily be used to test the assumption that only a pairwise additive potential need be employed in McMillan-Mayer level theory [25,28] in order to study primitive model

electrolyte solutions. This investigation is currently being carried out [187]. Another extension to the present study which is also in progress [133] is the examination of large colloidal particles and electric double layers in the same model electrolyte solutions considered here. Finally, more complicated but hopefully more realistic models might also be investigated using the methods outlined in this thesis.

We conclude by again stating that the purpose of the present study was not to develop and report results for an exact model of aqueous electrolyte solutions. Rather, its main purpose was to systematically examine simple models for these systems in order to learn what is important in determining ion solvation and to help understand how details of the ion solvation affect the measurable thermodynamic quantities.

## LIST OF REFERENCES

1. Murrell, J.N., and Boucher, E.A., Properties of Liquids and Solutions, Wiley, New York, 1982.
2. Franks, F., Water, The Royal Society of Chemistry, London, 1983.
3. Helper, L.G., and Smith, W.L., Principles of Chemistry, MacMillan, New York, 1975.
4. Franks, F., ed., Water; A Comprehensive Treatise, Vol. 1: The Physics and Physical Chemistry of Water, Plenum Press, New York, 1971.
5. Conway, B.E., Ionic Hydration in Chemistry and Biophysics, Elsevier Scientific Publishing Co., Amsterdam, 1981.
6. Harned, H.S., and Owens, B.B., Physical Chemistry of Electrolyte Solutions, 3rd ed., Reinhold Publishing Corp., New York, 1959.
7. Robinson, R.A., and Stokes, R.H., Electrolyte Solutions, 2nd ed., Academic Press, New York, 1959.
8. Guggenheim, E.A., and Stokes, R.H., Equilibrium Properties of Aqueous Solutions of Single Strong Electrolytes, Pergamon Press, Toronto, 1969.
9. Conway, B.E., and Barrads, R.G., eds., Chemical Physics of Ionic Solutions, Wiley, New York, 1966.
10. Wolynes, P.G., *Ann. Rev. Phys. Chem.*, **31**, 345 (1980).
11. Hamer, W.J., ed., The Structure of Electrolyte Solutions, Wiley, New York, 1959.
12. Friedman, H.L., *Chem. Sci.*, **25**, 42 (1985).
13. Enderby, J.E., and Neilson, G.W., *Rep. Prog. Phys.*, **44**, 593 (1981).
14. Enderby, J.E., Howells, W.S., and Howe, R.A., *Chem. Phys. Lett.*, **21**, 109 (1973).
15. Narten, A.H., Vaslow, F., and Levy, H.A., *J. Chem. Phys.*, **58**, 5017 (1973).
16. Enderby, J.E., *Ann. Rev. Phys. Chem.*, **34**, 155 (1983).
17. Clausius, R., *Poggendorffs Annalen*, **101**, 338 (1857).
18. van't Hoff, J.H., *Z. Physik. Chem.*, **1**, 481 (1887).
19. Planck, M., *Z. Physik. Chem.*, **1**, 577 (1887).
20. Arrhenius, S., *Z. Physik. Chem.*, **1**, 631 (1887).

21. Falkenhagen, H., Electrolytes, trans: R.P. Bell, Clarendon Press, Oxford, 1934.
22. Debye, P., and Hückel, E., *Physik. Z.*, **24**, 185, 305 (1923).
23. Onsager, L., *Physik. Z.*, **28**, 277 (1927)
24. Outhwaite, C.W., A Specialist Periodical Report: Statistical Mechanics, Vol. 2, The Chemical Society, London, 1975.
25. Anderson, H.C., Modern Aspects of Electrochemistry, eds. B.E. Conway and J. O'M. Bockris, Vol. 11, 1975.
26. McMillan, W.G., and Mayer, J.E., *J. Chem. Phys.* **13**, 276 (1945).
27. Hansen, J.P., and McDonald, I.R., Theory of Simple Liquids, Academic Press, London, 1976.
28. Friedman, H.L., *Ann. Rev. Phys. Chem.*, **32**, 179 (1981).
29. Ramanathan, P.S., and Friedman, H.L., *J. Chem. Phys.*, **54**, 1086 (1971).
30. Rasaiah, J.C., *J. Sol. Chem.*, **2**, 301 (1973).
31. Barker, J.A., and Watts, R.O., *Chem. Phys. Lett.*, **3**, 144 (1969).
32. Rahman, A., and Stillinger, F.H., *J. Chem. Phys.*, **55**, 3336 (1971).
33. Barker, J.A., and Henderson, D., *Rev. Mod. Phys.*, **48**, 587 (1976).
34. Levesque, D., Weiss, J.J., and Hansen, J.P., Applications of the Monte Carlo Method in Statistical Physics, ed., K. Binder, Springer-Verlag, New York, 1984.
35. Reimers, J.R., and Watts, R.O., *Chem. Phys.*, **91**, 201 (1984).
36. Reimers, J.R., Watts, R.O., and Klein, M.L., *Chem. Phys.*, **64**, 95 (1982).
37. Barnes, P., Finney, J.L., Nicholas, J.D., and Quinn, J.E., *Nature*, **282**, 459 (1979).
38. Wojcik, M., and Clementi, E., *J. Chem. Phys.*, **84**, 5970 (1986).
39. Jorgensen, W.L., *J. Am. Chem. Soc.*, **103**, 335 (1981).
40. Kuharsky, R.A., and Rossky, P.J., *J. Chem. Phys.*, **82**, 5164 (1984).
41. Jorgensen, W.L., Chandrasekhar, J., Madura, J.D., Impey, R.W., and Klein, M.L., *J. Chem. Phys.*, **79**, 926 (1983).
42. Mezei, M., Swaminathan, S., and Beveridge, D.L., *J. Chem. Phys.*, **71**, 3366 (1979).

43. Lie, G.C., Clementi, E., and Yashimine, M., *J. Chem. Phys.*, **64**, 2315 (1976).
44. Stillinger, F.H., and Rahman, A., *J. Chem. Phys.*, **60**, 1545 (1974).
45. Neumann, M., *J. Chem. Phys.*, **82**, 5663 (1985).
46. Neumann, M., *J. Chem. Phys.*, **85**, 1567 (1986).
47. Wood, D.W., Water: A Comprehensive Treatise, ed. F. Franks, Vol. 6: Recent Advances, Plenum Press, New York, 1979.
48. Sceats, M.G., Stavola, M., and Rice, S.A., *J. Chem. Phys.*, **70**, 3927 (1979).
49. Matsuoka, O., Yoshimine, M., and Clementi, E., *J. Chem. Phys.*, **64**, 1351 (1976).
50. Bounds, D.G., *Molec. Phys.*, **54**, 1355 (1985).
51. Chandrasekhar, J., Spellmeyer, D.C., and Jorgensen, W.L., *J. Am. Chem. Soc.*, **106**, 903 (1984).
52. Mills, M.F., Reimers, J.R., and Watts, R.O., *Molec. Phys.*, **57**, 777 (1986).
53. Mezei M., and Beveridge, D.L., *J. Chem. Phys.*, **74**, 6902 (1981).
54. Impey, R.W., Madden, P.A., and McDonald, I.R., *J. Chem. Phys.*, **87**, 5071 (1983).
55. Heinzinger, K., and Vogel, P.C., *Z. Naturforsch.*, **31A**, 463 (1976).
56. Szasz, G.J., Heinzinger, K., and Reide, W.O., *Z. Naturforsch.*, **36A**, 1067 (1981).
57. Clementi, E., and Barsotti, R., *Chem. Phys. Lett.*, **59**, 21 (1978).
58. Heinzinger, K., *Pure Appl. Chem.*, **57**, 1031 (1985).
59. Rossky, P.J., *Ann. Rev. Phys. Chem.*, **36**, 321 (1985).
60. Watts, R.O., A Specialist Periodical Report: Statistical Mechanics, Vol. 1, Chemical Society, London, 1973.
61. Stell, G., Patey, G.N., and Hoyer, J.S., *Adv. Chem. Phys.*, **38**, 183 (1981).
62. Patey, G.N., *Molec. Phys.*, **34**, 427 (1978).
63. Patey, G.N., *Molec. Phys.*, **35**, 1413 (1978).
64. Patey, G.N., Levesque, D., and Weis, J.J., *Molec. Phys.*, **38**, 1635 (1979).
65. Patey, G.N., Levesque, D., and Weis, J.J., *Molec. Phys.*, **38**, 219 (1979).

66. Wertheim, M.S., *J. Chem. Phys.*, **55**, 4291 (1971).
67. Carnie, S.L., and Patey, G.N., *Molec. Phys.*, **47**, 1129 (1982).
68. Fries, P.H., and Patey, G.N., *J. Chem. Phys.*, **82**, 429 (1985).
69. Levesque, D., Weis, J.J., and Patey, G.N., *Molec. Phys.*, **51**, 333 (1984).
70. Lee, L.Y., Fries, P.H., and Patey, G.N., *Molec. Phys.*, **55**, 751 (1985).
71. Perkyns, J.S., Fries, P.H., and Patey, G.N., *Molec. Phys.*, **57**, 529 (1986).
72. Carnie, S.L., Chan, D.Y.C., and Walker, G.R., *Molec. Phys.*, **43**, 1115 (1981).
73. Chan, D.Y.C., Mitchell, D.J., and Ninham, B.W., *J. Chem. Phys.*, **70**, 2946 (1979).
74. Levesque, D., Weis, J.J., and Patey, G.N., *J. Chem. Phys.*, **72**, 1887 (1980).
75. Levesque, D., Weis, J.J., and Patey, G.N., *Phys. Lett.*, **66A**, 115 (1978).
76. Outhwaite, C.W., *Molec. Phys.*, **37**, 1229 (1977).
77. Adelman, S.A., and Chen, J.H., *J. Chem. Phys.*, **70**, 4291 (1979).
78. Adelman, S.A., and Deutch, J.M., *J. Chem. Phys.*, **60**, 3935 (1974).
79. Patey, G.N., and Carnie S.L., *J. Chem. Phys.*, **78**, 5183 (1983).
80. Kusalik, P.G., and Patey, G.N., *J. Chem. Phys.*, **79**, 4468 (1983).
81. Kusalik, P.G., "A Theoretical Study of Dilute Aqueous Electrolyte Solutions", Master's Thesis, University of British Columbia, 1984.
82. Pettitt, B.M., and Rossky, P.J., *J. Chem. Phys.*, **84**, 5836 (1986).
83. Kusalik, P.G., and Patey, G.N., to be published.
84. Kusalik, P.G., and Patey, G.N., to be published.
85. Kusalik, P.G., and Patey, G.N., accepted, *J. Chem. Phys.*
86. Kusalik, P.G., and Patey, G.N., submitted, *J. Chem. Phys.*
87. Friedman, H.L., A Course in Statistical Mechanics, Prentice-Hall, Englewood Cliffs, New Jersey, 1985.
88. McQuarrie, D.A., Statistical Mechanics, Harper and Row, New York, 1976.
89. Hill, T.L., An Introduction to Statistical Thermodynamics, Addison-Wesley, Reading, Massachusetts, 1960.

90. Ornstein, L.S., and Zernike, F., *Proc. Acad. Sci. Amsterdam*, **17**, 793 (1914).
91. Lebowitz, J.L., and Percus, J.K., *Phys. Rev.*, **144**, 251 (1966).
92. Percus, J.K., and Yevick, G.J., *Phys. Rev.*, **110**, 1 (1958).
93. Van Leeuwen, J.M., Groeneveld, M.J., and De Boer, J., *Physica*, **25**, 792 (1959).
94. Meeron, E., *J. Math. Phys.*, **1**, 192 (1960).
95. Morita, T., *Prog. Theor. Phys.*, **23**, 829 (1960).
96. Rushbrooke, G.S., *Physica*, **26**, 259 (1960).
97. Verlet, L., *Nuovo Cimento*, **18**, 77 (1960).
98. Perera, A., Kusalik, P.G., and Patey, G.N., *Mol. Phys.*, In Press.
99. Perera, A., Kusalik, P.G., and Patey, G.N., submitted, *J. Chem. Phys.*
100. Perera, A., Kusalik, P.G., and Patey, G.N., to be published.
101. Blum, L., and Torruella, A.J., *J. Chem. Phys.*, **56**, 303 (1971).
102. Blum, L., *J. Chem. Phys.*, **57**, 1862 (1972).
103. Blum, L., *J. Chem. Phys.*, **58**, 3295 (1973).
104. Kirkwood, J.G., and Buff, F.P., *J. Chem. Phys.*, **19**, 774 (1951).
105. Born, M., and Oppenheimer, J.R., *Ann. Phys. (Leipz.)*, **84**, 457 (1927).
106. Hirschfelder, J.O., Curtiss, C.F., and Bird, R.B., Molecular Theory of Gases and Liquids, Wiley, New York, 1954.
107. Kielich, S., A Specialist Periodical Report: Dielectric and Related Molecular Processes, Vol. 1, The Chemical Society, London, 1972.
108. Messiah, A., Quantum Mechanics, Wiley, New York, 1958.
109. Rotenberg, M., Bevins, R., Metropolis, N., and Wooten, N., The 3-j and 6-j Symbols, Massachusetts Institute of Technology, Cambridge, 1959.
110. Perkyins, J.S., "The Solution to the Reference Hypernetted Chain Approximation for Fluids of Hard Spheres With Dipoles and Quadrupoles with Application to Liquid Ammonia", Master's Thesis, University of British Columbia, 1985.
111. Walker, G.R., "Fluids with Angle-Dependent Potentials", Ph.D. Dissertation, Australian National University, 1983.



112. Buckingham, A.D., *Quart. Rev. Chem. Soc. Lond.*, **13**, 183 (1959).
113. Price, S.L., Stone, A.J., and Alderton, M., *Molec. Phys.*, **52**, 987 (1984).
114. Stogryn, D.E., and Stogryn, A.P., *Molec. Phys.*, **11**, 371 (1966).
115. John, I.G., Bacskay, G.B., and Hush, N.S., *Chem. Phys.*, **51**, 49 (1980).
116. Newmann, D., and Moskovitz, J.W., *J. Chem. Phys.*, **49**, 2056 (1968).
117. Huiszoon, C., *Molec. Phys.*, **58**, 865, (1986).
118. Dyke, T.R., and Muentner, J.S., *J. Chem. Phys.*, **59**, 3125 (1973).
119. Verhoeven, J., and Dymanuys, A., *J.Chem. Phys.*, **52**, 3222 (1970).
120. Ciccariello, S., and Domenico, G., *J. Chem. Soc., Faraday*, **81**, 1163 (1985).
121. Narten, A.H., and Levy, H.A., *J. Chem. Phys.*, **55**, 2263 (1971).
122. Soper, A.K., and Phillips, M.G., *Chem. Phys.*, **107**, 47 (1986).
123. Pauling, L., The Nature of the Chemical Bond, 3rd ed., Cornell University Press, Ithaca, N.Y., 1960.
124. Morris, D.F.C., *Struct. Bonding*, **4**, 63 (1968).
125. Adelman, S.A., *J. Chem. Phys.*, **64**, 724 (1976).
126. Brigham, E.O., and Morrow, R.E., The Fast Fourier Transform, IEEE Spectrum, New York, 1967.
127. Lado, F., *J. Comp. Phys.*, **8**, 417 (1971).
128. Abramowitz, M., and Stegun, I.A., eds., Handbook of Mathematical Functions, Dover, New York, 1970.
129. Lado, F., *Molec. Phys.*, **31**, 1117 (1976).
130. Lee, L.L., and Levesque, D., *Molec. Phys.*, **26**, 1351 (1973).
131. Verlet, L., and Weis, J.J., *Phys. Rev. A.*, **5**, 939 (1972).
132. Perkyns, J.S., Kusalik, P.G., and Patey, G.N., *Chem. Phys. Lett.*, **129**, 258 (1986).
133. Torrie, G.M., Kusalik, P.G., and Patey, G.N., to be published.
134. Gerald, C.F., Applied Numerical Analysis, 2nd ed., Addison-Wesley, Don Mills, Ontario, 1978.
135. Chan, D.Y.C., Mitchell, D.J., Ninham, B.W., and Pailthorpe, B.A., *J. Chem. Phys.*, **69**, 691 (1978).

136. Mendenhall, W., Introduction to Probability and Statistics, 4th ed., Duxbury Press, North Scituate, Massachusetts, 1975.
137. Hasted, J.B., Aqueous Dielectrics, Chapman and Hall, London, 1973.
138. Frölich, H., Theory of Dielectrics, 2nd ed., Oxford University Press, Oxford, 1958.
139. Böttcher, C.J.F., Theory of Electric Polarization, 2nd ed., Elsevier Scientific, Amsterdam, 1973.
140. Weidner, R.T., and Sells, R.L., Elementary Classical Physics, Vol. 2, Allyn and Bacon, Boston, 1973.
141. Hubbard, J.B., Colonomos, P., and Wolnes, P.G., *J. Chem. Phys.*, **71**, 2652 (1979).
142. Kirkwood, J.G., *J. Chem. Phys.*, **4**, 592 (1936).
143. Høye, J.S., and Stell, G., *J. Chem. Phys.*, **64**, 1952 (1976).
144. Stillinger, F.A., and Lovett, R., *J. Chem. Phys.*, **49**, 1991 (1968).
145. Friedman, H.L., and Ramanathan, P.S., *J. Chem. Phys.*, **74**, 3756 (1970).
146. Beeby, J.L., *J. Phys. Chem.*, **6**, 2262 (1973).
147. Hall, D.G., *J. Chem. Soc., Faraday Trans.*, **67**, 2516 (1971).
148. Rasaiah, J.C., and Friedman, H.L., *J. Chem. Phys.*, **50**, 3965 (1969).
149. Friedman, H.L., Krishman, C.V., and Jolicoeur, C., *Ann. New York Academy Sci.*, **204**, 19 (1973).
150. Castellan, G.W., Physical Chemistry, Addison Wesley, Reading, Massachusetts, 1971.
151. Rasaiah, J.C., and Friedman, H.L., *J. Chem. Phys.*, **48**, 2742 (1968).
152. Høye, J.S., and Stell, G., *J. Chem. Phys.*, **71**, 1985 (1979).
153. Rasaiah, J.C., Isbister, D.J., and Stell, G., *J. Chem. Phys.*, **75**, 4707 (1981).
154. Rasaiah, J.C., *J. Chem. Phys.*, **77**, 5711 (1982).
155. Patey, G.N., and Valleau, J.P., *Chem. Phys. Lett.*, **58**, 157 (1978).
156. Wertheim, M.S., *Ann. Rev. Phys. Chem.*, **30**, 471 (1979).
157. Venkatasubramanian, V., Gubbins, K.E., Gray, C.G., and Joslin, C.G., *Molec. Phys.*, **52**, 1441 (1984).

158. Caillat, J.M., Levesque, D., Weis, J.J., Kusalik, P.G., and Patey, G.N., *Molec. Phys.*, **55**, 65 (1985).
159. Patey, G.N., Torrie, G.M., and Valleau, J.P., *J. Chem. Phys.*, **71**, 96 (1979).
160. Vesley, F.J., *Chem. Phys. Lett.*, **56**, 390 (1978).
161. Pollock, E.L., Alder, B.J., and Patey, G.N., *Physica A.*, **108**, 14 (1981).
162. Murad, S., *Molec. Phys.*, **51**, 525 (1984).
163. Patey, G.N., Levesque, D., and Weis, J.J., *Molec. Phys.*, **57**, 337 (1986).
164. Murphy, W.F., *J. Chem. Phys.*, **67**, 5877 (1977).
165. Spiegel, M.R., Mathematical Handbook of Formulas and Tables, McGraw-Hill, New York, 1968.
166. Steinhauser, O., and Bertagnolli, H., *Ber. Bunsenges. Phys. Chem.*, **85**, 45 (1981).
167. Pollock, E.L., Alder, B.J., and Pratt, L.R., *Proc. Natl. Acad. Sci. U.S.A.*, **77**, 49 (1980).
168. Kusalik, P.G., and Patey, G.N., unpublished work.
169. Weast, R.C., ed., CRC Handbook of Chemistry and Physics, 56th ed., CRC Press, Cleveland, Ohio, 1975.
170. Jansoon, V.M., and Franck, E.U., *Ber. Bunsenges. Phys. Chem.*, **76**, 943 (1972).
171. Eisenberg, D., and Kauzmann, W., The Structure and Properties of Water, Clarendon, Oxford, 1969.
172. Coulson, C.A., and Eisenberg, D., *Proc. R. Soc. A.*, **291**, 445 (1966).
173. Perera, A., Kusalik, P.G., and Patey, G.N., to be published.
174. Washburn, E.W., ed., International Critical Tables, McGraw-Hill, New York, 1926.
175. Conway, B.E., and Verrall, R.E., *J. Phys. Chem.*, **70**, 3952 (1966).
176. Behret, H., Schmithals, F., and Barthel, J., *Z. Phys. Chem. Neue Folge.*, **96**, 73 (1975).
177. Harris, F.E., and O'Konski, C.T., *J. Phys. Chem.* **61**, 310 (1957).
178. Geise, K., Kaatz, U., and Pottel, R., *J. Phys. Chem.*, **74**, 3718 (1970).
179. Haggis, G.H., Hasted, J.B., and Buchanan, T.J., *J. Chem. Phys.*, **20**, 1452 (1952).

180. Barthel, J., Krüger, J., and Schallmeyer, E., *Z. Phys. Chem. Neue Folge.*, **104**, 59 (1977).
181. Gucker, F.T., Chernick, C.L., and Roy-Chowdhury, P., *Proc. Natl. Acad. Sci. U.S.A.*, **55**, 12 (1966).
182. Wen, W.I., and Saito, S., *J. Phys. Chem.*, **68**, 2639 (1964).
183. Millero, F.J., *Chem. Rev.*, **71**, 147 (1971).
184. Franks, F., and Smith, H.T., *Trans. Faraday Soc.*, **63**, 2586 (1967).
185. Hamer, W.J., and Wu, Y.C., *J. Phys. Chem. Ref. Data*, **1**, 1047 (1972).
186. Lindenbaum, S., and Boyd, G.E., *J. Phys. Chem.*, **68**, 911 (1964).
187. Patey, G.N., and Kusalik, P.G., to be published.
188. Springer, J.F., Prohant, M.A., and Stevens, F.A., *J. Chem. Phys.*, **58**, 4863 (1973).
189. Lado, F., *Molec. Phys.*, **31**, 1117 (1976).
190. Patey, G.N., *J. Chem. Phys.*, **72**, 5763 (1980).

## APPENDIX A

### TREATMENT OF POTENTIAL TERMS IN $c(12)$

In general, care must be taken in handling the long-range tails in  $c_{\mu\nu;a\beta}^{mnl}(r)$  and  $\eta_{\mu\nu;a\beta}^{mnl}(r)$  when numerically performing both forward and backward Hankel transforms (cf. eqs. (2.32), (2.34) and (2.46), (2.47)). For the hard-sphere multipolar fluids being considered in this study, it is the long-range contributions due to  $\beta u_{a\beta}(12)$  that are of primary concern, since  $c_{a\beta}(12) \rightarrow -\beta u_{a\beta}(12)$  as  $r \rightarrow \infty$ . We find it convenient to define the *short-range* functions

$$c_{\mu\nu;a\beta}^{mnl;S}(r) = c_{\mu\nu;a\beta}^{mnl}(r) + \lambda_{\mu\nu;a\beta}^{mnl}(r) , \quad (A.1a)$$

where for  $mnl \neq 0$

$$\lambda_{\mu\nu;a\beta}^{mnl}(r) = \begin{cases} \beta u_{\mu\nu;a\beta}^{mnl}(r), & \text{for } r > d_{a\beta} \\ 0, & \text{for } r < d_{a\beta} \end{cases} \quad (A.1b)$$

and  $d_{a\beta}$  is the hard-sphere contact distance. We note that  $\lambda_{00;a\beta}^{000}(r)$  is defined below. In eq. (A.1b) we assume that all potential terms that are not multipolar are short-ranged, and therefore are not included in  $\lambda_{\mu\nu;a\beta}^{mnl}(r)$ .

First let us consider a system which contains no charged species. For this system we need to consider only terms for which  $l \geq 2$ . It follows from eqs. (2.10b) and (3.38a) that none of the Hankel transforms,  $\tilde{c}_{\mu\nu;a\beta}^{mnl}(k)$ , will have divergent behaviour at small  $k$ . In fact, all but  $\tilde{c}_{00;a\beta}^{112}(k)$  will go to

zero as  $k \rightarrow 0$ . Furthermore, the integral transforms of the functions

$\lambda_{\mu\nu;a\beta}^{mnl}(r)$  can be performed analytically, and it can be shown [103] that for  $r \geq d_{a\beta}$   $\hat{\lambda}_{\mu\nu;a\beta}^{mnl}(r) = 0$ . Hence, the potential term makes no contribution to  $\hat{c}_{\mu\nu;a\beta}^{mnl}(r)$  for  $r \geq d_{a\beta}$ . For  $r \leq d_{a\beta}$ ,  $\hat{\lambda}_{\mu\nu;a\beta}^{mnl}(r)$  evaluates to a constant term which can then be added to the hat transform of the short-range  $c$  to obtain the full  $\hat{c}_{\mu\nu;a\beta}^{mnl}(r)$ .

For a system containing both ionic and dipolar species, two additional terms require special treatment, namely  $c_{00;a\beta}^{011}(r)$  and  $c_{00;a\beta}^{000}(r)$ . We point out that there are normally no integral transforms associated with these terms. It can be shown [61,135] that as  $k \rightarrow 0$ ,  $\tilde{c}_{00;a\beta}^{011}(k)$  will diverge as  $1/k$  (of course, this is only the case when particle  $a$  has a charge and particle  $\beta$  has a dipole moment). We take advantage of the linearity of Fourier transforms and transform only the short-range  $c$  numerically;  $\lambda_{00;a\beta}^{011}(r)$  can be transformed analytically. Using eqs. (2.10b) and (A.1b) we write that

$$\lambda_{00;a\beta}^{011}(r) = A/r^2, \quad (\text{A.2})$$

where  $A$  will depend upon the charge and dipole moment of particles  $a$  and  $\beta$ , respectively. Then inserting eq. (A.2) into eq. (2.34b) and evaluating the integral yields

$$\tilde{\lambda}_{00;a\beta}^{011}(k) = \frac{4\pi i A}{d_{a\beta} k^2} \sin(k d_{a\beta}), \quad (\text{A.3})$$

where  $i = \sqrt{-1}$ . We note that  $\tilde{\lambda}_{00;a\beta}^{011}(k)$  has the correct [135] small  $k$  behaviour. From the definition of  $\eta_{a\beta}^{(12)}$  (cf. eq. (2.38)) it clearly follows that  $\tilde{\eta}_{00;a\beta}^{011}(k)$  will also diverge as  $1/k$  as  $k \rightarrow 0$ . Fortunately, this divergent behaviour will pose no numerical problems in the back Hankel transform (cf. eq. (2.46b)) because the divergent terms in the integral will cancel exactly at

small  $k$ .

When both particles  $a$  and  $\beta$  are charged, it can be shown [61,135] that  $\tilde{c}_{00;a\beta}^{000}(k)$  diverges as  $1/k^2$  as  $k \rightarrow 0$ . Thus, we again split  $c_{00;a\beta}^{000}(r)$  into a short-range function, which can be easily Fourier transformed numerically, and a long-range function,  $\lambda_{00;a\beta}^{000}(r)$ , whose transform can be derived analytically. Following previous workers [188-190], we define

$$\lambda_{00;a\beta}^{000}(r) = \beta \frac{q_a q_\beta}{r} (1 - e^{-\sigma r}) , \quad (\text{A.4a})$$

which can be Fourier transformed analytically to give

$$\tilde{\lambda}_{00;a\beta}^{000}(k) = 4\pi\beta q_a q_\beta \left[ \frac{\sigma^2}{k^2(k^2 + \sigma^2)} \right] , \quad (\text{A.4b})$$

where  $q_a$  and  $q_\beta$  are the charges on the ions. The constant  $\sigma$  must be chosen with care so as not to cause  $\lambda_{00;a\beta}^{000}(r)$  to become *large* at small  $r$ , but it must also allow  $\lambda_{00;a\beta}^{000}(r) \rightarrow \beta q_a q_\beta / r$  at some reasonable value of  $r$ . It is again the case that  $\tilde{\eta}_{00;a\beta}^{000}(k)$  will have the same divergent behaviour as  $\tilde{c}_{00;a\beta}^{000}(k)$ ; we note that at finite concentrations  $h_{00;a\beta}^{000}(r)$  must be screened, and hence its Fourier transform will not contribute. Thus, we define the *short-range* function

$$\tilde{\eta}_{00;a\beta}^{000;S}(k) = \tilde{\eta}_{00;a\beta}^{000}(k) - \tilde{\lambda}_{00;a\beta}^{000}(k) , \quad (\text{A.5})$$

which can be Fourier transformed numerically without difficulty.

For an ionic system at infinite dilution, the fact that the functions  $h_{\mu\nu;a\beta}^{mnl}(r)$  are no longer screened requires that special attention be paid to certain functions. First, the long-range tail of  $h_{00;a\beta}^{000}(r)$  must be corrected for the  $k=0$  point which was ignored in the numerical integration (*i.e.*, by the FFT [126] ) of  $\tilde{\eta}_{00;a\beta}^{000;S}(k)$ . Also, the long-range tail of  $h_{00;a\beta}^{011}(r)$ , which

has a  $1/r^2$  dependence at large  $r$  [61], will affect both  $c_{00;a\beta}^{000}(r)$  and  $c_{00;a\beta}^{022}(r)$ . Within the HNC theory, both functions have a dependence upon  $[h_{00;a\beta}^{011}(r)]^2$  at large  $r$ . The resulting  $1/r^4$  tails are truncated during a numerical calculation (both in the closure calculation and in the Hankel transform), but analytical expressions which correct for this truncation can be derived. We remark that these correction terms are small and relatively unimportant (except when determining  $C_{is}$ ) for univalent ions, but can become quite significant for larger charges.



## APPENDIX B

### REPRESENTATIVE EXAMPLES OF EXPONENTIAL INTEGRALS

First we will consider an integral of the general form

$$F = a \int_d^\infty r^2 \left[ (1+\kappa r) \frac{e^{-\kappa r}}{r^2} \right]^2 dr , \quad (\text{B.1})$$

where  $a$  is some constant. It is the behaviour of  $F$  as  $\kappa \rightarrow 0$  that is of interest here. It is convenient to write eq. (B.1) in the form

$$F = a[I_0 + I_1 + I_2] , \quad (\text{B.2a})$$

where

$$I_0 = \int_d^\infty \frac{e^{-2\kappa r}}{r^2} dr , \quad (\text{B.2b})$$

$$I_1 = 2\kappa \int_d^\infty \frac{e^{-2\kappa r}}{r} dr \quad (\text{B.2c})$$

and

$$I_2 = \kappa^2 \int_d^\infty e^{-2\kappa r} dr . \quad (\text{B.2d})$$

Then using standard tables of integrals [165], it is possible to show that

$$I_0 = \frac{e^{-2\kappa d}}{d} - 2\kappa \int_d^\infty \frac{e^{-2\kappa r}}{r} dr \quad (\text{B.3a})$$

and

$$I_2 = \frac{\kappa}{2} e^{-2\kappa d} . \quad (\text{B.3b})$$

We can then insert eqs. (B.2c) and (B.3) into eq. (B.2a) to obtain

$$F = a \left[ \frac{1}{d} + \frac{\kappa}{2} \right] e^{-2\kappa d} \quad (\text{B.4})$$

and expanding the exponential yields

$$F = a \left[ \frac{1}{d} - \frac{3}{2} \kappa + \kappa^2 d - \dots \right] . \quad (\text{B.5})$$

Therefore, in the limit  $\kappa \rightarrow 0$ , we have that

$$F = a \left[ \frac{1}{d} - \frac{3}{2} \kappa \right] . \quad (\text{B.6})$$

We will now examine the  $\kappa \rightarrow 0$  dependence of an integral of the general form

$$F = a \int_{R-d}^{R+d} (1+\kappa r) \frac{e^{-\kappa r}}{r^2} \left[ (r^2 + R^2 - d^2)^2 - (2rR)^2 \right] dr , \quad (\text{B.7})$$

where again  $a$  is some constant. Equation (B.8) can then be written as

$$F = a \left[ I_3 + I_2 + I_1 + I_0 + I_{-1} + I_{-2} \right] , \quad (\text{B.8a})$$

where

$$I_3 = \kappa \int_{R-d}^{R+d} r^3 e^{-\kappa r} dr , \quad (\text{B.8b})$$

$$I_2 = \int_{R-d}^{R+d} r^2 e^{-\kappa r} dr , \quad (\text{B.8c})$$

$$I_1 = -2\kappa(R^2 + d^2) \int_{R-d}^{R+d} r e^{-\kappa r} dr , \quad (\text{B.8d})$$

$$I_0 = -2(R^2 + d^2) \int_{R-d}^{R+d} e^{-\kappa r} dr , \quad (\text{B.8e})$$

$$I_{-1} = \kappa(R^2 - d^2)^2 \int_{R-d}^{R+d} \frac{e^{-\kappa r}}{r} dr \quad (\text{B.8f})$$

and

$$I_{-2} = (R^2 - d^2)^2 \int_{R-d}^{R+d} \frac{e^{-\kappa r}}{r^2} dr . \quad (\text{B.8g})$$

Using standard forms for the integrals in eqs. (B.8b-e) and (B.8g) as given in tables [165], we can rearrange eq. (B.8a) to obtain

$$F = a \left[ e^{-\kappa r} \left[ \left( -r^3 - \frac{4}{\kappa} r^2 - \frac{8r}{\kappa^2} - \frac{8}{\kappa^3} \right) + 2(R^2 + d^2) \left( r + \frac{2}{\kappa} \right) - \frac{1}{r} (R^2 - d^2)^2 \right] \right]_{R-d}^{R+d}. \quad (\text{B.9})$$

If we then evaluate eq. (B.9) at its limits, we find that

$$F = a e^{-\kappa R} \left[ e^{-\kappa d} \left[ \frac{-8}{\kappa^3} - \frac{8R}{\kappa^2} - \frac{8d}{\kappa^2} - \frac{8Rd}{\kappa} \right] - e^{\kappa d} \left[ \frac{-8}{\kappa^3} - \frac{8R}{\kappa^2} + \frac{8d}{\kappa^2} + \frac{8Rd}{\kappa} \right] \right], \quad (\text{B.10})$$

which we can write as

$$F = a e^{-\kappa R} \left[ \left[ \frac{8}{\kappa^3} + \frac{8R}{\kappa^2} \right] \left[ e^{\kappa d} - e^{-\kappa d} \right] - \left[ \frac{8d}{\kappa^2} + \frac{8Rd}{\kappa} \right] \left[ e^{\kappa d} + e^{-\kappa d} \right] \right]. \quad (\text{B.11})$$

Now, it is the  $\kappa \rightarrow 0$  limiting behaviour of eq. (B.11) we wish to determine.

By expanding the exponentials, we can show that at small  $\kappa$

$$e^{\kappa d} - e^{-\kappa d} = 2\kappa d + \frac{1}{3}\kappa^3 d^3 \quad (\text{B.12a})$$

and

$$e^{\kappa d} + e^{-\kappa d} = 2 + \kappa^2 d^2. \quad (\text{B.12b})$$

Inserting eqs. (B.12) into eq. (B.11) and simplifying yields

$$F = \frac{-16a}{3d^3} (1 + \kappa R) e^{-\kappa R}. \quad (\text{B.13})$$

## APPENDIX C

### TRANSFORMATION OF THE ROTATIONAL INVARIANT $\Phi^{123}_{(12)}$

As in the text, we will make use of the notation of Steinhauser and Bertagnolli [166] in our discussion. Using the rotation matrix given by eq. (39) of Ref. 166, it is easy to show that in the  $(\hat{x}, \hat{y}, \hat{z})$  frame of reference (see Figure 6(b))

$$\hat{x}_2 = \begin{bmatrix} \cos a_2 \cos \beta_2 \cos \gamma_2 - \sin a_2 \sin \gamma_2 \\ \sin a_2 \cos \beta_2 \cos \gamma_2 + \cos a_2 \sin \gamma_2 \\ -\sin \beta_2 \cos \gamma_2 \end{bmatrix}, \quad (C.1a)$$

$$\hat{y}_2 = \begin{bmatrix} -\cos a_2 \cos \beta_2 \sin \gamma_2 - \sin a_2 \cos \gamma_2 \\ -\sin a_2 \cos \beta_2 \sin \gamma_2 + \cos a_2 \cos \gamma_2 \\ \sin \beta_2 \sin \gamma_2 \end{bmatrix}, \quad (C.1b)$$

$$\hat{z}_2 = \begin{bmatrix} \sin \beta_2 \cos a_2 \\ \sin \beta_2 \sin a_2 \\ \cos \beta_2 \end{bmatrix}. \quad (C.1c)$$

In the ion reference frame we take advantage of the restriction on  $\beta_2^I$  as given by eq. (4.66a) and write

$$\hat{x}_2^I = \begin{bmatrix} -\sin a_2^I \sin \gamma_2^I \\ \cos a_2^I \sin \gamma_2^I \\ -\cos \gamma_2^I \end{bmatrix}, \quad (C.2a)$$

$$\hat{y}_2^I = \begin{bmatrix} -\sin a_2^I \cos \gamma_2^I \\ \cos a_2^I \cos \gamma_2^I \\ \sin \gamma_2^I \end{bmatrix}, \quad (C.2b)$$

$$\hat{z}_2^I = \begin{bmatrix} \cos a_2^I \\ \sin a_2^I \\ 0 \end{bmatrix}. \quad (C.2c)$$

In order to take the unit vectors  $\hat{x}_2^I$ ,  $\hat{y}_2^I$  and  $\hat{z}_2^I$  from the ion frame of reference to the  $(\hat{x}, \hat{y}, \hat{z})$  reference frame, we multiply the unit vectors by the rotation matrix  $\underline{R}$ , as given by eq. (4.69), which yields

$$\hat{x}_2 = \begin{bmatrix} -\sin a_2^I \sin \gamma_2^I \cos \omega + \cos \gamma_2^I \sin \omega \\ \cos a_2^I \sin \gamma_2^I \\ -\sin a_2^I \sin \gamma_2^I \sin \omega - \cos \gamma_2^I \cos \omega \end{bmatrix}, \quad (C.3a)$$

$$\hat{y}_2 = \begin{bmatrix} -\sin a_2^I \cos \gamma_2^I \cos \omega - \sin \gamma_2^I \sin \omega \\ \cos a_2^I \cos \gamma_2^I \\ -\sin a_2^I \cos \gamma_2^I \sin \omega + \sin \gamma_2^I \cos \omega \end{bmatrix}, \quad (C.3b)$$

$$\hat{z}_2 = \begin{bmatrix} \cos a_2^I \cos \omega \\ \sin a_2^I \\ \cos a_2^I \sin \omega \end{bmatrix}. \quad (C.3c)$$

We can now obtain expressions relating the two sets of Euler angles associated with the two different frames of reference by equating components of the two forms for  $\hat{x}_2$ ,  $\hat{y}_2$  and  $\hat{z}_2$ . From eqs. (C.1c) and (C.3c) we have that

$$\sin \beta_2 = \frac{\cos a_2^I \cos \omega}{\cos a_2} = \frac{\sin a_2^I}{\sin a_2} \quad (C.4a)$$

and

$$\cos \beta_2 = \cos a_2^I \sin \omega. \quad (C.4b)$$

Similarly, we use the z-components of  $\hat{x}_2$  and  $\hat{y}_2$ , as given by eqs. (C.1a), (C.3a) and (C.1b), (C.3b), to obtain

$$\cos\gamma_2 = \sin a_2 \left[ \sin\gamma_2^I \sin\omega + \frac{\cos\gamma_2^I \cos\omega}{\sin a_2^I} \right] \quad (C.5a)$$

and

$$\sin\gamma_2 = \sin a_2 \left[ -\cos\gamma_2^I \sin\omega + \frac{\sin\gamma_2^I \cos\omega}{\sin a_2^I} \right] . \quad (C.5b)$$

Then using the trigonometric identities [165]

$$\cos 2\gamma = \cos^2\gamma - \sin^2\gamma , \quad (C.6a)$$

$$\cos 2\gamma = 2\sin\gamma \cos\gamma , \quad (C.6b)$$

and the requirement that  $\sin 2\gamma_2^I = 0$ , which follows from eq. (4.66b), it can be shown that

$$\cos 2\gamma_2 = \cos 2\gamma_2^I \sin^2 a_2 \left[ \frac{\cos^2 \omega}{\sin^2 a_2^I} - \sin^2 \omega \right] \quad (C.7a)$$

and

$$\sin 2\gamma_2 = -2\cos 2\gamma_2^I \sin^2 a_2 \left[ \frac{\sin\omega \cos\omega}{\sin a_2^I} \right] . \quad (C.7b)$$

If one substitutes eqs. (C.4) and (C.7) into eq. (4.64b) and takes  $a_1 = 0$ , one can obtain the result

$$\begin{aligned} \Phi^{123}(12) = \sqrt{6} & \left[ 3\cos\beta_1 (\cos^2\omega - \sin^2 a_2^I \sin^2\omega) \cos 2\gamma_2^I \right. \\ & + 2\sin\beta_1 \cos 2\gamma_2^I \left[ \cos a_2^I \cos a_2 \sin\omega \left[ \frac{\sin a_2}{\sin a_2^I} \cos^2\omega \right. \right. \\ & \left. \left. - \sin a_2 \sin a_2^I \sin^2\omega \right] + 2\sin^2 a_2 \sin\omega \cos\omega \right] \right] . \quad (C.8) \end{aligned}$$

From eq. (C.4a) we have the identities

$$\cos a_2 = \frac{\sin a_2 \cos a_2^I \cos\omega}{\sin a_2^I} \quad (C.9a)$$

and

$$\sin a_2 = \frac{\cos a_2 \sin a_2^I}{\cos a_2^I \cos \omega} . \quad (C.9b)$$

Using these relationships, together with simple trigonometric identities [165], we simplify eq. (C.8) which can eventually be written as the expression for  $\underline{\Phi}^{123}(12)$  given in eq. (4.70).